Influence of Aging in the Warm Forming of 6xxx series Aluminum Alloys

Vasco Manuel Neto Simoes

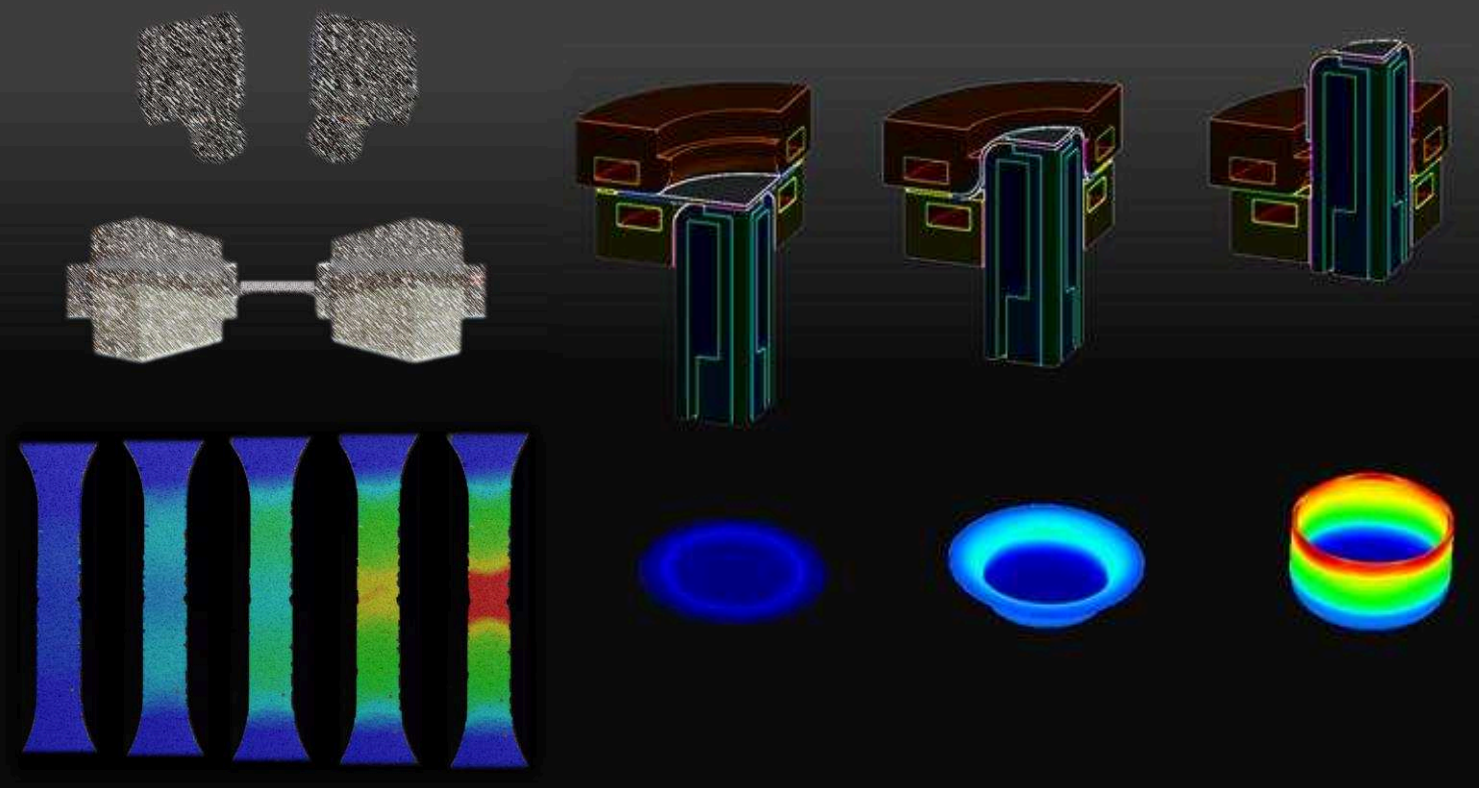

Vasco Manuel Neto Simões

Influence of Aging in the Warm Forming of 6xxx series Aluminum Alloys

Doctoral Thesis in Mechanical Engineering, branch of Production Technologies,
under the supervision of Hervé Laurent, Luís Filipe Martins Menezes and Marta Cristina Cardoso de Oliveira,
submitted to the Department of Mechanical Engineering, Faculty of Sciences and Technology of the University of Coimbra.
Thesis in cotutelle between the University of Coimbra and the University of South Brittany.

August 2017

· U C ·

UNIVERSIDADE DE COIMBRA

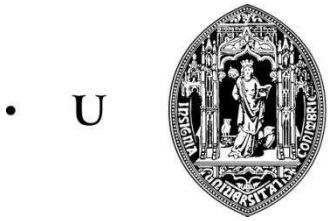

Influence of Aging in the Warm Forming of 6xxx series Aluminum Alloys

Dissertation in cotutelle presented to the Department of Mechanical Engineering of the University of Coimbra, as a requirement to obtain the doctoral degree in Mechanical Engineering, by the University of Coimbra and by the University of South Brittany, carried out under the supervision of Hervé Laurent, Luís Filipe Martins Menezes and Marta Cristina Cardoso de Oliveira.

Vasco Manuel Neto Simões

Department of Mechanical Engineering

Faculty of Sciences and Technology

University of Coimbra

Coimbra

2017

Dedicated to my Father

"Science is a social process.
It happens on a time scale longer than a human life.
If I die, someone takes my place.
If you die, someone takes your place.
What's important is to get it done."

Alfred Wegener (1880 – 1930)
Alfred Wegener proposed in 1912 the theory of continental drift
by hypothesizing that the continents are slowly drifting around the Earth.
Died in November 1930 (aged 50) in his fourth Greenland expedition,
before the theory was scientifically accepted.

(Page intentionally left blank)

Acknowledgements

The research work present in this PhD thesis has been carried out in a cooperation between the University of Coimbra and the University of Southern Brittany, namely in the research centers: Centre for Mechanical Engineering, Materials and Processes – CEMMPRE (Research Unit nº 285 of the Portuguese Foundation for Science and Technology), and; Institut de Recherche Dupuy de Lôme – IRDL (FRE CNRS 3744). The opportunity to perform this PhD in international cooperation was very fruitful for my research and engineering education, as well as in my personal development.

First, I want to express my sincere gratitude to my scientific advisers Professor Marta Oliveira, Professor Hervé Laurent, and Professor Luís Filipe Menezes. Your wise guidance and investigation freedom allowed me to improve the knowledge in the warm forming of aluminum alloys. I sincerely thank your friendship, dedication, and availability, as well as guidelines and teachings that I have always received.

I would like to thank the technical staff of IRDL namely Anthony Jégat, William Berckmans and Hervé Bellegou, for their help, teaching and technical advice that surely improve the quality of the experimental work here presented.

I also would like to thank Professor Valdemar Fernandes, the availability to discuss and scientific advice that help me in better understating the microstructural deformation mechanisms.

I am grateful to the colleagues and friends at IRDL, their help in my integration, the friendship out of office teaching me French culture. I greatly thank Jean-Baptiste Tutiaux, Julien Cochet, Nelson Souto for their help, support and scientific discussions.

I am also grateful for the support given by my colleagues and friends at CEMMPRE, André Diogo, João, Pedro Barros and Pedro Prates by their good mood, funny discussions at coffee break and lunchtime, and scientific discussions

I cannot forget the joyful moments and relaxation during my journey and I thank to my friends. From Coimbra, Inês and José, and Sofia. In Erasmus at KIT, Alex, Marta and Pedro. From Lorient, Leo le flatmates Bourgo's family. "Os Moscãoteiros", Bruno, Daniel and João.

My affectionate and special thanks to my Parents and Sister, Clémence, and Clémence's family, for their unconditional support, patience, encouragement, and presence during this journey.

I greatly acknowledge the financial support of this work, provided by: Foundation for Science and Technology (FCT), PhD Grant SFRH/BD/90669/2012; national funds from the French Ministry of Higher Education and Research; national funds from FCT via the project P2020-PTDC/EMS-TEC/6400/2014 (POCI-01-0145-FEDER-016876) and by UE/FEDER funds through the program COMPETE 2020, under the project CENTRO-01-0145-FEDER-000014 (MATIS).

Abstract

The transport industry faces sustainability challenges that demand vehicles' weight reduction, while safety requirements impose the increase of their structural strength. One of the approaches adopted to address this goal is the continuous development of lightweight materials, as the aluminum alloys. However, when compared with the traditionally mild steels used in sheet metal forming operations, they present lower formability and higher springback. In this context, warm forming was proposed as a solution to solve these problems. However, the warm forming of heat treatable aluminum alloys is still a challenge, since the recommended range of temperature for the forming process is similar to the one used for heat treatments. Thus, warm conditions can result in precipitation hardening, which changes the material thermo-mechanical behavior. These changes need to be predicted during the process virtual try-out to avoid defects in the production line. Moreover, heat treatable alloys are prone to natural aging, which can lead to variability and defects in the production line. Thus, the main goal of this work is to analyze the warm forming conditions of heat treatable aluminum alloys, taking into account the natural aging, in order to propose solutions that can contribute to the increase of robustness of sheet metal forming operations.

Two heat treatable Al-Mg-Si (6xxx series) alloys were selected for the study: the EN AW 6016-T4 and the EN AW 6061-T6. Their thermo-mechanical behavior was characterized using uniaxial tensile tests in a Gleeble 3500 machine between room temperature (RT) and 300 °C. Additional, uniaxial tensile tests were performed in an Instron 4505 machine coupled with a classical furnace, at 200 °C, enabling the analysis of different heat-holding times. The strain field was measured using optical system GOM-ARAMIS 4M. The cylindrical cup tests were performed in a Zwick/Roell Amsler BUP200 sheet metal testing equipment, adapted with specific tools for warm forming. All warm forming tests were performed considering non-isothermal conditions, with the die and the blank-holder heated up to the desired temperature, while the punch is refrigerated to keep its temperature close to RT. The cylindrical cup tests were performed between RT and 250 °C, for different punch (ram) speeds and heat-holding times. After the forming operation the cup thickness and the cup height were measured, as well as the springback, using the split-ring test. Finally, the influence of natural aging was evaluated for the period from 1 to 18 months, which required the duplication of some tests.

Globally, it is possible to correlate the thermo-mechanical results to those obtained in the forming tests, validating the macroscopic approach adopted for the result analysis. The EN AW 6061-T6 mechanical behavior shows a small natural aging effect, while it has a strong effect for the EN AW 6016-T4 alloy, leading to an increase of the yield stress and tensile strength and, consequently, of the springback. In this context, warm forming tests at 200 and 250 °C, prove to be an effective solution to reduce the variability caused by natural aging.

Both alloys present a negligible strain rate sensitivity at RT, while it is positive for warm temperatures. The warm forming tests performed at 200 °C show that high punch speeds are advantageous, since the formability and the springback remained stable or improved with the punch speed increased. In fact, low punch speed leads to a high exposure time, which promotes dynamic precipitation hardening for the EN AW 6016-T4 alloy, i.e. the punch force and the springback increase. The same effect is observed with the increase of the heat-holding time, at 200 °C. On the other hand, for the EN AW 6061-T6, the increase of the heat-holding time has a negligible impact on the formability and springback. Moreover, whatever the punch speed adopted, the variability caused by natural aging was negligible at warm forming, which validate the effectiveness of this solution. Thus, the heating system selected for the warm forming must guarantee a high heating rate, which is also advantageous from the production point of view.

Throughout this work, the split-ring test was used to evaluate springback. In this context, a numerical study was performed, in order to improve knowledge concerning the impact of the ironing stage in the circumferential residual stresses in the ring. Globally, the results show that the introduction of an ironing stage changes the characteristic distribution of the residual stress component throughout the vertical wall, even for relatively small ironing strains. This study was important to the results analysis since it explained the lower sensitivity of the ring located in the top of the cup (ironed zone) to the changes in material and process conditions. The analysis of the other rings clearly shows that warm forming contributes to springback reduction, when performed under non-isothermal conditions, with high punch speeds and heating rates.

Keywords : Warm forming, Aluminum Alloys of 6xxx series,
Natural Aging, Artificial Aging,
Springback, Numerical Simulation

Resumo

A indústria de transportes enfrenta desafios de sustentabilidade que exigem a redução de peso dos veículos, enquanto os requisitos de segurança impõem o aumento da resistência estrutural. Uma das abordagens adotadas para atingir estes objetivos é o desenvolvimento de materiais de elevada resistência específica, como as ligas de alumínio. No entanto, estas ligas apresentam menor conformabilidade e maior retorno elástico do que os aços tradicionalmente utilizados nas operações de estampagem. A conformação a temperaturas moderadas foi proposta como alternativa para ultrapassar estes problemas. No entanto, a sua utilização para ligas de alumínio tratáveis termicamente é ainda um desafio, uma vez que a gama de temperaturas recomendada para o processo de estampagem é semelhante à utilizada nos tratamentos térmicos. Assim, a conformação nesta gama de temperaturas pode conduzir a encruamento por precipitação, o que altera o comportamento termo-mecânico do material. Esta alteração deve ser prevista na conceção virtual para evitar a ocorrência de defeitos na linha de produção. Além disso, estas ligas são propensas a envelhecimento natural, responsável por introduzir variabilidade e defeitos na linha de produção. O principal objetivo deste trabalho é analisar as condições de conformação a temperaturas moderadas de ligas de alumínio tratáveis termicamente, incluindo o efeito de envelhecimento natural, a fim de propor soluções que possam contribuir para aumentar a robustez das operações de estampagem.

Neste trabalho procedeu-se à caracterização do comportamento termo-mecânico, de duas ligas de Al-Mg-Si (série 6xxx) tratáveis termicamente: a EN AW 6016-T4 e a EN AW 6061-T6. Tal envolveu a realização de ensaios de tração entre a temperatura ambiente (TA) e 300 °C num equipamento Gleebe. De modo a estudar diferentes tempos de aquecimento-manutenção a 200 °C utilizou-se uma máquina tração Instron equipada com um forno. O campo de deformação foi medido com o sistema ótico GOM-ARAMIS 4M. Foram também realizados ensaios de estampagem de taças cilíndricas, entre TA e 250 °C, em condições não-isotérmicas, com a matriz e o cerra-chapas aquecidos à temperatura desejada, e o punção refrigerado para manter uma temperatura próxima da TA. Nestes ensaios foram ainda estudadas diferentes velocidades de deslocamento do punção e tempos de aquecimento-manutenção. O equipamento utilizado foi Zwick/Roell Amsler BUP200, com ferramentas adaptadas para conformação a temperaturas moderadas. Após a operação de conformação, foi medida a espessura e a altura da taça, bem como o retorno elástico com base no ensaio de corte de anel. Finalmente, foi avaliada a influência do envelhecimento natural para o período de 1 a 18 meses, o que exigiu a duplicação de alguns ensaios.

Globalmente, a abordagem macroscópica adotada para a análise de resultados foi validada pela correlação entre os resultados dos ensaios de caracterização termo-mecânica e os de conformação. O comportamento mecânico da liga 6061-T6 é pouco sensível ao envelhecimento natural, enquanto a liga 6016-T4 apresenta um aumento da tensão limite de elasticidade e máxima não desprezável, que resultam no aumento do retorno elástico. Neste contexto, a conformação a quente para temperaturas entre 200 e 250 °C, revela-se uma solução eficaz para reduzir a variabilidade induzida pelo envelhecimento natural no processo de estampagem.

As ligas apresentam uma sensibilidade à velocidade de deformação negligenciável à TA, que passa a ser positiva com o aumento da temperatura. Os testes de conformação realizados a 200 °C mostram que a utilização de uma velocidade do punção elevada pode ser vantajosa, uma vez que a conformabilidade e o retorno elástico permanecem estáveis ou melhoram com o aumento da velocidade. De facto, velocidades do punção reduzidas conduzem a tempos de exposição elevados, o que promove o endurecimento por precipitação dinâmica da liga EN AW 6016-T4, i.e. a força de estampagem e o retorno elástico aumentam. O mesmo efeito é observado com o aumento do tempo de aquecimento-manutenção, a 200 °C. Pelo contrário, para a liga EN AW 6061-T6, o aumento deste tempo tem um impacto negligenciável na conformabilidade e no retorno elástico. Além disso, qualquer que seja a velocidade do punção, a variabilidade causada pelo envelhecimento natural da liga EN AW 6016-T4 é negligenciável para 200 °C, o que valida a eficácia desta solução. Assim, o sistema de aquecimento selecionado para a conformação a temperaturas moderadas deve garantir uma velocidade de aquecimento elevada, o que também é vantajoso do ponto de vista industrial.

Ao longo deste trabalho, o ensaio de corte de anel foi utilizado para avaliar o retorno elástico. Neste contexto, foi realizado um estudo numérico, para melhorar o conhecimento sobre o impacto da etapa de estiramento na distribuição das tensões residuais circunferenciais no anel. Os resultados mostram que a introdução da etapa de estiramento altera a distribuição característica das tensões residuais ao longo da parede vertical, mesmo para pequenas reduções de espessura. Este estudo foi importante para a análise dos resultados, uma vez que justifica a menor sensibilidade do anel localizado no topo do copo (zona estirada) às mudanças nas condições de comportamento do material e de processo. A análise dos outros anéis mostra claramente que a conformação a temperaturas moderadas, em condições não isotérmicas, contribui para a redução do retorno elástico, se realizada com velocidades do punção e de aquecimento elevadas.

Palavras-chave : Estampagem a quente, Ligas de Alumínio da serie 6xxx, Envelhecimento Natural, Envelhecimento Artificial, Retorno Elástico, Simulação Numérica

Résumé

L'industrie du transport fait actuellement face à des contraintes environnementales qui exigent des réductions de la masse des véhicules tandis que les contraintes de sécurité imposent l'augmentation de la résistance des structures. Pour répondre à ces deux objectifs, l'une des approches adoptées consiste à utiliser des matériaux métalliques légers, comme par exemple les alliages d'aluminium. Cependant, ces alliages présentent une plus faible formabilité et un retour élastique plus élevé que les aciers traditionnellement utilisés dans les opérations d'emboutissage. Dans ce contexte, l'emboutissage à température tiède apparaît comme une solution très intéressante pour résoudre ces problèmes. Néanmoins, l'emboutissage à tiède des alliages d'aluminium reste toujours un défi car la gamme de température utilisée est proche de celle utilisée lors des traitements thermiques de ces alliages. Ainsi l'augmentation de la température peut entraîner un durcissement par précipitation, modifiant le comportement thermomécanique du matériau. Ces changements doivent être prédits pour éviter des variations dans le process de production. En outre, les alliages d'aluminium à traitement thermique, sont susceptibles de vieillir naturellement, ce qui peut entraîner des défauts à la fin de l'emboutissage. Dans ce contexte, l'objectif principal de ce travail a été d'analyser les conditions d'emboutissage à tiède des alliages d'aluminium à traitement thermique en tenant compte du vieillissement naturel, afin de proposer des solutions permettant d'améliorer la robustesse des opérations d'emboutissage.

Deux nuances d'alliages d'aluminium à traitement thermique Al-Mg-Si, de la série 6xxx, ont été sélectionnées pour l'étude : l'EN AW 6016-T4 et l'EN AW 6061-T6. Leurs comportements thermo mécaniques ont été caractérisés en utilisant des essais de traction sur une machine Gleeble 3500 entre la température ambiante (TA) et 300 °C. Des essais supplémentaires pour analyser l'influence du temps de maintien en température à 200 °C ont été effectués sur une machine Instron 4505 avec l'utilisation d'une enceinte thermique. Le champ de déformation a été mesuré par le système de corrélation d'images GOM ARAMIS 4M. Des essais d'emboutissage de godets cylindriques ont été également effectués entre TA et 250 °C avec des conditions non isothermes sur une machine Zwick / Roell Amsler BUP200, la matrice et le serre-flanc étant chauffés jusqu'à la température voulue alors que le poinçon est refroidi pour conserver sa température proche de la TA. Au cours de ces essais, la vitesse d'emboutissage et le temps de maintien en température du flan ont aussi été étudiés. Après l'opération d'emboutissage, l'épaisseur et la hauteur du godet ont été mesurés, ainsi que le retour élastique selon l'essai d'ouverture d'anneau (essai dit de Demeri). Enfin, l'influence du vieillissement naturel a été évaluée pour une période allant de 1 à 18 mois, ce qui a nécessité la duplication de certains essais.

Globalement, il est possible de corréler les résultats thermo mécaniques avec ceux obtenus au cours des essais d'emboutissage, en validant l'approche macroscopique adoptée pour l'analyse des résultats de traction. Le comportement mécanique de l'EN AW 6061-T6 montre un faible vieillissement naturel, alors qu'il a un effet important pour l'alliage EN AW 6016-T4. Ce vieillissement entraîne une augmentation de la limite d'élasticité et de la résistance maximale à la traction et par conséquent, du retour élastique. Dans ce contexte, les essais d'emboutissage à 200 et 250 °C se révèlent être une solution efficace pour réduire la variabilité causée par le vieillissement naturel.

Les deux alliages présentent une sensibilité négligeable à la vitesse de déformation à la TA, alors qu'elle est positive à hautes températures. Les essais d'emboutissage à tiède effectués à 200 °C montrent que les vitesses d'emboutissage élevées sont avantageuses, la formabilité et le retour élastique restant stables ou améliorés avec l'augmentation de la vitesse d'emboutissage. En fait, une faible vitesse d'emboutissage entraîne un temps d'exposition élevé qui favorise le durcissement dynamique par précipitation dans le cas de l'alliage EN AW 6016-T4 provoquant une augmentation de la force d'emboutissage et du retour élastique. Les essais de traction avec les étapes de relaxation ont été extrêmement utiles pour comprendre les phénomènes de précipitation dynamique à 200°C. En outre, quelle que soit la vitesse d'emboutissage adoptée, la variabilité causée par le vieillissement naturel est restée négligeable lors de l'emboutissage à tiède, ce qui a permis de valider l'efficacité de cette solution. Globalement, il est apparu que le système de chauffage utilisé pour l'emboutissage à tiède doit garantir une vitesse de chauffe rapide, ce qui est également avantageux pour le temps de production.

Tout au long de ce travail, l'essai d'ouverture d'anneau a été utilisé pour évaluer le retour élastique. Dans ce contexte, une étude numérique a été réalisée afin de mieux comprendre l'impact de l'étape d'étirage dans les contraintes résiduelles circonférentielles dans l'anneau. Globalement, les résultats montrent que l'introduction d'une étape d'étirage modifie la répartition classique des contraintes résiduelles dans toute la paroi verticale, même pour les petites déformations d'étirage. Cette étude a été importante pour l'analyse des résultats puisqu'elle a expliqué la faible sensibilité de l'ouverture de l'anneau situé au sommet du godet (zone étirée). L'analyse des autres anneaux montre clairement que l'emboutissage à tiède contribue à la réduction du retour élastique lorsqu'il est réalisé dans des conditions non isothermes, avec des vitesses d'emboutissage élevées et avec une vitesse de chauffe rapide.

Mots clés : Emboutissage à Tiède, Alliages d'Aluminium de la série 6xxx, Vieillissement Naturel, Vieillissement Artificiel, Retour Élastique, Simulation Numérique

Contents

List of Figures

List of Tables

(Page intentionally left blank)

Chapter 1.

Introduction

This chapter presents the motivation for investigating the topics addressed in the thesis. The main challenges and objectives in the context of warm forming of heat treatable alloys are highlighted and the outline of the thesis is detailed.

(Page intentionally left blank)

1.1. Framework

In the last decades, accelerated by the globalization, the movement of people and goods has significantly increased requiring higher mobility. Thus, higher capacity and travel speed of the transport modes is required, i.e. more and faster vehicles. Additionally, the increasing requirements related to the social impacts of accidents and life quality imposes to the transport industry an increase on vehicles' security and comfort. On the other hand, the demand for sustainable development imposes to the transport industry the challenge of reducing human footprint. This lead to the concept of Green Vehicle, which are the ones presenting very low carbon energy resources, have very low air pollutant and noise emissions and can be easily recycled. From the structural point of view, in order to be ecological, vehicles must be lighter and use recyclable materials. However, in order to be safer and more comfortable, vehicles require supplementary equipment, which leads to weight increases. This is one of the challenges of transport industry: increase the safety and comfort while reducing weight. Facing that, new lightweight materials with high specific strength (the tensile strength divided by alloys density), together with processing technologies, are in continuous development. The advantages resulting from weight reduction are summarized in Table 1.1, on its left side, while the most cited lightweight materials are presented on its right side. Please note that all materials can contribute to the advantages pointed out for mass reduction.

Table 1.1 – The advantages of weight reduction (at left side), and the new materials used to reduce weight of vehicles (at right side).

Advantages in Mass Reduction	Materials to improve mass reductions
+ Acceleration	• Ultra-high strength Steel (UHSS)
+ Braking	• Advanced high strength Steel (AHSS)
+ Handling	• Aluminum Alloys
+ Driving comfort	• Magnesium Alloys
+ Road preservation	• Titanium Alloys
– Fuel ; Emissions (CO_2)	• Carbon fiber reinforced polymer (CFRP)

The specific tensile strength of some of these materials is shown in Figure 1.1. Carbon fiber reinforced polymer (CFRP) is a composite material with specific strength approximately ten times higher than metallic alloys. On the other hand, CFRP is more expensive than metallic alloys and its recycling is very limited, while metallic alloys have very good recycling rates. Additionally, the materials used in road vehicles must respect the end-of-life-vehicle directive of the European Union (DIRECTIVE 2000/53/EC), which states that the reuse and recovery shall be increased to a

minimum of 95 % of the average weight, per vehicle. Moreover, the use of recycled metallic alloys contributes to reduce the cost of raw materials. The environmental impact of metallic alloys is analyzed by (Ingarao et al., 2011), which presents an overview of their sustainability issues, when used in sheet metal forming processes. Within metallic alloys, steel is the one that requires fewer resources in its production as raw material, followed by aluminum and magnesium alloys. Titanium alloys are too expensive for most large series industrial applications. However, these alloys have extraordinary corrosion resistance and the ability to withstand extreme temperatures. Magnesium alloys are often less required than aluminum alloys due to its reduced formability and higher environmental cost. Another relevant issue connected with sheet metal forming processes is the fact that, for metallic alloys, as the specific strength increases the formability at room temperature decreases, as shown in Figure 1.1.

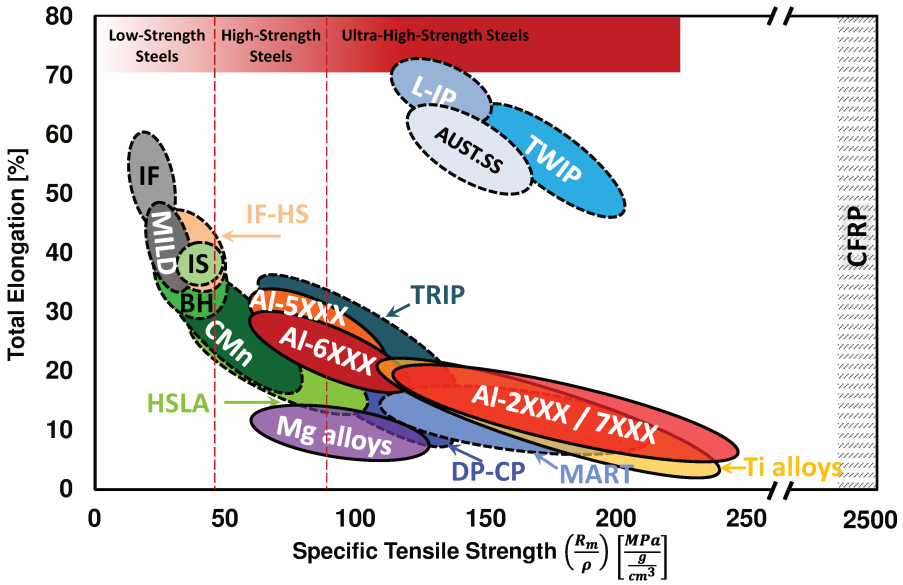

Figure 1.1 –Comparison of the total elongation versus the specific tensile strength for materials with potential for use on road vehicles (adapted from (eaa, 2011)).

The choice of the right material for a given usage is a difficult task since various materials can fulfill the set of requirements needed, even when taking into account the constraints imposed by the manufacturing process and the cost per part. Aiming to reduce the human footprint, the choice of material selection should be based on Life Cycle Assessment (LCA). The LCA estimates the environmental aspects and the potential impacts throughout products' lifetime, from raw material extraction through materials processing, manufacture, distribution, use, repair and maintenance, and end of life recycling.

In order to illustrate the impact of LCA in materials selection, Figure 1.2 present two examples of the materials used in the aeronautical and the automotive transport sector (Airbus, 2013)(Audi AG, 2011b). Nowadays, in the aeronautical sector, CFRP is the most used material in the fuselage, replacing mostly the aluminum alloys (Dursun and Soutis, 2014). In fact, for the long aeronautical life cycles, CFRP presents the best LCA results (Khalil, 2017). Although the increased use of CFRP reduced the role of aluminum alloys up to some extent, high strength aluminum alloys remain important in airframe construction (Dursun and Soutis, 2014). Titanium alloys are used to support jet engines in wings due to their resistance to extreme conditions. In brief, the A350 XWB's fuselage is constructed with components made of CFRP plus aluminum-lithium and titanium alloys (see Figure 1.2 a)), resulting in lower fuel consumption and easier maintenance. These materials reduce the need for overall fatigue and corrosion maintenance tasks, while enhancing the jetliner's overall operating efficiency (Airbus, 2013).

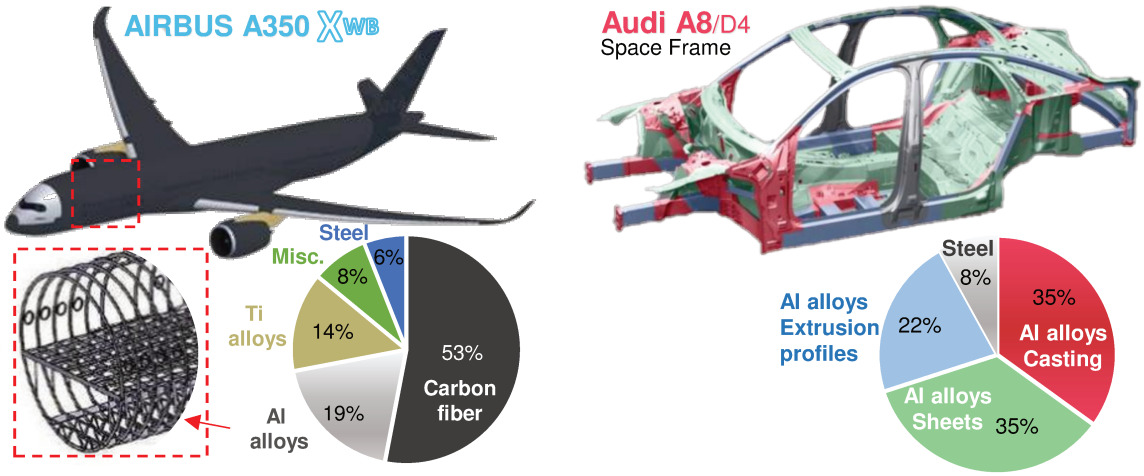

a) b)

Figure 1.2 – The percentage by mass of materials used in: a) Airbus, the A350 XWB's (Airbus, 2013); b) Audi A8 (D4) space frame (Audi AG, 2011b).

In the automotive industry, the demand for aluminum alloys and high strength steels has increased, replacing traditionally predominant steels (Neugebauer et al., 2006). According to (Audi AG, 2011a), an Aluminum Space Frame body can weight over 40 percent less than a comparable steel construction. The example shown in Figure 1.2 b) refers to an Audi A8, which presents a space frame with a total weight of 231 kilograms. In this advanced Body-in-white, hot-shaped steels serve as B-pillars and several aluminum alloys, using multiple manufacturing processes, are combined to produce a lightweight body (making the passenger cell stronger and safer). In summary, aiming the weight reduction, the new vehicles are made combining distinct

types of materials through the different manufacturing process. As stated by (Carle and Blount, 1999), it is most probable that the car body of the future will be a composite of steel, aluminum and several kinds of plastics. This trend is also predicted by other authors, as shown in Figure 1.3. Only the right material, with the right manufacturing technology, in the right place, can ensure maximum benefits (Carle and Blount, 1999).

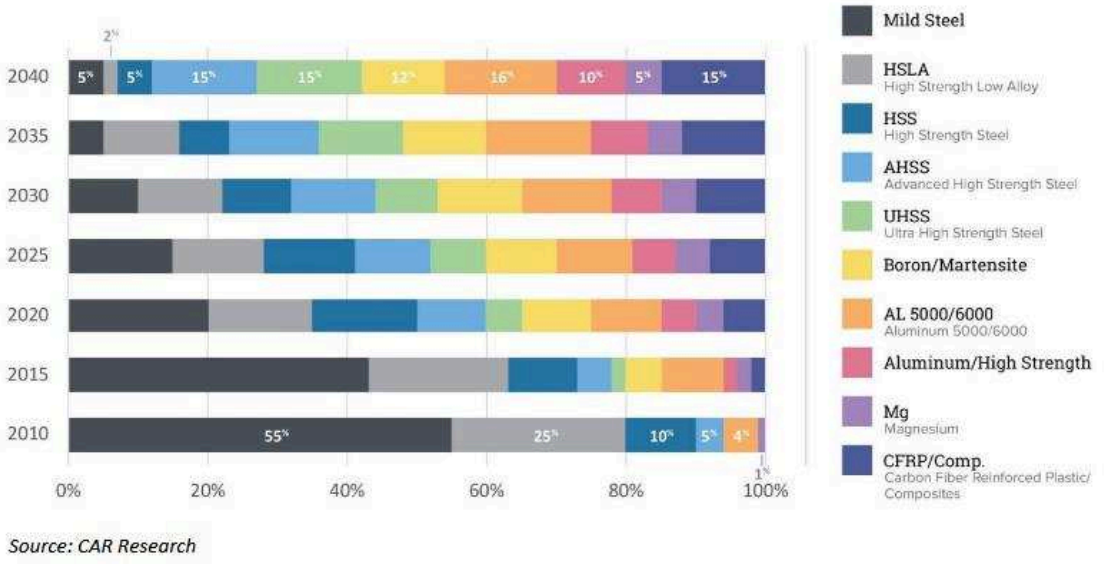

Figure 1.3 –Material distribution in the U.S. fleet (Body-in-white plus closures) (Smith et al., 2016).

1.2. The automotive industry: aluminum alloys or steel?

In the automotive industry, UHSS/AHSS and aluminum alloys are the most used materials in the body-in-white construction. Although carbon fiber composites, magnesium and titanium alloys are also used (mostly in performing sport automotive vehicles) they are not currently in daily life vehicles. (Mayyas et al., 2012) compares the different material options for the body-in-white, based on LCA, concluding that the aluminum and the magnesium intensive structures were found to result in less energy consumption over the life of the vehicle, which is assumed around 200000 miles. However, when the lifetime decreased to around 50000 miles, mild steel and the AHSS ranked the highest in terms of savings in energy and CO^2 emission. On the other hand, CFRP shows the most detrimental LCA value, whatever the lifetime considered. In this context, the analysis made to the Audi A8 (D4) model reports that, although the production of primary aluminum requires more energy than the production of steel, the weight advantage of the aluminum body quickly equalizes the balance during operation of the vehicle, after roughly 50000 kilometers (Audi AG,

2011c). At the end of the vehicles life, the aluminum scrap has a higher value than steel. However, its recycling cost is also higher. Comparing the body-in-white of the Audi A8 (D4) with its newer version (D5, from 2017), the amount of mild steel and UHSS/AHSS increased from 8% to 40%, while the amount of aluminum alloys reduced from 92% to 58%, which resulted in a weight increase of 51 kg. Constructors prefer to use aluminum alloys in sport and luxury/executive vehicles, while steels are a primary option for cheaper vehicles (McCallion, 2012). Often the choice is linked with the average lifetime planned for the vehicle, as highlighted by the LCA, and the performance requests.[1]

The demand for UHSS/AHSS and aluminum alloys in the automotive industry has been increasing and, as shown in Figure 1.4, it is expected to continue to grow. However, as shown in Figure 1.1, the formability of these alloys is limited. The main process used in the body-in-white manufacturing is sheet metal forming (see Figure 1.2 b)), which makes low formability a big issue. Additionally, the reduced young modulus of aluminum and magnesium alloys leads to the increase of the springback after stamping operations. The high strength of UHSS/AHSS requires higher forming forces and also leads to higher springback. In order to overcome these issues, the material softening, induced by the increase of temperature, has been explored (Neugebauer et al., 2006). Examples of this type of approach are the warm forming of aluminum (Toros et al., 2008) and magnesium alloys (Koh et al., 2015), and the hot forming of UHSS/AHSS alloys (Karbasian and Tekkaya, 2010). The distinction between warm and hot forming is based on the recrystallization temperature. Warm forming is carried out below recrystallization temperature without allowing grain growth. As a result of the temperature increase, strain hardening recovery mechanisms are enhanced. On the other hand, forming operations performed above the recrystallization temperature are referred as hot forming. Hot forming has higher energetic costs and requires more expensive tools, as compared to warm forming. Additionally, at temperatures above 450°C, a deterioration of the tribological conditions occurs for hot forming of UHSS/AHSS (Neugebauer et al., 2006). The hot forming of UHSS/AHSS involves heat treatment and fast quenching, leading the steel microstructure to change from ferrite and perlite to 100% martensitic (ArcelorMittal, 2017). It leads to changes in the crystalline structure during the process and non-negligible thermal expansions, which increases the complexity of hot forming of UHSS/AHSS, as compared to warm forming of aluminum alloys. Despite all, UHSS/AHSS are good competitors against aluminum alloys, although hot formed

[1] Additional information concerning the aluminum alloys and steel in transports (automotive) industry can be found in: www.drivealuminum.org european-aluminium.eu; www.worldsteel.org; www.cargroup.org.

components are mainly available for non-visible parts, due to poor surface quality (ArcelorMittal, 2017).

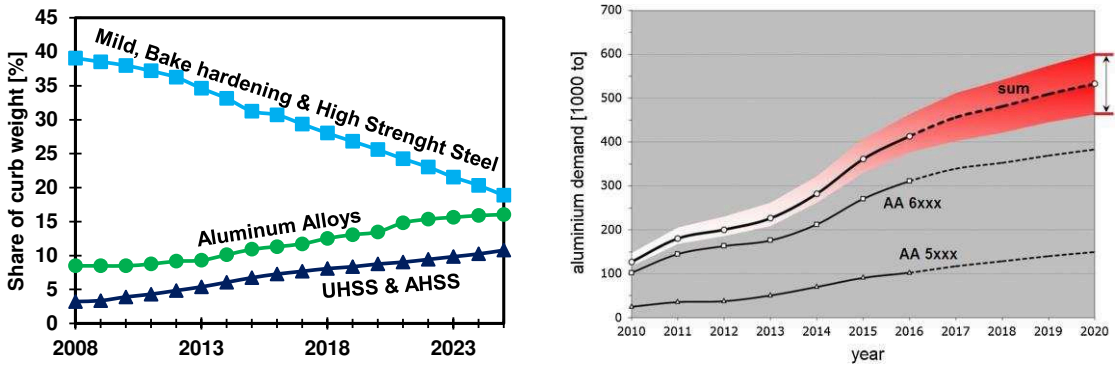

Figure 1.4 – The increase in demand of lightweight alloys: a) materials share as percent of vehicle curb weight (source: Ducker Worldwide (Djukanovik, 2016)); b) Forecast of European demand for rolled aluminum sheet products of the AA 5xxx and AA 6xxx series (Engler et al., 2016).

1.2.1. Aluminum alloys in the automotive industry

In the automotive industry, casting of aluminum alloys is used to produce parts with complex geometries and to increase local stiffness in high load bearing areas (see Figure 1.2 b)). Aluminum extruded parts are used in particular for the bolt-on front crash management system and the roof bow. Aluminum rolled sheets are used in stamping operations to produce the most of structural and outer skin parts. According to (Hirsch, 2014), in the first Audi models, the aluminum alloys were primarily used as extrusion or casting profiles, but the trend has evolved to sheet metal forming. Figure 1.5 presents some examples of the usage of these alloys in automotive vehicles, highlighting the presence of aluminum sheet metal formed components. The main aluminum wrought alloys used in automotive and rail vehicles are from the 5xxx series (Al-Mg alloys) and the 6xxx series (Al-Mg-Si alloys). The 5xxx series is mostly used in structural parts and inner panels; while the 6xxx series is standard for extrusion, structural parts and outer panels. Within aluminum alloys, both series are characterized by presenting medium strength and good formability, corrosion resistance and welding ability. The 5xxx series are non-heat treatable alloys that tend to form stretcher strain markings during forming (Portevin-Le Chatelier effect), which appear as uneven surface (bad surface quality), limiting its use in outer panels. The 6xxx series are heat treatable alloys and their strength can triplicate by heat treatment. This strength improvement depends of the heat treatment conditions and chemical composition. The heat treatment to improve strength is called artificial aging and is often performed after the forming operations. Another advantage of heat treatable alloys is the local laser heat treatment that enables the tailoring of the

materials properties, in the manufacturing of lightweight and crash-proof components for the Body in white (Merklein et al., 2012).

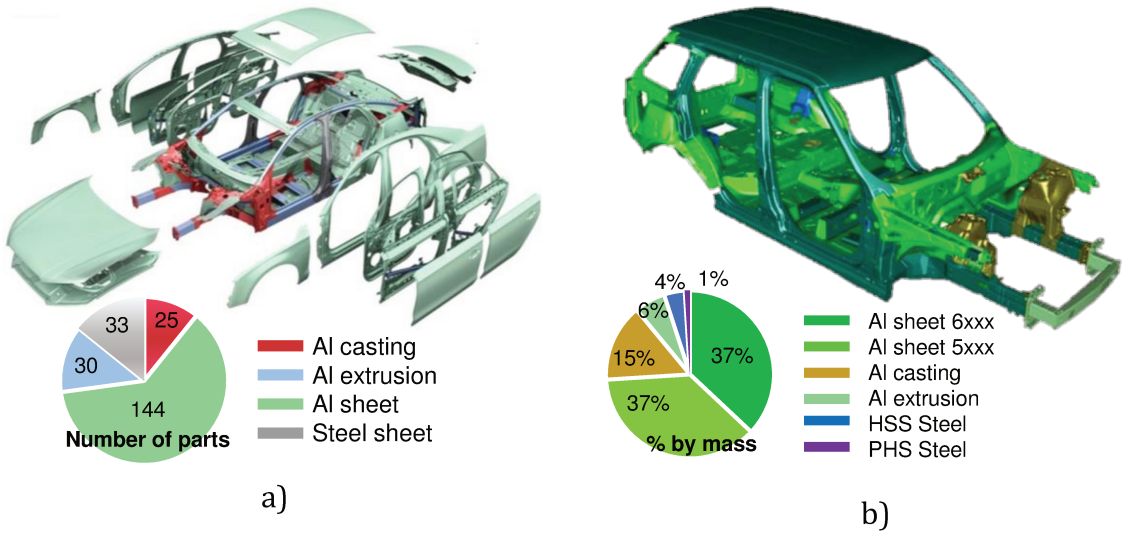

Figure 1.5 – Examples of body design with aluminum alloys in automotive vehicles: a) aluminum space frame of the Audi A8 (D4); b) the all-aluminum monocoque body structure in Range Rover (L405). Source: (eaa, 2013)

1.2.2. The advantages of warm forming in Aluminum alloys

Warm forming in aluminum alloys requires lower forming forces than conventional room temperature (RT) processing, while increases formability and reduces the springback, as shown in Figure 1.6. It results from the thermally activated strain recovery mechanisms. Additionally, in the 5xxx series warm forming suppresses the stretcher strain markings during forming, improving the range of usage for this series (Bernard et al., 2017).

Warm forming can be performed under isothermal or non-isothermal conditions. Nevertheless, previous studies have shown than non-isothermal conditions, with the temperature of the punch lower than the one of the die and the blank-holder, contribute for an increase of the formability (Palumbo and Tricarico, 2007). However, warm forming brings additional costs in energy to heat the tools and in tools manufacturing due to its higher complexity, particularly for non-isothermal conditions. Nevertheless, such costs are redressed with the possibility of reducing the number of forming stages required, with a consequently lower processing time and additional savings on the number of forming tools required.

a) b)

Figure 1.6 – Advantages of warm forming: a) formability increase (Bolt et al., 2001); b) springback decrease (Grèze et al., 2010)

1.2.3. The challenge of warm forming of Al-Mg-Si Alloys

The possibility of performing heat treatment after forming, combined with good formability and post forming strength, leads to higher demand for the 6xxx series than for the 5xxx series, see Figure 1.4 b). However, its thermo-mechanical behavior, namely in warm forming conditions, was not fully understood, particularly at the beginning of this thesis. In fact, the recommended temperature range for warm forming of the 6xxx series coincides with the recommended temperature range for its heat treatment. As outlined in Figure 1.7, the main challenge is understanding the influence of warm forming in post forming mechanical behavior. As shown in Figure 1.7, a lower warm forming processing time allows forming the alloy without changing the initial heat treatment conditions, while a higher processing time can lead to changes. Moreover, an excessive warm forming processing time can result in over aging, causing the loss of in-service behavior strength. Therefore, the control of the warm forming processing time seems to be crucial, but improved knowledge is required concerning the admissible ranges. Additionally, the combined effect of deformation and artificial aging on the mechanical properties of Al-Mg-Si alloys allows an increase of strength (Cai et al., 2004; Kolar et al., 2012). Thus, warm forming of heat treatable alloys can be exploited to match strain hardening with artificial age hardening, in order to improve the strength of the final components. In fact, despite warm forming advantages, the influence of warm forming in the formability, residual stresses and springback, and in-service behavior of the final components is still a challenge, particularly for heat treatable alloys. Finally, the improvements achieved in warm forming of 6xxx series alloys can be useful to understand the thermo-mechanical of other heat treatable aluminum or magnesium alloys.

Another factor that contributes to supplementary difficulties in the forming operations of the 6xxx series alloys is the natural aging. Natural aging occurs due to the precipitation of the alloying elements (solute atoms) in the aluminum matrix (Al-matrix). It leads to the strength increase as the storage time at RT increases, and

consequently, the variability of mechanical behavior that affects the forming operation, the springback and also the in-service behavior. In fact, as compared to non-natural aged alloys, natural aging reduces the medium strength obtained after T6 heat treatment (artificial aging), known as the negative effect of natural aging in artificial aging. Despite some methods proposed in the literature can reduce the natural aging phenomenon (see e.g. (Ding et al., 2016; Engler et al., 2015; Yan, 2014)), but not definitely suppress it. In fact, these methods can only stabilize the natural aging during reduced time spans (up to few days), which is not enough for industrial practice. Thus, the control of natural aging is always an open issue for heat treatable aluminum alloys.

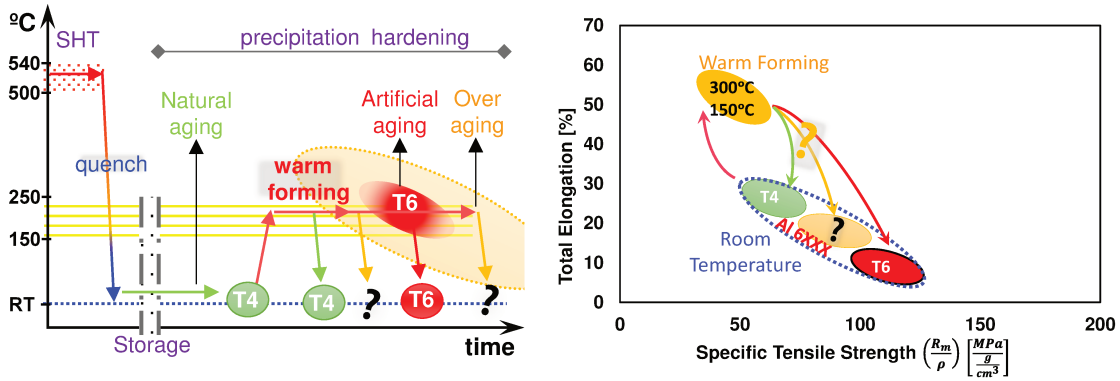

Figure 1.7 – a) Warm forming of heat treatable alloys b) the final mechanical properties after warm forming

In summary, the main challenges connected with the improved understanding of the warm forming conditions for 6xxx series alloys concern:

- The control of natural aging, and its influence in warm forming;
- The influence of non-isothermal conditions (including tools thermal dilatation);
- The influence of the forming speed in the process;
- The control of the heating and the exposure time.

1.3. Objectives

The main challenge in warm forming of 6xxx series lies in the coincidence between warm forming and artificial aging temperature, and in the variability of the mechanical behavior due to natural aging. Both can lead to variability and defects in the production line, which need to be predicted. However, at present, the influence of warm forming in natural aging and springback still has to be analyzed. Thus, the main goal of this work is to analyze the warm forming conditions of heat treatable aluminum alloys, taking into account the natural aging, in order to propose solutions that can contribute to improve the robustness of sheet metal forming operations. This requires study the process variables, like the forming temperature and speed, heat-holding time and storage time at RT, in order to understand their influence on the forming force, on the parts thickness distributions and springback, as well as on the evolution of the temperature gradient in the sheet and tools. In this context, the two alloys selected for this study are the EN AW 6016-T4 and the EN AW 6061-T6, which are commonly used for skin applications and for structural components in the automotive industry, respectively.

1.4. Thesis outline

In order to facilitate the reading and understanding of this thesis, the current section presents the structure as well as a brief summary of the topics covered in each chapter. The content is organized in seven chapters; this first chapter defines the framework and motivation. Chapter 2 presents an overview of the plastic deformation mechanisms, particularly of heat treatable aluminum alloys, and a resume of the tests performed. Chapter 3 corresponds to the manuscript, of a submitted article, that analyzes the impact of natural aging and warm forming conditions in the forming and springback. Chapter 4 presents the work on the influence of the punch speed in warm forming and springback of the two heat treatable alloys. Chapter 5 corresponds to the manuscript that analyzes the influence of the exposure time in warm forming and springback, of the same alloys. The article corresponding to the numerical analysis of the influence of the clearance between the die and the punch on springback, using the split-ring test, is presented in Chapter 6. Finally, Chapter 7 summarizes the main issues addressed in this work, emphasizing the main conclusions, and giving some recommendations and suggestions for future work.

References

Airbus, 2013. Fast special edition: A350 XWB. Bruno Piquet 25.

ArcelorMittal, 2017. Steels for hot stamping - Usibor® and Ductibor® [WWW Document]. URL http://automotive.arcelormittal.com/europe/products/UHSS/Usibor/EN (accessed 8.10.17).

Audi AG, 2011a. Audi Technology Portal - Audi Space Frame [WWW Document]. Audi Technol. Portal. URL https://www.audi-technology-portal.de/en/body/aluminium-bodies/audi-spaceframe-en (accessed 8.5.17).

Audi AG, 2011b. Audi Technology Portal - Semi-finished components [WWW Document]. Audi Technol. Portal. URL https://www.audi-technology-portal.de/en/body/aluminium-bodies/semi-finished-components (accessed 8.5.17).

Audi AG, 2011c. Audi Technology Portal - Aluminium as a material [WWW Document]. Audi Technol. Portal. URL https://www.audi-technology-portal.de/en/body/aluminium-bodies/aluminium-as-a-material (accessed 8.7.17).

Bernard, C., Coër, J., Laurent, H., Manach, P.Y., Oliveira, M., Menezes, L.F., 2017. Influence of Portevin-Le Chatelier Effect on Shear Strain Path Reversal in an Al-Mg Alloy at Room and High Temperatures. Exp. Mech. 57, 405–415. doi:10.1007/s11340-016-0229-z

Bolt, P.J., Lamboo, N., Rozier, P., 2001. Feasibility of warm drawing of aluminium products. J. Mater. Process. Technol. 115, 118–121.

Cai, M., Field, D.P., Lorimer, G.W., 2004. A systematic comparison of static and dynamic ageing of two Al–Mg–Si alloys. Mater. Sci. Eng. A 373, 65–71. doi:10.1016/j.msea.2003.12.035

Carle, D., Blount, G., 1999. The suitability of aluminium as an alternative material for car bodies. Mater. Des. 20, 267–272. doi:10.1016/S0261-3069(99)00003-5

Coër, J., 2013. Mise en forme par emboutissage en température d'un alliage d'aluminium AA5754-O (PhD-thesis). Université de Bretagne Sud.

Ding, L., Weng, Y., Wu, S., Sanders, R.E., Jia, Z., Liu, Q., 2016. Influence of interrupted quenching and pre-aging on the bake hardening of Al–Mg–Si Alloy. Mater. Sci. Eng. A 651, 991–998. doi:10.1016/j.msea.2015.11.050

Djukanovik, G., 2016. Steel cannot compete with aluminium in vehicle lightweighting [WWW Document]. Alum. Insid. URL http://aluminiuminsider.com/steel-cannot-compete-with-aluminium-in-vehicle-lightweighting/ (accessed 8.6.17).

Dursun, T., Soutis, C., 2014. Recent developments in advanced aircraft aluminium alloys. Mater. Des. 56, 862–871. doi:10.1016/j.matdes.2013.12.002

eaa, 2013. European Aluminium Association, Aluminium Automotive Manual – Applications – Car body – Body structure.

eaa, 2011. European Aluminium Association, Aluminium Automotive Manual – Design – Design with Aluminium.

Engler, O., Hirsch, J., 2002. Texture control by thermomechanical processing of AA6xxx Al–Mg–Si sheet alloys for automotive applications—a review. Mater. Sci. Eng. A 336, 249–262. doi:10.1016/S0921-5093(01)01968-2

Engler, O., Schäfer, C., Brinkman, H.-J., Brecht, J., Beiter, P., Nijhof, K., 2016. Flexible rolling of aluminium alloy sheet—Process optimization and control of materials properties. J. Mater. Process. Technol. 229, 139–148. doi:10.1016/j.jmatprotec.2015.09.010

Engler, O., Schäfer, C., Myhr, O.R., 2015. Effect of natural ageing and pre-straining on strength and anisotropy in aluminium alloy AA 6016. Mater. Sci. Eng. A 639, 65–74. doi:10.1016/j.msea.2015.04.097

Grèze, R., Manach, P.Y., Laurent, H., Thuillier, S., Menezes, L.F., 2010. Influence of the temperature on residual stresses and springback effect in an Aluminium alloy. Int. J. Mech. Sci. 52, 1094–1100. doi:10.1016/j.ijmecsci.2010.04.008

Hirsch, J., 2014. Recent development in aluminium for automotive applications. Trans. Nonferrous Met. Soc. China 24, 1995–2002. doi:10.1016/S1003-6326(14)63305-7

Ingarao, G., Di Lorenzo, R., Micari, F., 2011. Sustainability issues in sheet metal forming processes: an overview. J. Clean. Prod. 19, 337–347. doi:10.1016/j.jclepro.2010.10.005

Karbasian, H., Tekkaya, A.E., 2010. A review on hot stamping. J. Mater. Process. Technol. 210, 2103–2118. doi:10.1016/j.jmatprotec.2010.07.019

Khalil, Y.F., 2017. Eco-efficient lightweight carbon-fiber reinforced polymer for environmentally greener commercial aviation industry. Sustain. Prod. Consum. 12, 16–26. doi:10.1016/j.spc.2017.05.004

Koh, Y., Kim, D., Seok, D.-Y., Bak, J., Kim, S.-W., Lee, Y.-S., Chung, K., 2015. Characterization of mechanical property of magnesium AZ31 alloy sheets for warm temperature forming. Int. J. Mech. Sci. 93, 204–217. doi:10.1016/j.ijmecsci.2015.02.001

Kolar, M., Pedersen, K.O., Gulbrandsen-Dahl, S., Marthinsen, K., 2012. Combined effect of deformation and artificial aging on mechanical properties of Al–Mg–Si Alloy. Trans. Nonferrous Met. Soc. China 22, 1824–1830. doi:10.1016/S1003-6326(11)61393-9

Laurent, H., Coër, J., Manach, P.Y., Oliveira, M.C., Menezes, L.F., 2015. Experimental and numerical studies on the warm deep drawing of an Al–Mg alloy. Int. J. Mech. Sci. 93, 59–72. doi:10.1016/j.ijmecsci.2015.01.009

Manach, P.-Y., Coër, J., Jégat, A., Laurent, H., Yoon, J.W., 2016. Benchmark 3 - Springback of an Al-Mg alloy in warm forming conditions. J. Phys. Conf. Ser. 734, 22003. doi:10.1088/1742-6596/734/2/022003

Mayyas, A.T., Qattawi, A., Mayyas, A.R., Omar, M.A., 2012. Life cycle assessment-based selection for a sustainable lightweight body-in-white design. Energy, Sustainable Energy and Environmental Protection 2010 39, 412–425. doi:10.1016/j.energy.2011.12.033

McCallion, R., 2012. Manufacturing with UHSS. Automot. Manuf. Solut.

Merklein, M., Böhm, W., Lechner, M., 2012. Tailoring Material Properties of Aluminum by Local Laser Heat Treatment. Phys. Procedia, Laser Assisted Net shape Engineering 7 (LANE 2012) 39, 232–239. doi:10.1016/j.phpro.2012.10.034

Neugebauer, R., Altan, T., Geiger, M., Kleiner, M., Sterzing, A., 2006. Sheet metal forming at elevated temperatures. CIRP Ann. - Manuf. Technol. 55, 793–816. doi:10.1016/j.cirp.2006.10.008

Palumbo, G., Tricarico, L., 2007. Numerical and experimental investigations on the Warm Deep Drawing process of circular aluminum alloy specimens. J. Mater. Process. Technol. 184, 115–123. doi:10.1016/j.jmatprotec.2006.11.024

Smith, B., Spulber, A., Modi, S., Fiorelli, T., 2016. Technology Roadmaps: Intelligent Mobility Technology, Materials and Manufacturing Processes, and Light Duty Vehicle Propulsion.

Toros, S., Ozturk, F., Kacar, I., 2008. Review of warm forming of aluminum–magnesium alloys. J. Mater. Process. Technol. 207, 1–12. doi:10.1016/j.jmatprotec.2008.03.057

Yan, Y., 2014. Investigation of the negative and positive effect of natural aging on artificial aging response in Al-Mg-Si alloys (PhD-thesis). Technische Universität Berlin, Berlin.

Chapter 2.

Materials and test conditions

This chapter presents the materials studied and the test conditions selected for their thermo-mechanical characterization. The first subchapter provides an overview of the mechanisms of plastic deformation, with focus on heat-treatable aluminum alloys. The second presents a brief description of the production process of aluminum alloys sheets, including the heat treatments. Further details concerning the aluminum alloys selected for the present work are briefly described in the third subchapter. The fourth presents a resume of the experimental tests and procedures adopted in this work. Finally, the fifth subchapter resumes the influence of some process parameters in the warm forming of heat-treatable aluminum alloys.

(Page intentionally left blank)

2.1. Overview on the physical mechanisms of deformation

The deformation refers to changes in shape and volume of the material, while the mass remains unchanged. The deformation behavior of metallic materials depends of their atomic crystal structure. When considering a single crystal, the application of an external load leads to the **slip** between atomic planes that cause the deformation of the crystal structure, which can be reversible (elastic) or permanent (plastic). A slip plane and a slip direction define a slip system. The single crystal plastically deforms when the shear stress between the two adjacent slip planes exceeds a critical value, referred as the critical resolved shear stress (CRSS). In addition to slip, plastic deformation in some metallic materials can also occur by mechanical **twinning**. This involves the simultaneous rearrangement of the several atomic planes of the crystal structure (distorted part), in such a way that the distorted part becomes a mirror image of the non-distorted one. As for slip, it is possible to define twin planes and directions in the crystal structure (Callister, 2000; Campbell, 2008).

The crystal structure defines the number of slip and twinning systems, the atomic packing factor, and the coordination number. Table 2.1 presents the characteristic values for the Hexagonal-Close Pack (HCP), the Face-Centered Cubic (FCC) and the Body-centered cubic (BCC) structures. Slip preferably occurs in planes containing the greatest number of atoms per area (close-packed planes) in directions of most atoms per length (close-packed directions), since they present a lower CRSS (Campbell, 2008). Each slip system has a different resolved shear stress, because they present a different orientation relative to the orientation of the external stress. The slip commences on the most favorably oriented slip system, which corresponds to the one that presents the better alignment relative with the applied external stress (higher Schmid factor) (Schmid and Boas, 1935). When a structure presents a high number of slip systems, the probability of their favorable alignment relatively to the external stress increases.

Table 2.1 – Physical properties of crystal structures (Campbell, 2008).

	HC	FCC	BCC
Slip Planes	1	4	6
Slip Direction	3	3	2
Slip Systems	3	12	12
Coordination Number	12	12	8
Atomic Packing Factor	0.74	0.74	0.68
Alloys	Magnesium	Aluminum	Iron (steel)

From the knowledge concerning the metallic bond, it is possible to derive a theoretical value for the stress required to produce slip between atomic planes in a metallic perfect crystal. However, the strength actually obtained experimentally on single crystals is only about one-thousandth of this theoretical value. Thus, this mechanism of atomic slip cannot describe the strength associated with plastic deformation. This can only be explained by the presence of defects in the lattice, which are particularly important for polycrystalline materials. Several types of defects have been identified in the literature that can be separated, according to the alterations induced in the crystal structure, in: point, line, planar and bulk. Some of these defects are presented in Figure 2.1 (Campbell, 2008).

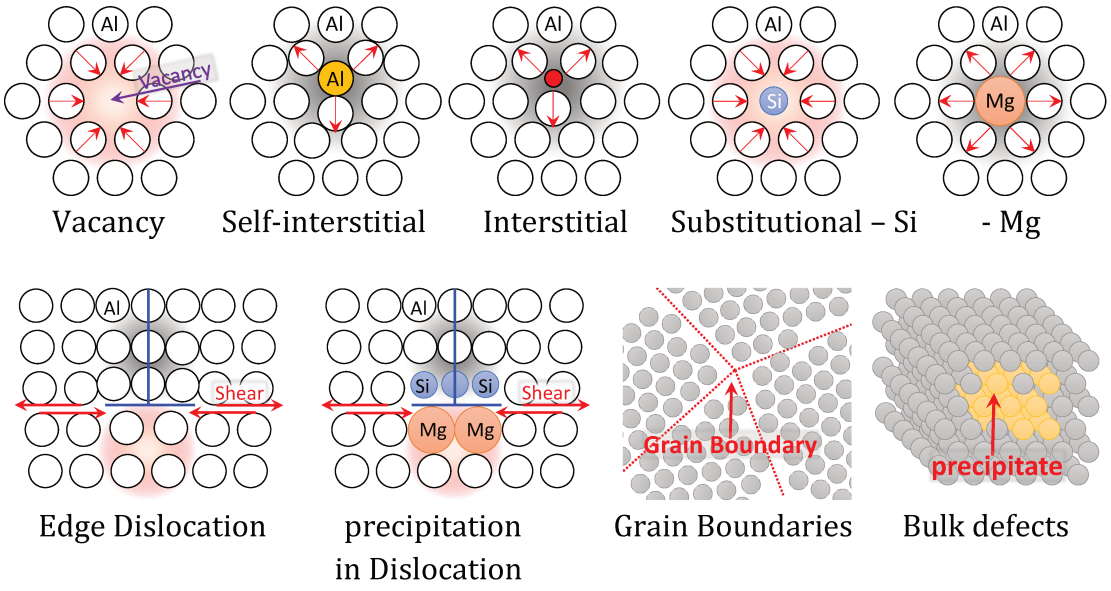

Figure 2.1 – Crystallographic defects. Tensile stresses in the lattice are presented in pink, while compressive stresses are in grey (adapted from (Callister, 2000; Mondolfo, 1976) for the Al-Mg-Si alloys).

The point defects are the simplest ones and correspond to an irregularity in the lattice, associated with a missing atom (vacancy), an extra atom (interstitial), or an impurity (substitutional) atom. Line defects correspond to dislocations, which can be of one of three types: edge, screw and mixed (which exhibit components of both previous types and are the most common). Planar defects include grain boundary, twin boundary and stacking faults. Bulk defects correspond to precipitates, inclusions and voids (Callister, 2000; Campbell, 2008).

Each defect creates a strain field in the lattice, which extends to the surrounding atoms, and its magnitude decreases with the radial distance from the defect (Smith, 1995). Due to their small size, point defects generally produce only local distortions in the crystal lattice, which are compressive or tensile stresses. A vacancy or a substitutional atom, smaller than the matrix ones, produces a tensile stress in the

neighboring atoms. On the contrary, an interstitial atom or substitutional atom, bigger than the matrix ones, produces a compressive stress in its neighbors. In case of Al-Mg-Si alloys, Si promotes tensile stresses while Mg results in compressive ones (Mondolfo, 1976). Screw dislocations only promote a shear stress. Edge dislocations lead to tensile stresses, for the atoms below the dislocation line, and compressive stresses, for the ones above. Moreover, in the dislocation slip plane there is also a shear stress. Planar and bulk defects occur on a much bigger scale than the previous ones and lead to a stress state that is different for each case.

The interaction between strain fields promoted by different defects is complex. However, defects tend to organize themselves in order to promote the reduction of the internal energy of the crystal, eventually annihilating each other. For example, dislocations in the same slip plane with opposite strain fields tend to attract each other, promoting their annihilation. Moreover point defects can also move to the dislocation core in order to reduce their stress field (Callister, 2000; Campbell, 2008). In case of Al-Mg-Si alloys, the atoms of Mg and Si diffuse towards dislocation creating small precipitate clusters (Engler et al., 2015) (see precipitation in Dislocation in Figure 2.2).

In polycrystalline materials, the slip systems of each grain have an orientation different of that of their neighbor grains. Therefore, each grain tends to deform in a different way, with the consequent formation of voids or overlaps between neighboring grains (Shimokawa et al., 2005). To prevent this from happening, local internal stresses arise, which are algebraically added to the external ones. The internal stresses vary from grain to grain of the polycrystalline and may even depend, in a sensitive way, on the region considered therein. Thus, in terms of deformation, the grains of a polycrystalline aggregate are subject to complex boundary conditions, that do not exist in single crystals. This requires the simultaneous activation of several slip systems in each grain. There is also an additional barrier to dislocation slip at the grain boundaries. Thus, the material strength increases as the grain size reduce (grain size hardening) (Hansen, 2004). As consequence, the deformation of polycrystals generally requires the application of higher stresses than those required to deform single crystals. The condition of continuity along the grain boundaries is, therefore, the essential characteristic that distinguishes the deformation of polycrystals from that of single crystals. During deformation, the grains of the polycrystalline aggregate rotate, relatively to the axis of the applied stress, which can lead to preferential orientations (crystallographic texture) (Shimokawa et al., 2005).

Plastic deformation of polycrystalline materials occurs associated with dislocation slip. This corresponds to a step-by-step movement, where a plane of atoms breaks and immediately bonds with new ones, as schematically shown in Figure 2.2 (Callister, 2000). In slip, the dislocation moves in a surface defined by its line and Burger's vector, which represents the magnitude and direction of the lattice

distortion resulting from the dislocation. Slip is a conservative motion since the motion is reversible, i.e. if the sign of the shear stress is reversed, the dislocation can move in the opposite direction and, eventually, restore the original configuration. The other basic type of dislocation motion is climb. In climb, the dislocation moves out of the slip plane, resulting in a non-conservation type of motion, since the motion cannot be easily reversed by a simple change of the sign of shear stress, requiring additional work to create point defects (Campbell, 2008).

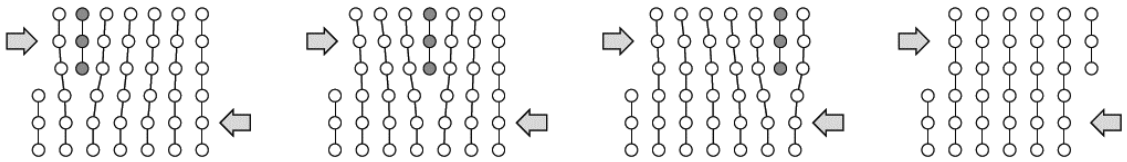

Figure 2.2 – Schematic representation of the slip motion of an edge dislocation (adapted from (Callister, 2000)).

Dislocation slip is the main mechanism for plastic deformation of polycrystalline materials with FCC and BCC crystallographic materials[2], due to the large number of slip systems available (see Table 2.1). Conversely, due to the fewer slip systems available in HCP alloys, plastic deformation occurs mainly by twinning. However, twinning occurs also in FCC and BCC alloys when the resolved shear stress for slip becomes higher than for twinning (Christian and Mahajan, 1995).

In most metallic materials, the dislocation density increases drastically during plastic deformation due to their multiplication, resulting from the interaction with defects, particularly with other dislocations. The best-known mechanism of dislocation generation is the Frank-Read source, which may be characterized as a localized intragranular dislocation source. In this mechanism a dislocation segment lying on an active slip plane - and whose ends are pinned by, e.g. other parts of the dislocation lying outside the plane - bows out under an applied stress (Shimokawa et al., 2005). At critical stress, this dislocation segment can generate dislocation loops, as a result of which dislocation multiplication can occur. The second mechanism is the cross slip, which is the process when screw dislocation moves from a given slip plane to another that contains the direction of the Burgers vector. This cross slip can also result in a pinning segment that multiplies similarly to the Frank-Read source (Messerschmidt and Bartsch, 2003). Finally, slip transmission may occur when a slip

[2] According with Taylor's model, each grain of the polycrystalline deforms homogeneously by sliding in five independent systems. Typically, the CRSS is lower for slip than for twinning, which facilitates the dislocation slip, as long as the slip systems available are properly oriented with the applied stress.

dislocation moving into a grain boundary promotes the generation of a dislocation in an adjacent grain. In fact, three fundamental reactions may take place when a slip dislocation collides with a grain boundary. Besides this transmission mechanism, the dislocation may also be absorbed or reflected, i.e. to move back into the original grain (de Koning et al., 2003). Since the amount of defects increases during plastic deformation, the stored energy in the crystal structure also increases, and the remaining energy is dissipated as heat (Callister, 2000; Campbell, 2008).

The dislocation movement in its slip systems can be restrained, or even blocked, due to the crystallographic defects. Therefore, their motion and generation is particularly influenced by the amount of defects, but also by temperature. The influence of temperature is related with the fact that there is an equilibrium concentration for the number of vacant lattice sites, which increases with the increase of temperature. This is related with the single atomic movements that occur through crystal structure and grain boundaries, i.e. **diffusion**. This is a thermally activated mechanism, since the temperature should be high enough to overcome the energy barriers to atomic motion. That is why diffusion is often negligible at RT and becomes relevant for temperatures greater than approximately one third of the absolute melting temperature (Antczak and Ehrlich, 2007). Moreover, diffusion is also time dependent, since it involves the transport of elements until attaining an equilibrium. Diffusion can promote the atomic motion to a lattice site (substitutional diffusion) or an interstice (interstitial diffusion). In case of substitutional diffusion, the atomic motion is assisted by vacancies (vacancies assisted diffusion) (Liu et al., 2017). Thus, structures like FCC and HCP are more favorable to substitutional diffusion than BCC, since their atomic packing factor and coordination number is higher. On the other hand, BCC structures are more favorable to interstitial diffusion than FCC and HCP, since the interstitial free space is higher (see Table 2.1). The diffusion mechanism is fundamental to enable dislocations to overcome crystallographic defects assisted by climb (Ayas et al., 2014).

The mechanisms of multiplication and mutual interaction of dislocations allow to explain certain aspects of the plastic deformation of metallic materials: during its course, the density of dislocations inside the material increases and simultaneously the material strength increases (strain hardening behavior). Experimental observations suggested that, during the plastic deformation, the shear stress of a slip system is a function of the dislocations density. It can be assumed that the evolution of the dislocations density is dictated by the competition between the rate of generation and of mutual annihilation. During plastic deformation, the probability of dislocation annihilation also increases, due to the increase of the dislocation density (Nix et al., 1985). The rate of generation is independent of both temperature and time, while the rate of annihilation depends of both.

As previously introduced, strain hardening depends on the interaction between dislocation motion and crystallographic defects. In case of aluminum heat-treatable alloys, the alloying elements tend to form second-phase particles, like solute clusters or precipitates. The interaction between a dislocation and second-phase particles depends of their size, shape and their relative distance. Dislocations can either cut through the second-phase particle (see Figure 2.3 a)) or bend around and bypass it (see Figure 2.3 b)). The cut mechanism is easier for small particles like solute clusters, which are coherent with the aluminum matrix. Hard particles in the grains (that are not cut), can accumulate dislocation loops (Orowan mechanism), although their effectiveness as strength mechanism declines as their spacing increases (McQueen et al., 2011).

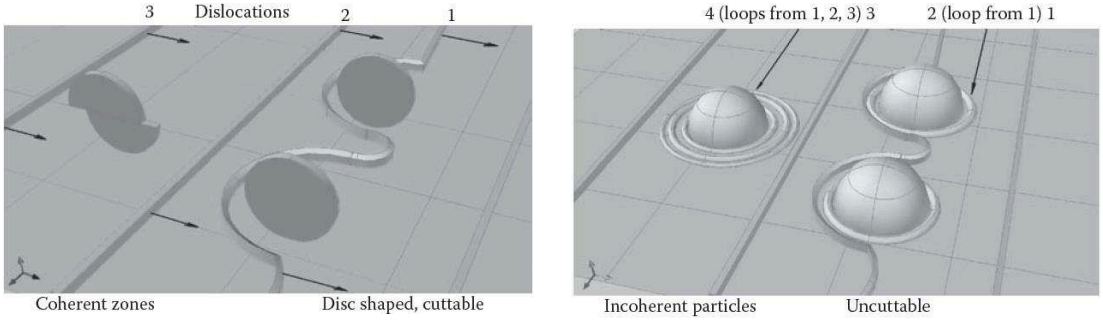

a) Cutting of second-phase particles

b) bend around and bypass second-phase particles

Figure 2.3 – Schematic representation of the interaction between dislocation and second-phase (McQueen et al., 2011).

Figure 2.4 summarize the strengthening and softening mechanisms that can coexist in Al-Mg-Si alloys, including the relations between them, which is dictated by their by their positioning in the same line. Besides grain size and strain hardening, there are also two other strengthening mechanisms. Solute hardening results from the presence of the alloying elements, which as explained in the previous section, deforms the crystal lattice. Therefore, there is no softening mechanism associated. The age hardening results from the precipitation of solute atoms in finely dispersed second-phase particles in a supersaturated matrix, thus, it is also known as precipitation hardening. It is a temperature and time dependent process, since it involves diffusion of the alloying elements. The rise in strength upon aging depends on the interaction between dislocations and second-phase particles. In case of metal sheets, the grain size (and shape) and solute hardening are mostly controlled during the alloy production phase. On the other hand, the strain and precipitation strengthening mechanism can be used to attain desired properties in the production phase or during the forming phase (namely at warm forming temperatures, as highlighted in Figure 2.4).

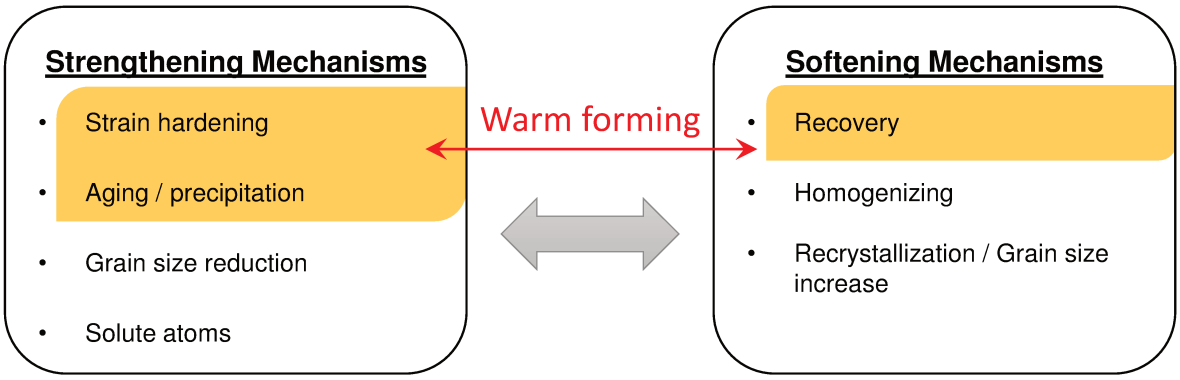

Figure 2.4 – Al-Mg-Si alloys strengthening and softening mechanisms, highlighting their importance in warm forming processes.

The softening mechanisms are mainly dictated by the increase of the rate of dislocation annihilation with the increase of the temperature, since it promotes the dislocations rearrangement and, eventually, their annihilation. Moreover, this rearrangement is assisted by thermal energy, which aids in both climb and slip mechanisms. Since impurities and alloying elements are attracted to both vacancies and dislocations, their presence decreases the mobility of the defects (Galindo-Nava et al., 2012). There are several softening mechanisms, which are temperature and holding time dependent. When considering a pre-deform material, the annihilation and rearrangement of defects can be promoted by the increase of temperature. This corresponds to the recovery where several processes occur: (1) the annihilation of excess point defects, particularly vacancies; (2) the rearrangement of dislocations into lower energy configurations, which also annihilates many of them; and (3) the formation of sub-grains that grow and interlock into sub-boundaries. Thus, there is a relief of stored internal strain energy by rearrangement of dislocations into lower-energy configurations; however, the grain shape and orientation remain the same. The further increase of temperature and time results in recrystallization, which is the replacement of the pre-deformed grains by new strain-free grains. The driving force for recrystallization is the remaining stored energy that was not eliminated during recovery. New orientations, new grain sizes and new grain shapes form during recrystallization. In fact, during this process some of the recrystallized grains grow at the expense of other recrystallized grains. Since fine-grained materials offer the best combination of strength and ductility, in almost all cases, grain growth is an undesirable process. If the material is held at the recrystallization temperature for an extended period of time, further increase of the average grain size occurs. This process is accomplished by the migration of grain boundaries. The heat treatment process which involves recovery, recrystallization, grain growth and a slow cooling, is known as annealing (Campbell, 2008). Finally, homogenizing involves submitting the alloy to a high temperature and holding it for a sufficient time that enables achieving a nearly homogeneous solid solution. The time and temperature required should be

long enough for diffusion to occur, in order to produce a supersaturated solid solution (SSSS) when fast quenching. In case of metal sheets, all these softening mechanisms can be used to attain desired properties in the production phase, considering static or dynamic conditions, i.e. with or without imposing deformation.

In case of Al-Mg-Si alloys, as highlighted also in Figure 2.4, the warm forming process can combine the strain and age hardening with the recovery softening, in order to improve the process conditions as well as the in-service behavior of the component. However, the Al-Mg-Si alloys present a strain rate sensitivity that is negligible at RT, but for temperatures greater than approximately one third of the absolute melting, the strain rate effect on the strength cannot be neglected. As previously mentioned, this is related with the fact that diffusion influences the rate of dislocation annihilation. Therefore, warm forming process conditions involve the definition of processing temperature and strain-rate.

2.2. The production process of aluminum wrought alloys

2.2.1. Aluminum alloys

Aluminum is the most abundant metallic element on earth. The primary aluminum is produced from alumina (aluminum oxide) by the Hall–Héroult process. In turn, alumina is obtained refining bauxite, mostly using the Bayer process. However, bauxite only contains 30–60% of alumina, and therefore its refining produces a high amount of side-products, as red mud. Red mud is environmentally dangerous, however it can be reused in the production of cement (Pontikes and Angelopoulos, 2013) or other ceramic materials (Pérez-Villarejo et al., 2012), as a source for other metals (namely: iron) (Liu and Naidu, 2014), and in catalytic applications (Sushil and Batra, 2008). In fact, the aluminum production requires a high amount of energy, which reduces its usage. Nevertheless, aluminum recycling (secondary aluminum) requires only 5% of the cost associated with the production of primary aluminum, which encourages recycling and increases its life cycle (Wallace, 2011). Low density and melting point, high electrical conductivity and corrosion resistance, give to aluminum alloys a multitude of applications, especially in engineering solutions for the transport industry.

The aluminum alloys are divided as wrought and cast alloys, which are further subdivided as heat-treatable and non-heat-treatable. Casting is normally required for making complex shapes, as for example automotive space frames. Aluminum wrought alloys are the most used, for example as metal sheets and extrusions profiles. They are divided into 8 series in function of the alloying elements, as shown in Figure 2.5. In the international designation systems adopted for aluminum wrought alloys, each

alloy is given a four-digit number, where: the first digit indicates the major alloying elements; the second, if different from 0, indicates a variation of the alloy; and the third and fourth digits identify the specific alloy in the series. The aluminum specification is normally complemented with a letter that designates the heat treatment (temper). The basic temper designations correspond to the letters F (as fabricated), O (annealed), H (strain-hardened), W (solution heat treated) and T (thermally treated to produce stable tempers, different from the previously mentioned). When required, the letter is followed by one or more digits, which indicate sub-divisions of the basic tempers (Kaufman, 2000). The Al-Mg-Si heat treatable alloys, from 6xxx series, are the ones used in present work.

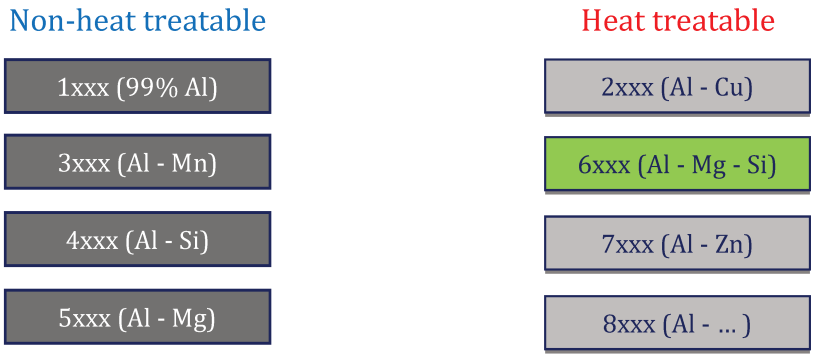

Figure 2.5 – International designation system for aluminum wrought alloys.

2.2.2. The heat treatment

The heat treatment is a thermal process that, under controlled conditions, allows changing the mechanical behavior of aluminum alloys. It is related with the presence of solute atoms that form cluster or precipitates, which interact with the dislocations (see e.g. Figure 2.3). As previously mentioned, these interactions are a function of the cluster or precipitates size, shape and relative distance. Therefore, it is possible to obtain different mechanical properties for the same alloy.

In order to perform a heat treatment the aluminum alloy is heated up to 500 °C (see Solution Heat Treatment (SHT) in Figure 2.6 a)), then it is hold at this temperature for the time required to dissolve eutectic and other phases in an uniform solid solution, and is fast quenched to RT. With the fast quenching, the alloying elements remain dissolved in the aluminum matrix and form a solid solution: the ductility is maximal while the strength is minimum (see Figure 2.6 b)). Due to the fast quenching, the alloying elements are in the SSSS in the Al matrix. In order to reduce the supersaturation, they move and form solute clusters. This phenomenon occurs at RT and is called **natural aging**, the state T4 in Figure 2.6 b). In order to obtain a harder material, the alloy can be heated up to about 200 °C, which allows the formation of precipitates (see Figure 2.6 a)). This phenomenon is called **artificial**

aging, and leads to the peak aged T6 state (maximal yield strength) in Figure 2.6 b). The increase of the holding time at the heat treatment temperature can lead to over-aging and consequent loss of strength (see Figure 2.6 b)), as the precipitates become non-coherent with the aluminum matrix and their relative distance increases (McQueen et al., 2011). Figure 2.7 presents the globally accepted precipitation sequence of Al-Mg-Si alloys, also highlighting the shape of the clusters and the precipitates in the aluminum matrix. The precipitation highly depends on the temperature and time since it occurs by diffusion mechanisms. The Mg and Si are substitutional elements in the Al-matrix, thus "vacancy-assisted diffusion" is the main diffusion mechanism (Falahati et al., 2012; Pogatscher et al., 2011).

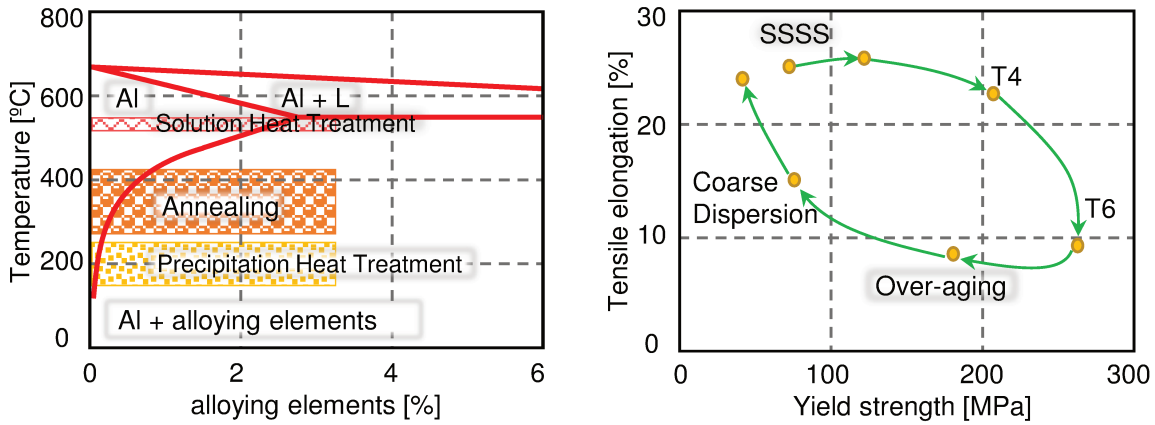

Figure 2.6 – a) Phase equilibrium diagram; b) effect of precipitation on the yield strength and elongation for an EN AW 2036 alloy (adapted from (Hatch, 1984)).

Precipitates	Comment
Clusters of discrete Mg or Si atoms	Clustering of Si may be detrimental to strength
Coclusters of Mg and Si atoms	May be GP zones resulting from ordering transformation
Coherent β'' (Mg_2Si/MgSi) as needles along <100>α	Monoclinic
Semicoherent β' (Mg_2Si) as rods along <100>α	Hexagonal, may forms from β''
Semicoherent B' (Mg_2Si) as laths along <100>α	Hexagonal, forms together with β' favored by high Si:Mg ratios
β (Mg_2Si) as platelets on {100}α	FCC may transform directly from β'

Precipitation sequence

Figure 2.7 – Precipitation sequence for the Al-Mg-Si alloys, highlighting the shape of the clusters and the precipitates in the aluminum matrix (adapted from (Hetnarski, 2013)).

Figure 2.8 presents examples of time–temperature–hardness diagrams for two Al-Mg-Si alloys. These diagrams highlight the importance of considering the joint contribution of temperature and heat-holding time, when evaluating the alloys mechanical properties. When considering warm forming of heat-treatable alloys, it can be expected that the process influences the local strength of the component and, consequently, its post forming in-service behavior.

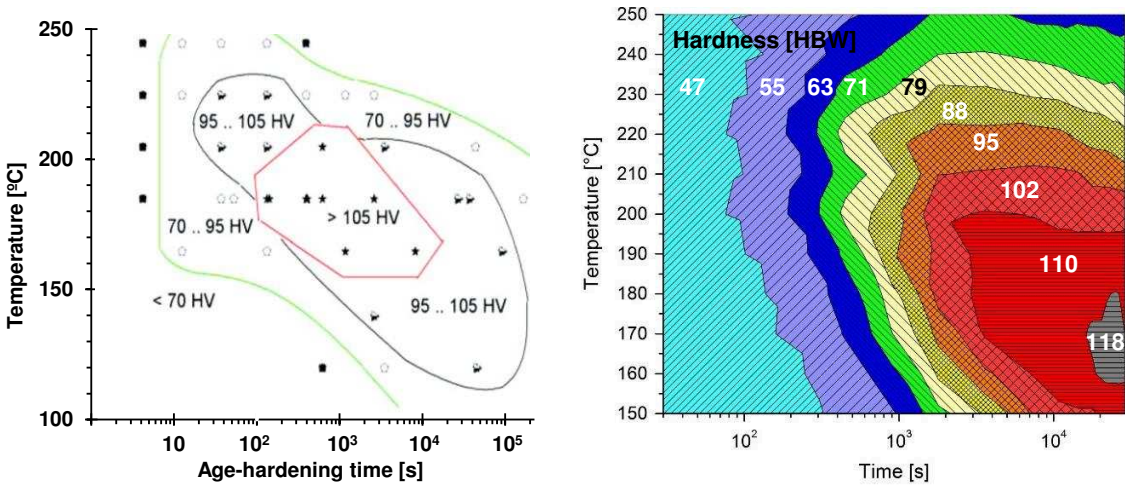

a) EN AW 6016 b) EN AW 6061

Figure 2.8 – Time–temperature–hardness diagrams obtained for two heat treatment alloys (a) adapted from (Schiffmann et al., 2004) and b) from (Pogatscher et al., 2011)).

2.3. Selected alloys

Two Aluminum wrought alloys were selected for this study, the EN AW 6016-T4 and the EN AW 6061-T6, which are commonly used for skin applications and for structural components, respectively. The alloys of the 6xxx-series show a good resistance to corrosion, especially to atmospheric corrosion, a high level of mechanical properties, a good formability and weldability.

Figure 2.9 presents some examples of the applications of both alloys. The EN AW 6016-T4 alloy is mostly used in the automotive industry, with two examples of such applications in Figure 2.9 a) and b). Figure 2.9 a) corresponds to the (spare wheel) trunk recess of the Mercedes-Benz SL (R231), which is produced with a recycled aluminum with a secondary content of 90% (AMAG, 2012). Figure 2.9 b) shows the urban 100% electric Bolloré Bluecar, were all sidewall modules are made using only the EN AW 6016-T4, allowing an optimal recycling at end of life (Hydro, 2012). This car-sharing vehicle is present in French cities (Paris, Lyon, Bordeaux and others) and due to aluminum good corrosion properties its exterior body is often unpainted,

which allows additional environmental economy. Other examples of the application of the EN AW-6016 for outer body panels are: the Audi A2 and A8-D2/3, made of Anticorodal ®-120 alloy; the BMW-Z8; the Rolls Royce Phantom; and the Lamborghini Gallardo (eaa, 2013a).

EN AW 6016-T4

a) Trunk recess – Mercedes-Benz SL (R231)

EN AW 6061-T6

c) All-aluminum assembled engine cradle

d) Compression Fit joint

b) Bolloré Bluecar (100% electric)

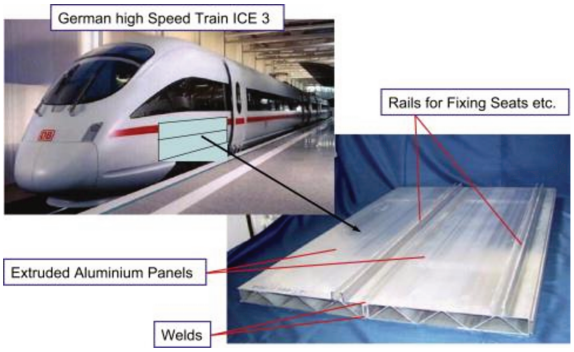

e) German ICE 3

Figure 2.9 – Examples of applications of the: (left) EN AW 6016-T4 alloy and (right) EN AW 6061-T6 alloy (a) (AMAG, 2012); b) (Hydro, 2012); c) (eaa, 2013b); d) (eaa, 2002); e) (Zheng et al., 2009)).

The EN AW 6061-T6 was developed in 1935 and was initially applied in the construction of commercial and military aircraft structures, including wings and fuselages. Nowadays, this alloy presents a wide range of applications as sheets or extrudates, being a common aluminum alloy for general-purpose use. Its typical applications are as structural sections, and include small airplanes (home-built), automotive, shipbuilding and railways (Kaufman, 2000). In the automotive industry it is used, for example, in the engine cradle (see Figure 2.9 c)) (eaa, 2013b) and in the compression fit joint (see Figure 2.9 d)), which is commonly used for building aluminum vehicle frames (eaa, 2002). It was also used in the Chevrolet Corvette Z06, for extruded seatback beam (eaa, 2013a), and in the rear frame (which supports the spare wheel and the fuel tank) of the Corvette ZR-1/LT-1 (C5) (eaa, 2013b).

Additionally, a study was performed to evaluate the potential weight savings with the replacement of the mild-steel by the EN AW 6061-T4, in the door panels of a 2011 Chevrolet Silverado, showing a reduction of 13kg (Stevens et al., 2016). In rail transport, the EN AW 6061-T6 is used in Advanced High Speed trains for the panels and structural components, as shown in Figure 2.9 e), for German ICE 3 (Zheng et al., 2009), or also in German Transrapid (Goran Djukanovik, 2017) and in Japanese Series 200 Shinkansen (Yoshida, 2010). Lastly, the EN AW 6061-T6 is also highly used in the construction of sportive bicycle frames.

The EN AW 6016-T4 alloy was produced and provided by Constellium. The date of the SHT is known for this alloy; therefore, its storage time at RT is counted after the date of the SHT. The EN AW 6061-T6 alloy was acquired in the retail market, and the date of SHT and T6 heat treatment is unknown; therefore, its storage time at RT is counted after its reception in the laboratory.

Table 2.2 presents the mass fraction of the main alloying elements (in percent composition by mass, wt.%) for each of the alloys under study. The amount of Mg+Si+Cu [wt.%] and the Mg/Si ratio are also presented, since they influence the aging strength and kinetics. The EN AW 6016-T4 is known to present a Mg/Si ratio lower than one; in opposition, the EN AW 6061-T6 presents a Mg/Si ratio usually higher than 1.5.

Table 2.2 – Chemical composition, in percent composition by mass (wt.%), of the EN AW 6016-T4 (supplier results) and the EN AW 6061-T6 (The Aluminum Association, 2015) alloys.

	Si	Mg	Cu	Fe	Mn	Mg+Si+Cu	Mg/Si
EN AW 6016-T4	0.91	0.41	0.10	0.255	0.17	1.42	0.46
EN AW 6061-T6	0.4-0.8	0.8-1.2	0.15-0.4	<0.70	<0.40	1.35-2.4	1.0-3.0

The mechanical properties of both alloys at RT are presented in Table 2.3. For the EN AW 6016-T4 alloy, the mechanical properties were determined from uniaxial tensile tests performed at 4 days of maturation (supplier results); while for the EN AW 6061-T6 alloy, they correspond to typical values (Kaufman, 2008). The terms and definitions used throughout this work are according to (ISO 6892-1: 2009) (i.e. R_m tensile strength; $R_{p0.2}$ proof strength at 0.2% of the extensometer gauge length; A_g percentage of non-proportional elongation at maximum force) and the (ISO 10275: 2007) (i.e. the strain hardening exponent (n), which in this case was evaluated between 4 and 6 % of plastic deformation, n_{4-6}, and 10 and 15 %, n_{10-15}).

The mechanical behavior of both alloys is distinct. The EN AW 6016-T4 alloy presents a lower strength and a higher elongation value than the EN AW 6061-T6. However, these differences in the mechanical behavior of both alloys are mainly linked with their heat treatments, since the T4 heat treatment is used to attain higher ductility, while the T6 heat treatment is used to improve the strength.

The producers of the materials indicate that they have a thickness of 1 mm. After the reception, a control on the thickness and surface texture was performed for both alloys. The results are discussed in the following sections.

Table 2.3 – Mechanical properties of the EN AW 6016-T4 at 4 days of maturation (supplier results) and the EN AW 6061-T6 (Kaufman, 2008) alloys. The thickness presented corresponds to the average value obtained with fifty measurements.

	$R_{p0.2}$	R_m	A_g	n_{4-6}	n_{10-15}	Thickness
EN AW 6016-T4	88 MPa	198 MPa	24.6 %	0.32	0.27	1.05 mm
EN AW 6061-T6	≈275 MPa	≈310 MPa	≈10 %	–	–	0.98 mm

2.3.1. Thickness measurements

The thickness of each material was measured considering fifty points randomly distributed over the sheets. The sheets of both alloys present an area of 1×2 m^2, the points at a distance of 50 mm border were not considered in the measurements in order to avoid the border effects. Figure 2.10 a) and b) presents the frequency distribution of the thickness values obtained, for the EN AW 6016-T4 and EN AW 6061-T6, respectively. Small differences to the thickness value indicated by the producers were noticed, which can correspond up to 5%. Moreover, the thickness distribution differs for the both alloys: the EN AW 6016-T4 presents a frequency distribution that can be described by the normal distribution, while the EN AW 6061-T6 is more random. The average value is the one reported in Table 2.3.

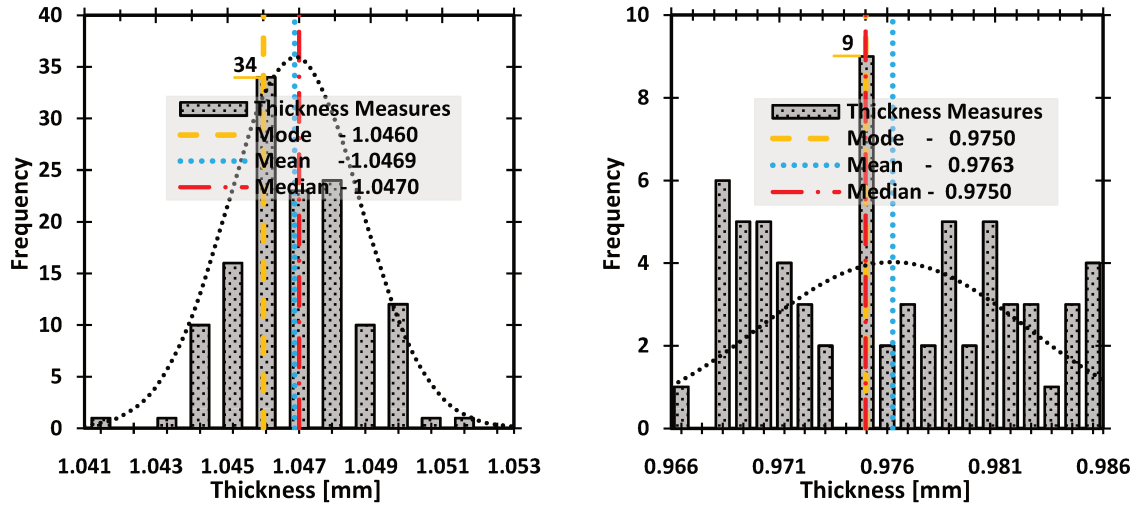

a) EN AW 6016-T4 b) EN AW 6061-T6

Figure 2.10 – Thickness measurement control.

A study by finite element analysis on the impact of small initial thickness deviations, and the impact of natural aging, in the final thickness of a formed component was performed for the EN AW 6016-T4 alloy, considering the alloy mechanical behavior at RT. The DD3IMP in-house code (Menezes and Teodosiu, 2000; Neto et al., 2017; Oliveira et al., 2008) was used to evaluate the forming behavior of a cylindrical cup, considering four condition: an initial thickness of 1.000 mm or 1.047 mm, both were analyzed taking into account the mechanical properties evaluated at 1 and 18 months natural aging. The maximum punch force and average thickness were lower when using an initial thickness of 1 mm or for 1 month of natural aging. Moreover, the numerical simulations show a very good prediction of the experimental thickness evolution, when using the measured thickness value. Therefore, the initial sheet thickness input in the numerical simulation is a major factor for the accurate prediction of the thickness distribution. This becomes crucial when using the thickness distribution to evaluate the constitutive models performance. See Appendix 1, (Simões et al., 2016).

2.3.2. Surface texture

The surface texture of both materials was analyzed by Scanning Electron Microscope (SEM). The alloy EN AW 6016-T4 shows a surface typical of electrical discharge texturing (EDT) and the alloy EN AW 6061-T6 shows one typical of mill finish (MF), as presented in Figure 2.11. While the MF surface exhibits a directional texture, the EDT presents a regular pattern. In automotive applications, the EDT surface allows an attractive appearance after painting (Miller et al., 2000; Tobiyama and Abotani, 2004). More than appearance, the surface texture affects the lubrication conditions and, consequently, can alter the friction value. In fact, some studies on aluminum alloys showed that EDT can improve formability, when compared with MF surfaces (Emmens, 1997; Tobiyama and Abotani, 2004). This improvement of formability is justified by better lubrication conditions, since the isolated pockets on the textured surface serve as a reservoir for the lubricant. Moreover, the lubrication conditions are independent of the sliding direction, leading to an isotropic friction coefficient. In the opposite, the MF surface leads to earlier thinning during the forming operation, which is attributed to the anisotropic lubrication conditions promoted by the directional texture (Masters et al., 2013; Zhou et al., 2011).

However, the literature results for aluminum alloys can be contradictory, showing their dependency of roughness and closed-void volume. In fact, the surface roughness increases as the material plastically deforms. (Masters et al., 2013) shows that the MF surface presents anisotropic lubrication conditions even at relatively high deformation, whatever the strain path analyzed. Moreover, the friction coefficient increases with the deformation level, due to the increase of roughness. This causes a

transition from hydrodynamic to a mixed friction regime, where metal-to-metal contact is increased. For an EDT surface, the roughening effects due to plastic deformation can be completely overcome, such that the friction value remains constant (Masters et al., 2013). A higher closed-void volume results in lower friction values (Batalha and Stipkovic Filho, 2001) and less sensitivity to galling (Zhou et al., 2011). Moreover, the results indicate that the friction coefficient decreases with the increase of pressure and sliding speed (Batalha and Stipkovic Filho, 2001; Emmens, 1997; Zhou et al., 2011). The influence of pressure was also studied by (Zhou et al., 2011), showing that whatever the sliding speed, for a contact pressure lower than 5 MPa, the EDT surface presents a higher friction value and the transverse direction to the milling one of the MF surface (see Figure 2.11). However, for a contact pressure higher than 110 MPa this behavior inverts. Based on the experimental tests performed during this work, it is not possible to state that the surface texture has a strong influence in the forming process.

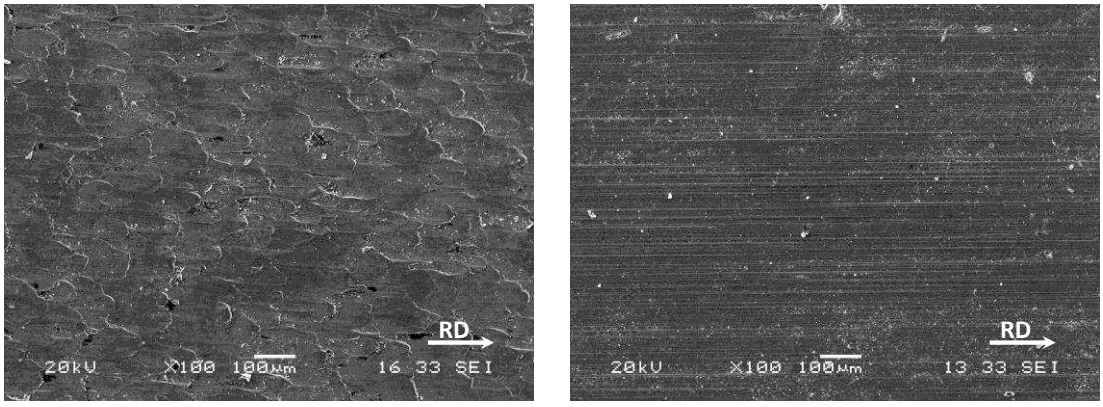

a) EN AW 6016-T4 b) EN AW 6061-T6

Figure 2.11 – Surface texture of both alloys in study was analyzed by Scanning Electron Microscope. a) electrical discharge texturing (EDT) for the EN AW 6016-T4. b) mill finish (MF) for the EN AW 6061-T6

2.4. Experimental tests

2.4.1. Tensile test

The mechanical behavior of metal sheets is usually evaluated submitting the material to specific stress conditions, resembling the stress states attained in forming process, such as: uniaxial tensile, plane strain tension, biaxial tensile and shear. The uniaxial tensile test is the most commonly used for characterizing the mechanical behavior of metal sheets, due to its standardization and simplicity. The test allows attaining relatively small uniform strain, due to the plastic instability (necking).

Figure 2.12 presents an illustration of an engineering stress-strain curve obtained from a tensile test. The response of material in this test is divided in two main regimes, elastic and plastic. The Yield point defines the transition between the two regimes. This point is not always easily defined based on the shape of the stress-strain curve. Therefore, an offset yield point is commonly set at 0.2% plastic strain, in order to avoid its arbitrary definition (the green line in Figure 2.12). The specimen is submitted to a homogeneous deformation up to the maximal load, designated by ultimate tensile strength (the red point in Figure 2.12). Afterwards, the deformation localizes and necking occurs, followed by fracture (the purple point in Figure 2.12). In this work the true stress-strain curves are presented only up to the ultimate tensile strength, since the onset of necking induces a triaxial stress state. The point corresponding to the ultimate tensile strength is not always easily defined, particularly for materials that present stagnation of the engineering stress during post-uniform elongation, since several points may present similar stress values.

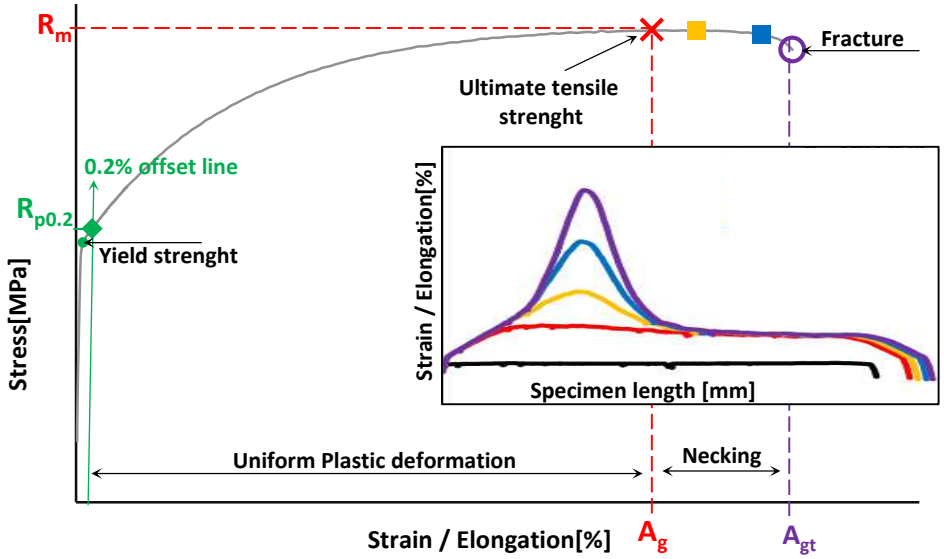

Figure 2.12 – Schematic representation of an engineering stress-strain curve obtained from a tensile test, highlighting the correlation with the strain distribution in the specimen. The same color scheme is used for the strain distribution and the points in the curve.

Uniaxial tensile tests were performed considering different temperatures, strain rates and natural aging periods. Figure 2.13 a) resumes the tests performed. The temperature range considered was from RT up to 300 °C, at strain rates of $2x10^{-4}s^{-1}$, $2x10^{-3}s^{-1}$ and $2x10^{-2}s^{-1}$. The strain rate value of $2x10^{-3}s^{-1}$ was adopted as reference and, consequently, was used in most of the tests performed. Static strain aging, due to material storage at RT, was evaluated for the EN AW 6016-T4 alloy at 1, 4, 7 and 18 months of storage time. For the EN AW 6061-T6, the tests were performed at 1 and 7

months after receiving the alloy. Stress relaxations tests were also performed to get knowledge concerning dynamic precipitation hardening.

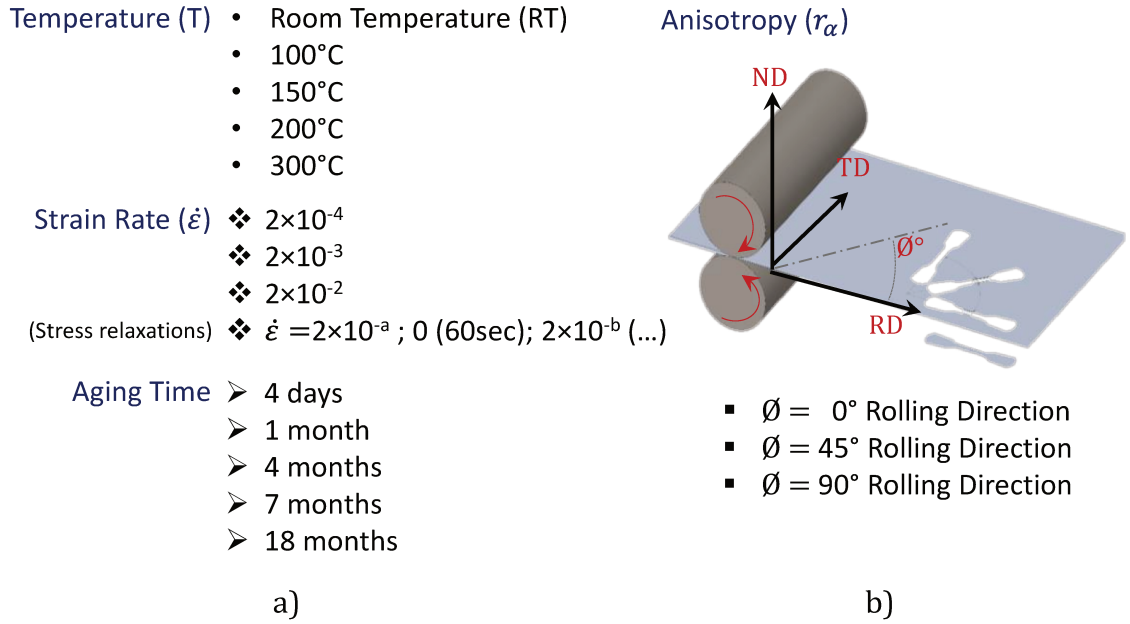

Figure 2.13 – List of uniaxial tensile tests performed and its processing conditions.

Metal sheets are prone to present anisotropic mechanical behavior, i.e. the mechanical properties are directional dependent in sheet plane, due to the rolling process and the grain texture. In particular, the rolling process tends to induce a specific case of anisotropic behavior, called orthotropy. The orthotropic behavior is characterized by the symmetry of the mechanical properties with respect to three orthogonal planes, and the intersection lines of these symmetry planes are the orthotropy axes, as shown in Figure 2.13 b).

The uniaxial tensile test enables the evaluation of the anisotropy coefficient *r*, which is defined as:

$$r_\alpha = \frac{\varepsilon_{yy}^p}{\varepsilon_{zz}^p}., \qquad 2.1$$

where ε_{yy}^p and ε_{zz}^p are the plastic strains perpendicular to the tensile direction and in the through-thickness direction, respectively. In order to measure these plastic strain (ε_{yy}^p and ε_{zz}^p (this value is obtained by the incompressibility condition)) during the test, the strain fields were measured using the digital image correlation (DIC) system from GOM-ARAMIS 4M. This is a non-contact and material independent measuring system, which uses two cameras (for 3D surface coordinates) to take pictures of a stochastic pattern. The acquisition rate was defined in function of test strain rate, in order to keep the adequate amount of data.

Due to the orthotropic behavior, the anisotropy coefficient is usually determined from tensile tests along different angles θ with the rolling direction (RD), as shown in Figure 2.13 b). The orthotropic behavior was studied for both alloys, using specimens cut along three different directions in the sheet plane: 0°, 45° and 90° with RD. Additionally, for the EN AW 6016-T4 alloy tensile tests 1, and 7 months of storage time were also performed for these three directions. These tests were performed at the reference strain rate ($2x10^{-3}s^{-1}$) in the temperature range from RT to 200 °C.

Based on the anisotropy coefficients along θ = 0°, 45° and 90° with the RD, r_0, r_{45}, and r_{90}, it is possible to determine the average anisotropy coefficient, also known as the normal anisotropy coefficient (r_n),, defined as:

$$r_n = \frac{(r_0+2\times r_{45}+r_{90})}{4}, \qquad 2.2$$

This coefficient gives information about the material ability to deform in the thickness direction. If the coefficient is greater than one, the width strains will be dominant (the 'thinning resistance' is more pronounced) (Banabic, 2010). It is also possible to determine the planar anisotropy coefficient (Δr), which is defined as:

$$\Delta r = \frac{(r_0-2\times r_{45}+r_{90})}{2}, \qquad 2.3$$

This coefficient is a measure of the variation of the anisotropy coefficient with the angle to the rolling direction and is related to the earing amplitude of the deep-drawn cups. More precisely, if the value of the anisotropy coefficient is the same along all the directions in the plane of the sheet metal, the earring phenomenon will not be observed.

The uniaxial tensile tests were carried out in a Gleeble 3500 device and in an Instron 4505 machine coupled with a classical furnace, in order to improve knowledge concerning the influence in the mechanical behavior of the temperature gradient along the specimen, which always occurs in the Gleeble device, since the specimen is heated by direct resistance. Moreover, different heat-holding times were used to evaluate the influence on the thermo-mechanical behavior. A minimum of two tests was performed for each condition under analysis (temperature, strain-rate, in-plane direction and aging time). The results were always reproducible, with an average scatter of true stress less than ±1MPa, for the same value of true strain.

2.4.2. Cylindrical cup

The cylindrical cup benchmark test is one of the most widely studied in order to evaluate formability. This test allows analyzing the effect of different process parameters for large deformations, including the ones related with ironing. Also, it permits the analysis of different defects such as earing, wrinkles, ring prints and fracture (Banabic, 2010). Ironing will occur if the gap between the punch and the die is not sufficiently large to allow the blank material to flow into the die cavity. The ironing process typically imposes high contact forces, normal to the surface of the

punch and the die, which can lead to the occurrence of galling, particularly for aluminum alloys. Considering the high contact forces attained, it is also interesting to test the lubrication conditions. Figure 2.14 presents the processing conditions for the cylindrical cup tests performed, for the EN AW 6016-T4 and the EN AW 6061-T6 alloys.

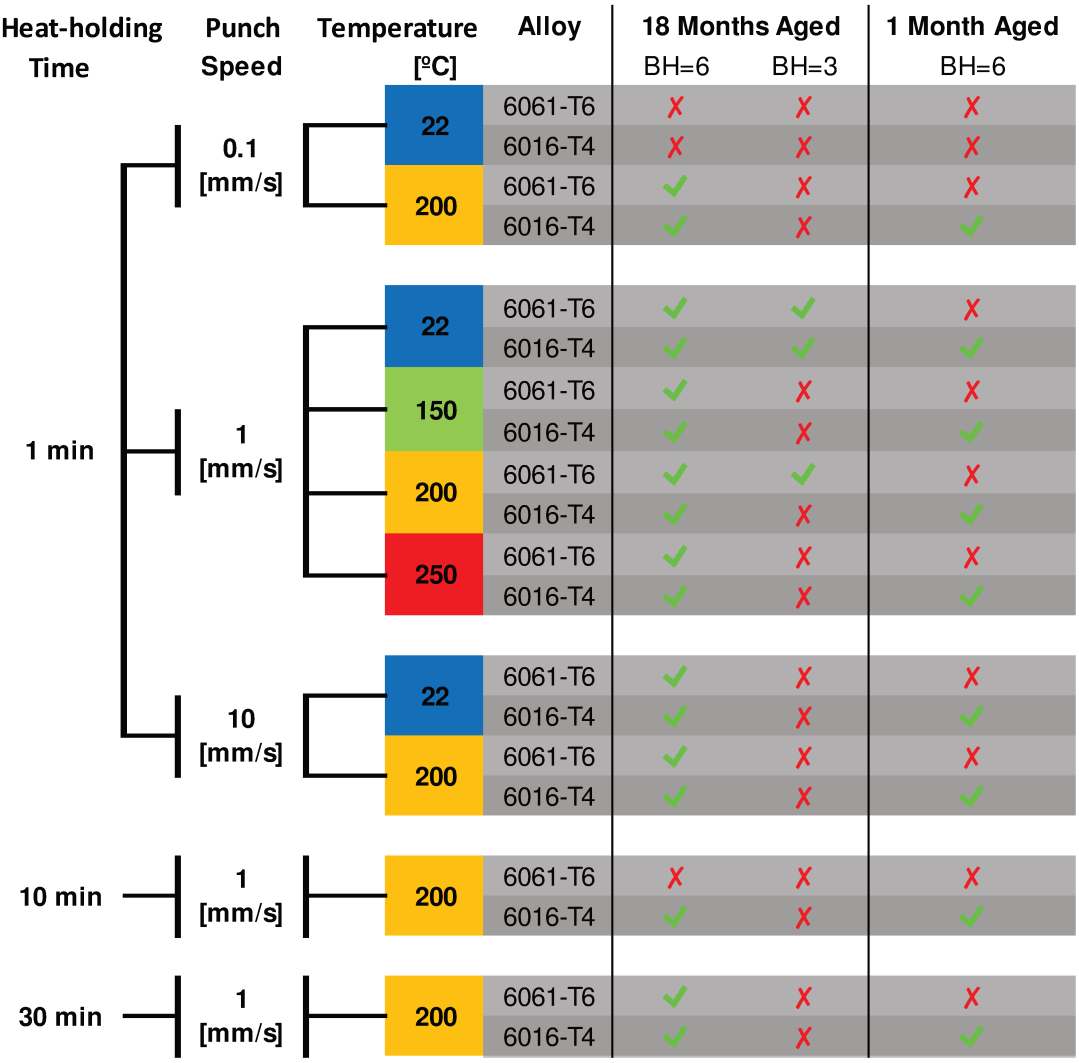

Figure 2.14 – List of cylindrical cup tests performed and their process conditions. The temperature indicated corresponds to the initial blank temperature and BH=3 corresponds to a blank holder force of 3kN, for example.

The tests were performed in a Zwick/Roell Amsler BUP200 sheet metal testing equipment, adapted with specific tools for warm forming. The warm forming tests were all performed considering non-isothermal conditions, with the die and the blank-holder heated by internal electrical heating rods up to the desired temperature, while the punch is refrigerated to keep its temperature close to RT. Moreover, several heat-holding times and punch (ram) speeds were tested, enabling the analysis of

different process conditions. During each test, the punch force and its displacement, the blank-holder (BH) force and the temperature were acquired, as a function of time

Additionally, after the forming operation, it is possible to evaluate the springback with a simple trimming operation, as shown in Figure 2.15. This test consists in cutting a ring specimen from a full drawn cup and then to split the ring longitudinally along a radial plane. The difference between the ring diameters, before and after splitting, gives a direct measure of the springback phenomenon, and indirectly, of the amount of residual stresses in the drawn cup (Demeri et al., 2000). The split-ring test, provides a simple benchmark for correlating the springback predicted by finite element analysis with experimental measurements. The main reason for the springback phenomenon are the tangential stresses, perpendicular to the split plane, which are present in the cup due to the deep drawing process, as shown by (Gnaeupel-Herold et al., 2005; Laurent et al., 2011). In this work, two modifications were added to the standard procedure, related with the trimming sequence and the number of rings cut from the cup, which will be detailed Chapter 3.

Figure 2.15 – Split- ring test, 1 – initial cup, 2 – split-ring, 3 – cup's bottom and top after the trimming of the ring.

2.4.3. Temperature measurements

The temperature was measured using type K thermocouples (Alumel-Chromium thermocouple) with a wire of 250μm diameter, see Figure 2.16 a) – bottom. These thermocouples have a range of temperature between -200 °C and 1250 °C, with a standard accuracy of +/- 0.75%. In order to obtain a good weld joint between the thermocouple and the sheet, the surfaces oxidation was locally removed, by sandblasting. The sandblast sheet surface is shown in Figure 2.16 a) – top. The thermocouples were welded (Figure 2.16 b)) to the sheet using a 35200 Thermocouple Welder from Dynamic System Inc (Gleeble Systems), with a welding

voltage of 45V-DC in less than 1.2 milliseconds. In the tensile test specimens, the thermocouples were welded in a straight line at the middle of their width, one at the center followed by other three with a distance of six millimeters between each other. Moreover, the local influence of the thermocouple and the weld point is considered irrelevant in the mechanical properties measurement, since in the tensile test, the rupture never occurs in the weld zone (Figure 2.16 c)).

Two thermocouples were welded in the blanks used in the cylindrical cup tests, one on its center and the second in a line at 22.5º to the RD, which guarantees an accurate measurement of the cup thickness along the selected directions, of 0º, 45º and 90º to the RD. After the test, the thermocouples are removed (Figure 2.16 c)) showing a good welded adhesion between the thermocouple and the sheet. This procedure is used for all temperature measurements presented in this work.

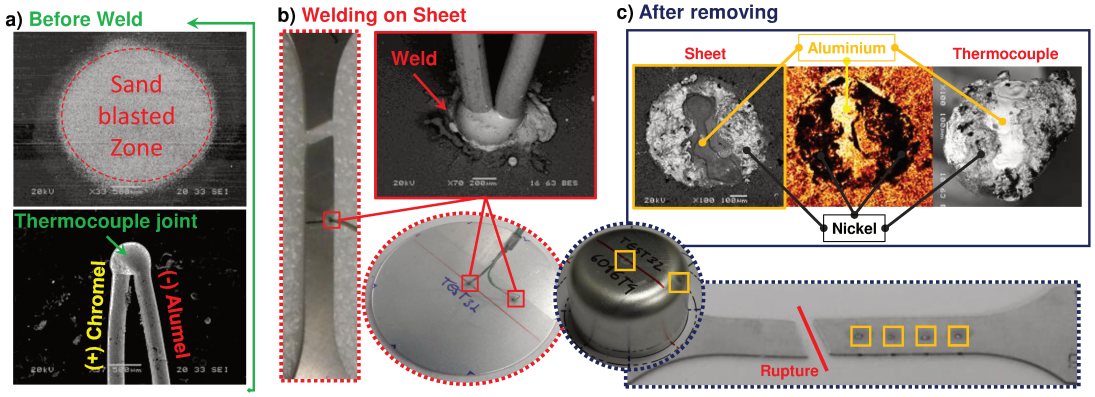

Figure 2.16 – Thermocouple welding steps in the sheet: a) sand blasted local region in sheet and thermocouple join; b) welding positions on the sheet and detail of the welded thermocouple; c) welding positions on the sheet after the thermocouple removal and details highlighting the transfer of materials.

2.5. Final Remarks

As previously discussed, the time and the temperature significantly affect the thermo-mechanical behavior of the heat treatable 6xxx aluminum alloys. Figure 2.17 presents a resume of the influence of the aging time, the temperature, the strain rate and the heat-holding time the mechanical behavior of heat treatable alloys, based on results from the literature review, but also from the ones obtained in this study, which will be detailed in the following chapters. At RT, as the storage time increases the material becomes harder, see Figure 2.17 a). For a low heat-holding time, as the temperature increases the alloys becomes softer and easier to deform, see Figure 2.17 b). Regarding the strain sensitivity, in warm forming the alloys have a different thermo-mechanical behavior, which depends of the heat treatment condition. As

shown in Figure 2.17 c), the alloys artificial aged are generally more stable and present positive strain rate sensitivity; while the alloys natural aged presents initial positive strain rate sensitivity, changing to negative strain rate sensitivity for higher values of deformation. Lastly, concerning the influence of heat-holding time, it is expected that: the alloys in T4 heat treatment condition precipitate towards T6, and therefore its strength increase; while the alloys T6 heat treatment condition, precipitate towards over aging and its strength decrease (Figure 2.17 d)).

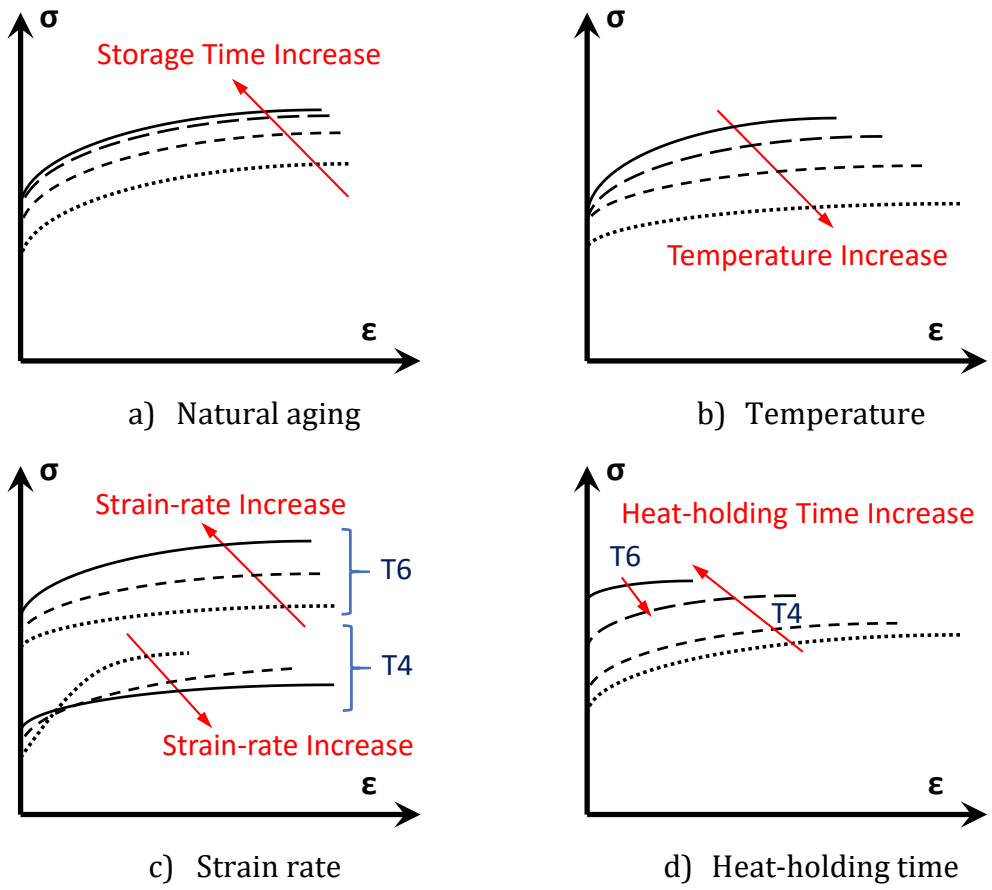

Figure 2.17 – The influence of time and temperature on the stress-strain curve of 6xxx aluminum alloys.

References

AMAG, 2012. Structure - AMAG Austria Metall AG [WWW Document]. AMAG Austria Met. AG. URL https://www.amag.at/en/our-aluminium/automotive/structure.html (accessed 8.22.17).

Antczak, G., Ehrlich, G., 2007. Jump processes in surface diffusion. Surf. Sci. Rep. 62, 39–61. doi:10.1016/j.surfrep.2006.12.001

Ayas, C., van Dommelen, J.A.W., Deshpande, V.S., 2014. Climb-enabled discrete dislocation plasticity. J. Mech. Phys. Solids, Sixtieth anniversary issue in honor of Professor Rodney Hill 62, 113–136. doi:10.1016/j.jmps.2013.09.019

Banabic, D., 2010. Sheet Metal Forming Processes: Constitutive Modelling and Numerical Simulation. Springer Science & Business Media.

Batalha, G.F., Stipkovic Filho, M., 2001. Quantitative characterization of the surface topography of cold rolled sheets — new approaches and possibilities. J. Mater. Process. Technol., 5th Asia Pacific conference on Materials processing 113, 732–738. doi:10.1016/S0924-0136(01)00607-0

Callister, J.W.D., 2000. Fundamentals of Materials Science and Engineering: An Interactive e . Text, 5th Edition, 5 edition. ed. Wiley, New York.

Campbell, F.C., 2008. Elements of Metallurgy and Engineering Alloys. ASM International, Materials Park, Ohio.

Christian, J.W., Mahajan, S., 1995. Deformation twinning. Prog. Mater. Sci. 39, 1–157. doi:10.1016/0079-6425(94)00007-7

de Koning, M., Kurtz, R.J., Bulatov, V.V., Henager, C.H., Hoagland, R.G., Cai, W., Nomura, M., 2003. Modeling of dislocation–grain boundary interactions in FCC metals. J. Nucl. Mater., Proceedings of the Second IEA Fusion Materials Agreement Workshop on Modeling and Experimental Validation 323, 281–289. doi:10.1016/j.jnucmat.2003.08.008

Demeri, M.Y., Lou, M., Saran, M.J., 2000. A Benchmark Test for Springback Simulation in Sheet Metal Forming (SAE Technical Paper No. 2000-01–2657). SAE Technical Paper, Warrendale, PA.

eaa, 2013a. European Aluminium Association, Aluminium Automotive Manual – Applications – Car body – Body structure.

eaa, 2013b. European Aluminium Association, Aluminium Automotive Manual – Applications – Car body – Body components.

eaa, 2002. European Aluminium Association, Aluminium Automotive Manual – Materials – Alloy constitution.

Emmens, W.C., 1997. Tribology of Flat Contacts and its Application in Deep Drawing (PhD-thesis). University of Twente.

Engler, O., Schäfer, C., Myhr, O.R., 2015. Effect of natural ageing and pre-straining on strength and anisotropy in aluminium alloy AA 6016. Mater. Sci. Eng. A 639, 65–74. doi:10.1016/j.msea.2015.04.097

Falahati, A., Lang, P., Kozeschnik, E., 2012. Precipitation in Al-Alloy 6016 – The Role of Excess Vacancies. Mater. Sci. Forum 706–709, 317–322. doi:10.4028/www.scientific.net/MSF.706-709.317

Galindo-Nava, E.I., Sietsma, J., Rivera-Díaz-del-Castillo, P.E.J., 2012. Dislocation annihilation in plastic deformation: II. Kocks–Mecking Analysis. Acta Mater. 60, 2615–2624. doi:10.1016/j.actamat.2012.01.028

Gnaeupel-Herold, T., Foecke, T., Prask, H.J., Fields, R.J., 2005. An investigation of springback stresses in AISI-1010 deep drawn cups. Mater. Sci. Eng. A, Measurement and Interpretation of Internal/Residual Stresses 399, 26–32. doi:10.1016/j.msea.2005.02.017

Goran Djukanovik, 2017. Aluminium use in the production of trains steams ahead [WWW Document]. Alum. Insid. URL http://aluminiuminsider.com/aluminium-use-production-trains-steams-ahead/ (accessed 8.18.17).

Hansen, N., 2004. Hall–Petch relation and boundary strengthening. Scr. Mater., Viewpoint set no. 35. Metals and alloys with a structural scale from the micrometer to the atomic dimensions 51, 801–806. doi:10.1016/j.scriptamat.2004.06.002

Hatch, J.E., 1984. Aluminum: Properties and Physical Metallurgy, Subsequent edition. ed. ASM International, Metals Park, Ohio.

Hetnarski, R.B. (Ed.), 2013. Encyclopedia of Thermal Stresses, 2014 edition. ed. Springer, New York.

Hind, A.R., Bhargava, S.K., Grocott, S.C., 1999. The surface chemistry of Bayer process solids: a review. Colloids Surf. Physicochem. Eng. Asp. 146, 359–374. doi:10.1016/S0927-7757(98)00798-5

Hydro, 2012. Aluminium macht Car-sharing in Paris mobil [WWW Document]. Hydro Dtschl. URL http://www.hydro.com/de/hydro-in-deutschland/Presse/Nachrichten/2012/Aluminium-macht-Car-sharing-in-Paris-mobil/ (accessed 8.22.17).

ISO 6892-1:2009, 2009. Metallic materials - Tensile testing - Part 1: Method of test at room temperature. International Organization for Standardization, Geneva, Switzerland.

ISO 10275:2007, 2007. Metallic materials - Sheet and strip - Determination of tensile strain hardening exponent. International Organization for Standardization, Geneva, Switzerland.

Kaufman, J.G., 2008. Properties of Aluminum Alloys: Fatigue Data and Effects of Temperature, Product Form, and Processing. ASM International, Materials Park, Ohio : Washington, D.C.

Kaufman, J.G., 2000. Introduction to Aluminum Alloys and Tempers. ASM International.

Kvande, H., 2011. 3 - Production of primary aluminium, in: Lumley, R. (Ed.), Fundamentals of Aluminium Metallurgy, Woodhead Publishing Series in Metals and Surface Engineering. Woodhead Publishing, pp. 49–69.

Laurent, H., Coër, J., Grèze, R., Manach, P.Y., Andrade-Campos, A., Oliveira, M.C., Menezes, L.F., 2011. Mechanical behaviour and springback study of an Aluminium alloy in warm forming conditions. Int. Sch. Res. Not. 2011, e381615. doi:10.5402/2011/381615

Liu, F., Liu, Z., Lin, P., Zhuang, Z., 2017. Numerical investigations of helical dislocations based on coupled glide-climb model. Int. J. Plast. 92, 2–18. doi:10.1016/j.ijplas.2017.02.015

Liu, Y., Naidu, R., 2014. Hidden values in bauxite residue (red mud): Recovery of metals. Waste Manag. 34, 2662–2673. doi:10.1016/j.wasman.2014.09.003

Masters, I.G., Williams, D.K., Roy, R., 2013. Friction behaviour in strip draw test of pre-stretched high strength automotive aluminium alloys. Int. J. Mach. Tools Manuf. 73, 17–24. doi:10.1016/j.ijmachtools.2013.05.002

McQueen, H.J., Spigarelli, S., Kassner, M.E., Evangelista, E., 2011. Hot Deformation and Processing of Aluminum Alloys, 1 edition. ed. CRC Press, Boca Raton.

Menezes, L.F., Teodosiu, C., 2000. Three-dimensional numerical simulation of the deep-drawing process using solid finite elements. J. Mater. Process. Technol. 97, 100–106. doi:10.1016/S0924-0136(99)00345-3

Messerschmidt, U., Bartsch, M., 2003. Generation of dislocations during plastic deformation. Mater. Chem. Phys. 81, 518–523. doi:10.1016/S0254-0584(03)00064-6

Miller, W.S., Zhuang, L., Bottema, J., Wittebrood, A.J., De Smet, P., Haszler, A., Vieregge, A., 2000. Recent development in aluminium alloys for the automotive industry. Mater. Sci. Eng. A 280, 37–49. doi:10.1016/S0921-5093(99)00653-X

Mondolfo, L.F., 1976. Aluminum alloys: Structure and properties. Butterworths, London ; Boston.

Neto, D.M., Oliveira, M.C., Menezes, L.F., 2017. Surface Smoothing Procedures in Computational Contact Mechanics. Arch. Comput. Methods Eng. 24, 37–87. doi:10.1007/s11831-015-9159-7

Nix, W.D., Gibeling, J.C., Hughes, D.A., 1985. Time-dependent deformation of metals. Metall. Trans. A 16, 2215–2226. doi:10.1007/BF02670420

Oliveira, M.C., Alves, J.L., Menezes, L.F., 2008. Algorithms and Strategies for Treatment of Large Deformation Frictional Contact in the Numerical Simulation of Deep Drawing Process. Arch. Comput. Methods Eng. 15, 113–162. doi:10.1007/s11831-008-9018-x

Pérez-Villarejo, L., Corpas-Iglesias, F.A., Martínez-Martínez, S., Artiaga, R., Pascual-Cosp, J., 2012. Manufacturing new ceramic materials from clay and red mud derived from the aluminium industry. Constr. Build. Mater. 35, 656–665. doi:10.1016/j.conbuildmat.2012.04.133

Pogatscher, S., Antrekowitsch, H., Leitner, H., Ebner, T., Uggowitzer, P.J., 2011. Mechanisms controlling the artificial aging of Al–Mg–Si Alloys. Acta Mater. 59, 3352–3363. doi:10.1016/j.actamat.2011.02.010

Pontikes, Y., Angelopoulos, G.N., 2013. Bauxite residue in cement and cementitious applications: Current status and a possible way forward. Resour. Conserv. Recycl. 73, 53–63. doi:10.1016/j.resconrec.2013.01.005

Power, G., Loh, J., 2010. Organic compounds in the processing of lateritic bauxites to alumina: Part 1: Origins and chemistry of organics in the Bayer process. Hydrometallurgy 105, 1–29. doi:10.1016/j.hydromet.2010.07.006

Schiffmann, R., Haug, J., Banhart, J., 2004. Evolution of Precipitates during Age-hardening of AW 6016 Alloy, in: Materials Forum. pp. 604–609.

Schmid, E., Boas, W., 1935. Kristallplastizität: Mit Besonderer Berücksichtigung der Metalle.

Shimokawa, T., Nakatani, A., Kitagawa, H., 2005. Grain-size dependence of the relationship between intergranular and intragranular deformation of nanocrystalline Al by molecular dynamics simulations. Phys. Rev. B 71, 224110. doi:10.1103/PhysRevB.71.224110

Simões, V.M., Laurent, H., Oliveira, M.C., Menezes, L.F., 2016. Natural aging effect on the forming behavior of a cylindrical cup with an Al-Mg-Si alloy. AIP Conf. Proc. 1769, 200021. doi:10.1063/1.4963639

Smith, W.F., 1995. Principles of Materials Science and Engineering, 3 Sub edition. ed. Mcgraw-Hill College, New York.

Stevens, M., Modi, S., Chess, M., 2016. Mixed Materials Solutions : Alternative Materials for Door Assemblies. Center for Automotive Research.

Sushil, S., Batra, V.S., 2008. Catalytic applications of red mud, an aluminium industry waste: A review. Appl. Catal. B Environ. 81, 64–77. doi:10.1016/j.apcatb.2007.12.002

The Aluminum Association (Ed.), 2015. International Alloy Designations and Chemical Composition Limits for Wrought Aluminum and Wrought Aluminum Alloys.

Tobiyama, Y., Abotani, K., 2004. Hot-Dip Galvanized Steel Sheet with Excellent Surface Quality for Automotive Outer Panels. JFE Technical Report 4, 48–52.

Wallace, G., 2011. 4 - Production of secondary aluminium, in: Lumley, R. (Ed.), Fundamentals of Aluminium Metallurgy, Woodhead Publishing Series in Metals and Surface Engineering. Woodhead Publishing, pp. 70–82.

Yoshida, H., 2010. Alloy Development for Transportation in Sumitomo Light Metal, in: Kumai, S., Umezawa, O., Takayama, Y., Tsuchida, T., Sato, T. (Eds.), Alloy Development & Application 1. Presented at the 12th International Conference on Aluminium Alloys, The Japan Institute of Light Metals, Yokohama, Japan, pp. 54–61.

Zheng, L., Petry, D., Rapp, H., Wierzbicki, T., 2009. Characterization of material and fracture of AA6061 butt weld. Thin-Walled Struct. 47, 431–441. doi:10.1016/j.tws.2008.08.008

Zhou, R., Cao, J., Wang, Q.J., Meng, F., Zimowski, K., Xia, Z.C., 2011. Effect of EDT surface texturing on tribological behavior of aluminum sheet. J. Mater. Process. Technol. 211, 1643–1649. doi:10.1016/j.jmatprotec.2011.05.004

(Page intentionally left blank)

Chapter 3.

The influence of warm forming in natural aging and springback of Al-Mg-Si alloys

This chapter contains the paper submitted to the International Journal of Material Forming, with the same title as the chapter. This work discusses the thermo-mechanical behavior of the two Al-Mg-Si alloys, in function of temperature (from 22 to 300°C) and storage time (from 1 to 18 months), using uniaxial tensile tests, cylindrical cup tests and split ring (springback) tests. It shows that warm conditions can be used as an effective solution to minimize the variability caused by the natural aging in forming operations of heat treatable aluminum alloys.

.

(Page intentionally left blank)

Highlights

1. The material strength increases with natural aging, leading to parts shape variability at room temperature forming operations.
2. The temperature increase reduces the influence of natural aging in the variation of yield stress and tensile strength.
3. Whatever the natural aging time, temperature increase leads to decrease yield stress and work hardening while post-uniform elongation increases.
4. Whatever the natural aging time, warm forming reduces the influence of natural aging in parts shape variability, namely springback.

Graphical Abstract

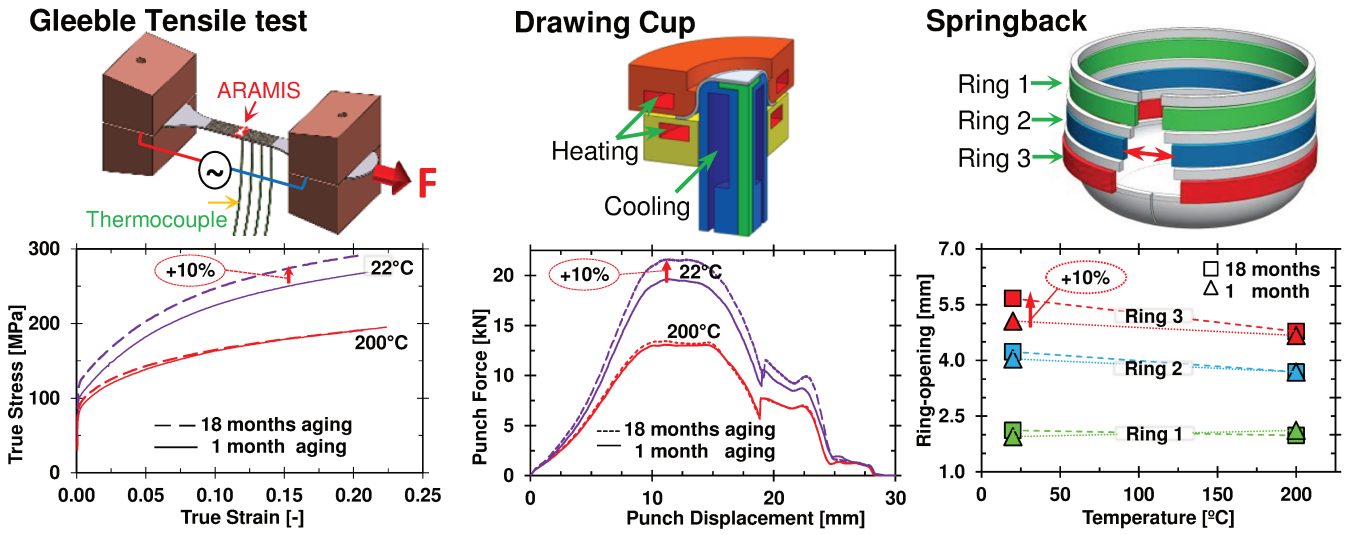

(Page intentionally left blank)

The influence of warm forming in natural aging and springback of Al-Mg-Si alloys

Vasco Simões [a,b,*], Hervé Laurent [a], Marta Oliveira [b], Luís Menezes [b]

[a] Univ. Bretagne Sud, FRE CNRS 3744, IRDL, F-56100 Lorient, France.

[b] CEMMPRE, Department of Mechanical Engineering, University of Coimbra, Polo II, Rua Luís Reis Santos, Pinhal de Marrocos, 3030-788 Coimbra, Portugal

* Corresponding author: vasco.simoes@uc.pt (+351 912536771)

Abstract

Natural aging is an open issue for heat treatable aluminum alloys, since it causes variability in sheet metal forming operations, namely in the parts shape, as well as in-service behavior. Warm forming is a very interesting solution to improve formability and reduce springback. Therefore, this work aims to study the contribution of warm forming to reduce the variability caused by natural aging in sheet metal forming operations. The thermo-mechanical behavior of two Al-Mg-Si alloys, EN AW 6016-T4 and EN AW 6061-T6, is studied in function of temperature (from 22 to 300 ºC) and storage time (from 1 to 18 months), using uniaxial tensile tests, cylindrical cup tests and split ring (springback) tests. At 22 ºC, the EN AW 6061-T6 shows negligible variations of mechanical behavior due to natural aging, while the EN AW 6016-T4 shows a clear increase of the yield stress and of the work hardening and, consequently, of the springback. Warm forming temperatures between 200 and 250 ºC reduce the yield stress and the work hardening and, consequently, minimize the effects of natural aging. Thus, warm conditions can be used as an effective solution to minimize the variability caused by the natural aging in forming operations of heat treatable aluminum alloys.

Keywords: Al-Mg-Si; Natural Aging; Warm Forming; Springback

1 Introduction

The increasing demand of aluminum alloys in the automotive sector is linked with their good strength-to-weight ratio, leading to lower weight and consequent emissions reduction during vehicles life cycle [1, 2]. Within aluminum alloys, the heat treatable present good ductility in T4 heat treatment and medium strength in T6 heat treatment [1, 2]. Ductility is required for sheet metal forming operations while strength is required for in-service behavior. However, during storage at room temperature (RT) of heat treatable alloys, the alloying elements (or solute atoms) precipitate in the aluminum matrix into more stable phases. This spontaneous phenomenon usually leads to the increase of the alloys strength, as function of storage time at RT, which is called natural aging. Precipitation can be accelerated by heating above RT in an operation referred as artificial aging.

Natural aging is currently a crucial problem for sheet metal forming of heat treatable aluminum alloys. Natural aging generates two problems for the automotive industry: the first is an increase of variability during forming operations and springback; the second is, a negative effect of natural aging on subsequent artificial aging. However, at present, only some solutions to minimize the negative effect of natural aging were proposed. The present work aims to reduce the variability caused by natural aging in forming operations and springback. The Al-Mg-Si wrought alloys (6xxx series) were selected since they are highly demanded in the automotive industry for body-in-white components, due to good ductility and post forming strength.

It is known that the variability of the mechanical behavior due to the natural aging, can lead to the lack of dimensional accuracy in sheet metal forming production lines [3, 4]. For example, Suri et al. [3] concluded that natural aging can lead to 23% of strain variation and 9% of thickness variation in the stretch forming of an aircraft skin. In turn, Marretta and Lorenzo showed by numerical studies [5] that the yield stress and the strain hardening exponent (n) are the most influential parameters in springback and thinning variability, respectively. Zhong et al. [6] performed experimental studies for the EN AW 6016 alloy at RT, confirming that natural aging leads to an increase of the yield stress and of the work hardening, although the n value can decrease. Concerning the orthotropic behavior, Leacock et al. [7] observed that the EN AW 7075 alloy changes from in-plane isotropic behavior, in as-quenched state, to in-plane anisotropy,

during the first 15 min of natural aging. However, after this abrupt change, the degree of anisotropy appears to remain constant. Prillhofer et al. [4] studied the influence of the natural aging, between two and six months of storage at RT, on the formability of four different Al-Mg-Si alloys (EN AW 6016, 6005A, 6063 and 6013 alloys). They concluded that the forming limit curves (FLC) and the bendability present a weak decrease due to natural aging.

In literature, the most reported influence of natural aging is the material strength increase in function of storage time. According to Esmaeili and Lloyd [8] and Hirth et al. [9], the material strength evolution follows a linear relationship with the logarithm of storage time, enabling the determination of a natural aging kinetics parameter and thus, the prediction of the strength increase. However, recent studies reported the existence of five different natural aging stages in Al-Mg-Si alloys, each one with its own kinetics [10, 11]. Therefore, the natural aging kinetics parameter is valid only within a limited storage time range. Moreover, the natural aging kinetics and magnitude of strength increase seem dependent of storage temperature, chemical composition and degree of supersaturation [10, 12]. For example, for an EN AW 6061 alloy, Pogatscher et al [13] refers that the evolution of the strength saturates after around 7 days of natural aging; while, Hunsicker [12] shows that natural aging occurs at least during 10 years, although 90% of the strength increase occurs during the first year. However, the uncertainty of the natural aging phenomenon makes its control and prediction very difficult. Additionally, in industrial practice the time span between solution heat treatment and sheet metal forming can be delayed from several weeks up to a few months [14]. Therefore, Suri et al. [3] conclude that in order to minimize the natural aging influence, the storage time must be standardized, otherwise the material strength at the forming instant is continuously changing.

Some solutions have been proposed in the literature aiming to reduce the negative effect of natural aging in artificial aging. These solutions are: interrupted quenching [15], pre-aging [15, 16], pre-strain [16, 14], and pre-strain followed by pre-aging [16]. All these methods lead to an increase of the initial yield stress value. Engler et al. [14] alerts that pre-strain also leads to an increase of the in-plane anisotropy, which was attributed to anisotropic hardening after the change in strain path. However, none of these methods can definitely suppress the natural aging. In fact, they can only stabilize the natural aging during reduced time spans (up to few days), which is not enough for industrial practice. Besides, some disadvantages were also pointed out concerning

their usage. For example, Ding et al. [15] observed that interrupted quenching treatments produce quench-induced precipitates and wide precipitates free zones along the grain boundaries, which can cause fracture toughness problems in Al–Mg–Si alloys. Recently, a new strategy was proposed by Werinos et al. [10], which consists on the addition of Sn in the composition of Al–Mg–Si alloys, allowing temporary suppression of natural aging for approximately 6 months.

According to differential scanning calorimetry studies, performed for various compositions of Al-Mg-Si alloys, the natural aging precipitates dissolve in a temperature range between 200 and 250 ℃ [16]. Therefore, Pogatscher et al, [13] proposed an increase of the usual artificial aging temperature (160-180 ℃) to 210 ℃, which contributes to dissolve natural aging precipitates and reduce the negative effect of natural aging in artificial aging. This temperature range corresponds to the one used in warm forming. Warm forming is an effective solution to improve formability [17–19], contributing to reduce the internal stress of formed components and, consequently, springback [20, 21]. Moreover, according to Mahabunphachai and Koç [22], the change of grain size due to the effects of warm temperature and strain rate as compared to RT was not significant; therefore, it was concluded that the decrease in the flow stress at warm forming temperatures was mainly due to the thermally activated dislocation. Therefore, since warm forming enhances dislocation movement, it is expected to minimize its interaction with natural aging precipitates. Both mechanisms, precipitates dissolution and dislocation enhancement, are expected to minimize the natural aging effect for warm forming condition.

This work aims to improve the knowledge about the influence of natural aging in the mechanical behavior of Al-Mg-Si alloys, particularly its consequences on the variability of sheet metal forming operations performed at RT, which is only reported in a few studies. The main goal is to evaluate the potential of using warm forming conditions to reduce variability in sheet metal forming operations, namely in springback. The use of warm forming as a strategy to reduce the influence of natural aging phenomenon on forming operations has not been previously reported. The influence of natural aging in the thermo-mechanical behavior was studied following a macroscopic approach, using uniaxial tensile tests, cylindrical cup tests and the split ring tests on two Al-Mg-Si alloys, EN AW 6016-T4 and EN AW 6061-T6.

Most of the studies concerning natural aging kinetics resort to indirect methods to analyze precipitation evolution [8–10, 15, 16]. However, the experience shows that these methods have to be combined, since a single indirect technique is not powerful enough to clearly reveal the subtle changes in natural aging [16, 23]. In fact, according to Banhart et al. [23], among of all the imaging techniques, only 3D Atom Probe Tomography has the potential to resolve the clusters formed during natural aging, since the identification of natural aging precipitates is extremely difficult due to its nanometer size. However, 3D Atom Probe Tomography is not a very accessible method. Consequently, since the aim of this work is not to analyze the kinetics of natural aging precipitates, no microscopic results by indirect methods are shown. A macroscopic approach is adopted in this paper to study the natural aging impact in forming operations.

This paper is organized as follows. In Section 2, the alloys selected for this study are introduced and a review concerning the precipitation mechanisms is presented to support the macroscopic approach. Section 3 details the experimental procedure adopted for the thermo-mechanical analysis of the material behavior and presents its results, including the study of the natural aging effect. Section 4 describes the cylindrical cup benchmark test, which is used to analyze the influence of warm forming conditions and the results are presented and discussed. Finally, the main conclusions are summarized in Section 5.

2 Al-Mg-Si alloys and its precipitation mechanisms

2.1 Materials

The two alloys selected for this study are the EN AW 6016-T4 and the EN AW 6061-T6, which are commonly used for skin applications and for structural components in the automotive industry, respectively. The designation T4 indicates solution heat treated, rapid quenching, and naturally aged to a substantially stable condition [12]. The designation T6 indicates solution heat treated, rapid quenching, followed by artificial aging [12]. The term natural aging is often linked with the T4 heat treatment. However, according to Prillhofer et al. [4] which, as previously mentioned, analyzed the natural aging of four Al-Mg-Si alloys in the period between two and six months after solution heat treatment (SHT), the natural aging is susceptible to occurs in both heat treatments: for the T4 heat treatment natural aging always leads to a strength increase, while for T6 it can lead to both strength increase or decrease.

The EN AW 6016-T4 alloy was produced and provided by Constellium, and the date of the SHT is known; therefore, its storage time at RT is counted after the date of the SHT. The EN AW 6061-T6 alloy was acquired in the retail market, and the date of SHT and T6 heat treatment is unknown; therefore, its storage time at RT is counted after its reception in the laboratory. The mechanical properties of both alloys are presented in Table 1. The terms and definitions used throughout this work are according to ISO 6892-1:2009 [24] (i.e. R_m tensile strength; $R_{p0.2}$ proof strength at 0.2% of the extensometer gauge length; A_g percentage of non-proportional elongation at maximum force) and the ISO 10275:2007 [25] (i.e. the strain hardening exponent (n), which in this case was evaluated between 4 and 6 % of plastic deformation, n_{4-6}, and 10 and 15 %, n_{10-15}).

For the EN AW 6016-T4 alloy, the mechanical properties at RT, presented in Table 1, were determined from uniaxial tensile tests performed at 4 days of maturation (supplier results); while for the EN AW 6061-T6 alloy, they correspond to typical values [26]. The mechanical behavior of both alloys is distinct. The EN AW 6016-T4 alloy presents a lower strength and a higher elongation value than the EN AW 6061-T6. However, these differences in the mechanical behavior of both alloys are mainly linked with the heat treatments, since the T4 heat treatment is used to attain higher ductility while the T6 heat treatment is used to improve the strength. The thickness of both alloys is approximately 1 mm, with the measured experimental value presented in Table 1.

Table 2 presents the mass fraction of the main alloying elements (in percent composition by mass, wt.%) for each of the alloys under study. For the 6xxx series the Mg and Si are the alloying elements that promote precipitation hardening [12]. The EN AW 6016-T4 is known to present a Mg/Si ratio lower than one; in opposition, the EN AW 6061-T6 presents a Mg/Si ratio usually higher than 1.5. According to Ding et al. [27], for the same Mg+Si [wt.%] content, the alloys with a Mg/Si ratio ≈0.5 (Si-rich) present higher natural aging strength than the ones with a Mg/Si ratio ≈2.0 (Mg-rich), which indicates that Si atoms have higher solid solution strengthening than Mg atoms. Nevertheless, these authors [27] also conclude that the natural aging rate depends more on the Mg+Si content than on the Mg/Si ratio. Moreover, it is known that Cu also promotes clustering during natural aging [8]. Therefore, in the present work the amount of Mg+Si+Cu [wt.%] was adopted as a reference (see Table 2), since alloys with a higher content of these alloying elements are more saturated, and therefore, the driving force for precipitation is higher.

	$R_{p0.2}$	R_m	A_g	n_{4-6}	n_{10-15}	Thickness
EN AW 6016-T4	88 MPa	198 MPa	24.6 %	0.32	0.27	1.05 mm
EN AW 6061-T6	≈275 MPa	≈310 MPa	≈10 %	–	–	0.98 mm

Table 1 – Mechanical properties of the EN AW 6016-T4 alloy at 4 days of maturation (supplier results) and the EN AW 6061-T6 alloy [26]. The thickness presented corresponds to the average value obtained with fifty measures.

	Si	Mg	Cu	Fe	Mn	Mg+Si+Cu	Mg/Si
EN AW 6016-T4	0.91	0.41	0.10	0.255	0.17	1.42	0.46
EN AW 6061-T6	0.4-0.8	0.8-1.2	0.15-0.4	<0.70	<0.40	1.35-2.4	1.0-3.0

Table 2 – Chemical composition, in percent composition by mass (wt.%), of the EN AW 6016-T4 (supplier results) and the EN AW 6061-T6 [28] alloys.

2.2 Precipitation mechanisms

In heat treatable Al-Mg-Si alloys, the macroscopic mechanical behavior is dependent of the microstructural mechanisms of precipitation hardening, which occurs by natural and artificial aging. Nonetheless, as mentioned in the introduction, the identification of natural aging precipitates is extremely difficult due to its nanometer size, particularly for Al-Mg-Si alloys [23]. This occurs due to the small content of Mg and Si (as shown in Table 2) and because Mg, Al, and Si are neighboring elements in the periodic table. Hence, it is necessary to combine different indirect methods to analyze the subtle changes during natural aging or to use a technique like 3D

Atom Probe, to be able to resolve the clusters formed [23]. However, it is crucial to understand the heat treatments and their precipitation sequences (see Figure 1). Thus, in this section, a review is presented concerning the precipitation mechanisms that occur during natural and artificial aging, which influences the alloys strength and ductility.

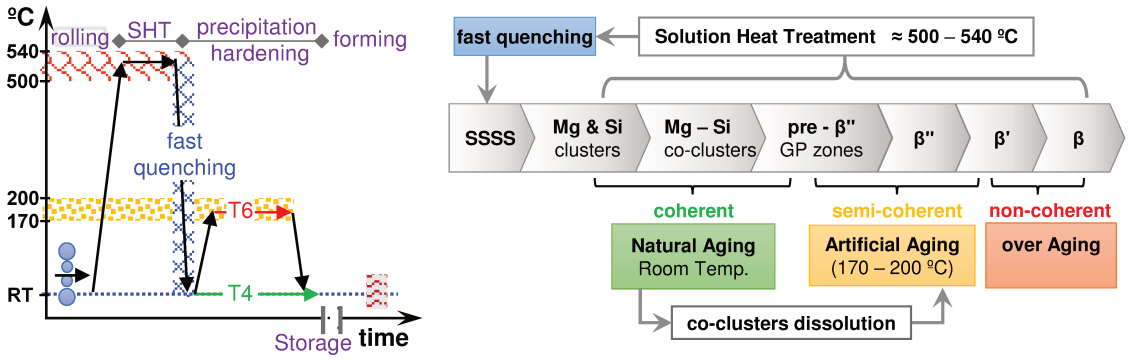

a) b)

Figure 1 – a) Heat treatment sequence; b) Precipitation sequence in Al-Mg-Si alloys (according to [23])

The heat treatment starts with SHT, which consists on a heating stage, followed by a holding stage between 500 to 540 ℃ and fast quenching to RT (see Figure 1 a)) [12]. The SHT creates a solid solution by dissolving the precipitates of alloying elements. A slow quenching from SHT to RT leads to quench-induced precipitation during cooling, which disables subsequent heat treatments [29]. On contrary, the fast quenching keeps the alloying elements dissolved in the aluminum matrix at RT, in a supersaturated solid solution (SSSS) (see Figure 1 b)). The SSSS occurs since the solubility of Mg and Si atoms is lower at RT than at SHT temperature [12]. At SSSS, the alloy presents mainly solid solution strengthening and maximal ductility. Afterwards, precipitation hardening occurs by natural or artificial aging. In both, the precipitation of Mg and Si atoms offers supplementary strength for dislocations motion, which depends of the precipitates size and shape, and its coherence with the Al-matrix [15].

The precipitation sequence is shown in Figure 1 b). According to Wenner et al. [30], the generic precipitation sequence is: SSSS → solute clusters (coherent) → hardening precipitates (semi-coherent) → non-hardening precipitates (non-coherent). The SSSS is the driving force for the precipitation of Mg and Si atoms in the Aluminum matrix [12], which may start immediately after quenching. Natural aging occurs at RT due to the formation of solute clusters which are coherent

with the Al-matrix and follow the precipitation sequence: from Mg and Si clusters to Mg-Si co-clusters [16]. The artificial aging requires a new heating stage at a temperature range between 170 and 200 ºC. Thus, it is characterized by a different behavior, in which the strength increases due to the precipitation of hardening precipitates (β'' – needles) until a maximum value (the T6 heat treatment). The extended holding at artificial aging temperature leads to a strength decrease, known as over-aging, which is caused by the formation of non-hardening β' and β precipitates [31].

In Al-Mg-Si alloys, the precipitation occurs mainly by "vacancy-assisted diffusion" mechanism, since, as mentioned before, the Mg and Si are substitutional elements in the Al-matrix. The vacancies are mainly formed due to fast quenching, i.e. "quenched-in vacancies" [30]. The formation of solute clusters trap the vacancies and reduces the number of atoms in SSSS, which leads the aging process progressively to stop [10, 11]. Thus, the strategies proposed in the literature to reduce the natural aging are based on the reduction of "vacancy-assisted diffusion". For example, interrupted quenching and pre-aging methods are performed at temperatures from 70 up to 150 ºC, for a short period of time (see Figure 2 a) and b)). These methods promote the formation of pre-β'' precipitates during this short period of artificial aging (see Figure 1 b)). The pre-β'' precipitates significantly reduce the number of "quenched-in vacancies" and supersaturation of alloying elements [15]. Concerning the pre-strain method (see Figure 2 c)), the dislocations act as vacancy sinks which lead to lower clusters formation [14]. Lastly, also the addition of Sn in the composition of Al–Mg–Si alloys, proposed by Werinos et al. [10], consists on reducing the concentration of excess vacancies allowing temporary suppression of natural aging.

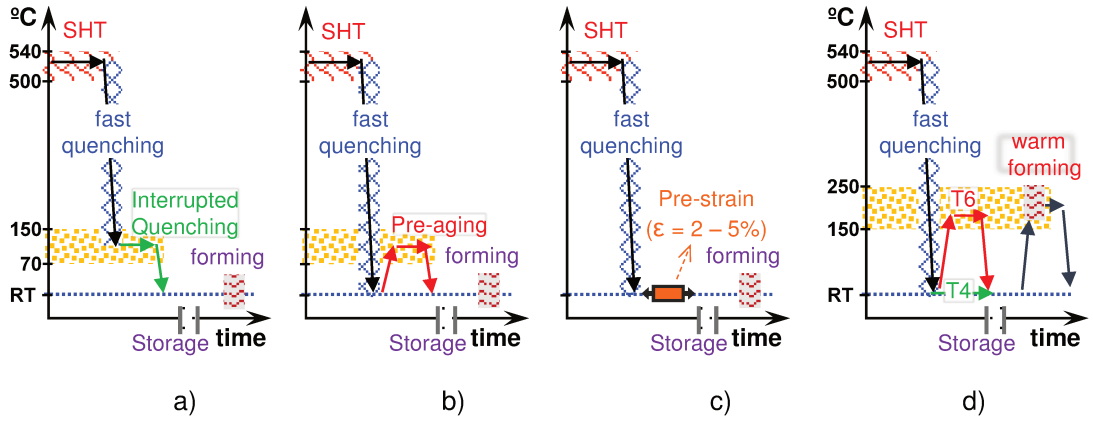

Figure 2 – Solutions to avoid natural aging: a) Interrupted Quenching b) Pre-aging c) Pre-strain; d) Warm forming (our solution).

Warm forming is analyzed in this work to control natural aging as shown in Figure 2 d). The temperature increase promotes the diffusion rate and the vacancies amount increase, which contribute to enhance the dislocation movements, minimizing the interactions between solute clusters and dislocations. Simultaneously, the solute clusters are expected to dissolve between 200 and 250 ºC [13, 16]. Thus, warm forming in this temperature range may contribute to reduce the influence of natural aging in the variability of the mechanical properties of the material used in the forming operation. However, during warm forming it is necessary to control the holding time in order to avoid artificial aging. Thus, in the present work, the total time considered for heating and forming was always below 2 min, which prevents the occurrence of any heat treatment change. In this work, the storage time and the temperature are controlled, aiming to find the temperature range which reduces the natural aging influence on the material behavior variability. The influence of temperature is analyzed first using tensile tests, in the following section.

3 Thermo-mechanical characterization

3.1 Experimental procedure

The thermo-mechanical behavior of both alloys was evaluated by performing uniaxial tensile tests in a Gleeble 3500 device. The uniform section of the specimen measures 40 mm length and 10 mm width. The strain fields were measured using the digital image correlation (DIC) system from ARAMIS 4M – GOM. Figure 3 presents the Gleeble 3500 device highlighting the relative position of the ARAMIS 4M cameras. The temperature was measured using type K thermocouples welded on the specimen surface. As shown in Figure 3 c), one thermocouple of control (TC1) was placed in the specimen's middle, followed by three measurement thermocouples in the same straight line, with a distance of six millimeters between each other (TC2, TC3 and TC4). In the Gleeble device the specimen is heated by direct resistance (Joule heating effect), which results in a higher temperature on its center [32, 33]. This thermal gradient in the specimen's length direction can promote heterogeneous mechanical properties [34]. Therefore, in order to minimize this effect in the determination of the stress-strain curves, a rectangular gauge measurement area of 3 mm length and 6 mm width, positioned in the specimen's middle (see Figure 3 c)), is used to compute the strain. According to Coër et al. [34], this gauge area assures a temperature gradient lower than 1℃. Lastly, the heating time is fixed to 20 seconds in order to minimize microstructural modifications and assuring that the required temperature in the specimen center is achieved. The heating stage is immediately followed by the tensile test, corresponding to the warm forming step shown in Figure 2 d).

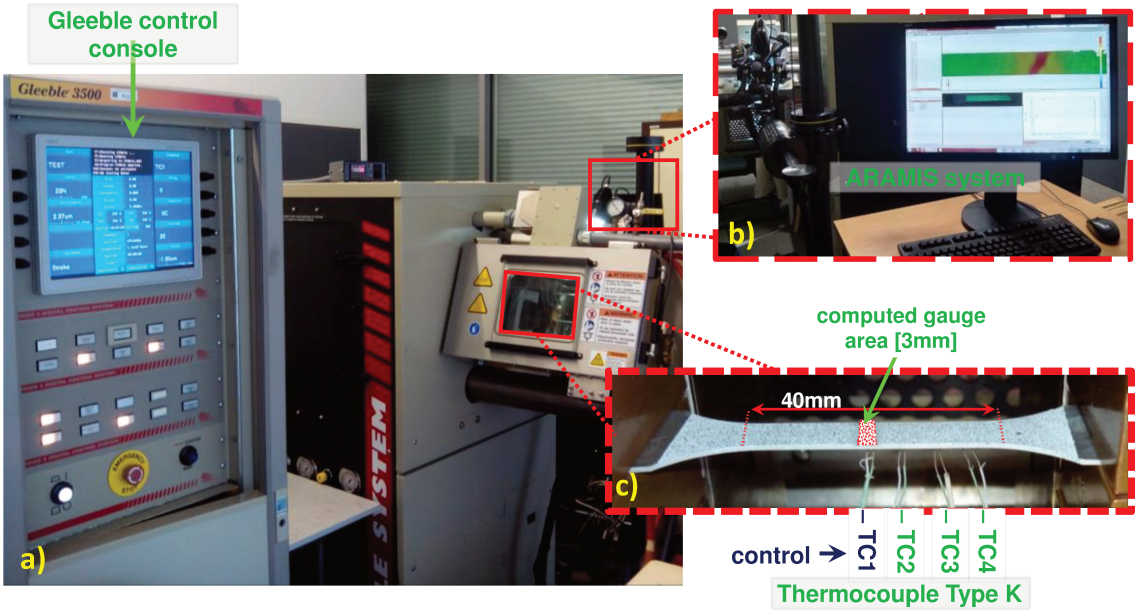

Figure 3 – a) Gleeble 3500 device and ARAMIS 4M system, highlighting: b) the cameras position and, c) the tensile test specimen.

The tensile tests were performed at RT (≈22), 100, 150, 200 and 300 ℃, considering an imposed initial strain rate of ≈ $2x10^{-3}s^{-1}$. The in-plane anisotropic behavior was studied from RT up to 200 ℃, using specimens cut along three different directions in the sheet plane: 0, 45 and 90 °, with the rolling direction (RD).

The natural aging effect was evaluated for both alloys by performing tensile tests at 1 and 7 months of storage time. For the EN AW 6016-T4 alloy, the analysis of the natural aging effect was performed considering the temperature range from RT, 100, 150 and 200 ℃, while for the EN AW 6061-T6 alloy only the two extreme values were considered. A minimum of two tensile tests were performed for each test condition. The reproducibility was confirmed through the average scatter of the true stress, which was less than ±1MPa for the same true strain value. Therefore, only one representative test is presented for each condition. The tensile test results are presented as true stress – true strain plotted until the maximum load.

3.2 Results analysis and discussion

3.2.1 The hardening behavior

As explained in Section 2.1, for the EN AW 6061-T6 alloy, the storage time corresponds to the time after the reception. The true stress – true strain curves are presented in Figure 4 a) and b) for the EN AW 6016-T4 and EN AW 6061-T6 alloys, respectively. A noteworthy variation of the mechanical properties due to the storage time is observed for the EN AW 6016-T4 alloy, while for the EN AW 6061-T6 alloy it presents a negligible effect.

The dependence of the material behavior to temperature is similar for both alloys, as the temperature increases flow stress decreases and consequently, it results in lower values of $R_{p0.2}$ and R_m. These tendencies were also reported by [35, 22]. However, for the same temperature, the mechanical behavior of both alloys is distinct. In fact, the EN AW 6061-T6 alloy presents always a higher strength and a lower elongation value than the EN AW 6016-T4 alloy. At RT, Ozturk et al. [36] performed a study analyzing the mechanical behavior of the EN AW 6061 alloy in function of heat treatments. They show that the mechanical behavior of the EN AW 6061 alloy in T4 conditions is very similar to the one observed for the EN AW 6016-T4 alloy in this study. Therefore, the differences observed here-in between both alloys are mainly linked with the different heat treatments: T4 or T6.

Concerning the EN AW 6016-T4 alloy (see Figure 4 a)), the natural aging leads to an increase of the material strength, introducing also a variation of the work hardening behavior. Comparing the stress-strain curves at 1 and 7 months of natural aging, the difference in stress values for the same strain value reduces as the temperature and the strain increases. In fact, the higher difference between stress-strain curves at 1 and 7 months of natural aging is obtained at RT, and the lower at 200 ℃. At 200 ℃, the natural aging effect is still observed by the increase of the $R_{p0.2}$ value. However, for strain values higher than 10%, the stress-strain curves of 1 and 7 months aged specimens present a similar hardening behavior with approximately the same R_m value. In fact, previous studies have report a dissolution of Mg-Si co-clusters that occurs for the temperature range from 200 ℃ to 250 ℃ [13, 16]. At 200 ºC, the time necessary to attain a strain of 10% is 40 seconds. Taking into account the heating time of 20 seconds, the analysis of the

stress-strain curves indicates that the time to dissolve natural aging Mg-Si co-clusters is about 60 seconds.

In order to better understand the influence of temperature on the natural aging, the true stress-true strain curves shown in Figure 4 are normalized by their stress value at 0.01, i.e. $\Delta\sigma = \sigma - \sigma_{\varepsilon=0.01}$. This normalization, presented in Figure 5, suppresses the influence of the initial yield stress value, allowing the direct comparison of the work hardening behavior for each different storage period and temperature. At RT, for both alloys, the work hardening slightly increases due to increasing storage time, as observed for other Al-Mg-Si alloys [6, 31, 37]. As the test temperature increases, the magnitude of work hardening decrease with the temperature increase is higher at 7 months of natural aging than at 1 month. This effect is more evident for the EN AW 6016-T4 alloy than for EN AW 6061-T6 alloy. In fact, for the EN AW 6016-T4 alloy, it is noticed that at RT and 100℃, the 7 months aged alloy presents a higher work hardening than the 1 month aged, while at 150℃ and 200℃ the opposite behavior is observed (see Figure 5). Thus, it can be concluded that the work hardening decreases as the test temperature increases, but such dependence to temperature is also a function of natural aging (storage time).

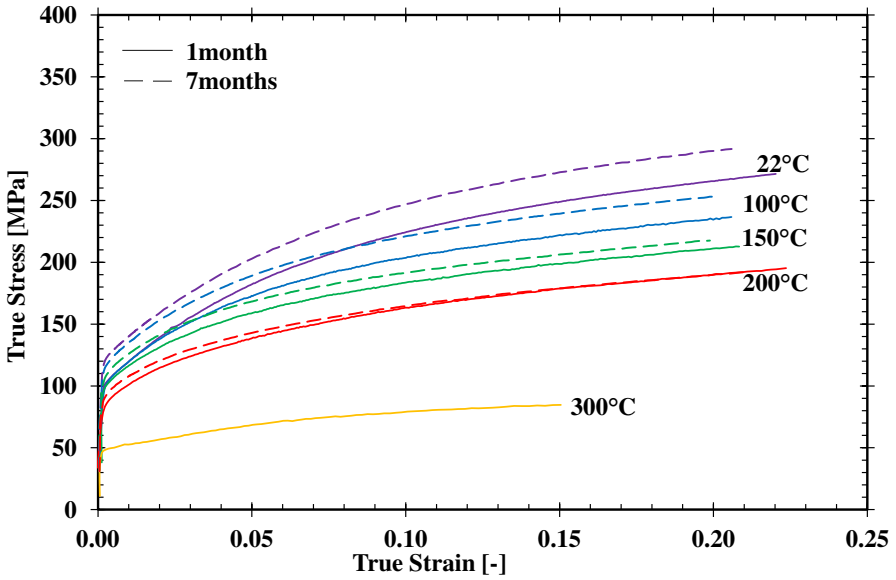

a) EN AW 6016-T4

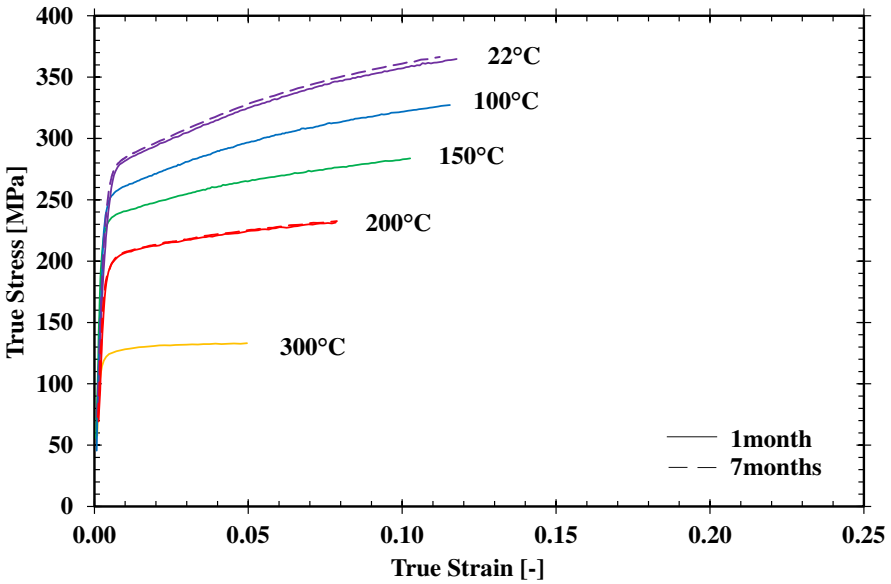

b) EN AW 6061-T6

Figure 4 – Influence of the natural aging on the true stress – true strain curves obtained from uniaxial tensile tests performed at different temperatures, for specimens oriented along the RD at 1 and 7 months of storage time. The 1 month aged material is shown by the solid line and the 7 months by the dashed line.

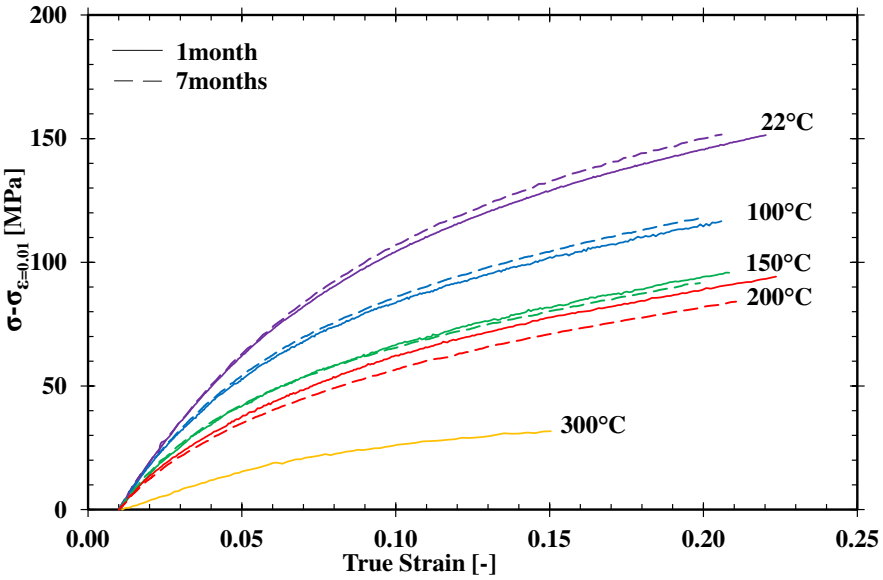

a) EN AW 6016-T4

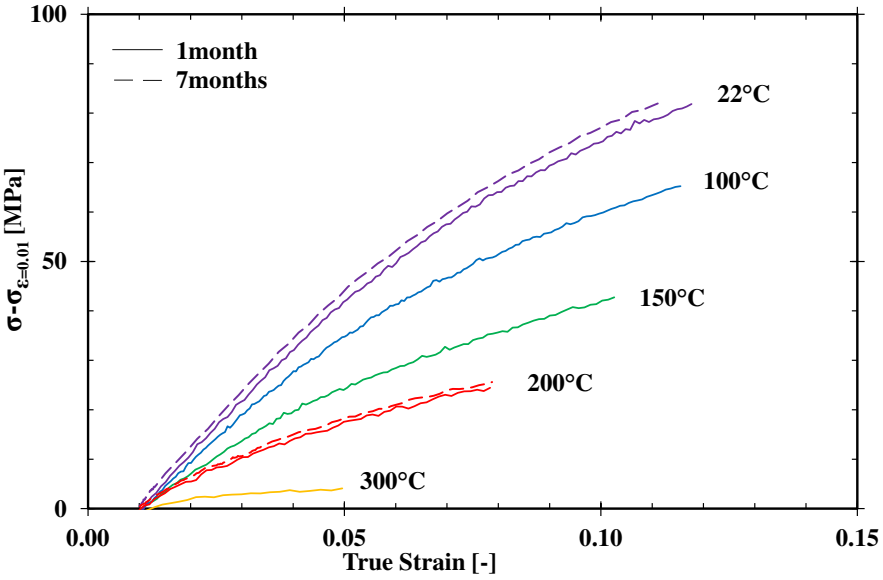

b) EN AW 6061-T6

Figure 5 – Dependence of the work hardening on natural aging and temperature: variation of true stress – true strain curves obtained by normalizing each of the curves shown in Figure 4 by its stress value at ε=0.01. Note that the scale of Figure 5 a) is twice the one of Figure 5 b).

Figure 6 presents the logarithm of the true stress as a function of the logarithm of the true strain, enabling the evaluation of the strain hardening exponent (n), which corresponds to the curves' slope; the greater this slope, the greater the n value. For the EN AW 6016-T4 alloy, the n value was determined for a strain range of 4 to 6 % (n_{4-6}) and 10 to 15% (n_{10-15}), since it presents a slight variation with strain, as shown in Table 1 (see also Figure 6 a)). For the EN AW 6061-T6

alloy, the n value was not determined for the range between 10 and 15%, since the maximum force was achieved prior to 15% of strain (see Figure 6 b)). However, the results for this alloy show that the slope is almost constant, indicating a small variation of the n value with the strain increase. At 300 ºC it presents a perfectly plastic behavior. The n values determined for both alloys are summarized in Table 3.

Globally, the results show that both alloys present a decrease of the n values with temperature and storage time increase. Moreover, whatever the temperature, the n values are always lower for the 7 months aged specimens than for 1 month ones, which for the EN AW 6016-T4 alloy are also lower than the values reported by the supplier at 4 days of maturation at RT (see Table 1). Additionally, at RT the n_{4-6} value is higher than the n_{10-15} value (also noticeable in the supplier results presented in Table 1). However, the difference between the n_{4-6} and the n_{10-15} value decreases with the temperature increase, becoming negligible for temperatures higher than 100 ºC. Lastly, for the same temperature conditions, the n value and the work hardening are lower for the EN AW 6061-T6 than for the EN AW 6016-T4 alloy. Similar dependence of the n value was reported but for other aluminum alloys, with temperature [38, 39] and with natural aging, only at RT [6, 39].

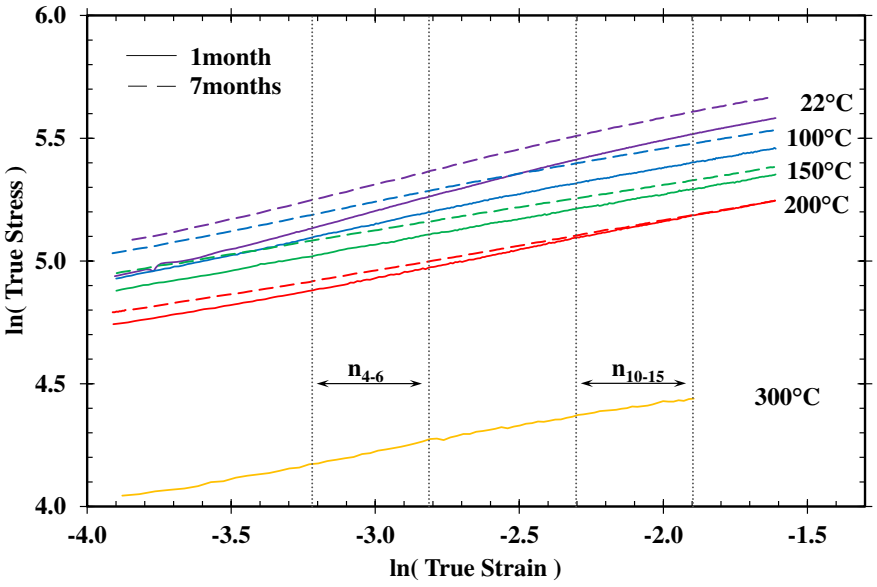

a) EN AW 6016-T4

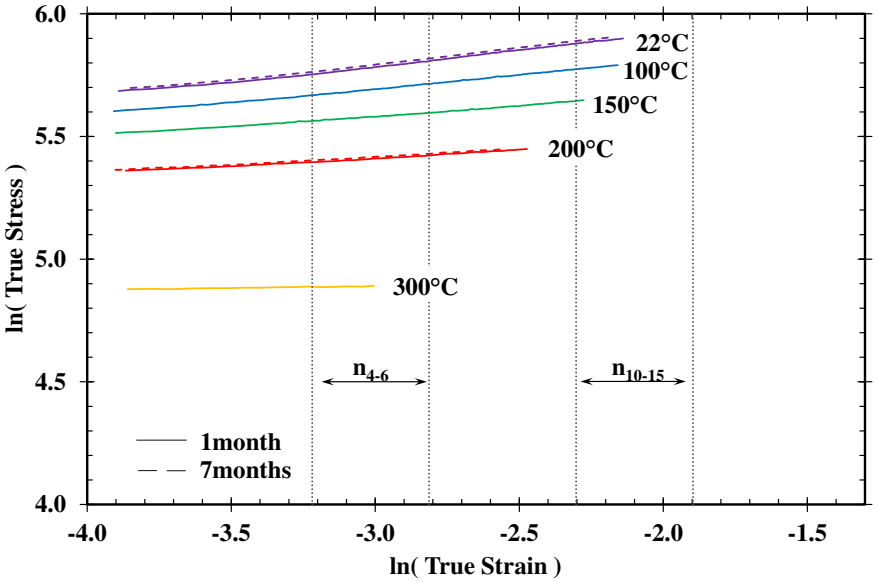

b) EN AW 6061-T6

Figure 6 – Dependence of the n value on natural aging and temperature: log (true stress) – log (true strain) curves to highlight the variations of the n value with strain. The curves are plotted over a strain range from about 0.01 up to 0.2 (for the EN AW 6016-T4) or up to the maximum load (for the EN AW 6061-T6). The results presented correspond to ones of Figure 4.

	EN AW 6016-T4				EN AW 6016-T4	
	1 month		7 months		1 month	7 months
	n_{4-6}	n_{10-15}	n_{4-6}	n_{10-15}	n_{4-6}	n_{4-6}
RT	0.318	0.258	0.275	0.239	0.135	0.129
100	0.255	0.206	0.239	0.197	0.116	-
150	0.209	0.195	0.191	0.181	0.081	-
200	0.229	0.223	0.192	0.203	0.068	0.067
300	0.230	-	-	-	-	-

Table 3 – Strain hardening exponent for the EN AW 6016-T4 and the EN AW 6061-T6 alloys. The values presented were determined along the RD.

The percentage of total elongation as a function of the temperature is presented in Figure 7, for both alloys, considering the results obtained at 1 and 7 months of storage time. The total elongation is the sum of the elastic and the plastic one ISO 6892-1:2009 [24], and its analysis is performed at maximum force (A_{gt}) and at fracture (A_t). At warm temperature, the occurrence of voids coalescence makes it difficult to identify the strain value at fracture. Therefore, the A_t values presented in Figure 7 corresponds to the first strain value (after the A_{gt}) with a stress value (σ_{At}) that complies with the requirement: $\sigma_{At} \approx R_m \times 0.9$. The values reported in Figure 7 correspond to the average of the several uniaxial tensile tests performed, including all the in-plane orientations (0, 45, 90°) to the RD. Thus, the error bars present the global minimum and maximum values obtained, with the black color associated to the 7 months tests.

Figure 7 shows that, for both alloys and whatever the temperature, the 7 months aged specimens presents a slightly lower elongation value at A_{gt} and A_t than the 1 month ones. Concerning the temperature influence between RT and 200 ℃, the A_t value increases with temperature, presenting an increase greater than 10%, for both alloys. On the other hand, the A_{gt} value remains almost constant, for the EN AW 6016-T4, or even decreases, for the EN AW 6061-T6 alloy. Moreover, in a temperature range from 200 to 300 ℃, the A_{gt} values presents an abrupt decrease for the both alloys, while the A_t values keeps increasing. It denotes that, the ductility enhancement at elevated temperatures is achieved primarily by the post-uniform elongation (i.e. the diffuse necking, the strain difference between the on-set of necking, A_{gt}, and A_t) which becomes dominant at elevated temperatures [38]. This behavior is similar to the one previously reported in [17, 18] but in that case for Al-Mg alloys, where it was stated that this overall increase of ductility

should be advantageous, since the industrial criterion for a successful sheet metal forming part only requires neither a severe thinning nor a crack in the part.

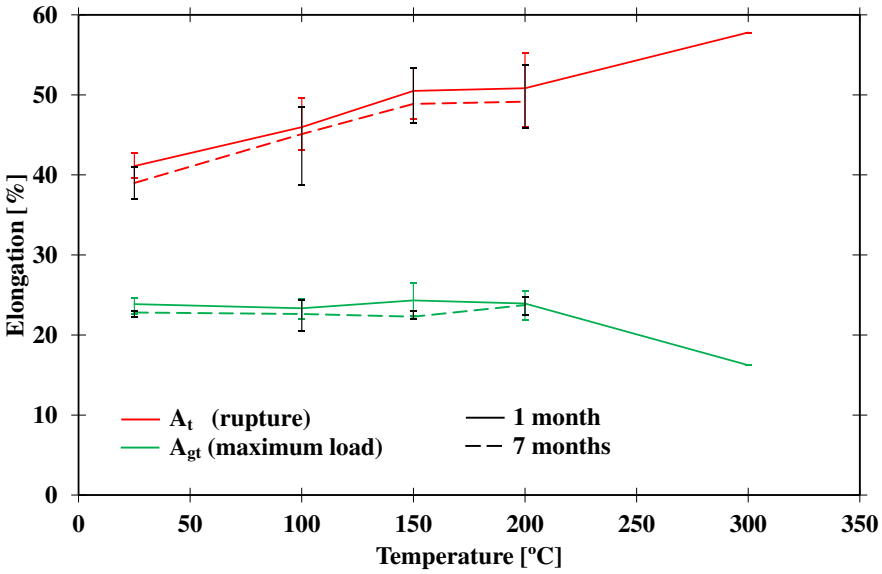

a) EN AW 6016-T4

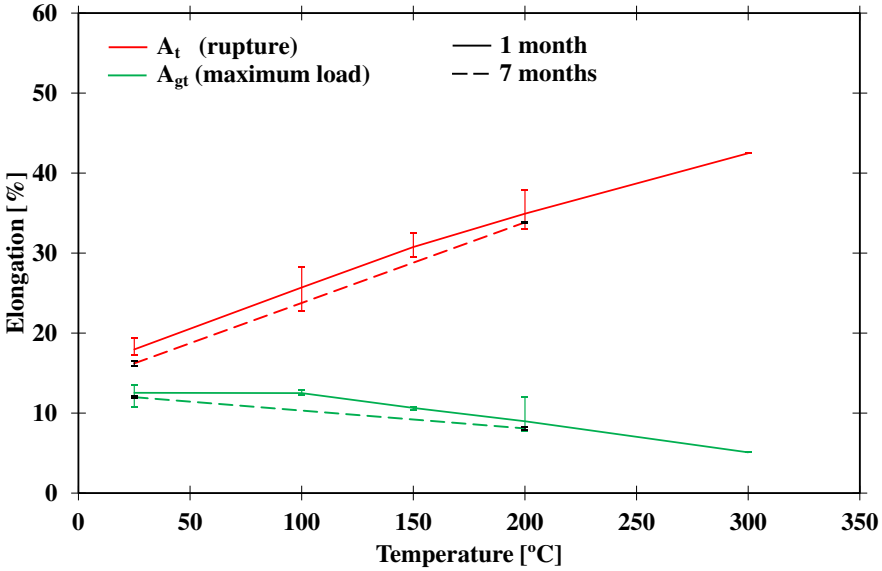

b) EN AW 6061-T6

Figure 7 – Evolution of the percentage of total elongation at maximum force (A_{gt}) and at fracture (A_t) in function of the temperature The error bars shows the minimum and maximum values obtained during all the tests performed (0, 45, 90° to the RD), with the black color associated to the 7 months' tests.

3.2.2 Strength evolution as a function of the storage time for the EN AW 6016-T4 alloy

As previously shown in Figure 4, the influence of the storage time in the change of the material behavior is more relevant for the EN AW 6016-T4 alloy and at RT. In order to better characterize the natural aging effect for this alloy, two additional tensile test were performed at RT. Figure 8 presents the true stress – true strain curves of the tensile tests performed at 1 month (26 days), 3.5 months (102 days), 7 months and 18 months of storage time, using specimens cut along the RD. Globally, the true stress – true strain curves confirm that the natural aging leads to an increase of both $R_{p0.2}$ and R_m values. This strength increase is more pronounced in the first months followed by a tendency to attain a saturation value after 7 months, showing that the formation of Mg-Si co-clusters attained a stabilization.

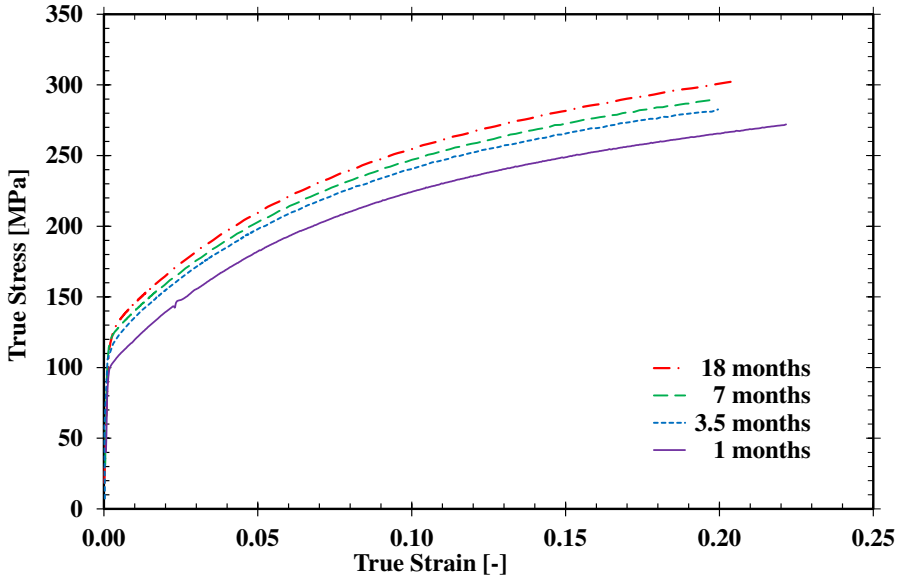

Figure 8 – The effect of natural aging for the EN AW 6016-T4 alloy on the true stress – true strain curves obtained from uniaxial tensile tests performed at RT, for specimens oriented along the RD, at 1, 3.5, 7, and 18 months of storage time.

As mentioned in the introduction, according to Esmaeili and Lloyd [8, 9] and Hirth et al. [8, 9], the strength evolution can be modeled by a logarithmic relationship with time, as follows:

$$R_{t_{NA}} = k \cdot \log(t_{NA}) + R_i, \quad (1)$$

where $R_{t_{NA}}$ is the yield stress, t_{NA} is the storage time, k is the natural aging kinetics parameter and R_i represents the initial yield stress of the alloy, measured after quenching and storage at RT

for ≈1 h [8]. According to Hirth et al. [9], although it is reasonable to apply this equation for times of commercial interest, it is not applicable for very short or very long natural aging times.

As presented in Figure 9 a), it is possible to use Equation 1 to correlate the stress evolution as a function of storage time. Both $R_{p0.2}$ and R_m values reflects a linear increase in function of the logarithm of the storage time. This enabled the determination of the parameters k and R_i of Equation 1, which are also presented in Figure 9 a). The natural aging kinetics parameter is slightly higher for the R_m value, which confirm the results of Figure 5, i.e. at RT, the natural aging also promotes an increase of the work hardening.

Figure 9 b) presents a summary of the results collected from literature for the EN AW 6016-T4 alloy, as well as the ones of Figure 9 a). The goal of Figure 9 b) is to try to present a range for the yield stress values in function of storage time, which can help to predict the influence of natural aging in sheet metal forming industrial applications. As mentioned previously, Figure 9 b) traduces the linear increase of the stress value in function of the logarithm of the storage time, according to Equation 1. Nonetheless, a high scatter of the yield stress values is observed for the same storage time, which disables any prediction of this yield stress in function of the natural aging based on literature results. In accordance with previous studies [8, 9, 27], this high scatter can be related to slight differences in the chemical composition. In fact, the parameters of Equation 1 are very sensitive to the alloy composition. Hirth et al. [9] showed that, for the EN AW 6016-T4 alloy, increasing the Si content from 1.06 to 1.39 [wt.%] (within standards chemical composition limits) the initial yield stress increases by 10%, while the natural aging kinetics remains unaltered. Indeed, Esmaeili and Lloyd [8] confirmed that increasing the Si content is linked with the initial yield stress increase. Moreover, they also showed that increasing the Cu content is linked with the increase of natural aging kinetics, while it also promotes a decrease of the initial yield stress.

In this context, it was decided to divide the literature results presented in Figure 9 b) into two groups: (i) the group of alloys where Mg+Si+Cu < 1.5 [wt.%] (in green) and (ii) the group where Mg+Si+Cu ≥ 1.5 [wt.%] (in red). The alloy considered in this study presents an amount of Mg+Si+Cu = 1.42 [wt.%] (see Table 2) and, its natural aging behavior is, in fact, similar to the other alloys located in the green region of Figure 9 b). However, the natural aging kinetics parameter also varies with the storage time, as discussed in [10, 11], and indicated in Figure 9 b)

by the change of slope for the green region. This highlights that Equation 1 is not applicable for very short or very long natural aging times [9]. Therefore, it is dangerous to extrapolate the behavior predicted by Equation 1.

In brief, it is difficult to establish a link between the parameters k and R_i and the weight percentage of the alloying elements (Mg+Si+Cu), even when considering a similar storage time, which indicates that more detailed studies are required to identify other factors affecting the natural aging. Figure 9 b) also highlights that most of the studies performed are mainly focused on short storage time periods, for which the strength variations are more significant. However, it is not possible to extrapolate the predicted behavior for the more common industrial storage time, as indicated in Figure 9 b) by the change in slope for the green region. Lastly, although the standardization of the storage time can be an effective solution to minimize the influence of natural aging on sheet metal forming parts variability [3], the results indicate that in order to be effective this requires that the amount of alloying elements remains also unchanged between different batches of the same alloy.

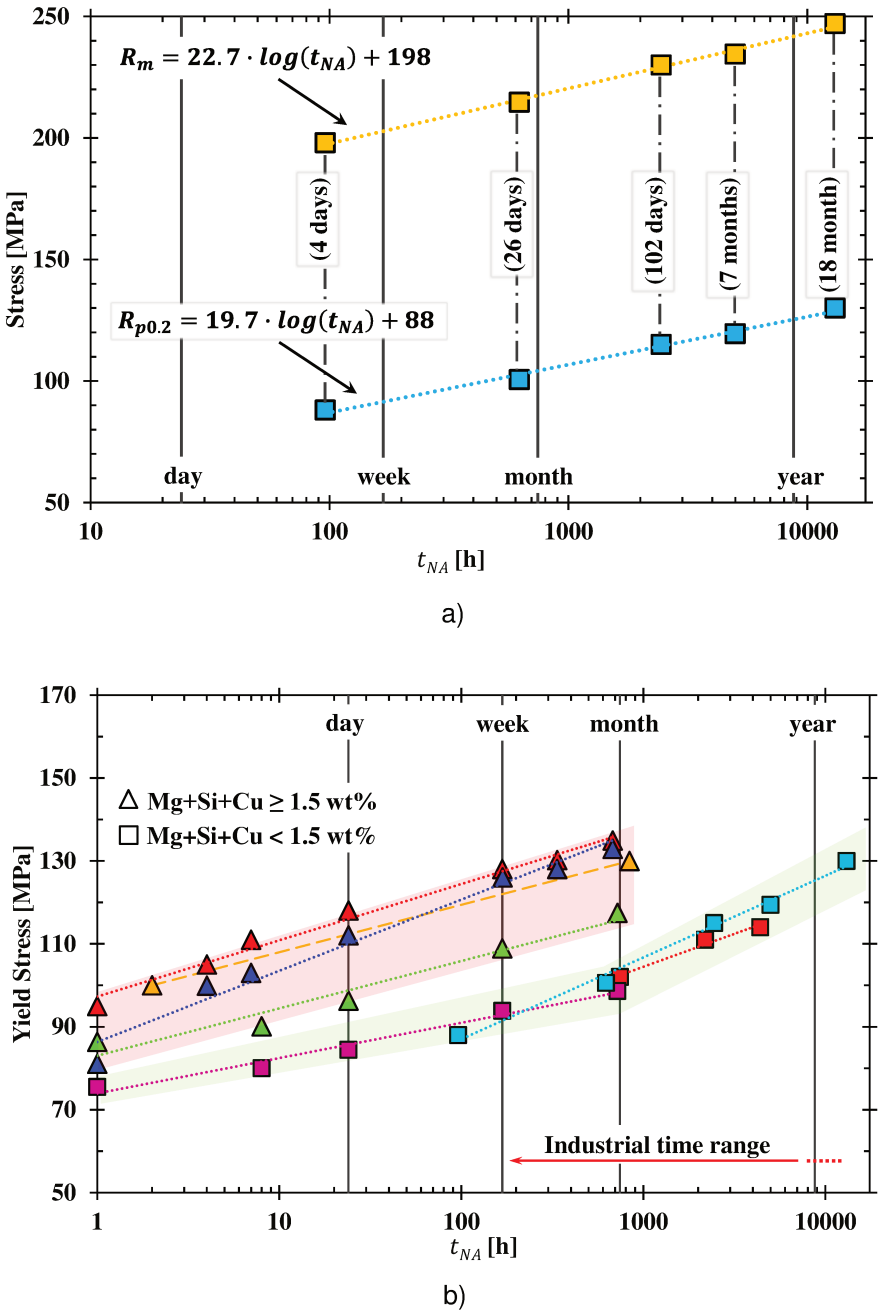

Figure 9 – The stress evolution as function of the storage time (t_{NA}) in logarithmic scale, according to Equation 1, for the EN AW 6016-T4 alloy. a) resumes the results obtained in our study, including the determination of the parameters for the Equation 1 for both $R_{p0.2}$ and R_m values; b) the results found in literature are presented with the ones of the present study in order to better understand the natural aging kinetics.

3.2.3 The orthotropic behavior

The objective of this section is to study the orthotropic behavior of both alloys in function of temperature and storage time. For the EN AW 6016-T4 alloy the in-plane anisotropic behavior was determined at 1 and 7 months of natural aging; while for the EN AW 6061-T6 alloy it was only determined at 1 month after its reception. Thus, the analysis of the evolution of orthotropic behavior in function of the storage time will be analyzed more precisely for the EN AW 6016-T4 alloy.

The anisotropy coefficient (r_α, α: angle with RD) represents the ratio between the plastic strain in the width direction (ε_{yy}^p) to the plastic strain in the thickness direction (ε_{zz}^p). During the uniaxial tensile test, the local total strain along the length (ε_{xx}) and the width (ε_{yy}) directions were acquired by the DIC system (see Figure 3). The plastic strain is obtained from the total strain by removing the elastic component. The thickness strain is determined based on the volume conservation assumption, i.e. $\varepsilon_{zz}^p = -(\varepsilon_{xx}^p + \varepsilon_{yy}^p)$. The r_α, were determined based on the linear fit between ε_{yy}^p and ε_{zz}^p, considering the test results up to the R_m point. The planar anisotropy coefficient (Δr) is calculated by: $\Delta r = (r_0 - 2 \times r_{45} + r_{90})/2$, and the normal anisotropy coefficient (r_n), by: $r_n = (r_0 + 2 \times r_{45} + r_{90})/4$.

Figure 10 presents the true stress – true strain curves obtained after 1 month of storage time for the three in-plane directions, 0, 45 and 90° to the RD, in a temperature range between RT and 200 °C, for both alloys. Globally, both alloys present a small variation of the flow stress in the sheet plane, particularly the EN AW 6061-T6 alloy. The EN AW 6016-T4 alloy shows a slightly higher strength at the RD. Additionally, although not shown here, the tensile tests performed for the EN AW 6016-T4 alloy after 7 months of storage also reveal a negligible anisotropy of the flow stress, i.e. although the natural aging effect increases the flow stress values, the trend between the different directions is the same.

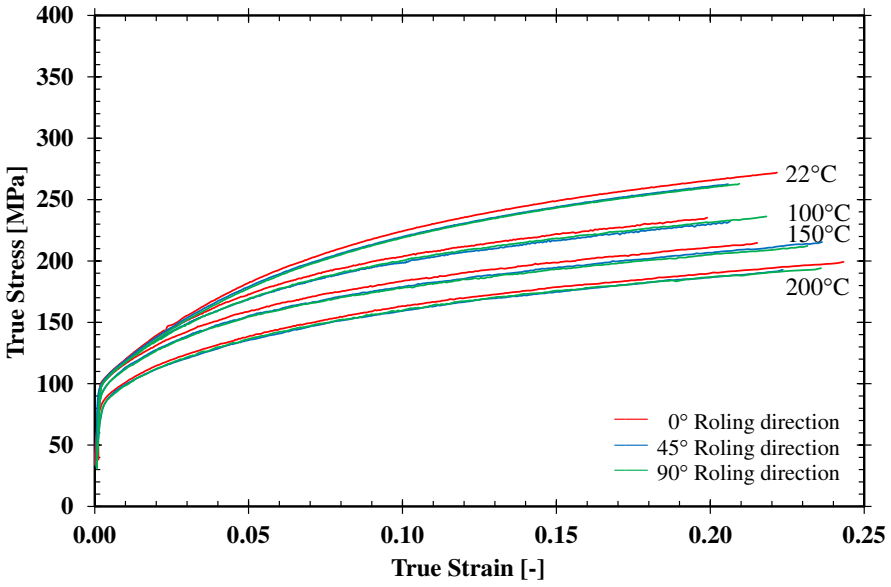

a) EN AW 6016-T4

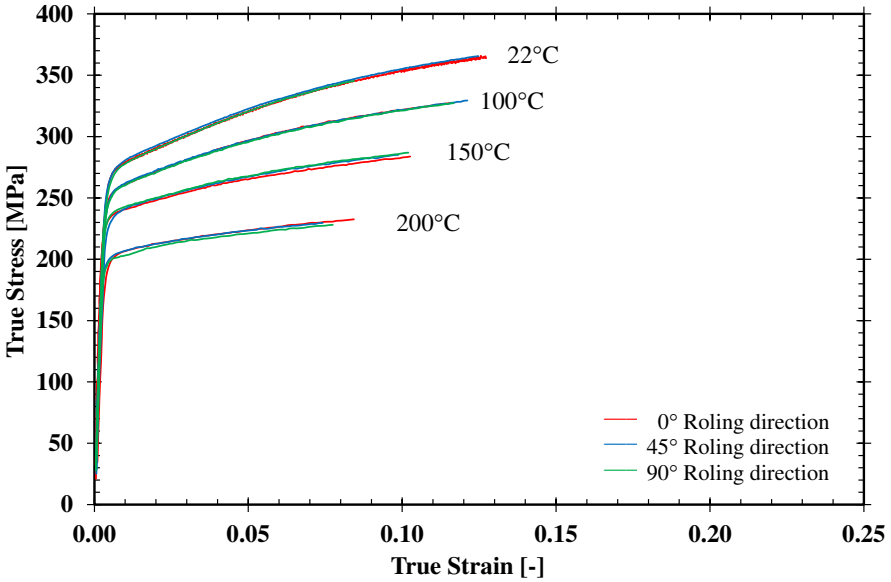

b) EN AW 6061-T6

Figure 10 – Influence of temperature and orientation to RD on the true stress – strain curves, performed from RT to 200 ℃; at 0, 45, 90° to RD. Tests performed at 1 month of storage time.

Figure 11 presents the yield stress values in function of the test temperature, for the three in-plane directions, for 1 month and 7 months of natural aging. Globally, the yield stresses in-plane anisotropic behavior is unaffected by the temperature increase. For the EN AW 6016-T4 alloy it is also visible that with the temperature increase the in-plane anisotropic behavior is not significantly affected by the natural aging.

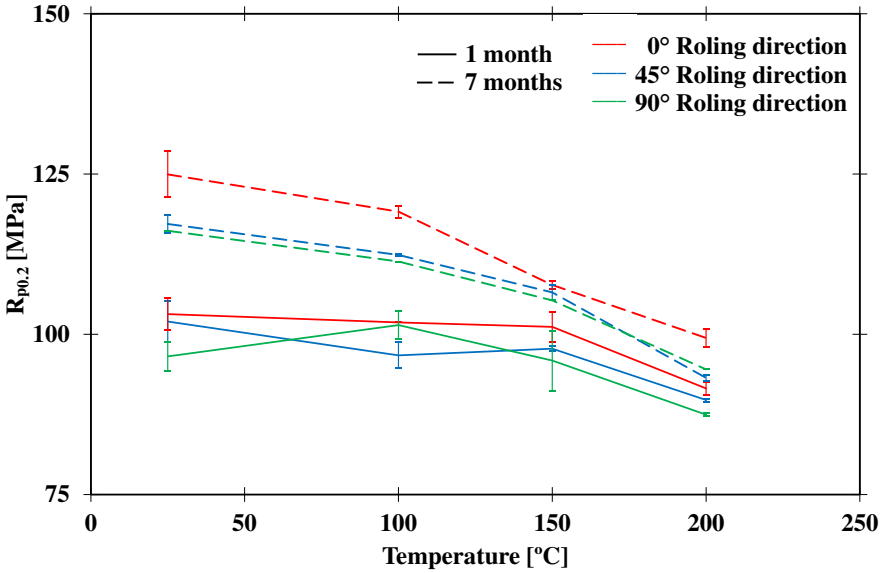

a) EN AW 6016-T4

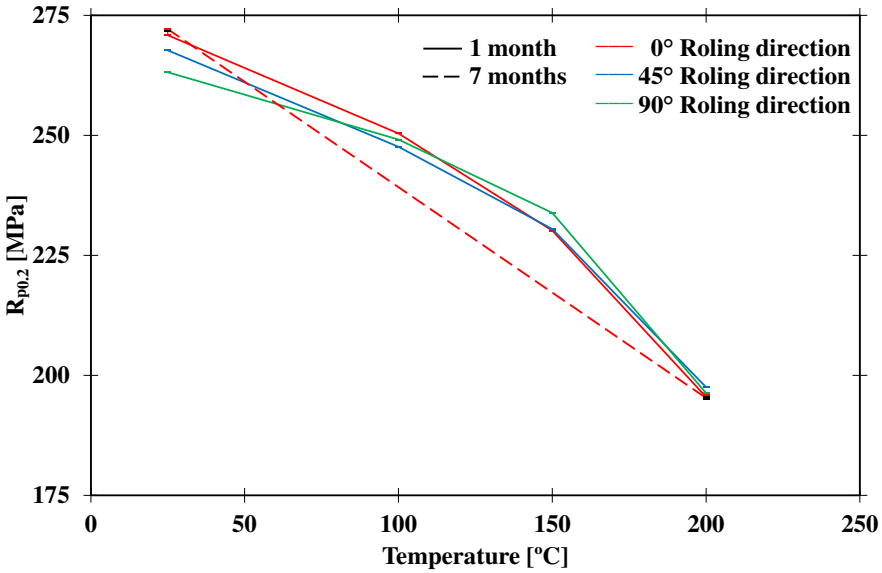

b) EN AW 6061-T6

Figure 11 – Evolution of the yield stress values as a function of the temperature, for 1 and 7 months of natural aging. The results for each temperature are an average of the tests performed at 0, 45, 90° to RD. The error bars show the minimum and maximum values obtained, with the black color associated to the 7 months' tests

The evolution of the r_α values in function of temperature, for 1 and 7 months of storage time, is presented in Figure 12 a) and b), for the EN AW 6016-T4 and the EN AW 6061-T6, respectively. For the EN AW 6016-T4, the r_α value is always lower at 45° and higher at RD, and for the EN AW 6061-T6 is lower at 90° and higher at RD, whatever the temperature under analysis. Moreover,

this trend for the r_α values remains unaltered throughout the natural aging for the EN AW 6016-T4.

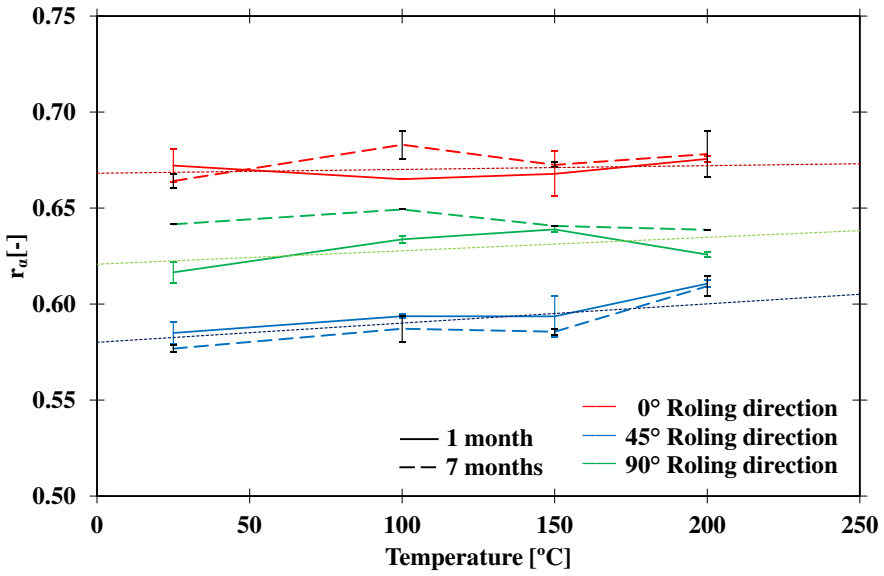

a) EN AW 6016-T4

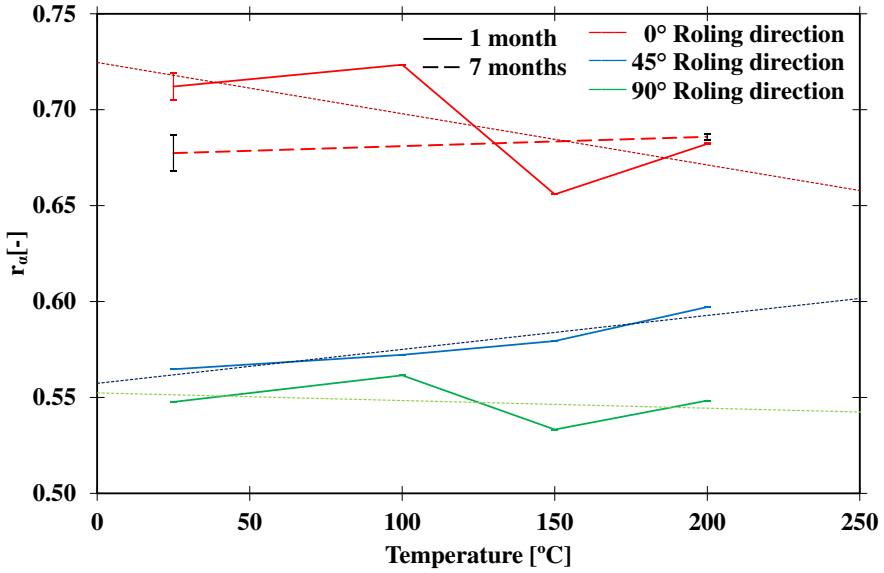

b) EN AW 6061-T6

Figure 12 – Evolution of the anisotropy coefficients as a function of temperature, at 0, 45, 90° to RD, for 1 and 7 months of natural aging. The error bars show the minimum and maximum values obtained, with the black color associated to the 7 months' tests. The dot line corresponds to the least squares trend line of results at 1 month of natural aging.

The anisotropy coefficients determined are summarized in Table 4, including the normal and the planar anisotropy coefficients. Globally, the variations of the r_n values with temperature and

natural aging are subtle. For the EN AW 6016-T4 alloy, the r_n value increases slightly with the increase of the temperature, as previously observed [40]. For the EN AW 6061-T6 alloy, the r_n value remains constant with the temperature increase. The increase of the r_n value with the increase of temperature represents an advantage, since it contributes to reduce the thinning problems during sheet metal forming. This is confirmed by the reduction of Δr value with the temperature increase, for both materials. In fact, this reduction of the Δr value indicates a trend to a more transverse isotropic behavior promoted by the temperature increase. The linear fit of the 1 month results, for the different directions, is shown in Figure 12 by the dot lines in order to highlight such trend. On other hand, for the EN AW 6016-T4 alloy, although the natural aging present negligible influence in the r_n value, it contributes to the increase of the Δr value, whatever the temperature. The present study is the first reporting the combined influence of natural aging and temperature dependence.

In brief, the degree of anisotropy remains constant, independently of the storage time, temperature or their combined influence. At RT, Leacock et al. [7] observed that prolonged natural aging of the EN AW 7075 alloy has a negligible effect on anisotropy. For the same alloys of the present study, Ghosh et al. [40] report that the temperature increase also has a negligible effect on anisotropy.

		EN AW 6016-T4					EN AW 6061-T6				
		r_0	r_{45}	r_{90}	r_n	Δr	r_0	r_{45}	r_{90}	r_n	Δr
1 month	RT	0.672	0.585	0.617	0.615	0.030	0.712	0.565	0.548	0.587	0.022
	100	0.665	0.594	0.634	0.622	0.028	0.723	0.572	0.562	0.607	0.035
	150	0.668	0.594	0.639	0.623	0.030	0.656	0.579	0.533	0.587	0.008
	200	0.676	0.611	0.626	0.631	0.020	0.682	0.597	0.548	0.606	0.009
	300	0.675	-	-	-	-	0.697	-	-	-	-
7 months	RT	0.664	0.577	0.642	0.615	0.038	0.677	-	-	-	-
	100	0.683	0.587	0.649	0.627	0.040	-	-	-	-	-
	150	0.672	0.586	0.641	0.621	0.036	-	-	-	-	-
	200	0.678	0.609	0.639	0.634	0.025	0.686	-	-	-	-

Table 4 –Average values of the anisotropy coefficients obtained for EN AW 6016-T4 and the EN AW 6061-T6 alloys, at 0, 45, 90° to RD, normal (r_n) and planar anisotropy coefficient (Δr).

4 Warm forming of a cylindrical cup

The thermo-mechanical analysis performed in the previous section indicates that natural aging and temperature have an important influence on the material mechanical behavior. However, only the EN AW 6016-T4 alloy is sensible to the natural aging, which is results in a strength increase. Moreover, it seems that the strengthening effect of natural aging becomes less important for higher test temperatures. Therefore, in the present section, the study of the impact of warm forming in the natural aging is performed only for the EN AW 6016-T4 alloy, considering 1 and 18 months of storage time. Regarding the EN AW 6061-T6 alloy, the tests were performed only for 18 months.

4.1 Experimental procedure

The cylindrical cup benchmark tests were performed in a Zwick BUP200 machine, adapted with specific tools for warm forming. This set-up was previously used to study the AA5754-O alloy [41, 42], and was also proposed in the conference Numisheet 2016, as a benchmark to evaluate the springback of an AA5086 alloy under warm forming conditions [43]. Before the forming process, a circular blank with 60 mm of diameter is cut out from the initial sheet by squaring shear in the Zwick BUP200, using a specific blade tool. To fully deep draw the cylindrical cup four tools were used: die, blank-holder, punch and ejector, as presented in Figure 13. The dimensions of the tools are also presented in Figure 13 a). All the tests were performed with a standard clamping force of 6 kN and a punch speed of 1 mm/s. During each test, the punch force and displacement, the blank-holder force and the temperature were acquired in function of time [41, 42]. A minimum of three reproducible tests were performed for each condition under analysis. Their reproducibility was confirmed through the average scatter of the punch force, which was less than ±0.1kN for the same displacement. Therefore, only one representative test is presented for each condition.

The procedure used to fully deep draw the cylindrical cup is presented in Figure 13 b) to e). Figure 13 b) shows the tools in the initial position, with the blank-holder clamping the sheet against the die. However, in the warm forming tests a previous heating step of the tools and blank is necessary. In this heating step, the die and the blank-holder are heated to the test desired temperature by internal electrical heating rods; while the punch was refrigerated to keep its temperature close to RT. When the die and the blank-holder attain the desired temperature, the

blank (lubricated with a high temperature aerosol grease 95cSt [44]) was positioned in the blank-holder. The blank is not heated at the same time than the tools, in order to reduce its heating time and, consequently, avoid microstructural modification induced by a prolonged heating stage. Due to the contact with the heated blank-holder, the blank (at RT) takes less than 60 seconds to attain the blank-holder temperature. Once the blank, the die and the blank-holder are at the test temperature (within a margin of error less than 2.5%), the blank-holder clamps the sheet against the die. Then, the punch was moved into the die's cavity (Figure 13 c)) to deform the blank to its final shape (Figure 13 d)). At the end of the drawing process the punch stops. Finally, the ejector was activated to remove the cup from the die's cavity (Figure 13 e)).

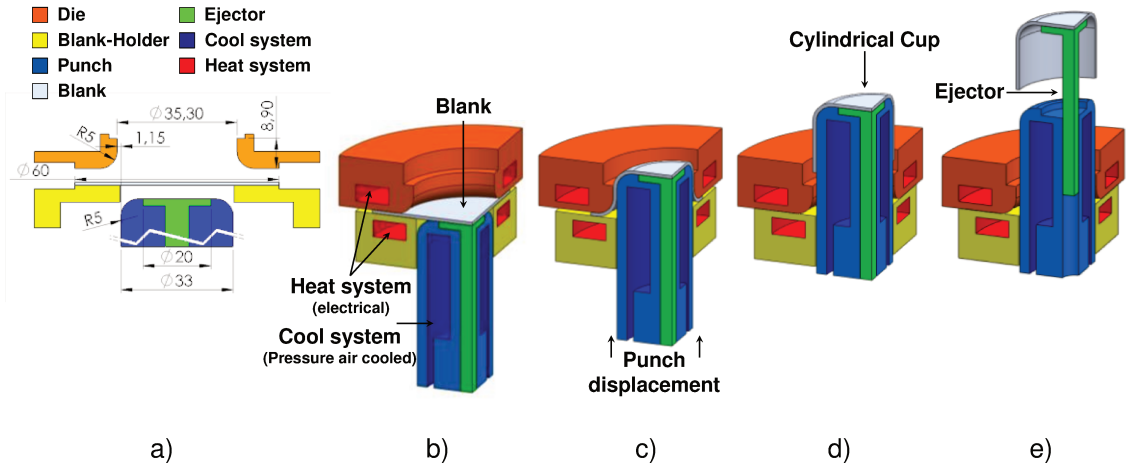

Figure 13 – Drawing of a cylindrical cup: a) Tools dimensions (in mm); b) Initial position; c) Cup drawing; d) Punch final position; and e) Ejection step.

The cylindrical cup test allows the analysis of three different type of results: a) the punch force evolution; b) the thickness distribution; and c) the cup height. Figure 14 presents the results of a test at RT, performed for the EN AW 6016-T4 alloy natural aged for 1 month, in order to enable the interpretation of common features. Figure 14 a) presents the punch force as a function of the punch displacement, highlighting two different phases: (i) the drawing and (ii) the ironing. For the test under analysis, as shown in Figure 14 a), the drawing phase occurs until a punch displacement of ≈ 21mm. During this phase, first the punch force increases rapidly until a displacement of ≈11 mm, which corresponds to the instant that the die and the punch shoulder radii are completely formed in the part (Figure 13 c)). Afterwards, it decreases until it reaches a

local minimum at ≈19mm of punch displacement, which is related to the fact that the tool presents no blank-holder stopper (see Figure 13 a)). This minimum occurs just before the loss of contact between the blank and the blank-holder, since at this stage the blank-holder promotes the movement of the sheet into the die cavity and, consequently, reduces the punch force (see detail ① in Figure 14 a)).

The ironing phase can be associated with the increase of the punch force until attaining a local maximum (≈23mm of punch displacement), followed by a decreasing until the end of the process. Ironing occurs since the gap between the punch and the die is not sufficiently large to allow the thicker material to flow. In fact, the gap between the punch and the die is 1.15 mm (see Figure 13 a)), which is higher than the initial sheet thickness (see Table 1). However, during the drawing phase, the material located in the flange area is submitted to a compression stress state in the circumferential direction (to reduce its diameter), which leads to an increase of thickness. Since, the material thickness becomes higher than the gap between the punch and the die, the ironing of the cup wall will occur (see detail ② in Figure 14 b)). Usually, the ironing is a process used to produce a more uniform wall thickness and increase the cup height. This process is very complex since the cup wall is simultaneously stretched along the axial direction and squashed between the punch and the die in the through-thickness direction [45, 46]. Moreover, the ironing process imposes high contact forces, normal to the surface of the punch and the die, which can lead to the occurrence of galling, particularly for aluminum alloys in dry contact conditions [47, 41, 42].

The thickness evolution along the cup profile is presented in Figure 14 b) as a function of the curvilinear distance from the cup center up to its top. Three distinct zones can be identified: cup bottom, punch radius and vertical wall, as shown in Figure 14 b). The two critical points, where the thickness reaches local minima, are at the entrance to the punch radius section and the confluence of the punch radius with the cup wall [48]. After that, along the cup wall, the thickness increases and attains a constant final value, due to the ironing phase. Regarding the cup height, it is mainly dependent of the initial blank diameter, but also of the friction conditions and of the magnitude of the ironing phase [47]. The cup height profile evolution is mainly linked with the material anisotropic behavior (see Figure 14 c)). However, according to Yoon et al. [46], the ironing phase tends to increase the cup height while reducing the earing profile.

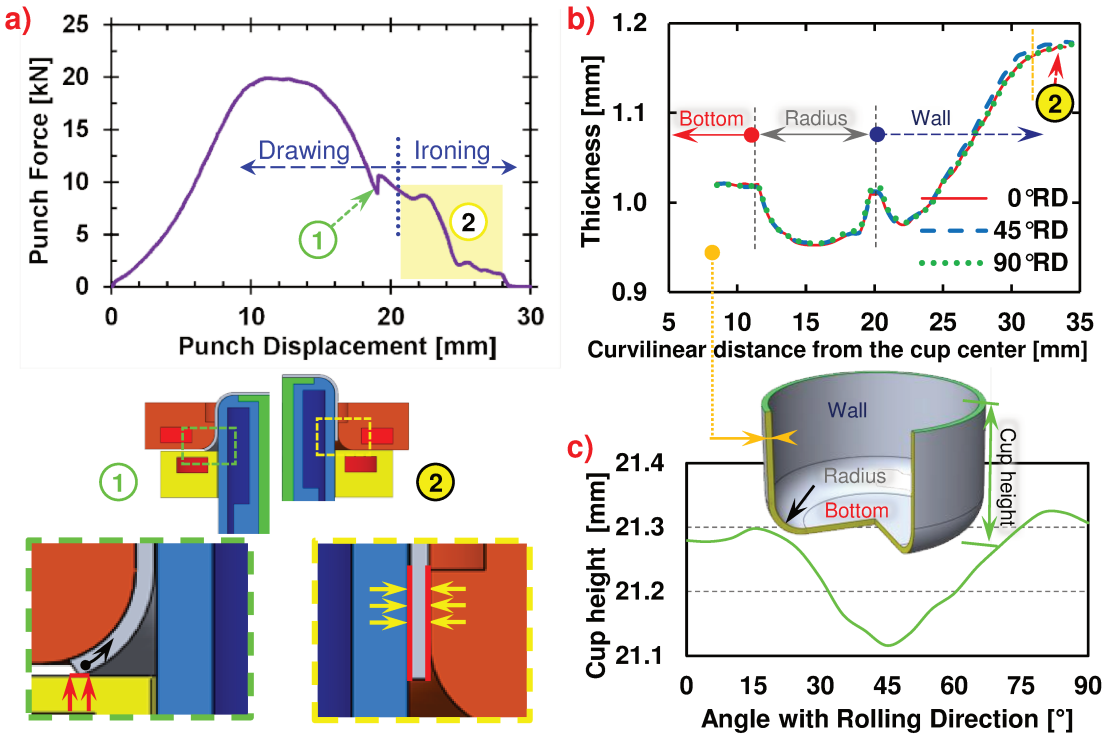

Figure 14 – Analysis of results obtained with the cylindrical cup test: a) punch force evolution as a function of its displacement; b) thickness evolution with the curvilinear distance from the cup center; and c) cup height evolution in function of the angle with RD. Detail ① the point of contact loss between the blank and the blank-holder. Detail ② the ironing phase. The results presented correspond to the EN AW 6016-T4 alloy with 1 month of natural aging, tested at RT.

The thickness and the cup height were measured at the end of the forming process using a 3D measurement machine "*Brown & Sharpe Mfg. Co.*" model "*MicroXcel PFX-454*". The thickness measurements were performed at each 45°, from 0 to 315° to RD (see Figure 15 a)), for each drawn cup. However, as presented in Figure 14 b), the thickness variations in function of the angle with RD are negligible and therefore are not analyzed in the present study. The cup height is measured at each 5° along the cup edge (the orange points on Figure 15 a)), with the first measurement point at 0° with the RD. In order to minimize the measurement errors related with axisymmetric deviations, the thickness and the height of the cup are presented as the average of the cup vertical axis symmetries (i.e. the presented 1st quadrant from 0 to 90° to RD is an average of the 1st, 2nd, 3th and 4th quadrants). It should be mentioned that the accuracy in the thickness measurements depends of: the 3D measurement machine accuracy (±3μm), the control of the positioning of the cup on the measurement device (±15μm), and of the angular deviations to the RD direction (±5μm) [41].

Springback is analyzed using the split ring test, which according to ASTM E2492-07(2012) [49], consist on: i) cut a ring from the cup wall (trimming); ii) open the ring along the RD (split ring); and iii) measure the ring opening. An electrical discharge machining (EDM) was used to open and cut the rings, as also suggested in ASTM E2492-07(2012) [49]. The variation of the ring diameter, before and after splitting, gives an indirect measure of the springback phenomenon and of the amount of the circumferential residual stresses present in the formed cup [21]. The ring opening was measured using a microscope to assure high measurement accuracy, and the EDM cut thickness (0.3 mm) was taken into account in the measured value.

In the present work two modifications were made to the standard procedure. The first is related with the sequence adopted to cut the ring from the cup: as shown in Figure 15 b), the cup was cut first along the axial direction and only afterward the rings were trimmed (Figure 15 c)). This approach was adopted to avoid the presence of any burrs on the split ring surface, which reduce the accuracy in the ring-opening measurements. In fact, with the standard procedure ASTM E2492-07(2012) [49], during the split ring operation the internal stresses present in the ring promote a sudden rupture, leading to a burr. By performing the vertical cut first, a progressive ring opening occurs during the trimming operation. It allows a better final surface and therefore accurate measurements of the ring-opening are possible. The second modification is related with the number of rings extracted from the vertical wall, which in the present case were three, each one with 3 mm height, as shown in Figure 15 c). This procedure allows a more detailed analysis of the springback behavior, since it was previously shown that the magnitude of the ring opening is influenced by its vertical position along the cup wall [50, 51].

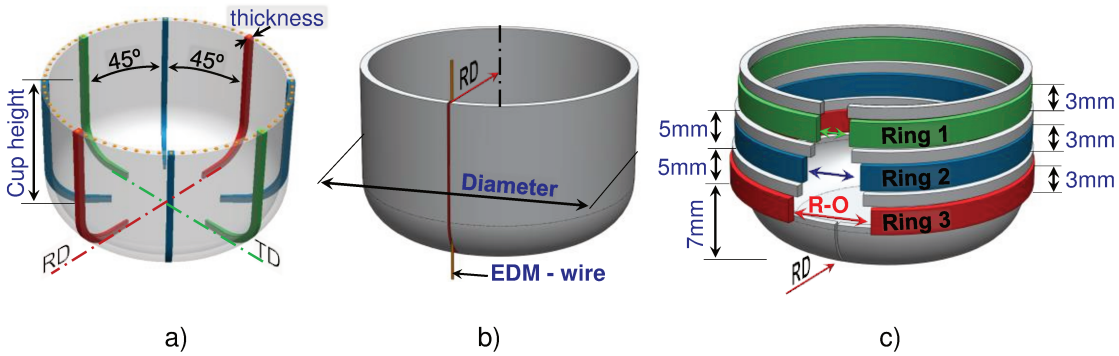

Figure 15 – Reference positions in the cylindrical cup for: a) measurements of thickness at each 45°, and of cup height at each 5° (the orange points) b) the vertical cut along RD with EDM-wire; and c) ring dimensions.

4.2 Results analysis and discussion

4.2.1 Punch force

The influence of temperature on the punch force evolution is presented in Figure 16 a) and b), for the EN AW 6016-T4 alloy and the EN AW 6061-T6 alloy, respectively. Globally, the punch force decreases with the temperature increase, which is linked to the material softening behavior resulting from the temperature increase [40, 42], as previously shown in Figure 4. The natural aging effect was evaluated only for the EN AW 6016-T4 alloy, by performing tests at 1 and 18 months of storage time. The results show an increase of the punch force due to the increase of the storage time, which is linked to the natural aging strengthening effect (see Figure 4 and Figure 9). However, this increase of the punch force due to natural aging becomes negligible as the temperature increases, which is in accordance with the results of the tensile tests (see Figure 4). Moreover, as described in Section 3.2.1, in the uniaxial tensile test at 200 ℃ the dissolution of natural aging clusters occurs for a test time of about 60 seconds. Therefore, since in the cylindrical cup test the heating phase takes 60 seconds, a significant dissolution of natural aging clusters is expected. This may contribute to minimize the variability in the punch force since the beginning of the drawing test.

The percentage variation of the maximum punch force as a function of temperature and natural aging is presented in Table 5, for the EN AW 6016-T4 and the EN AW 6061-T6 alloys, considering the drawing and the ironing stage. For both alloys, the result at RT and at 18 months of storage time is used as a reference for the percentage calculation. Regarding the influence of the

temperature increase, taking for instance the test performed at 250 ℃, it is observed a drawing force reduction of ≈50% and an ironing force reduction of ≈40%, for the EN AW 6016-T4 alloy; while for the EN AW 6061-T6 alloy, the drawing and the ironing phase present a similar percentage of punch force reduction of ≈40%. In fact, only for the EN AW 6016-T4 alloy the temperature increase seems to have a higher impact in the drawing stage than in the ironing one. Regarding the influence of natural aging on the punch force for the EN AW 6016-T4 alloy, at RT, 1 month aged specimens show a reduction of 8% in the drawing force and of 11% in the ironing force, as compared to the 18 months aged specimens. However, as the temperature increases, a decrease in the punch force variation between 1 month and 18 months aged specimens is observed.

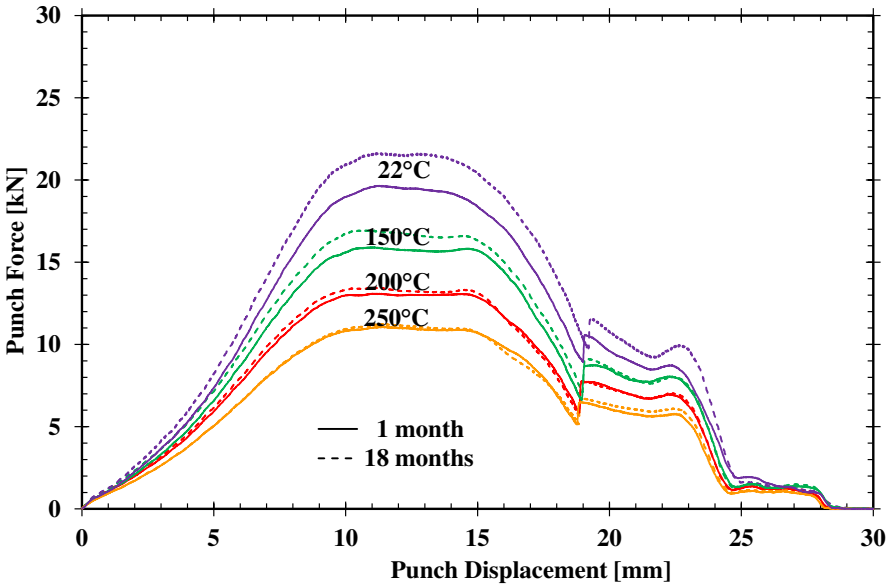

a) EN AW 6016-T4

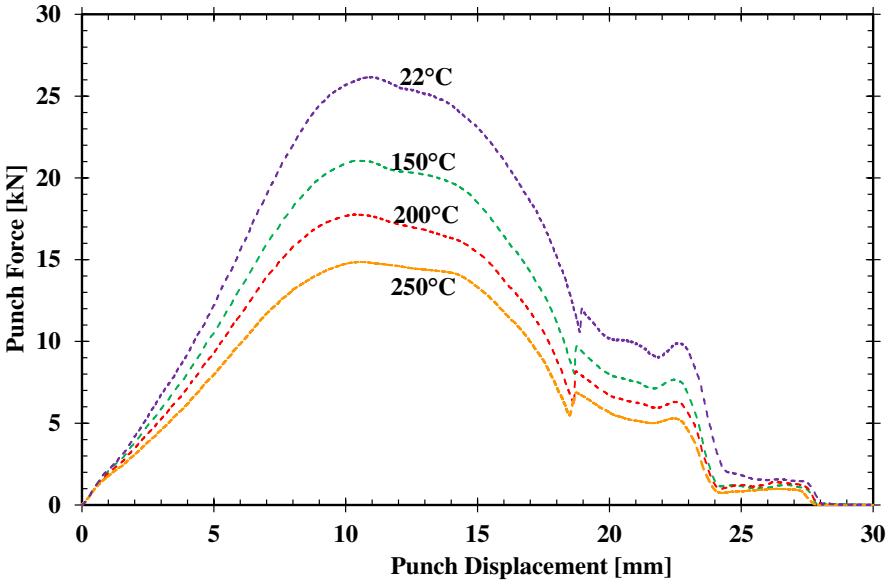

b) EN AW 6061-T6

Figure 16 – The influence of temperature and natural aging on the punch force evolution as a function of the punch displacement. The 1 month aged material is shown by the solid line and the 18 months by the dashed line.

	EN AW 6016-T4				EN AW 6061-T6	
	18 – m drawing	18 – m ironing	1 – m drawing	1 – m ironing	18 – m drawing	18 – m ironing
RT	0 %	0 %	8 %	11 %	0 %	0 %
150 ℃	21 %	21 %	25 %	20 %	19 %	21 %
200 ℃	37 %	30 %	39 %	31 %	32 %	34 %
250 ℃	48 %	38 %	48 %	38 %	42 %	40 %

Table 5 – Percentage variation of the maximum punch force as a function of temperature and natural aging, for the EN AW 6016-T4 and the EN AW 6061-T6 alloys. For both alloys, the results at RT and 18 months of storage time are chosen as reference.

4.2.2 Cylindrical Cup dimensions

The thickness evolution along the cup profile is shown in Figure 17 a) and b) for the EN AW 6016-T4 and the EN AW 6061-T6 alloys, respectively, considering only the measurements along RD. Globally, both alloys present a similar trend, with lower thickness values at the entrance to the punch radius section and the confluence of the punch radius with the cup wall. The fact that the EN AW 6061-T6 alloy presents lower thickness values is linked with its lower average initial value of 0.98mm, while the EN AW 6061-T6 alloy has 1.05mm (see Table 1).

Globally, both alloys present a similar trend with the increase of temperature. Between RT and 200 ℃, the thickness values attained for the same location in the cup are higher, with the increase of temperature. Above 200 ℃ the thickness values seem to stabilize. The higher thickness variations occur at the cup radius zone, particularly at the zone which corresponds to the entrance of the punch radius section. According to Palumbo and Tricarico [52], this can be related with the strengthening effect produced by the cooling action exerted by the punch and the material softening, due to the heated peripheral region, which reduces the required punch load and, consequently, the stress and strains levels on the punch radius section. Additionally, the maximum force attained in the ironing phase is always lower in the warm forming tests (see Figure 16), as compared to the RT one, which indicates that lower stress and strains levels are attained on the punch radius section. The lower value of maximum force attained in the ironing phase in warm forming tests is a consequence of the material thermal softening in the heated peripheral region, but it is also related with the thermal dilation of the die/punch and the consequent increase of the gap between them. In fact, considering that in warm forming conditions the temperature

distribution in the die/punch is uniform and that there are no constraints to its displacement in the radial direction, the die/punch will expand, such as:

$$\frac{r_f - r_i}{r_i} = \alpha\left[T_f - T_i\right], \quad (2)$$

where r is the radius, T is the temperature and the subscripts i and f are used for initial and final state, respectively. α is the thermal expansion coefficient, which can be assumed as constant with a value 1.19×10^{-5} K^{-1} [42]. Considering the initial radius (see in Figure 13 a)) and the maximum experimental temperature, measured for the ironing phase, the predicted gap changes from 1.15 mm to ≈1.16 mm. This increase of the gap with the increase of the test temperature is corroborated by the experimental results shown in Figure 17 and helps to explain why the warm formed cups always present a higher thickening.

As mentioned earlier, the material thickening in the flange area is a consequence of the compression stress state in the circumferential direction. The amount of thickening is mainly dictated by the material orthotropic behavior. As shown in Section 3.2.2, the changes in the alloy orthotropic behavior with the increase of temperature are very subtle. Thus, at the end of cup drawing, a similar thickening is expected whatever the test temperature. The warm forming tests present higher thickness values, as a consequence of the increase of the gap between the die and the punch, which allows a softer ironing stage.

Concerning the effect of natural aging for the EN AW 6016-T4 alloy, globally the cups obtained from 18 months stored material are slightly thicker than the ones stored during 1 month, particularly for the tests performed at RT. This seems to be mainly related with the increase in the hardening behavior induced by the natural aging (see Figure 8), which contributes to a slight change in the strain states even in the cup's bottom [53]. Moreover, this influence of natural aging in the thickness distribution reduces as the temperature increases (see Figure 17), which correlates with the hardening behavior presented in Figure 4.

The cup height distribution (or ear profile) is shown in Figure 18 a) and b) for the EN AW 6016-T4 and the EN AW 6061-T6 alloys, respectively. In the deep drawing of cylindrical cups, the ear profile is a consequence of the material anisotropic behavior. The shape of the ear profile is similar for both alloys, with maxima at RD and 90° to RD, and minimum at 45° to RD and equivalent positions. This is the expected behavior for materials presenting $\Delta r > 0$ [54](see Table 4).

Moreover, the shape of the ear profile is not affected by temperature or natural aging, confirming the subtle influence of these parameters in the materials anisotropic behavior (see Section 3.2.2). In fact, a slight decrease of the cylindrical cup ears amplitude (the difference between the maximum and minimum height) was noticed with the increase of temperature. This is in agreement with the lower value of Δr reported for the tensile tests at 200℃ (see Table 4) as well as with other warm forming results [40, 42]. Lastly, in agreement with the slight increase of the Δr value due to natural aging, the amplitude of the cup ears is higher for the 18 months aged material, when compared with 1 month.

To conclude, there is a relation between the average cup height and the thickness distribution, since a higher cup height occurs associated with a higher thinning at the cup radius zone. Therefore, the higher values of cup height are reported for the RT tests, and the cup height decreases with the increase of the temperature. Finally, concerning the effect of natural aging for the EN AW 6016-T4 alloy, as previously mentioned, the cups obtained from 18 months stored material are slightly thicker than the ones stored during 1 month and, consequently, its height profile is slightly lower. This effect is more relevant at RT and, according to results obtained with finite element analysis [53], are mainly related with the increase in the hardening behavior induced by the natural aging (see Figure 8). This also explains why the small differences in the cup thickness and height profile due to natural aging are minimized with the increase of the forming temperature.

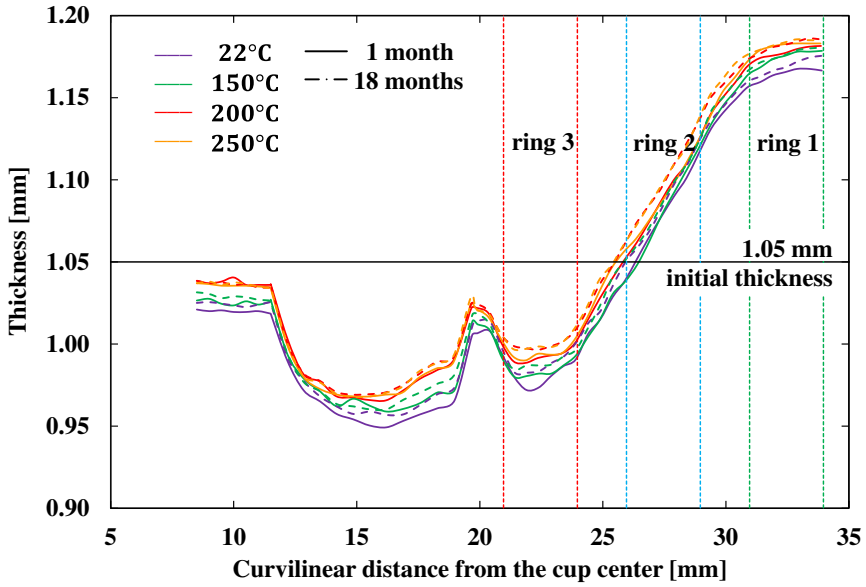

a) EN AW 6016-T4

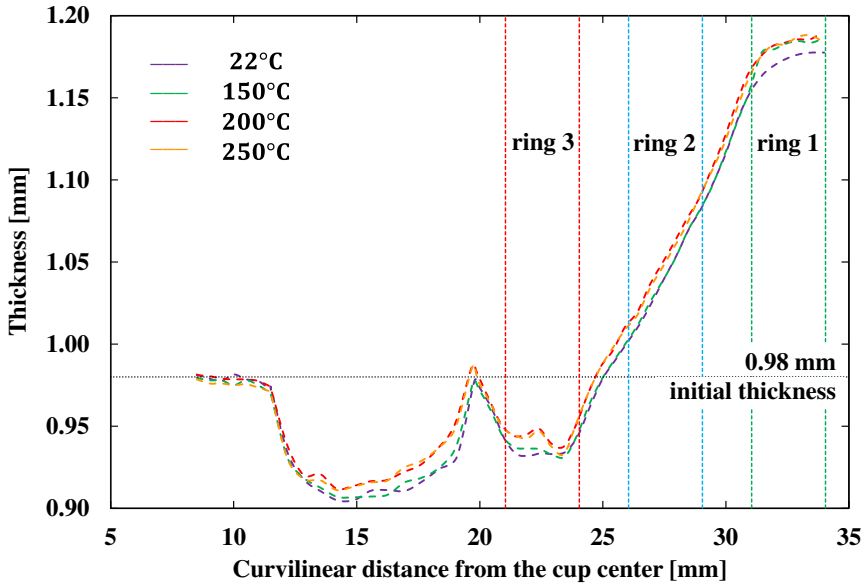

b) EN AW 6061-T6

Figure 17 – The influence of temperature and natural aging on the cup thickness. The 1 month aged material is shown by solid line and the 18 months by dash dot line.

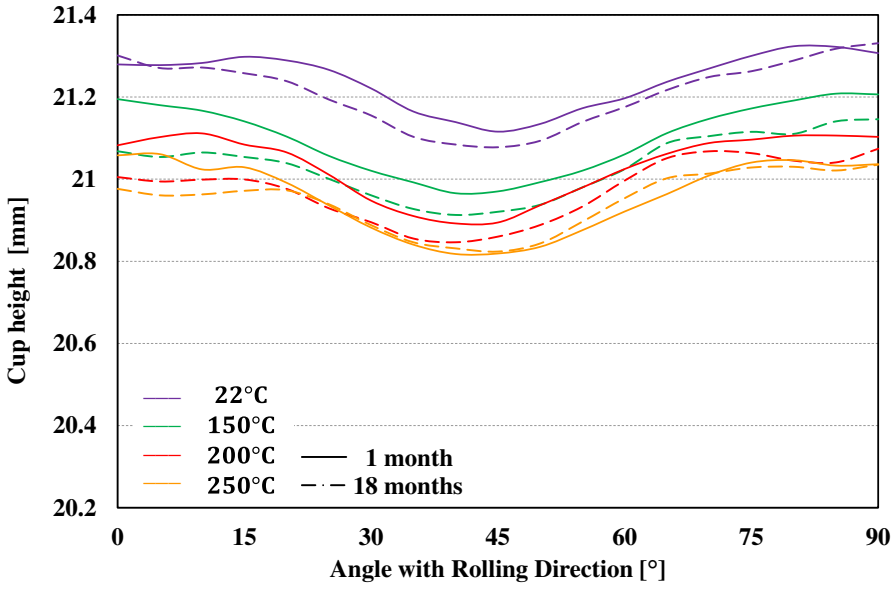

a) EN AW 6016-T4

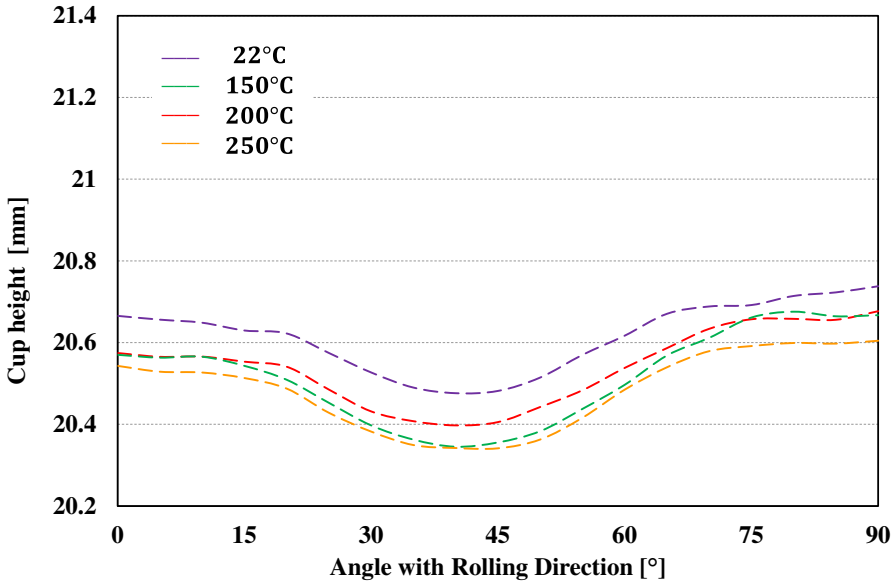

b) EN AW 6061-T6

Figure 18 – The influence of temperature and natural aging on the cup height. The 1 month aged material is shown by solid line and the 18 months by dash dot line.

4.2.3 Springback: the split ring test

As shown in Figure 15 c), three rings were cut out from the cup wall at various heights. The measurements of the three rings opening are shown in Figure 19 a) and b) for the EN AW 6016-T4 and the EN AW 6061-T6 alloys, respectively. Concerning the influence of the axial position of the ring in the cup wall, it is observed that ring 3 (near to cup bottom) presents the highest opening

value, while ring 1 (at the cup top) presents the lowest one, i.e. the ring opening shows a decreasing value as the distance to the cup bottom increases. This trend occurs for both materials tested, at RT and warm forming; therefore, it cannot be assigned to the test temperature and the material behavior. It should be mentioned that different trends have been reported, such as the increase of the ring opening with the increase of the distance to the cup bottom [50], or the highest ring opening for the one located closer to the middle of the vertical wall [51]. However, the ring opening trend is dictated by the distribution of the residual stresses in the cup, which depends on the specific combination of forming parameters selected to perform the deep drawing operation. This includes: the depth and diameter of the cup; the bending radii of the tools; the gap between the die and the punch, and; the blank-holder force [55]. In the particular case under analysis, it is also influenced by the occurrence of the ironing stage, which contributes to the reduction of the circumferential stress component through-thickness gradient, leading to a smaller ring opening, as observed in [56, 57].

The rings opening evolution as a function of temperature is similar for both alloys, i.e. the opening of the rings 2 and 3 (middle ring and bottom ring) decreases linearly as the temperature increases, while ring 1 (at the cup top) presents an opening value relatively constant. In rings 2 and 3, the springback reduction is attributed to the material softening behavior promoted by the temperature increase [21, 58], which reduces the magnitude of the circumferential residual stresses in the deep drawn cups and, consequently, the ring opening. The fact that ring 1 presents a relatively constant springback value as the temperature increases, seems to be connected to the reduction of the through-thickness gradient of the circumferential stress component, induced by the ironing stage (see Figure 17). Comparing the tests performed at RT with the ones at 250 ºC, and considering as example ring 2 (at the middle): the EN AW 6016-T4 alloy with 18 months of storage time presents a springback decrease of 16%; while the EN AW 6061-T6 alloy presents a decrease of 26%. In this context, the results are coherent with the fact that the increase of temperature presents a stronger effect in the yield stress for the EN AW 6061-T6 alloy (see Figure 4). In fact, it is known that for the same Young modulus value, springback increases with the increase of the yield stress [59]. Therefore, for the same temperature, the EN AW 6016-T4 alloy always presents a lower springback value.

As shown in Figure 19 a) for the EN AW 6016-T4, the influence of natural aging in the springback variability is maximal at RT and decreases as the temperature increases, being negligible from 200 ºC. The springback variability increases as the storage time increases, which is coherent with the variation reported for the yield stress as a function of natural aging (see Figure 4 and Figure 8). These results confirm the potential of warm forming to minimize the influence of natural aging on springback variability, while also reducing springback.

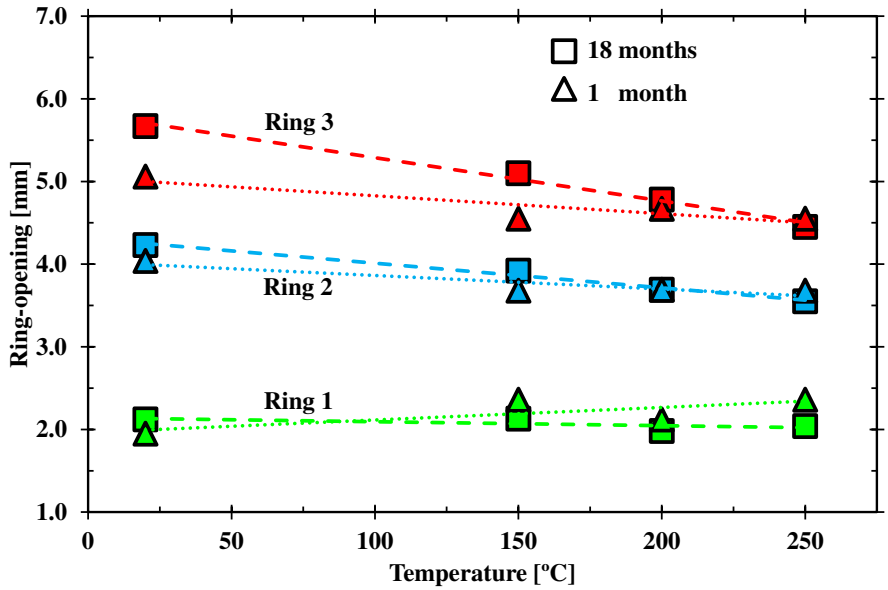

a) EN AW 6016-T4

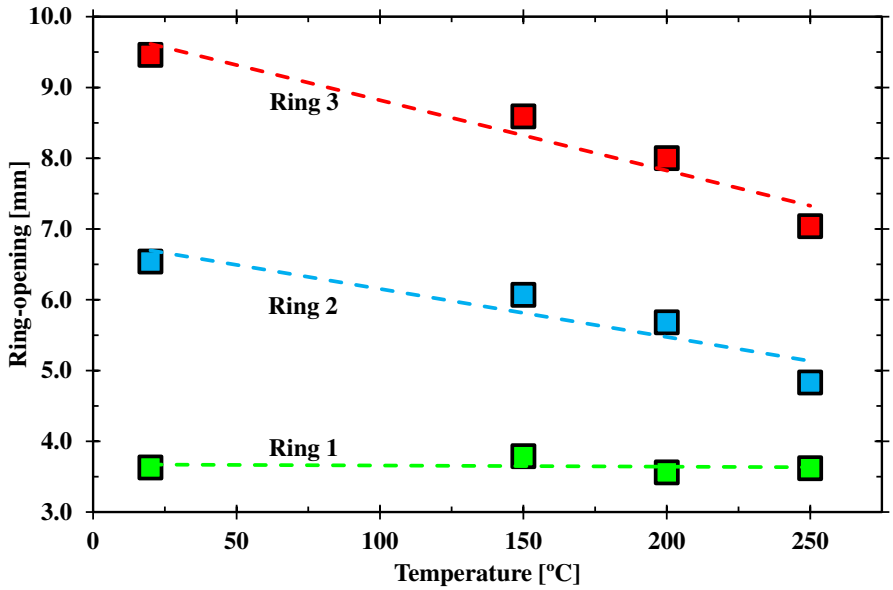

b) EN AW 6061-T6

Figure 19 – The influence of temperature and natural aging on the ring opening

5 Conclusions

Natural aging occurs in heat treatable aluminum alloys during its storage at RT. Storage time promotes the increase of the material strength and a slight variation of ductility and orthotropic behavior. These changes of the mechanical behavior cause variability in sheet metal forming operations, namely in the parts shape, as well as in-service behavior. The solutions proposed in the literature to control the natural aging cannot definitely suppress it; they can only stabilize the natural aging during reduced time spans, which is not enough for industrial practice. Therefore, the variability caused by the natural aging is still an open issue. Previous studies have shown that temperatures around 200 ºC contribute to dissolve natural aging solute clusters. Thus, the present work tests the effectiveness of warm forming conditions to reduce the variability of the mechanical behavior caused by natural aging, which never been reported in the literature.

Two Al-Mg-Si alloys (EN AW 6016-T4, EN AW 6061-T6) were analyzed using uniaxial tensile tests, cylindrical cup deep drawing tests and the split ring (springback) tests. The results show that:

- only the mechanical behavior of the EN AW 6016-T4 alloy is strongly influenced by natural aging. At RT (from 1 to 18 months), the yield stress and tensile strength increase as the storage time increases, which leads to an increase of the maximum drawing forces (about 10%) and springback (about 10%).
- for both alloys, the temperature increase leads to a decrease of the yield stress and the work hardening rate. Compared to RT, warm forming reduces the drawing forces, indicating the presence of lower internal stress, which leads to lower springback values.
- the temperature increase leads to an increase of the post-uniform elongation, which is higher for the EN AW 6061-T6 alloy than for the EN AW 6016-T4 alloy, although it has small influence in uniform elongation. This increase in ductility is advantageous to improve formability in sheet metal forming parts.
- concerning the orthotropic behavior, the trend does not change due to natural aging or temperature increase. However, the planar anisotropy coefficient slightly increases due to natural aging and decreases due to the temperature increase.

- the temperature increase reduces the influence of natural aging in the variations of yield stress and tensile strength. Thus, whatever the storage time, in warm forming between 200 and 250 ℃, the drawing force required to produce the cylindrical cups is nearly the same, as well as the thickness evolution along the cup, and the springback.

In summary, the results highlight the potential of warm forming in a temperature range from 200 to 250 ℃ as an effective solution to minimize the influence of natural aging in sheet metal forming parts variability. Moreover, warm forming contributes to the increase of formability and springback reduction. From an industrial point of view, warm forming can also be used to reduce the variability coming from different batches or different manufacturers.

Acknowledgements

The authors would like to acknowledge the funding that sponsored this research work: the national funds from the French Ministry of Higher Education and the Portuguese Foundation for Science and Technology (FCT) via the project P2020-PTDC/EMS-TEC/6400/2014 (POCI-01-0145-FEDER-016876) and by UE/FEDER funds through the program COMPETE 2020, under the project CENTRO-01-0145-FEDER-000014 (MATIS). The first author V. Simões is also grateful to the FCT for the PhD grant SFRH/BD/90669/2012. The authors are also grateful to Constellium (Estelle Muller) for supplying the material. Moreover, the authors acknowledge the technical staff of IRDL, for their help in some of the experimental procedures (Anthony Jégat and Hervé Bellegou).

Compliance with Ethical Standards

Funding: This study was funded by the French Ministry of Higher Education and the Portuguese Foundation for Science and Technology (FCT) via the project P2020-PTDC/EMS-TEC/6400/2014 (POCI-01-0145-FEDER-016876) and by UE/FEDER funds through the program COMPETE 2020, under the project CENTRO-01-0145-FEDER-000014 (MATIS). The first author V. Simões was also funded by the FCT for the PhD grant SFRH/BD/90669/2012.

Conflict of Interest: The authors declare that they have no conflict of interest.

References

1. Miller WS, Zhuang L, Bottema J, et al (2000) Recent development in aluminium alloys for the automotive industry. Mater Sci Eng A 280:37–49 . doi: 10.1016/S0921-5093(99)00653-X

2. Hirsch J (2011) Aluminium in innovative light-weight car design. Mater Trans 52:818–824

3. Suri R, Otto K, Boothroyd G (1999) Variation Modeling for a Sheet Stretch Forming Manufacturing System. CIRP Ann - Manuf Technol 48:397–400 . doi: 10.1016/S0007-8506(07)63211-9

4. Prillhofer R, Rank G, Berneder J, et al (2014) Property Criteria for Automotive Al-Mg-Si Sheet Alloys. Materials 7:5047–5068 . doi: 10.3390/ma7075047

5. Marretta L, Lorenzo RD (2010) Influence of material properties variability on springback and thinning in sheet stamping processes: a stochastic analysis. Int J Adv Manuf Technol 51:117–134 . doi: 10.1007/s00170-010-2624-4

6. Zhong H, Rometsch P, Cao L, et al (2010) Tensile properties and work hardening behaviour of alloy 6016 in naturally aged and pre-aged conditions. In: Proceedings of the 12th International Conference on Aluminium Alloys. Japan Institute of Light Metals, Tokyo, Japan, pp 2203–2208

7. Leacock AG, Howe C, Brown D, et al (2013) Evolution of mechanical properties in a 7075 Al-alloy subject to natural ageing. Mater Des 49:160–167 . doi: 10.1016/j.matdes.2013.02.023

8. Esmaeili S, Lloyd DJ (2004) Effect of composition on clustering reactions in AlMgSi(Cu) alloys. Scr Mater 50:155–158 . doi: 10.1016/j.scriptamat.2003.08.030

9. Hirth SM, Marshall GJ, Court SA, Lloyd DJ (2001) Effects of Si on the aging behaviour and formability of aluminium alloys based on AA6016. Mater Sci Eng A 319–321:452–456 . doi: 10.1016/S0921-5093(01)00969-8

10. Werinos M, Antrekowitsch H, Ebner T, et al (2016) Hardening of Al–Mg–Si alloys: Effect of trace elements and prolonged natural aging. Mater Des 107:257–268 . doi: 10.1016/j.matdes.2016.06.014

11. Banhart J, Lay MDH, Chang CST, Hill AJ (2011) Kinetics of natural aging in Al-Mg-Si alloys studied by positron annihilation lifetime spectroscopy. Phys Rev B 83:14101 . doi: 10.1103/PhysRevB.83.014101

12. H.Y. Hunsicker (1984) Chapter 5 - Metallurgy of Heat Treatment and General Principles of Precipitation Hardening. In: John E. Hatch (ed) Aluminum: Properties and Physical Metallurgy, Subsequent edition. ASM International, Metals Park, Ohio, pp 134–199

13. Pogatscher S, Antrekowitsch H, Leitner H, et al (2011) Mechanisms controlling the artificial aging of Al–Mg–Si Alloys. Acta Mater 59:3352–3363 . doi: 10.1016/j.actamat.2011.02.010

14. Engler O, Schäfer C, Myhr OR (2015) Effect of natural ageing and pre-straining on strength and anisotropy in aluminium alloy AA 6016. Mater Sci Eng A 639:65–74 . doi: 10.1016/j.msea.2015.04.097

15. Ding L, Weng Y, Wu S, et al (2016) Influence of interrupted quenching and pre-aging on the bake hardening of Al–Mg–Si Alloy. Mater Sci Eng A 651:991–998 . doi: 10.1016/j.msea.2015.11.050

16. Yan Y (2014) Investigation of the negative and positive effect of natural aging on artificial aging response in Al-Mg-Si alloys. PhD-thesis, Technische Universität Berlin

17. Ayres RA (1977) Enhanced ductility in an aluminum-4 Pct magnesium alloy at elevated temperature. Metall Trans A 8:487–492 . doi: 10.1007/BF02661760

18. Shehata F, Painter MJ, Pearce R (1978) Warm forming of aluminium/magnesium alloy sheet. J Mech Work Technol 2:279–290 . doi: 10.1016/0378-3804(78)90023-2

19. Bolt PJ, Lamboo N, Rozier P (2001) Feasibility of warm drawing of aluminium products. J Mater Process Technol 115:118–121

20. Kim HS, Koç M (2008) Numerical investigations on springback characteristics of aluminum sheet metal alloys in warm forming conditions. J Mater Process Technol 204:370–383 . doi: 10.1016/j.jmatprotec.2007.11.059

21. Grèze R, Manach PY, Laurent H, et al (2010) Influence of the temperature on residual stresses and springback effect in an Aluminium alloy. Int J Mech Sci 52:1094–1100 . doi: 10.1016/j.ijmecsci.2010.04.008

22. Mahabunphachai S, Koç M (2010) Investigations on forming of aluminum 5052 and 6061 sheet alloys at warm temperatures. Mater Des 1980-2015 31:2422–2434 . doi: 10.1016/j.matdes.2009.11.053

23. Banhart J, Chang CST, Liang Z, et al (2010) Natural Aging in Al-Mg-Si Alloys - A Process of Unexpected Complexity. Adv Eng Mater 12:559–571 . doi: 10.1002/adem.201000041

24. ISO 6892-1:2009 (2009) Metallic materials - Tensile testing - Part 1: Method of test at room temperature. International Organization for Standardization, Geneva, Switzerland

25. ISO 10275:2007 (2007) Metallic materials - Sheet and strip - Determination of tensile strain hardening exponent. International Organization for Standardization, Geneva, Switzerland

26. Kaufman JG (2008) Properties of Aluminum Alloys: Fatigue Data and Effects of Temperature, Product Form, and Processing. ASM International, Materials Park, Ohio : Washington, D.C

27. Ding L, Jia Z, Zhang Z, et al (2015) The natural aging and precipitation hardening behaviour of Al-Mg-Si-Cu alloys with different Mg/Si ratios and Cu additions. Mater Sci Eng A 627:119–126 . doi: 10.1016/j.msea.2014.12.086

28. The Aluminum Association (2015) International Alloy Designations and Chemical Composition Limits for Wrought Aluminum and Wrought Aluminum Alloys

29. Milkereit B, Starink MJ (2015) Quench sensitivity of Al–Mg–Si alloys: A model for linear cooling and strengthening. Mater Des 76:117–129 . doi: 10.1016/j.matdes.2015.03.055

30. Wenner S, Nishimura K, Matsuda K, et al (2013) Muon kinetics in heat treated Al (–Mg)(–Si) alloys. Acta Mater 61:6082–6092 . doi: 10.1016/j.actamat.2013.06.050

31. Deschamps A, Esmaeili S, Poole WJ, Militzer M (2000) Strain hardening rate in relation to microstructure in precipitation hardening materials. J Phys IV 10:Pr6-151-Pr6-156 . doi: 10.1051/jp4:2000626

32. Norris SD, Wilson I (1999) Application of 3D numerical modelling for thermal profile optimization on the Gleeble thermomechanical simulator. Model Simul Mater Sci Eng 7:297

33. Martins JMP, Alves JL, Neto DM, et al (2015) Numerical analysis of different heating systems for warm sheet metal forming. Int J Adv Manuf Technol 83:897–909 . doi: 10.1007/s00170-015-7618-9

34. Coër J, Bernard C, Laurent H, et al (2011) The Effect of Temperature on Anisotropy Properties of an Aluminium Alloy. Exp Mech 51:1185–1195 . doi: 10.1007/s11340-010-9415-6

35. Kurukuri S (2010) Simulation of thermally assisted forming of aluminium sheet. PhD-thesis, University of Twente

36. Ozturk F, Esener E, Toros S, Picu CR (2010) Effects of aging parameters on formability of 6061-O alloy. Mater Des 31:4847–4852 . doi: 10.1016/j.matdes.2010.05.050

37. Thuillier S, Le Maoût N, Manach PY (2011) Influence of ductile damage on the bending behaviour of aluminium alloy thin sheets. Mater Des 32:2049–2057 . doi: 10.1016/j.matdes.2010.11.050

38. Li D, Ghosh A (2003) Tensile deformation behavior of aluminum alloys at warm forming temperatures. Mater Sci Eng A 352:279–286 . doi: 10.1016/S0921-5093(02)00915-2

39. Zhang P, Li Z, Liu B, Ding W (2016) Tensile Properties and Deformation Behaviors of a New Aluminum Alloy for High Pressure Die Casting. J Mater Sci Technol. doi: 10.1016/j.jmst.2016.02.013

40. Ghosh M, Miroux A, Werkhoven RJ, et al (2014) Warm deep-drawing and post drawing analysis of two Al–Mg–Si alloys. J Mater Process Technol 214:756–766 . doi: 10.1016/j.jmatprotec.2013.10.020

41. Coër J, Laurent H, Oliveira MC, et al (2017) Detailed experimental and numerical analysis of a cylindrical cup deep drawing: Pros and cons of using solid-shell elements. Int J Mater Form 1–17 . doi: 10.1007/s12289-017-1357-4

42. Laurent H, Coër J, Manach PY, et al (2015) Experimental and numerical studies on the warm deep drawing of an Al–Mg alloy. Int J Mech Sci 93:59–72 . doi: 10.1016/j.ijmecsci.2015.01.009

43. Manach P-Y, Coër J, Laurent AJH, Yoon JW (2016) Benchmark 3 - Springback of an Al-Mg alloy in warm forming conditions. J Phys Conf Ser 734:22003 . doi: 10.1088/1742-6596/734/2/022003

44. Jelt Grease 5411 aerosol 95cSt. http://fr.rs-online.com/web/p/graisses/4612124/. Accessed 25 Nov 2015

45. Shi MF, Gerdeen JC (1989) A Theoretical study of the ironing process in sheet metal forming. J Mater Shap Technol 7:203–211 . doi: 10.1007/BF02834772

46. Yoon JW, Dick RE, Barlat F (2011) A new analytical theory for earing generated from anisotropic plasticity. Int J Plast 27:1165–1184 . doi: 10.1016/j.ijplas.2011.01.002

47. Simões VM, Coër J, Laurent H, et al (2013) Sensitivity Analysis of Process Parameters in the Drawing and Ironing Processes. Key Eng Mater 554–557:2256–2265 . doi: 10.4028/www.scientific.net/KEM.554-557.2256

48. Colgan M, Monaghan J (2003) Deep drawing process: analysis and experiment. J Mater Process Technol 132:35–41 . doi: 10.1016/S0924-0136(02)00253-4

49. ASTM E2492-07(2012) (2012) Standard Test Method for Evaluating Springback of Sheet Metal Using the Demeri Split Ring Test. ASTM Int 03.01: . doi: 10.1520/E2492-07R12

50. Gnaeupel-Herold T, Foecke T, Prask HJ, Fields RJ (2005) An investigation of springback stresses in AISI-1010 deep drawn cups. Mater Sci Eng A 399:26–32 . doi: 10.1016/j.msea.2005.02.017

51. Xia ZC, Miller CE, Ren F (2004) Springback Behavior of AA6111-T4 with Split-Ring Test. In: AIP Conference Proceedings. AIP Publishing, pp 934–939

52. Palumbo G, Tricarico L (2007) Numerical and experimental investigations on the Warm Deep Drawing process of circular aluminum alloy specimens. J Mater Process Technol 184:115–123 . doi: 10.1016/j.jmatprotec.2006.11.024

53. Simões VM, Laurent H, Oliveira MC, Menezes LF (2016) Natural aging effect on the forming behavior of a cylindrical cup with an Al-Mg-Si alloy. AIP Conf Proc 1769:200021 . doi: 10.1063/1.4963639

54. Hu P, Liu YQ, Wang JC (2001) Numerical study of the flange earring of deep-drawing sheets with stronger anisotropy. Int J Mech Sci 43:279–296 . doi: 10.1016/S0020-7403(99)00119-8

55. Xiao L-H, Yuan D-H, Xiang J-Z, et al (2016) Residual stress in the cylindrical drawing cup of SUS304 stainless steel evaluated by split-ring test. Acta Mech Sin 32:125–134 . doi: 10.1007/s10409-015-0516-4

56. Ragab MS, Orban HZ (2000) Effect of ironing on the residual stresses in deep drawn cups. J Mater Process Technol 99:54–61 . doi: 10.1016/S0924-0136(99)00360-X

57. Simões VM, Oliveira MC, Neto DM, et al (2017) Numerical study of springback using the split-ring test: influence of the clearance between the die and the punch. Int J Mater Form 1–13 . doi: 10.1007/s12289-017-1351-x

58. Laurent H, Grèze R, Manach PY, Thuillier S (2009) Influence of constitutive model in springback prediction using the split-ring test. Int J Mech Sci 51:233–245 . doi: 10.1016/j.ijmecsci.2008.12.010

59. Moon YH, Kang SS, Cho JR, Kim TG (2003) Effect of tool temperature on the reduction of the springback of aluminum sheets. J Mater Process Technol 132:365–368 . doi: 10.1016/S0924-0136(02)00925-1

Figure captions

Table captions

Chapter 4.

On the punch speed influence in warm forming and springback of two Al-Mg-Si alloys

This chapter contains the paper submitted to the Journal of Materials Processing Technology, with the same title as the chapter. This work discusses the thermo-mechanical behavior of the two Al-Mg-Si alloys, in function of temperature (at 22 to 200°C) and strain rate (from 2x10-4 to 2x10-2s-1), using uniaxial tensile tests and stress relaxation tests. The results of cylindrical cup tests and split ring (springback) tests performed for different punch speeds (from 0.1 to 10 mm/sec) are also discussed. It shows that at higher punch speed, the tools keep their temperature values nearly constant during the warm forming, allowing a better control of the process, including the temperature differential for the tools.

.

(Page intentionally left blank)

On the punch speed influence in warm forming and springback of two Al-Mg-Si alloys

V.M. Simões[1, 2], M.C. Oliveira[2], H. Laurent[1], L.F. Menezes[2]

[1] Univ. Bretagne Sud, FRE CNRS 3744, IRDL, F-56100 Lorient, France.

[2] CEMMPRE, Department of Mechanical Engineering, University of Coimbra, Polo II, Rua Luís Reis Santos, Pinhal de Marrocos, 3030-788 Coimbra, Portugal

Corresponding author: vasco.simoes@uc.pt

Highlights

- The punch speed influence in warm forming under non-isothermal conditions was analyzed for heat treatable aluminum alloys.
- The punch speed influences the exposure time and the heat transfer with the tools in warm forming.
- Dynamic precipitation (artificial aging) occurs in warm forming at low punch speed for natural aged alloys.
- Formability and springback remained stable or improved with the punch speed increased.

Abstract

In warm forming of aluminum alloys, the punch speed has a major influence on the success of sheet metal forming operations, namely in the parts shape, as well as in-service behavior. However, this process parameter is not often analyzed in the literature. Additionally, in warm forming of heat treatable aluminum alloys under non-isothermal conditions no study was reported concerning punch speed influence in springback. In the present work, two heat treatable Al–Mg–Si alloys (EN AW 6016-T4 and EN AW 6061-T6) are studied between 22ºC and 200ºC, using tensile tests and cylindrical cup forming followed by split ring (springback) tests. Monotonic tensile tests and stress relaxation tensile tests were performed at strain rates from $2x10^{-4}$ to $2x10^{-2}s^{-1}$. Dynamic strain aging (Lüders bands) was observed at 22ºC after each stress relaxation stages. For the EN AW 6016-T4 alloy, at 200ºC, when using low strain rates and stress relaxation stages, the occurrence of dynamic precipitation becomes more evident due to higher test time. Cylindrical cup tests were performed for punch speeds from 0.1 to 10 mm/s. In warm forming, a higher punch speed is advantageous since it minimizes the occurrence of dynamic precipitation and the heat transfer between the tools. Thus, formability and springback remained stable or improved with the punch speed increased. Additionally, higher punch speed is advantageous in industrial field since it allows higher production rates with a better control of the temperature difference between the tools.

Keywords: Al-Mg-Si; Warm Forming; Punch speed; Strain rate; Temperature gradient; Springback;

1 Introduction

The current environmental issues demand higher sustainability, namely in the transport sector, which includes the reduction of fuel consumption and its emissions but also the use of recyclable materials. Therefore, the transport sector looks for new materials and manufacturing strategies that allow reducing the components weight while increasing their strength and improves vehicles safety. The reduction of vehicle weight is crucial to reduce fuel consumption and its emissions. Aluminum alloys present good specific strength, high corrosion resistance and high recycling rate, which leads to the increasing demand for these alloys, as discussed in the overview by (Hirsch, 2011) concerning their application in lightweight vehicles. Within aluminum alloys, the heat treatable ones provide additional strength, by precipitation hardening after forming operations, which is an advantage when compared to the non-heat treatable aluminum alloys. Nevertheless, the aluminum alloys present low formability and non-negligible springback after the forming operation at room temperature (RT).

Warm forming has been shown to be an effective solution to improve formability for both non-heat treatable and heat treatable aluminum alloys. (Bolt et al., 2001) compared the warm forming behavior of non-heat treatable (Al-Mg) with heat treatable alloys (Al-Mg-Si). The results indicate that, although both alloys exhibit significant improvement in their formability compared with that at room temperature, the non-heat treatable alloys give higher part depths than the heat treatable. Additionally, the studies on the warm forming conditions reported a reduction of the springback behavior for non-heat treatable alloys, either using the U-rail test by (Moon et al., 2003) or the split-ring test by (Grèze et al., 2010). Recently, (Simões et al., 2017a) shown that warm conditions also reduce the springback for heat treatable aluminum alloys, with the advantage of being an effective solution to minimize the variability caused by the natural aging in forming operations of these alloys.

Warm forming can be performed under isothermal or non-isothermal (i.e. with a temperature gradient) conditions. (Wilson, 1988) review the warm forming of aluminum alloys concluding that large improvements in formability can be achieved if the flow strength of the material in the drawing zone is reduced, relative to that in the stretch-formed zone, by differential heating of the blank. In deep drawing operations, this can be achieved by decreasing the punch temperature relative to the one of the die/blank-holder. (Palumbo and Tricarico, 2007) and (Panicker et al., 2015) adopted this approach for studying a non-heat treatable Al-Mg alloy (EN AW 5754). (Palumbo and Tricarico, 2007) explain that the cooling action

exerted by the punch and the material softening at the heated peripheral region reduces the required punch load and, consequently, the stress and strain levels on the punch radius section. Thus, as shown by (Panicker et al., 2015), the non-isothermal warm forming is more effective to avoid excessive thinning than isothermal warm forming, where isothermal warm forming presents a thickness distribution similar to the one at RT. On the contrary, (Li and Ghosh, 2004) shown that increasing the punch temperature relative to the die/blank-holder temperature causes an increase in the ratio of the material being stretched over the punch relative to the material being drawn into the die.

The punch (ram) speed is an important process parameter in warm forming, since it influences the productivity. Aluminum alloys present a negligible strain rate sensitivity at RT, which increases as the temperature increases. It is generally accepted that the flow stress of aluminum alloys increases with increasing forming rates, especially in high temperature condition (Li and Ghosh, 2003). This positive strain rate sensitivity counterbalances the decrease of the flow stress for higher temperatures. (Shehata et al., 1978) and (Ayres and Wenner, 1979) studied the influence of the punch speed in the warm forming with a hemispherical punch, for non-heat treatable Al-Mg alloys, under isothermal conditions. (Shehata et al., 1978) concluded that in the range from 0.02 to 0.42 millimeters per second (mm/s) the influence of the punch speed may not be critical. However, (Ayres and Wenner, 1979) shown that formability decreases as the punch speed increases in the range from 0.8(3) to 83.(3) mm/s.

Under non-isothermal conditions, the temperature gradient is largely determined by the punch speed. This dependence of the temperature gradient to the punch speed is linked with the duration of the test (the exposure time). In fact, higher punch speeds lead to a lower exposure time and, consequently, minimize the heat transfer between the tools and the blank. (Palumbo and Tricarico, 2007) analyzed the influence of punch speed (range from 0.10 to 0.25 mm/s) on the evolution of the temperature difference between the peripheral zone of the blank (flange heated zone at 200 ºC) and the blank center (cold punch zone at RT) in function of the punch displacement, in the forming of an AA5754-O cylindrical cup. It was shown that the temperature difference between the flange heated zone and the blank center progressively increases during the process, due to the enlargement of the blank contact region with the (cooled) punch during the process; while simultaneously the blank peripheral is kept warm in the flange heated zone. The slope of the temperature difference evolution slightly decreases with the increase of punch speed, resulting in lower formability for a small temperature difference between the center and the flange of the blank. (Naka and Yoshida, 1999) analyzed the influence of the punch speed (range from 0.00(3) to 8.(3) mm/s) in

warm forming (range from RT to 180 ºC) of non-heat treatable alloys, concluding that for a punch speed lower than ≃2.00 mm/s the changes in the limiting drawing ratio are negligible. Whatever the temperature gradient considered, the studies for non-heat treatable aluminum alloys state that the formability decreases as the punch speed increases. In fact, for isothermal and non-isothermal conditions, the best formability was achieved for the tests performed at the higher temperature values but at the lowest punch speed values, which can be related with the positive strain rate sensitivity, at least for isothermal conditions.

On the other hand, (Ghosh et al., 2014) studied the influence of the punch speed during warm forming of two heat treatable Al-Mg-Si alloys at 250 ºC. It was observed that varying the punch speed, from 1.00 to 1.(3) mm/s for the 6016-T4 and from 1.23 to 2.00 mm/s for the 6061-T4, had no effect on the force – displacement response. However, the punch force presents a relevant increase for a sufficiently lower (i.e. 0.18(3) mm/s) punch speed, since the initial soft material gradually becomes harder and approaches the T6 condition (i.e. a change of initial heat treatment occurs as a result of the longer exposure time at 250 ºC). In this context, (Palumbo et al., 2015) studied the influence of the pressure rate during the warm hydroforming of a heat treatable Al-Mg-Si alloy, in a temperature range from RT to 350 ºC. The best formability improvement was achieved at 200 ºC using the highest pressure rate of 25 bar/s, to minimize the exposure of the material to the warm forming temperature employed. For an exposure time larger than 400 seconds, at temperatures equal or higher than 250 ºC, there is an increase of the yield stress and tensile strength and reduced ductility (Palumbo et al., 2015).

Besides good formability, to ensure a successful forming operation, it is also necessary to ensure a satisfactory performance in the application of the part. Thus, the part should not significantly lose its strength and ductility after forming, otherwise additional treatments have to be done to maintain the required properties. Concerning the post-forming mechanical properties and in-service behavior of warm formed aluminum components (non-heat and heat treatable alloys), (Li and Ghosh, 2004) remarked a high decrease of the post-forming yield stress, as compared with yield stress before the forming operation, when the temperature increases from 200 to 350 ºC. This decrease of post-forming yield stress occurs linked with the elongation increase. (Fan et al., 2016) investigated the warm forming and post-forming mechanical properties of a cylindrical cup for a heat treatable Al-Mg-Si alloy in a temperature range from 25 to 300 ºC, under isothermal conditions. The deep drawing test results show that enhanced formability and post-forming hardness could be obtained simultaneously between 150 and 200 ºC; however, both decline as the temperature increase to 300 ºC.

The analysis of the influence of warm forming in springback is usually evaluated using one of two benchmark tests: the cylindrical cup test followed by split-ring test and the U-rail. Using the split-ring test, under isothermal conditions with a punch speed of 0.5 mm/s, it was observed a decrease of springback for forming temperatures equal or above to 150 ºC, for a non-heat treatable Al-Mg alloy (the EN AW 5754-O) (Grèze et al., 2010). The same was observed under non-isothermal conditions, using a punch speed of 1 mm/s, for an Al-Mg alloy (the EN AW 5754-O) (Laurent et al., 2015) and for two Al-Mg-Si alloys (EN AW 6016-T4 and EN AW 6061-T6) (Simões et al., 2017a). A numerical analysis of the U-rail test was performed for an EN AW 5754-O alloy, comparing isothermal with non-isothermal heating conditions, for a punch speed of 10 mm/s, concluding that both conditions reduces springback (Kim and Koç, 2008). However, isothermal conditions presented the highest springback reduction. The influence of the punch speed (from 1 to 20 mm/s) on springback was also analyzed by the same authors, which concluded that in both cases, isothermal and non-isothermal conditions, the springback increases as the punch speed increases. According to the authors, this indicates that in general, to improve the dimensional accuracy of a formed part as well as to increase the formability, slow forming rate is preferred in warm forming (Kim and Koç, 2008). The same benchmark test was used to experimentally study the influence of the punch speed (in the range from 1 to 10 mm/s) for a non-heat treatable EN AW 1050 alloy, under non-isothermal conditions, with the same conclusions (Moon et al., 2003). Moreover, according to (Moon et al., 2003), the variations of the heat transfer between the tools and the blank, caused by punch speed changes, are the probable cause of some springback variations.

In brief, the studies concerning the influence of the punch speed in warm forming conditions were mostly performed for non-heat treatable aluminum alloys, with only a few considering the heat treatable ones. Moreover, no study analyzed the influence of punch speed and exposure time on the springback for heat treatable Al-Mg-Si alloys. This requires an improved analysis of the influence of the punch speed in the temperature gradient for non-isothermal warm forming conditions. The present study aims to understand the influence of the punch speed in the springback behavior and formability of two Al-Mg-Si alloys, under non-isothermal warm forming conditions.

In this context, section 2 presents the alloys selected for this study (EN AW 6016-T4 and EN AW 6061-T6) and the experimental characterization of their thermo-mechanical behavior at RT and 200 ºC, taking into account different strain rates and stress relaxation tests. The cylindrical cup tests are presented in section 3, including the results obtained at RT and 200 ºC, for different punch speeds. The experimental

results analyzed are the temperature evolution in function of time, the punch force evolution with its displacement, the thickness distribution along the cup wall and the earing profile, and the springback. For the EN AW 6016-T4 alloy, the influence of warm forming in the natural aging, at different punch speeds, is also evaluated. Finally, the analysis and discussion is presented in section 4 and the main conclusions are summarized in section 5.

2 Materials and Thermo-mechanical behavior

The two Al-Mg-Si alloys selected for this study were the EN AW 6016-T4 and the EN AW 6061-T6, which are commonly used for skin applications and for structural components, respectively. The designation T4 and T6 indicate that, after Solution Heat Treatment (SHT) and fast quenching to RT, the alloys were subjected to natural aging and artificial aging, respectively. The alloys with the T4 designation are more ductile than the ones with the T6 designation.

Figure 1 presents the difference between an Al-Mg-Si alloy in T4 and T6 heat treatment condition, concerning the production sequence and the precipitation state. After the rolling operation, used to obtain a thin metal sheet, the Al-Mg-Si alloys are submitted to SHT that consists on a heating phase followed by a holding stage between 500 to 540 °C and fast quenching to RT (see Figure 1 a)) (H.Y. Hunsicker, 1984). The SHT is required to achieve a re-dissolution of the secondary phases that have precipitated during the various preceding steps of the thermo-mechanical processing (Engler and Hirsch, 2002). Accordingly, SHT leads to a typical recrystallized microstructure consisting of fine, slightly elongated grains with a size of 20–30 μm. The fast quenching keeps the alloying elements dissolved in the aluminum matrix at RT, in a supersaturated solid solution (SSSS) (see Figure 1 b)). Afterwards, precipitation hardening occurs at RT, known as natural aging, up to a stabilization, which is designated by T4. Artificial aging (the T6 heat treatment) is promoted in a new holding stage at a temperature range between 170 and 200 °C (see Figure 1 a)), in which the strength increases until a maximum value, due to the precipitation of β'' – needles. The extended holding at artificial aging temperature leads to a strength decrease, known as over-aging, which is caused by the formation of non-hardening β' and β precipitates (see Figure 1 b)).

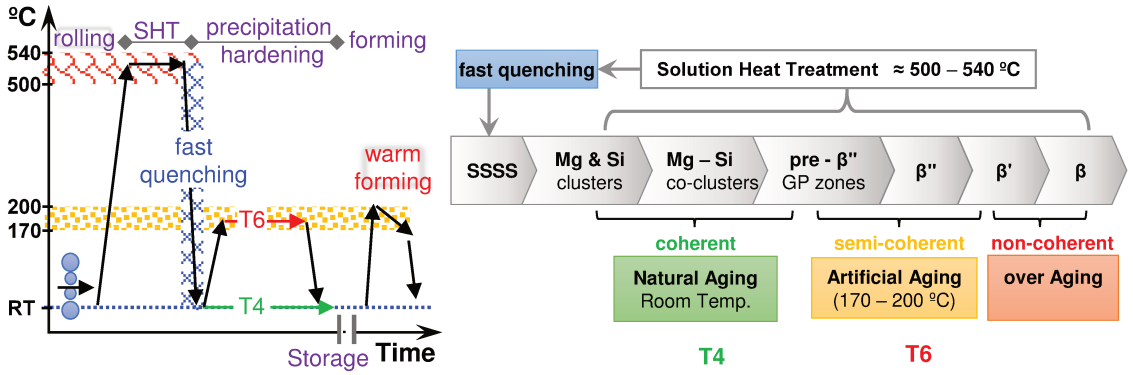

a) b)

Figure 1 – a) Thermal cycle of in production and heat treatment; b) Precipitation sequence in Al-Mg-Si alloys (according to (Banhart et al., 2010))

The temperature range for the warm forming of Al-Mg-Si alloys is similar to the temperature range used in their T6 heat treatment, as schematically shown in Figure 1. Therefore, microstructural precipitation hardening can occur during the warm forming process, being the thermo-mechanical behavior of the Al-Mg-Si alloys highly dependent of the heat treatment conditions. Considering the precipitation sequence shown in Figure 1 b), during warm forming an alloy in T4 condition may evolve to T6 heat treatment, and one in T6 heat treatment to over-aging condition; each heat treatment condition is more stable at warm temperature than the previous one. The precipitation is a diffusion phenomenon, which is time dependent, and its kinetics increases as the temperature increases. The precipitation hardening that occurs due to temperature and time is called static aging. However, the plastic deformation leads to dislocation-assisted precipitation, known as dynamic aging or dynamic precipitation (hardening). As shown by (Cai et al., 2004), at warm temperatures, the occurrence of plastic deformation highly reduces the exposure time required for precipitation hardening, as compared to the one associated with static aging. (Kolar et al., 2012) studied the influence of pre-strain at RT followed by precipitation hardening at 190 ºC (sequential mode) and warm forming at 190 ºC (simultaneous mode) in the material strength. They conclude that the simultaneous mode leads to higher in-service strength than the sequential mode. However, according with (Fan et al., 2016), warm forming at temperatures higher than 200 ºC can contribute to reduce post-forming mechanical properties and in-service behavior of aluminum components. Thus, in the present work, the results analysis must take into account the exposure time, the temperature and the strain rate, which are related with the punch speed.

The correlation between the punch speed and the strain rate imposed to the material in the warm forming of cylindrical cup test was studied using finite element analysis by (Palumbo and Tricarico, 2007) and (Neto et al., 2017). Both studies analyze a non-heat treatable Al-Mg alloy under non-isothermal conditions, with tools geometry identical to the one used in this study. (Neto et al., 2017) analyzed three different temperatures (RT, 150 and 240 ºC) and concluded that the strain rate in a point initially located in the flange (5 mm from the perimeter) is independent of the test temperature. For a punch speed of 5 mm/s, the plastic strain rate increases from about 10^{-2} to 10^{-1} s^{-1} during the sliding of the point over the die (flange region). Then, this value of plastic strain rate is kept roughly constant during the sliding of the point over the die radius (up to 18 mm of punch displacement). Finally, the plastic strain rate decreases abruptly when the point reaches the cup wall. (Palumbo and Tricarico, 2007) studied two punch speeds of 0.016 and 1 mm/s for four points, located at: (i) the cup bottom, (ii) cup radius, and two points on (iii) the flange zone. This study shows that after 12.5 mm of punch displacement, the points located at the cup bottom and radius present no plastic deformation. The higher strain rate was obtained for the point located at the cup radius, which presents the higher thickness reduction, which is comprised in a range between 10^{-4} and 10^{-3} s^{-1}, for a punch speed of 0.016 mm/s, and between 10^{-2} and 10^{-1} s^{-1}, for a punch speed of 1 mm/s. For the points located in the flange zone, the strain rate was comprised in a range between $2x10^{-4}$ and $6x10^{-4}$ s^{-1} for a punch speed of 0.016 mm/s and, $1x10^{-2}$ and $3x10^{-2}$ s^{-1} for a punch speed of 1 mm/s. In brief, the strain rate increase seems to be proportional to the punch speed increase, i.e. by doubling the punch speed the strain rate in the flange zone also doubles. Based on these results, the punch speeds between 0.1 and 10 mm/s can be related with maximum strain rate values in the range 10^{-3} s^{-1} and 10^{-1} s^{-1}, respectively. The influence of temperature and strain rate is analyzed first using uniaxial tensile tests.

2.1 Materials

The EN AW 6016-T4 alloy was produced and provided by Constellium, and the date of the SHT is known; therefore, its storage time at RT is counted after the date of the SHT. The EN AW 6061-T6 alloy was acquired in the retail market, and the date of SHT and T6 heat treatment is unknown; therefore, its storage time at RT is counted after its reception in the laboratory. In a previous work (Simões et al., 2017a), it was shown that the mechanical properties of the EN AW 6016-T4 alloy change during storage at RT, becoming relatively stable after 7 months. The mechanical properties of EN AW 6061-T6 remain relatively stable during the storage period. At RT, the natural aging effect leads to an increase of the tensile strength and consequent increase of the drawing forces; while its effects can be highly minimized in warm forming

conditions (Simões et al., 2017a). Therefore, in order to better understand the effect of natural aging in warm forming, the tests at different punch speed were performed considering the natural aging times of 1 and 18 months for the EN AW 6016-T4 alloy. For the EN AW 6061-T6 alloy, the natural aging study was not considered.

The mechanical properties of both alloys are presented in Table 1, according with the results presented in (Simões et al., 2017a), for the tensile test at RT at a strain rate of $2x10^{-3}s^{-1}$, with the specimens oriented along the rolling direction (RD). The terms and definitions used throughout this work are according to the ISO 6892-1:2009 (Central Secretariat ISO, 2009), i.e. R_m tensile strength; $R_{p0.2}$ proof strength at 0.2% of the extensometer gauge length; A_{gt} percentage of total elongation at maximum force; n_{4-6} strain hardening exponent between 4 and 6 % of plastic elongation; and n_{10-15} strain hardening coefficient between 10 and 15 % of plastic elongation. The thickness of both alloys is approximately 1 mm, with the average value of fifty measurements also presented in Table 1.

Table 1 – Mechanical properties of EN AW 6016-T4 and EN AW 6061-T6 along RD, at RT (Simões et al., 2017a). The thickness values presented are determined by the average **of** fifty measured points

	Aging time	$R_{p0.2}$	R_m	A_{gt}	n_{4-6}	n_{10-15}	Thickness
EN AW 6016-T4	1 month	101 MPa	215 MPa	23.9 %	0.32	0.26	1.05mm
	18 months	130 MPa	247 MPa	22.8 %	0.28	0.24	
EN AW 6061-T6	–	270 MPa	325 MPa	12%	0.14	–	0.98 mm

2.2 Thermo-mechanical behavior in uniaxial tension

Aiming the better understanding of the thermo-mechanical behavior during warm forming, uniaxial tensile tests were performed at RT (≈22 ºC) and 200ºC, at strain rates of: $2x10^{-4}s^{-1}$, $2x10^{-3}s^{-1}$ and $2x10^{-2}s^{-1}$, using specimens cut aligned with the RD. They were carried out in a Gleeble 3500 device and the strain field was acquired by digital image correlation with GOM-ARAMIS system. In the Gleeble device, the specimen is heated by direct resistance, resulting in a temperature gradient along the specimen length, with higher temperature on its center, which can promote heterogeneous mechanical properties along the specimen length direction. Therefore, it is expected that the specimen deforms preferentially at its middle where the temperature is higher. For the same reason the values indicated for the strain rates are not necessarily constant during the test, showing an increase with the increase of plastic strain. In order to minimize the effect of the temperature gradient in the determination of the true stress – true strain curves, a rectangular gauge measurement area of 6 mm width and 3 mm length, positioned in the specimen's

middle, is used to compute the strain. Detailed explanations about the experimental procedure used are given in (Coër et al., 2011) and (Simões et al., 2017a).

The uniaxial tensile tests were performed considering two types of loading conditions: **a)** monotonic loading up to rupture; **b)** multiple-step relaxation tests up to rupture, which consist of imposing a monotonic loading, interrupted by relaxation stages of 60 seconds, each followed by a loading, controlled with a fixed value for the grip displacement (named stress-relaxation tests). These stress-relaxation tests were performed considering two different conditions: **b)-i** a single strain rate of $2x10^{-3}s^{-1}$ was used in all loading stages up to rupture; **b)-ii** two strain rates were used alternately, such that the test starts with a strain rate of $2x10^{-4}s^{-1}$, followed by a stress-relaxation stage, then a load stage at $2x10^{-2}s^{-1}$, followed by a stress-relaxation stage. This cycle of load-relaxation (with two strain rates) is repeated alternately up to rupture. All the true stress – true strain curves are presented up to the maximal load, except in the cases corresponding to **b)-ii** condition. The goal of the stress-relaxation tests is to study the possibility of the occurrence of dynamic precipitation during warm forming. In fact, the dynamic precipitation is promoted by temperature, exposure time and strain hardening; therefore, stress-relaxation stages provide the necessary conditions to activate dynamic precipitation mechanism, allowing its evaluation.

2.2.1 EN AW 6016-T4

Figure 2 presents the true stress – true strain curves for the EN AW 6016-T4, obtained at RT and 200 °C, for three different strain rates: $2x10^{-4}$, $2x10^{-3}$ and $2x10^{-2}s^{-1}$. These tests were performed under monotonic uniaxial tensile tests (condition **a**)). Globally, the alloy presents a negligible strain rate sensitivity at RT while at 200 ºC it cannot be neglected. At both temperatures, with the increase of strain rate, the alloy presents a slight increase of the $R_{p0.2}$, while the hardening rate decreases. This results in a slight positive strain rate sensitivity, which is kept only for reduced values of plastic strain. However, as the plastic strain increases, the higher stress values correspond to the lower strain rates, which traduce a negative strain rate sensitivity. This is particularly remarkable at 200 ºC, with the test performed at $2x10^{-4}s^{-1}$ presenting the lower yield stress and the highest strain hardening rate, which saturates after a true strain of 0.05, resulting in the lower uniform elongation. On the other hand, the tests performed at strain rates of $2x10^{-3}$ and $2x10^{-2}s^{-1}$ present a smooth evolution of the work hardening. Nevertheless, the work hardening

rate is lower at $2x10^{-2}$ than at $2x10^{-3}s^{-1}$. Thus, although the test performed at $2x10^{-2}s^{-1}$ presents a higher $R_{p0.2}$, the value of R_m is lower than the one attained at $2x10^{-2}s^{-1}$.

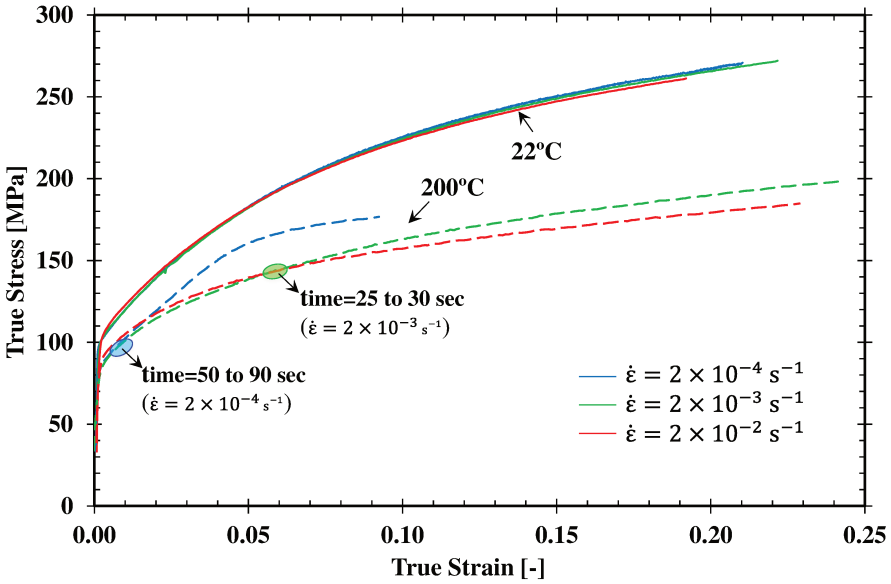

Figure 2 – Influence of the strain-rate on the true stress – true strain curves obtained from uniaxial tensile tests performed at 22 and 200 ºC, for the EN AW 6016-T4 in specimens oriented along the RD at 1 month of storage time (natural aging). The blue oval shape indicates the test time at which the curve a strain rate of $2x10^{-4}s$-1 is coincident with the curve of strain rate of $2x10^{-3}s^{-1}$; the green oval shape indicates the test time at which the curve of strain rate of $2x10^{-3}s^{-1}$ is coincident with the curve of strain rate of $2x10^{-2}s^{-1}$.

The thermo-mechanical behavior shown in Figure 2 at 200 ºC for a strain rate of $2x10^{-4}s^{-1}$ is similar to the one reported at 250 ºC by (Ghosh, 2011), at a strain rate of $2x10^{-3}s^{-1}$, for the EN AW 6016-T4. According to (Ghosh, 2011), such behavior is due to the microstructural phenomenon of dynamic precipitation hardening that occurs during the tensile test, such that the duration of the tensile test influences the stress-strain curves obtained. Additionally, their results at 250ºC, for strain rates of $2x10^{-2}s^{-1}$ and $2x10^{-1}s^{-1}$, are similar to the ones shown in Figure 2 at 200ºC, for $2x10^{-3}s^{-1}$ and $2x10^{-2}s^{-1}$, respectively. This indicates that at a higher temperature the dynamic precipitation hardening occurs quicker. In fact, as discussed previously the dynamic precipitation depends not only of the temperature but also of the exposure time. To help in the results interpretation, in Figure 2 the time intervals corresponding to the coincidence of the true stress – true strain curves are signed, with blue and green marks, associated to the test at $2x10^{-4}s^{-1}$ and at $2x10^{-3}s^{-1}$, respectively.

Figure 3 presents the distribution of true strain along the specimen length, measured for a section at the middle of the specimen width (purple dash line in the detail of the specimen), for the tests performed

at 200 ºC. The true strain profile is presented for four instants: two with similar true strain values at the specimen center, $\varepsilon = 0.02; 0.06$ and at R_m and at rupture. It can be observed that the strain profile present a different evolution with the strain rate. For the strain rates of $2x10^{-3}s^{-1}$ and $2x10^{-2}s^{-1}$, the true strain profile always presents preferential strain localization at the specimen center, whatever the strain value. This strain localization is linked with the temperature gradient along the specimen length, which that presents a higher temperature at its center. On the other hand, for a strain rate of $2x10^{-4}s^{-1}$, in the strain interval between $\varepsilon = 0.02$ and $\varepsilon = 0.08$, the specimen deforms preferentially in the adjacent regions to its center (see supplementary material video 1). This seems to be linked with the occurrence of dynamic precipitation hardening at the specimen center, due to its higher exposure time to the same temperature, caused by the slow strain rate. This leads to the increase of strength in the specimen center promoting the deformation of the adjacent regions, which are softer. However, after $\varepsilon = 0.08$ and up rupture, the specimen deforms also preferentially at its center, indicating the occurrence of dynamic precipitation in all the specimen gauge area. Moreover, for the strain rate of $2x10^{-3}s^{-1}$ and $2x10^{-2}s^{-1}$, in a strain interval up to $\varepsilon = 0.06$ both tests present a similar true stress – true strain curve (see Figure 2) as well as similar true strain profiles (see Figure 3). However, afterwards the test performed with a strain rate of $2x10^{-3}s^{-1}$ presents a higher stress value for the same true strain value. In fact, as shown in Figure 3, for the strain rate of $2x10^{-2}s^{-1}$ the deformation is more localized at the specimen center, while for the strain rate of $2x10^{-3}s^{-1}$ it is more spread along the length. This may also be linked with dynamic precipitation hardening occurring at the strain rate of $2x10^{-3}s^{-1}$, which increases the material strength at the specimen center due to its higher exposure time and leads the material to deform in the adjacent regions that are at lower temperatures.

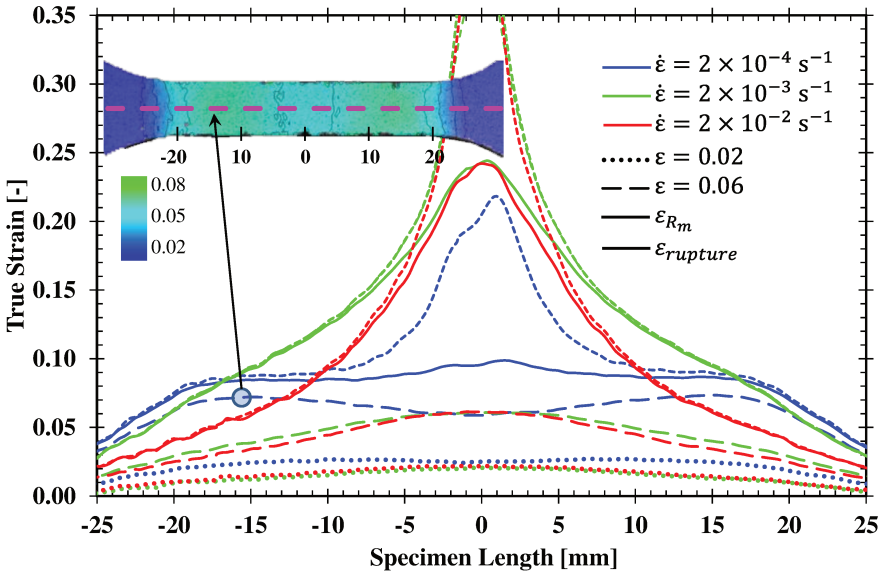

Figure 3 – Influence of the strain-rate on the true strain distribution along the specimen length for the uniaxial tensile tests performed at 200 ºC, for the EN AW 6016-T4 with specimens oriented along the RD at 1 month of storage time (natural aging). The true strain profiles are taken for four instants and correspond to the tests presented in Figure 2.

Stress-relaxation tests were performed to improve the knowledge concerning the occurrence of dynamic precipitation hardening in uniaxial tensile conditions. Figure 4 a) shows the results for the tests with a single strain rate of $2x10^{-3}s^{-1}$ (condition **b)-i**) and Figure 4 b) shows the test results obtained with the two alternate strain rates of $2x10^{-4}$ and $2x10^{-2}s^{-1}$ (condition **b)-ii**). In both figures, the curves of the monotonic tests presented in Figure 2 are added for comparison. Figure 5 a) and b) presents the true stress–time curves corresponding to true stress – true strain curves in Figure 4 a) and b), respectively. The aim of these figures is to improve knowledge concerning the influence of the exposure time (test duration) in the mechanical behavior of the EN AW 6016-T4 alloy.

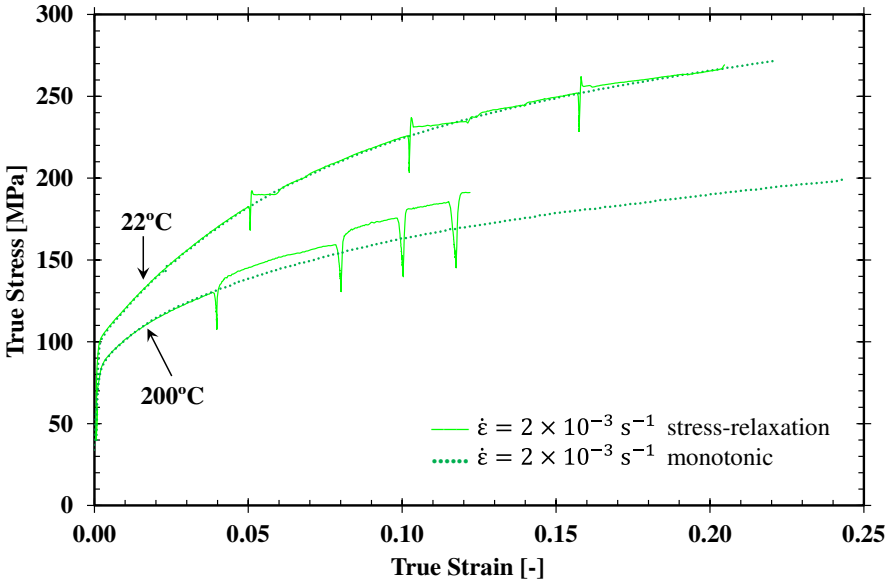

a) stress relaxation tests at single strain rate

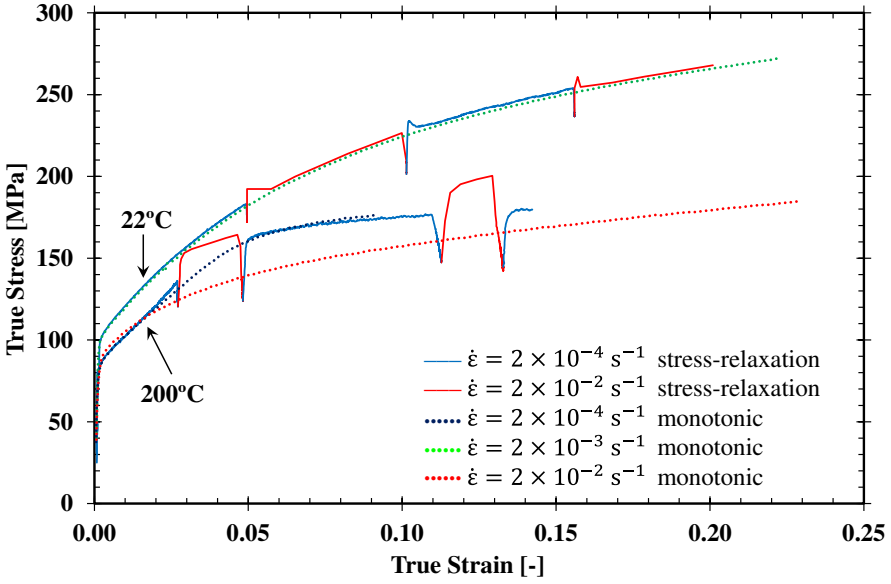

b) stress relaxation tests at multiple strain rate

Figure 4 – Influence of the strain-rate on the true stress – true strain curves obtained from stress relaxation uniaxial tensile tests performed at 22 and 200 ºC, for the EN AW 6016-T4 in specimens oriented along the RD at 1 month of storage time (natural aging).

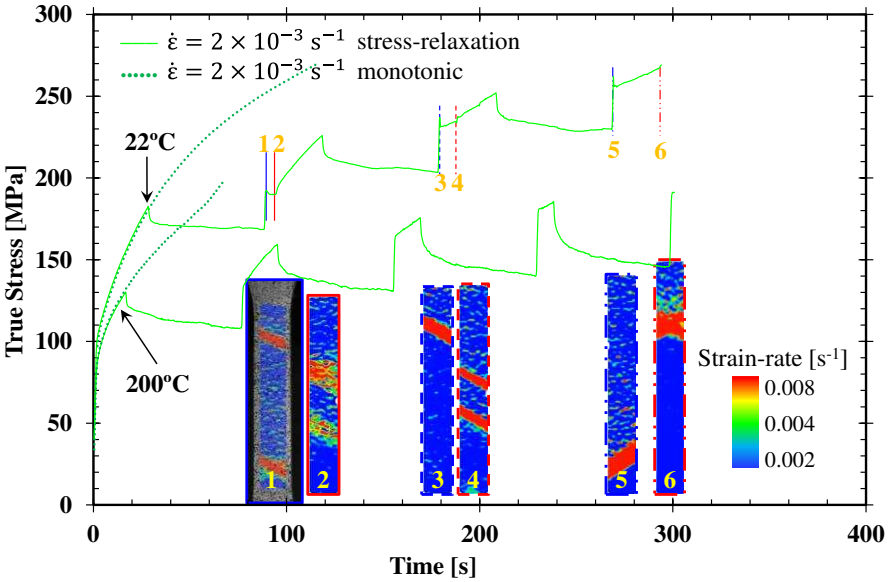

a) stress relaxation tests at single strain-rate

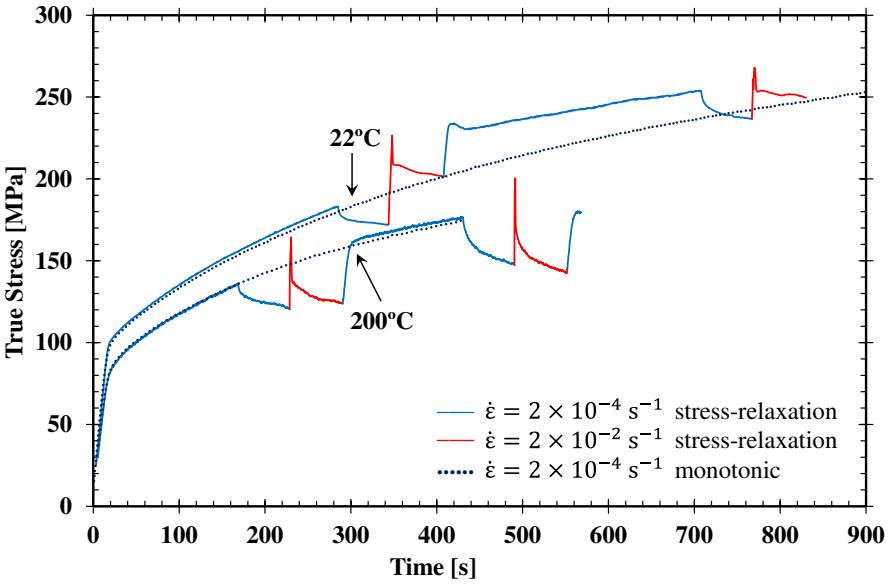

b) stress relaxation tests at multiple strain-rates

Figure 5 – Influence of the strain-rate on the true stress – time curves obtained from uniaxial tensile tests performed at 22 and 200 ºC, for the EN AW 6016-T4 in specimens oriented along the RD at 1 month of storage time (natural aging). The Figure 5 a) and b) presents the true stress – time curves of the tests presented in Figure 4 a) and b), respectively.

At RT, for both conditions, the results show that the stress-relaxation curves match the monotonic tensile curves. These results highlight that, at RT, the stress-relaxation stage at single and multiple strain rates have no significant contribution to the work hardening behavior. However, for both condition **b)-i** and **b)-ii**, after each relaxation stage, during new loading, the stress value suddenly increases attaining a local maximum and stabilizes into a plateau. After each stress-plateau, the formation and propagation of Lüders

bands (dynamic strain aging mechanism) was observed by digital image correlation, as shown in the detail in Figure 5 a) (see supplementary material video 2). According to (Picu et al., 2010), this is caused by the diffusion of Mg and Si atoms towards dislocations, originating Mg-Si precipitates. Such precipitates block the dislocations movement in subsequent loading stages, promoting an increase of stress to overcome it and, consequently, Lüders bands occur.

At 200 °C, the stress-relaxation stage has a non-negligible influence in the material behavior. As shown in see Figure 4 a), after each stress-relaxation stage, the stress-strain curve offsets upward as compared to the monotonic curve, while presenting a similar work hardening rate. Such behavior suggests that during each stress-relaxation stage some precipitation phenomenon occurs causing the strengthening of the alloy.

Concerning the stress-relaxation tests performed with two strain rates at 200 °C (see Figure 4 b)), during the 1st load stage, the stress-relaxation curve overlaps the monotonic one performed at $2x10^{-4}s^{-1}$. In the 2nd load stage a higher strain rate of $2x10^{-2}s^{-1}$ is imposed and the flow stress suddenly increases, indicating a positive strain rate sensitivity. However, in this 2nd load stage, the work hardening rate is lower than in 1st one and, consequently, the flow stress at the end of this stage, approaches a value similar to the one obtained in the monotonic tensile test at $2x10^{-4}s^{-1}$. In the 3rd load stage, at $2x10^{-4}s^{-1}$, a significant lower work hardening rate is observed as compared to the 1st one, which is similar to the one observed in the monotonic test at $2x10^{-4}s^{-1}$, being both curves overlapped. In the 4th load stage, at $2x10^{-2}s^{-1}$, the flow stress suddenly increases and presents a work hardening rate similar to the one of the 2nd load stage. Lastly, in the 5th load stage, the alloy presents a hardening behavior similar to the one of the 3rd load stage. In brief, at 200 °C, the stress-relaxation curve overlaps the equivalent monotonic one in all the periods performed with a strain rate value of $2x10^{-4}s^{-1}$, and diverges when the strain rate value of $2x10^{-2}s^{-1}$ is used. These results show the positive strain rate sensitivity of the EN AW 6016-T4 alloy at 200°C, being the higher stress values associated with higher strain rate values.

As shown in Figure 5 a), the exposure time of the stress-relaxation test with a single strain rate of $2x10^{-3}s^{-1}$ is about three times higher than the equivalent monotonic test, disabling any comparison except for the first load cycle. The same comment is valid for the two tests performed at RT shown in Figure 5 b). On the other hand, as shown in Figure 5 b), both tests performed at 200 °C have a similar exposure time, which results in the overlap of true stress – true strain curves (see also Figure 4 b)). It is interesting to note

that the monotonic tensile test at a strain rate of $2x10^{-4}s^{-1}$ and the stress-relaxation tensile test with two strain rate values, despite the different load sequence, present a similar true stress – true strain behavior when the specimen is loaded for the same instant of time at the same strain rate. It highlights that in warm forming of the EN AW 6016-T4 alloy, the control of the exposure time is crucial for determining the material behavior. In fact, for similar exposure time the material presents a positive strain rate sensitivity (see Figure 4 b)), but for different exposure times, leading to different rates of dynamic precipitation, a negative strain rate sensitivity can be observed (Figure 2).

2.2.2 EN AW 6061-T6

Figure 6 presents the true stress – true strain curves obtained from the uniaxial tensile tests performed at RT and 200 °C, for the EN AW 6061-T6. At RT, the monotonic tensile tests were performed for three strain rates: $2x10^{-4}$, $2x10^{-3}$ and $2x10^{-2}s^{-1}$. A stress-relaxation test was also performed considering a constant strain rate of $2x10^{-3}$ for each load cycle. The alloy presents negligible sensitivity to strain rate at RT. As for the EN AW 6016-T4 alloy, the stress-relaxation test at RT indicates no changes of the mechanical behavior and a stress-jump associated with the presence of Lüders bands.

At 200 ºC, a monotonic tensile test was performed for a strain rate of $2x10^{-3}$ s^{-1} as well as a stress-relaxation test, with two strain rate values: $2x10^{-4}$ and $2x10^{-2}$ s^{-1} (condition **b)-ii**). At this temperature, this alloy presents a positive sensitivity to strain rate, since the strength increases as the strain rate increases. The work hardening rate seems to be independent of the strain rate, since the monotonic and the stress-relaxation tests show a similar work hardening behavior. Moreover, a similar work hardening behavior in function of strain rate was observed by (Ghosh, 2011), for monotonic tensile tests performed on the EN AW 6061-T6 alloys, at 250 ºC with strain rates of $2x10^{-2}s^{-1}$ and $2x10^{-1}s^{-1}$. Lastly, no relevant material behavior change was noticed for this alloy as a result of the stress-relaxation stages, indicating that no significant microstructural change occurs and that the exposure time does not significantly affect the mechanical behavior of the EN AW 6061-T6 alloys, at 200 ºC.

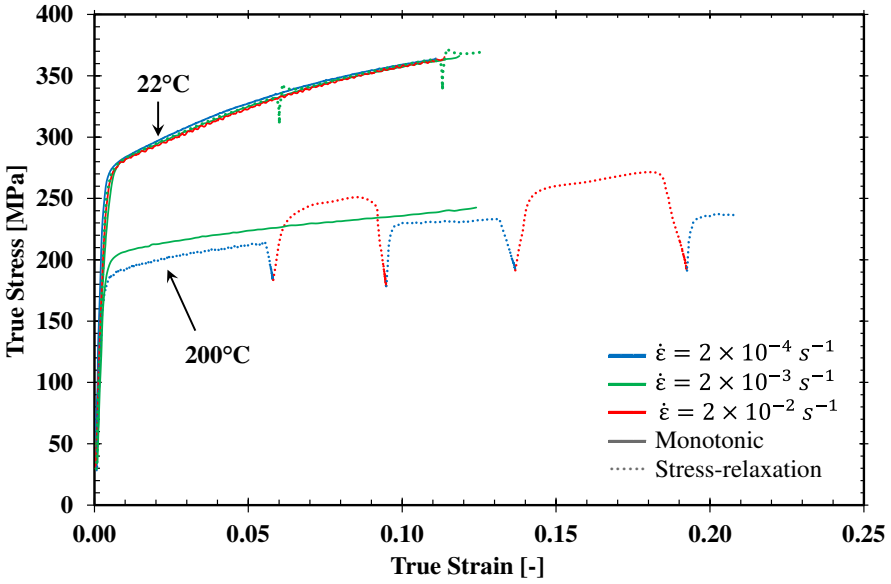

Figure 6 – Influence of the strain-rate on the true stress – true strain curves obtained from uniaxial tensile tests performed at 22 and 200 ºC, for the EN AW 6061-T6 in specimens oriented along the RD.

3 Cylindrical cup forming tests

3.1 Experimental procedure

The cylindrical cup tests consist in forming a metal sheet with a circular shape, the blank, into a forming die by the mechanical action of a punch. A blank-holder tool is used to avoid wrinkles and to control the material flow into the die. The dispositive used was a Zwick/Roell Amsler BUP200 sheet metal testing equipment, adapted with specific tools for warm forming (Coër, 2013). This dispositive was previously used to study the warm forming of an EN AW 5754-O alloy (Laurent et al., 2015) and was also proposed as a benchmark to evaluate the springback of an EN AW 5086 alloy (Manach et al., 2016). The blank has a circular shape with 60 mm of diameter. It was cut out previously to the forming process from the initial sheet by squaring shear in the Zwick BUP200 using a specific blade tool.

A schematic illustration of the procedure used in the warm forming of the cylindrical cup is presented in Figure 7. The warm forming procedure used to fully draw the cylindrical cup starts with the heating of the die and the blank-holder, up to the test desired temperature, by internal electrical heating rods (Figure 7 a)). While the punch is refrigerated to keep its temperature close to RT, the blank is positioned in the blank-holder, taking a few seconds to attain the desired test temperature (Figure 7 b)). The forming operation presented involves two distinct phases: (i) the drawing, as schematically shown in Figure 7 c); and the (ii) the ironing, which results from the fact that the gap between the die and the punch is smaller

than the thickening observed in the flange (see Figure 7 d)). At the end of the process the punch stops, and the ejector is activated to remove the cup from the die's cavity (Figure 7 e)).

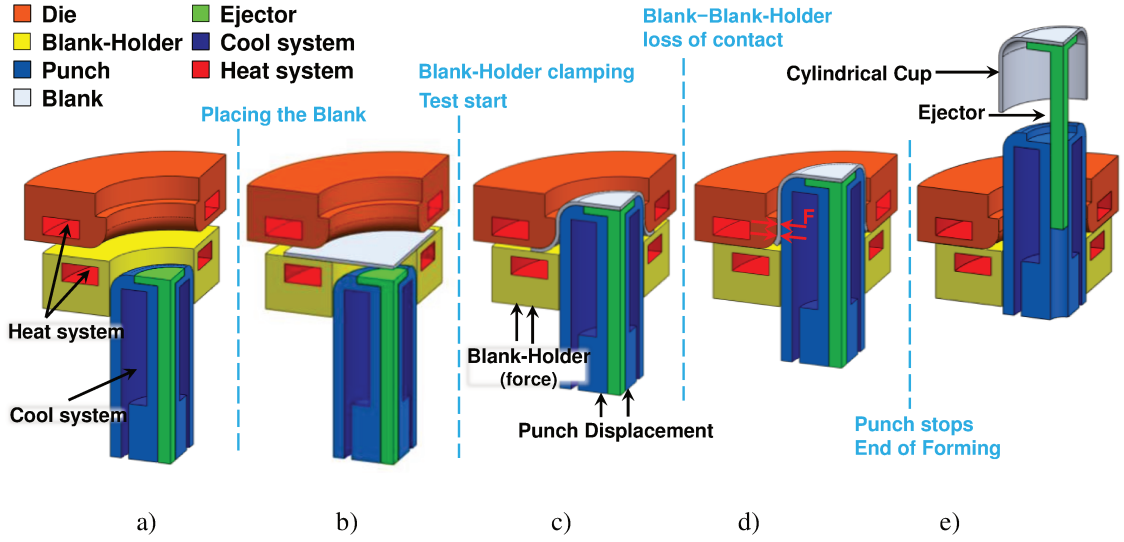

Figure 7 – Drawing of a cylindrical cup: a) Heating the die and blank holder to 200ºC, punch kept at RT by water cooling system; b) blank heating; c) Cup drawing; d) Ironing; e) Ejection step.

The dimensions of the tools (die, blank-holder, punch and ejector) and blank are presented in Figure 8. As shown in this figure, thermocouples are placed in a fixed position of the tools, enabling the acquisition of temperature values that corresponds to a local measure. A thermocouple is placed on the die radius (labeled TC Die); in the punch it is right below the ejector (labeled TC Punch); and in the blank-holder the thermocouple is at the flange zone, on the surface contacting with the sheet (labeled TC B-H). In the blank, the thermocouples are initially placed at the center (labeled TC Blank 1) and at 15 mm (limit of the punch radius) from the blank center (labeled TC Blank 2). However, the position relative to the tools of the thermocouples placed in the blank evolves during the warm forming test, meaning that the temperature values measured are a function of the punch displacement. Therefore, the analysis of the temperature evolution along the drawing test must be performed taking into account the evolution of thermocouples relative position. At the end of the forming operation, the thermocouple TC Blank 1 is still positioned on the cup bottom center while TC Blank 2 is located in the cup radius zone. This means that both will be in full contact with the cold punch during the forming process.

In the present work, the forming behavior of the two alloys selected is evaluated at RT and 200ºC, considering different punch speeds. The forming behavior of the EN AW 6016-T4 alloy was analyzed at

two natural aging times: 1 and 18 months; while for the EN AW 6061-T6 alloy the forming tests were only performed considering 18 months after its reception. The warm forming temperature was chosen based in the literature results which often refers 200 ºC as a temperature that enables the formability improvement, while keeping good post-forming mechanical properties (Fan et al., 2016). Additionally, in a previous study (Simões et al., 2017a) concludes that no significant improvement was found when the temperature was higher than 200 ºC. At RT, the punch speeds analyzed were 1 and 10 mm/s, while at 200ºC three values were considered: 0.1, 1 and 10 mm/s. As previously mentioned, this punch speed range corresponds to maximum strain rate values in the range 10^{-3} s^{-1} and 10^{-1} s^{-1}, respectively. The lower and higher punch speeds were imposed by the device characteristics. The water flow rate of the punch cooling system was equal in all the tests. All the tests were performed with a standard clamping force of 6 kN. The blanks were lubricated with ("Jelt Grease 5411 aerosol 95cSt," n.d.). The heating time was ~60 seconds (±15 seconds). During each test, the punch force and its displacement, the blank-holder force and the temperature were acquired, as a function of time. A minimum of three reproducible tests were performed for each condition under analysis. Their reproducibility was validated by two conditions: (i) the average scatter of the punch force, which was less than ±0.1kN for the same displacement; (ii) the difference in heating time was always inferior to ±15 seconds. Therefore, only one representative test is presented for each condition.

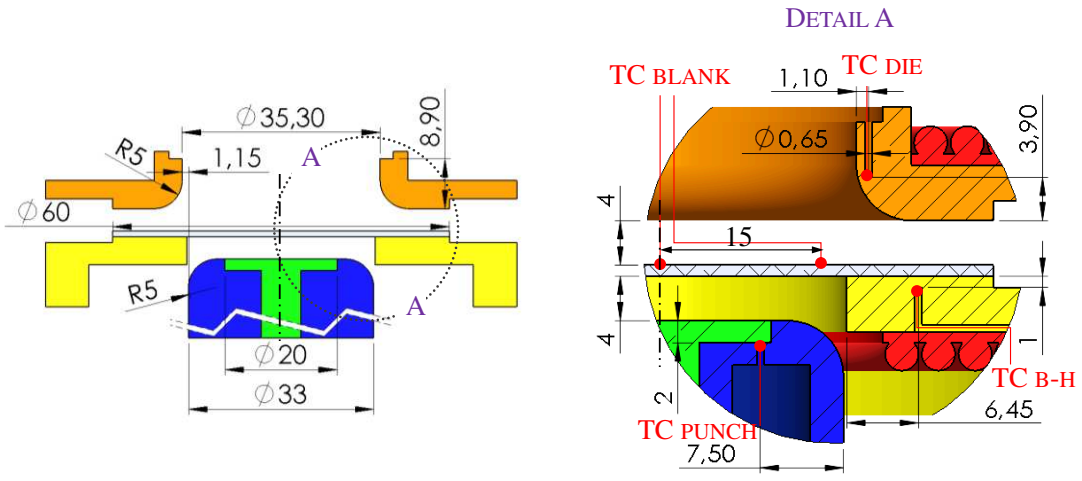

Figure 8 – Tools dimensions (in mm) and detail of thermocouples position.

After the forming operation the cup thickness and the cup height were measured, as schematically shown in Figure 9 a). The cup was measured using a 3D measurement machine "Brown & Sharpe Mfg. Co." model "MicroXcel PFX-454". In order to minimize measurement errors related with axisymmetric

deviations, the thickness and height of the cup are presented as the average of the cup vertical axis symmetries (i.e. the presented 1st quadrant 0º to 90º RD is an average of 1st, 2nd, 3th and 4th quadrants). The thickness measurements are performed along the interior and the exterior sides of the cup, in a normal direction to the surface, such that the difference between them corresponds to the thickness value. The measurements are performed at each 45º from 0º to 315ºRD. The cup height is measured at each 5º along the cup edge, and the first measurement point is at 0º to RD. The accuracy in the thickness measurements depends of: the 3D measurement machine accuracy (±3µm), the control of the positioning of the cup on the measurement device (±15µm), and of angular deviations to the RD direction (±5µm) (Coër, 2013). The results of cup dimensions were highly reproducible within the same test conditions.

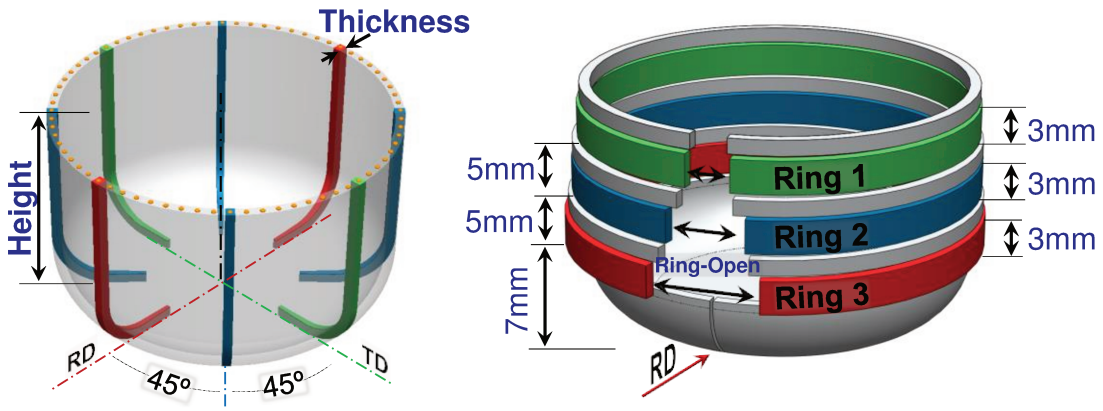

a) b)

Figure 9 – a) Cup dimensions, the thickness was measured at each 45º and the cup height at every five degrees; b) Cutting out the rings from cup wall, each ring has 3mm height.

Springback analysis was performed using the split-ring test. This test consists in: i) cut a ring from the cup wall (trimming); ii) open the ring along the RD (split-ring); and iii) measure the ring opening. The variation of the ring diameter, before and after splitting, gives an indirect measure of the springback phenomenon and of the amount of the circumferential residual stresses present in the formed cup (Grèze et al., 2010). As shown in Figure 9 b) three rings were cut from the cup wall. This procedure allows a more detailed analysis of the springback behavior, since it was previously shown that the magnitude of the ring opening is influenced by its vertical position along the cup wall (Xia et al., 2004). An electrical discharge machining (EDM) was used to cut and open the rings. The rings opening was measured using a microscope to assure high measurement accuracy, and the EDM cut thickness (0.3 mm) was taken into account in the

measured value. More details concerning the experimental procedure used are given in (Simões et al., 2017a).

3.2 Results of the forming process

3.2.1 The punch force analysis

The punch force evolution with its displacement is shown in Figure 10 a) and b), in function of the punch speed, for the EN AW 6016-T4 and the EN AW 6061-T6 alloys, respectively. Globally, with the temperature increase from RT to 200 ºC the punch force decreases, which is linked to the softening behavior resulting from the temperature increase, as previously discussed by (Simões et al., 2017a). Regarding the influence of the punch speed on the punch force evolution, globally the results show that at RT it has a negligible effect, while at 200 ºC it cannot be overlooked. This is valid for both alloys. According with the results presented in subsection 2.2, both alloys present negligible strain-rate sensitivity at RT but significant strain-rate sensitivity at 200 ºC. Thus, the sensitivity of the punch force evolution curves to the punch speed seems to be linked to the material strain rate sensitivity.

As shown in Figure 10 a), at 200 ºC, the EN AW 6016-T4 alloy shows a slightly higher punch force with a higher punch speed up to 9 mm of punch displacement. However, this behavior inverts after 10 mm of punch displacement. This inversion of punch force evolution occurs at about 90, 9 and 0.9 seconds for 0.1, 1 and 10 mm/s of punch speed, respectively. Moreover, for the punch speed of 0.1 mm/s an unusual increase of the drawing force is observed between 10 and 15 mm of punch displacement, which will be discussed in the following section. The same global trend is observed for the EN AW 6061-T6 alloy (Figure 10 b)), at 200 ºC, with higher punch forces linked to higher punch speeds up to 14 mm of punch displacement, followed by an inversion of this behavior. The time instant at which this inversion occurs is at about 150, 15 and 1.5 seconds, for 0.1, 1 and 10 mm/s of punch speed, respectively.

At RT the influence of natural aging (1 and 18 months) in the EN AW 6016-T4 alloy results in higher punch forces (see Figure 10 a)). However, the influence of natural aging in the punch force becomes negligible at 200 ºC, as previously observed by (Simões et al., 2017a). Additionally, the present study shows that at 200 ºC the influence of natural aging in the punch force was negligible, whatever the punch speed used.

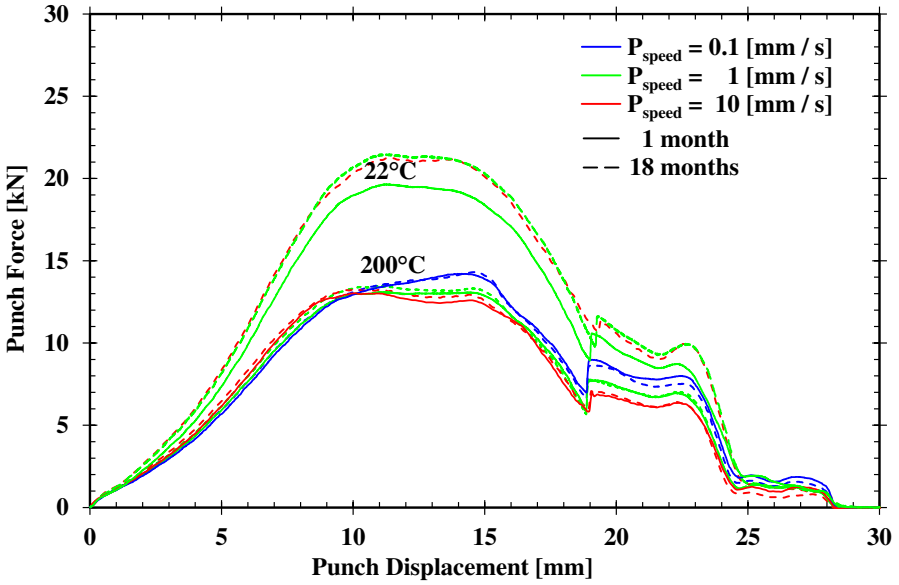

a) EN AW 6016-T4

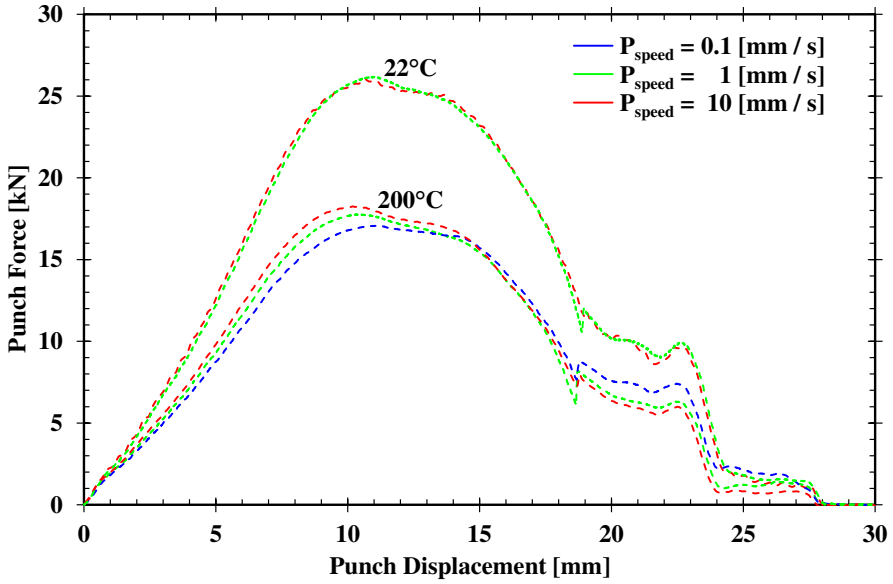

b) EN AW 6061-T6

Figure 10 – The influence of punch speed and temperature on the punch force evolution as function of punch displacement. For the EN AW 6016-T4 the natural aging influence is evaluated performing the tests at 1 and 18 months of storage time. The 1 month aged material is shown by solid line and the 18 months by dash dot line.

3.2.2 Cylindrical Cup dimension analysis

The thickness evolution along the curvilinear distance from the cup center and the cup height profile are presented in Figure 11 a) and b), respectively. The thickness evolution is presented only along RD, since the analysis of the other profiles leads to similar conclusions. For the EN AW 6016-T4 alloy, the results presented in Figure 11 corresponds to the tests performed only at 18 months of natural aging, since

the natural aging effect does not induces significant dimensional differences, as already reported by (Simões et al., 2017a).

As shown in Figure 11 a), globally both alloys present a similar trend for the thickness evolution, which is independent of the test temperature and punch speed. The thickness profile is constant at the cup bottom and close of the initial thickness value. The lower thickness values occur at the entrance to the punch radius section and the confluence of the punch radius with the cup wall. After that the thickness increases until attains a constant final value, due to the ironing phase. Comparing both alloys, it is visible that at the cup bottom and radius zone the EN AW 6061-T6 alloy presents lower thickness values. This difference is linked with the lower initial thickness value of 0.976 mm (see Table 1) for the EN AW 6061-T6 alloy. The EN AW 6016-T4 alloy has an initial thickness of 1.047 mm. In fact, the shape of the thickness profile is independent of the initial thickness value.

Globally, for the same location in the cup, the thickness values attained are higher for the cups performed at 200 ºC. Comparing the tests at 200 ºC with the ones at RT, the increase of temperature promotes the increase of the cup thickness at two distinct zones: (i) the cup radius zone; and (ii) the ironed zone. This temperature effect on the thickness evolution along the cup wall has been previously reported (Simões et al., 2017a). Regarding the cup radius zone, it is related to the cooling action exerted by the punch that produces a strengthening effect on the material located in the cup bottom and radius zone, which combined with a softening for the material located in the heated peripheral region, reduces the required punch load and, consequently, the stress and strains levels on the cup radius zone (Palumbo and Tricarico, 2007). Regarding the ironed zone, the temperature increase leads to the thermal dilation of the tools and, consequently, to the increase of the gap between the die and the punch (Simões et al., 2017a). Such increase explains the higher thickness observed in the ironed zone of the warm formed cups, since it is the gap between the die and the punch that determines the final thickness. Additionally, a higher gap results in a softer ironing phase with lower punch forces (see Figure 10) and, consequently, lower stress and strains levels on the cup radius zone, which also contributes to increase the thickness in the cup radius zone.

For both alloys, the punch speed has a negligible influence on the cup thickness at RT. Concerning the warm formed cups at 200 ºC, the thickness evolution in the ironed zone is affected by the punch speed for both alloys. For the EN AW 6016-T4 alloy, the thickness in the cup radius zone also seems to be slightly

affected by the punch speed. Globally, the thickness is higher for the cups performed at higher punch speeds.

The cup height profile in function of the angle to RD, also known as the ear profile, is shown in Figure 11 b). Globally, there is a relation between the average cup height and the thickness distribution, due to the conservation of the initial blank volume. Therefore, higher heights occur associated to thinner cups, i.e. with lower average thickness distribution. Thus, as shown in Figure 11 b), the higher values of the cup height occurs for the tests at RT while, on the contrary, the cup height is lower for tests performed at 200 ºC. At RT, the EN AW 6016-T4 alloy shows a decrease of the cup height with the increase of punch speed, while the EN AW 6061-T6 alloy shows the opposite behavior. At 200 ºC, the EN AW 6016-T4 alloy shows an increase of cup height with the increase of punch speed, while for the EN AW 6061-T6 alloy the cup height increases when the punch speed increases from 0.1 mm/s to 1 mm/s and decreases when the punch speed increases from 1 mm/s to 10 mm/s. Nevertheless, it should be mentioned that there are slight differences, particularly when taking into account that the results shown in Figure 11 b) are average values.

Lastly, the shape of the ear profile is similar for both alloys, with maxima at RD and 90° to RD, and minimum at 45° to RD and equivalent positions. This is the expected behavior for materials presenting $\Delta r > 0$ (Hu et al., 2001), which is the case of both alloys under study, as shown in (Simões et al., 2017a). Moreover, the global shape of the ear profile is not affected by temperature or punch speed, which indicates the subtle influence of temperature and strain rate in the variation of the materials orthotropic behavior. In fact, (Simões et al., 2017a) observed a slight decrease of the cylindrical cup ears amplitude (the difference between the maximum and minimum height) with the increase of temperature, which was linked with slight reduction of Δr value.

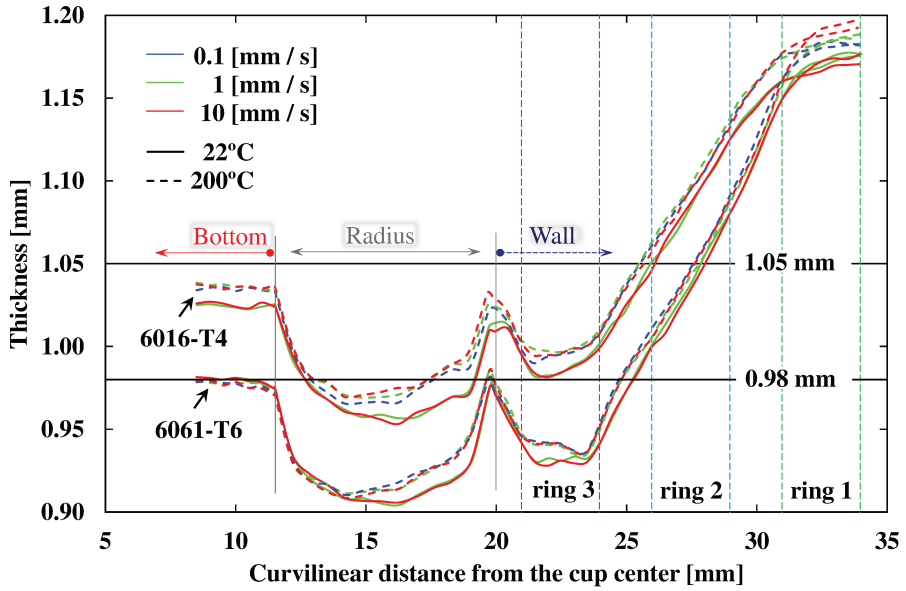

a) Cup Thickness

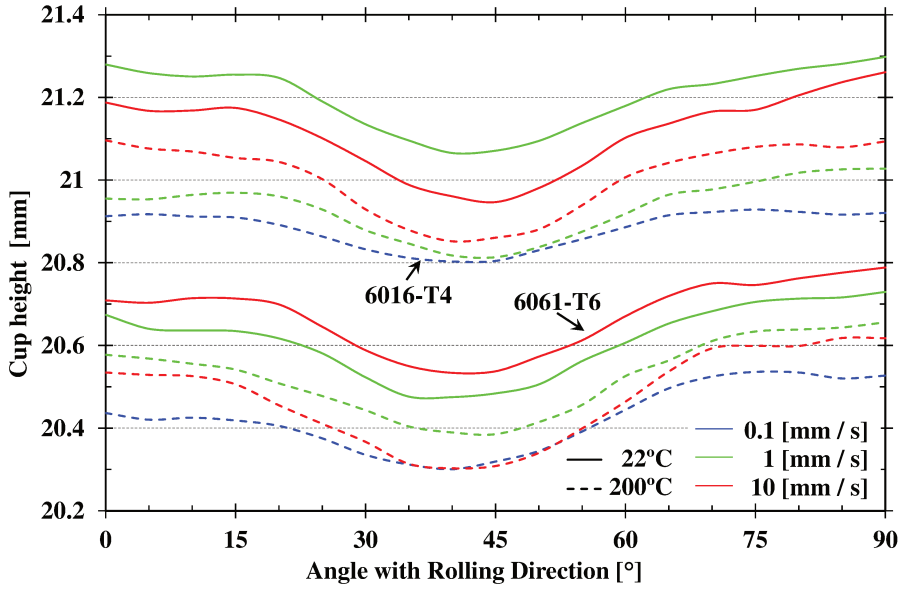

b) Cup Height

Figure 11 – The influence of punch speed and temperature on the full cup dimensions. The tests at RT are shown by solid line and the tests at 200 ºC are shown by dash dot line. The results presented correspond exclusively for the alloys natural aged of 18 months.

3.2.3 Springback analysis: the split-ring test

As presented in Figure 9 b), three rings were cut out from the cup wall at various heights. The measure of the rings opening in function of the punch speed is shown in Figure 12 a) and b) for the EN AW 6016-T4 and the EN AW 6061-T6 alloys, respectively. For the same temperature and punch speed conditions, the EN AW 6061-T6 alloy presents always higher springback values than the EN AW 6016-T4

alloy due to its higher yield stress, as shown in Table 1. In fact, it is known that for the same Young modulus value, springback increases with the increase of the yield stress (Moon et al., 2003).

Concerning the influence of the axial position of the ring in the cup wall, it is observed that the ring opening value decreases as the distance to the cup bottom increases. In fact, ring 3 (near to cup bottom) always presents the highest opening value, while ring 1 (at the cup top) presents the lowest. This trend occurs for both alloys and is independent of the punch speed and the forming temperature. In fact, the influence of the warm forming temperature was previously studied by (Simões et al., 2017a) for both alloys, using the same benchmark test, showing that the ring opening trend does not depend of the test temperature or of the alloy. Moreover, a numerical analysis of the stress condition for this benchmark test was presented by (Simões et al., 2017b), which highlights the impact of an ironing phase on the residual stress distributions in the cylindrical cup and, consequently, in the split-ring test. The results show that the ironing of the vertical wall changes the characteristic distribution of the axial and circumferential residual stresses in all locations of the cup wall, even for relatively small ironing strains. This affects the trend observed for the ring opening value, when rings are cut at different heights. In fact, since the ironing phase imposes high contact forces on the cup wall, which reduces the tangential stress, ring 1 presents a lower springback variation for the various test conditions. The fact that ring 1 presents a negligible springback variation with the increase of punch speed, seems to be connected to the reduction of the circumferential stress component through-thickness gradient induced by the ironing phase, as shown by (Simões et al., 2017b).

At RT, for both alloys (see Figure 12) the punch speed as a negligible effect on the ring opening. While at 200 ºC, for the EN AW 6016-T4 alloy (see Figure 12 a)), the ring opening value decreases linearly with the logarithmic punch speed increase, i.e. the higher ring opening variation occurs from a punch speed of 0.1 mm/s to 1 mm/s. Moreover, at 200 ºC the ring opening values are very similar for the material natural aged of 1 and 18 months. At 200 ºC, for the EN AW 6061-T6 alloy (see Figure 12 b)), the punch speed as a negligible effect on the ring opening value.

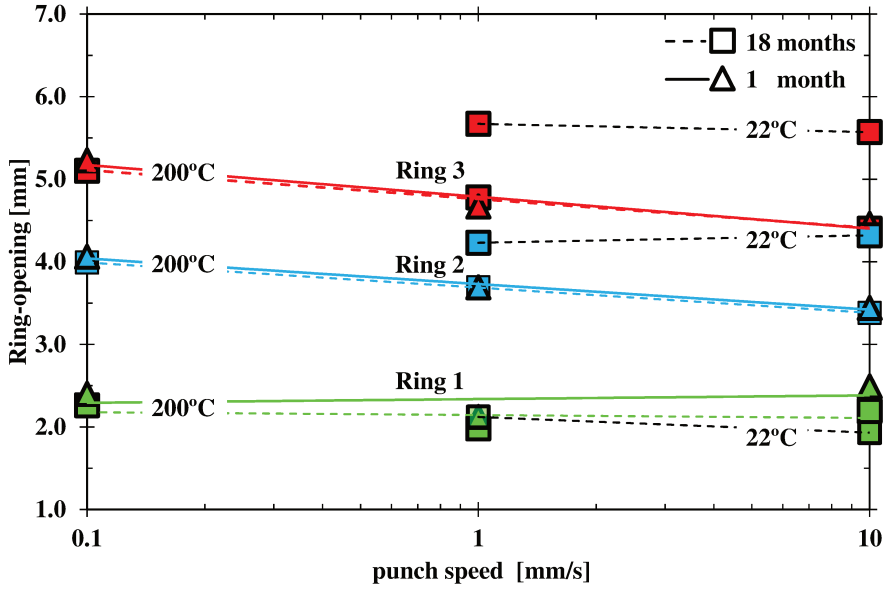

a) EN AW 6016-T4

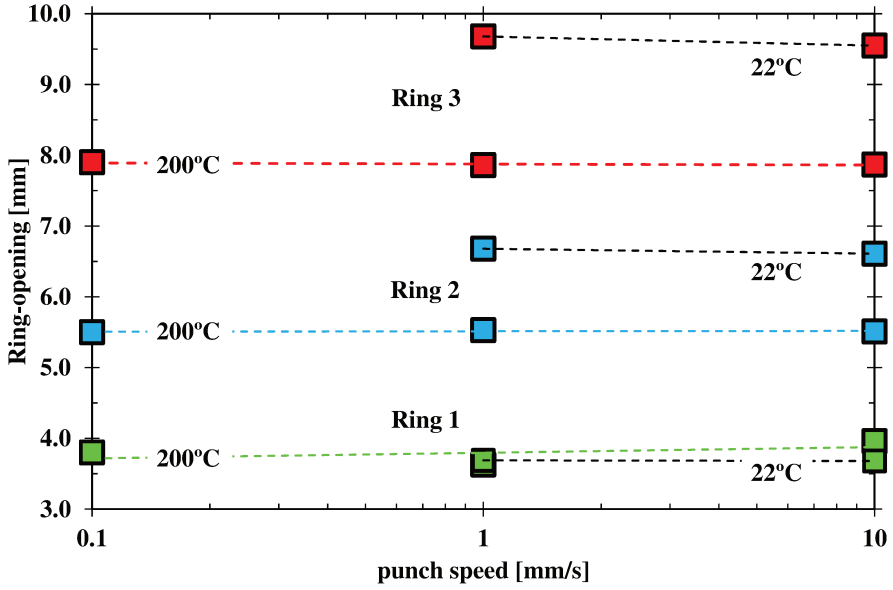

b) EN AW 6061-T6

Figure 12 – The influence of punch speed and temperature on ring opening. The punch speed axis is presented in a logarithmic scale. The 1 month aged material is only presented for the EN AW 6016-T4 alloy, for the tests at 200 ºC. The 1 month aged material is shown by solid line and the 18 months by dash dot line. These lines correspond to a logarithmic regression of the data presented.

4 Results analysis and discussion

In order to improve the understanding of the results obtained during the warm forming process, a detailed analysis of the temperature evolution is performed for the test at 200 ºC, for the EN AW 6016-T4 alloy (1 month aged), with a punch speed of 1 mm/s. Figure 13 a) presents the temperature evolution in

each of the thermocouples during the cylindrical cup test, while Figure 13 b) presents the punch force and blank-holder force evolutions. The negative time scale is used in Figure 13 to differentiate the heating phase from the forming phase, i.e. the negative time scale refers to the heating time countdown until the beginning of the forming phase.

Figure 13 connects the various steps, outlined in Figure 7, with the temperature and forces measured during the experimental test. **The heating phase** includes the steps presented in Figure 7 a) and b), which correspond to the negative time interval in Figure 13. In the first step, Figure 7 a), the die and the blank-holder were pre-heated by internal electrical heating rods up to the test temperature (200ºC), while the punch is refrigerated with water at RT in order to keep its temperature close to RT. The second step is the blank heating, which starts with the placement of the lubricated blank in the blank-holder (see Figure 7 b)). As shown Figure 13 a), since the blank is placed in the blank-holder, approximately 60 seconds elapse until the forming phase starts. The blank attains a temperature of thereabout 190ºC in 40 seconds (at minus 20 seconds). In fact, the first step of tools heating is performed in order to reduce the blank heating time. Moreover, the reduced heating time of approximately 60 seconds can help to minimize the occurrence of microstructural changes for the EN AW 6016-T4 alloy. Once the blank, the die and the blank-holder are at the test temperature (within a margin of error of less than 2.5%, Figure 13 a)), the blank-holder clamps the sheet against the die, until attaining a force of 6 kN (Figure 13 b)). After the blank-holder clamping, the die, the blank-holder and the sheet have the same temperature of about 200 $^{\pm 5}$ ºC, while the punch keeps its temperature close to RT. In fact, during the blank heating, the punch has no contact with the blank, since it is placed at approximately 4 mm from the blank (see Figure 7 b)). However, there is some heat transfer by convection and, consequently, the temperature of the blank center (TC Blank 1) is slightly lower than close to the flange zone (TC blank 2). The heating phase and blank-holder clamping force are similar for all test, whatever the punch speed.

The warm forming of the cylindrical cup begins at the instant of time equal to zero, when the punch contacts with the blank. Such contact leads to an abrupt drop in the blank temperature, in order to establish a thermal equilibrium between the cold punch and the heated die and blank-holder. TC Blank 1 presents a lower temperature than TC Blank 2 since the center of the blank establishes contact with the punch first. Then, the punch moves forward into the die cavity deforming the blank (Figure 7 c)). In the first 8 seconds, the punch force and temperature increases rapidly while the blank and the die temperature decreases. Between 8 and 13 seconds the punch force stabilizes, attaining a plateau, which corresponds to

the instant that the die and the punch shoulder radii are completely formed in the part (Figure 7 c)). During this time interval, the blank presents a significant contact area with the cold punch (punch bottom and radius) and with the heated die (die radius and flange). This high contact surface contributes to a stabilization of the punch and the die temperature, since the heat flows from the flange zone, through the blank, and is dissipated by the punch cooling system, promoting a thermal equilibrium. During this time interval, the blank temperature (TC Blank 1 and TC Blank 2) follows an almost linear decrease with a reduced slope, as shown Figure 13 a). This decrease is due to the heat transfer between the bottom of the cup and the cold punch.

After the plateau, the punch force decreases until it reaches a local minimum at ≈17.3 seconds, which corresponds to the instant the blank loses contact with the blank-holder. In fact, previous to this instant (at ≈15.4 seconds) the blank losses contact with the flange zone. However, since the tool presents no blank-holder stopper, the blank-holder promotes the movement of the sheet into the die cavity and, consequently, reduces the punch force (see Figure 13 b)). Once the blank loses its contact with the flange zone, it loses an important source of heat and, as consequence, its temperature decreases. During the **ironing phase**, which starts at ≈18.5 seconds, the temperature in the die radius (TC Die) also decreases with a slightly higher slope due to the high contact forces imposed. In fact, according to (Chang et al., 2016), higher contact pressure causes more deformation of the asperities at the interface (reducing the blank surface roughness), so the actual contacting area enlarges and the thermal contact resistance decreases, resulting in an increase of the interfacial heat transfer coefficient. These results support the temperature decrease in die radius during the ironing phase. During this phase, the punch force attains a local maximum (≈20 seconds), followed by a decrease until the ironing of the ears and then until the end of the process. After 22 seconds, as shown in Figure 13 a), the die temperature reverses its downward trajectory and increases again up to its initial temperature. The blank and the punch temperatures decrease linearly until the end of the forming process, presenting at the end the same temperature of ≈50ºC. At the end of the process, the punch stops and the ejector is activated to remove the cup from the die's cavity (Figure 7 e)).

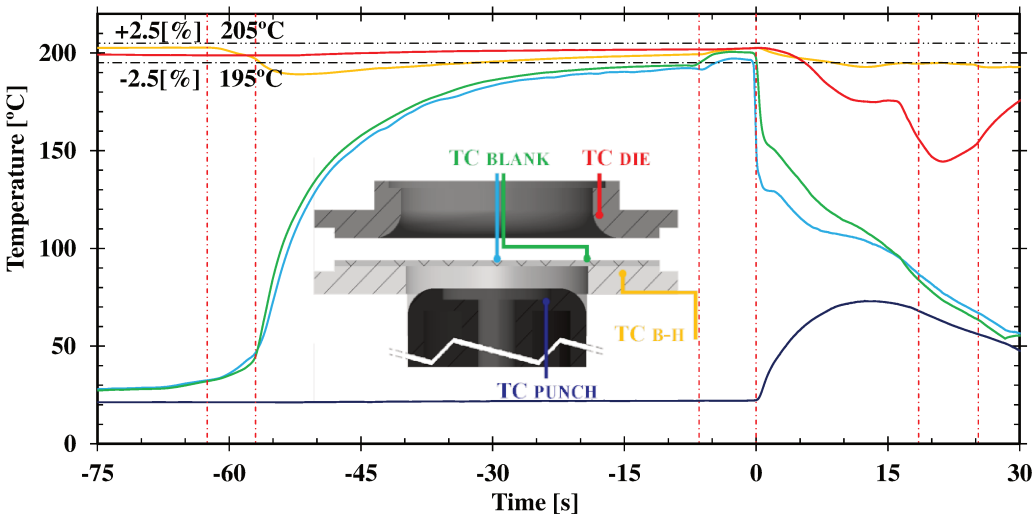

a) Temperature evolution

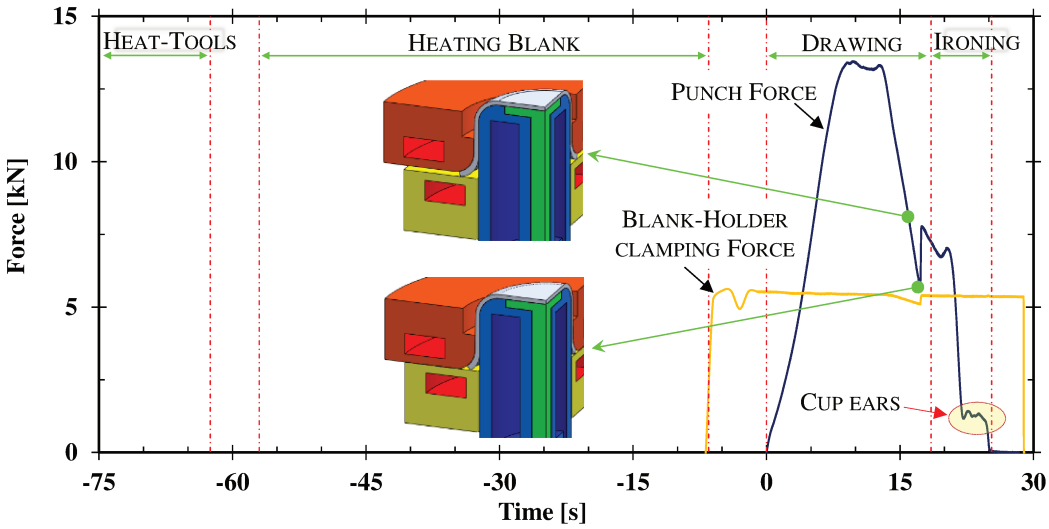

b) Punch and Blank-Holder force evolutions

Figure 13 – Cylindrical cup test at 200ºC, with pre-heated die and blank-holder and cold punch at a punch speed of 1 mm/s. The negative scale refers the heat time countdown to the beginning of drawing phase, and the positive scale refers the temperature gradient during drawing phase. The results presented corresponds to the EN AW 6016-T4 alloy natural aged of 1 month with a punch speed of 1 mm/s.

The results shown in Figure 13 highlight that, under non-isothermal conditions, the heat transfer phenomena that occur have a strong impact in the temperature of the blank during the forming process. The heat transfer is affected by the punch speed, since the duration of the forming phase will be in a range between ≈300 seconds (for 0.1 mm/s) and ≈3 seconds (for 10 mm/s), instead of the ≈30 seconds shown in Figure 13 for the punch speed of 1 mm/s. Figure 14 a) shows the analysis of the temperature evolution in function of the punch displacement for the three punch speeds, where the 0.1, 1 and 10 mm/s are presented by the dot, the solid and the dash line, respectively. The results presented correspond to the EN AW 6016-

T4 alloy at 18 months of natural aging, showing that the temperature evolution is similar to the one observed for the same alloy at 1 month of natural aging (see Figure 13 a)). Although not shown here, the same comment is valid for the temperature evolution for the EN AW 6061-T6 alloy and for different punch speeds.

As shown in Figure 14 a), the shape of the temperature evolution curves is quite similar for the punch speeds of 0.1 mm/s and 1 mm/s. In the drawing phase, the blank temperature (TC Blank 1 and TC Blank 2) is mostly coincident for both punch speeds. Nevertheless, it should be mentioned that the TC Die and the TC B-H show lower temperature values for the punch speed of 0.1 mm/s, while the TC Punch presents higher temperature values. In the ironing phase, the temperature in the tools and in the blank is lower at the punch speed of 0.1 mm/s. Concerning the temperature evolution for a punch speed of 10 mm/s, the temperature in TC B-H is stable during the entire test, while the TC Die presents a slight temperature decrease and the TC Punch a slight temperature increase. The temperature evolution in TC Blank 1 and TC Blank 2 presents an almost linear decrease, with a higher rate from the beginning of the test up to the instant of the maximum punch force. Thereafter, the TC Blank 1 and the TC Blank 2 temperature decreases linearly, but with a smaller rate. Globally, the average blank temperature is higher for the higher punch speeds.

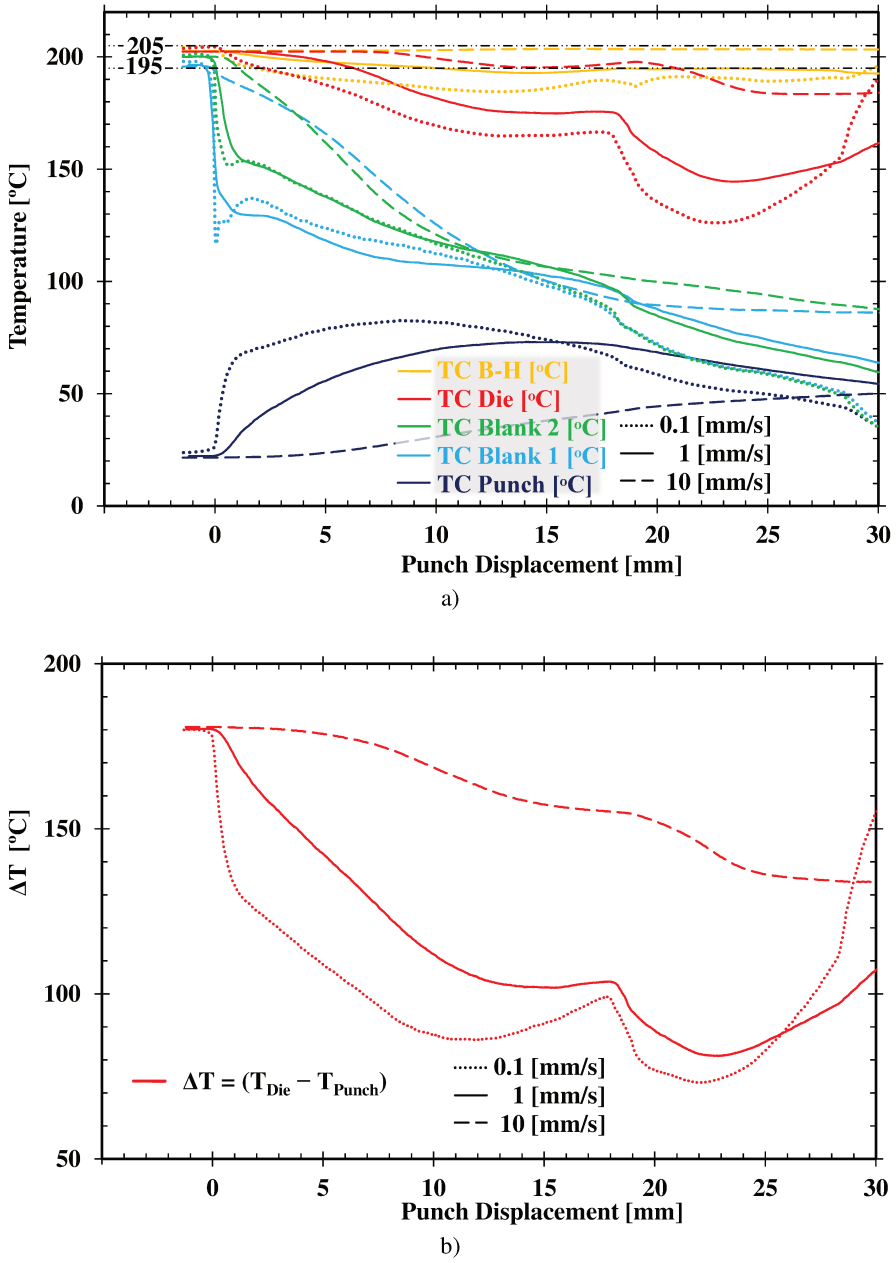

Figure 14 – Analysis of temperature gradient in function of punch displacement, in warm forming of a cylindrical cup at 200 ºC for the tested punch speeds (0.1, 1 and 10 mm/s): a) The temperature evolution in function of punch displacement; b) The temperature gradient between TC Die and TC Punch in function of punch displacement. The results presented correspond to tests for the EN AW 6016-T4 alloy natural aged of 18 months.

The temperature difference between TC Die and TC Punch, in function of punch displacement, is presented in Figure 14 b). The punch speed has a high influence on the heat transfer that occurs between the tools, through the blank. At the lowest punch speed (0.1 mm/s), the temperature difference between the heated die and the cooled punch is minimum, indicating that the heat exchanges during the forming process are maximal, i.e. the temperature of the cooled punch increases and the temperature of the heated die

decreases during the drawing phase, due to the thermal equilibrium associated with the long duration of the test. This also explains why the temperature of the punch tends to decrease when the blank loses contact with the flange area of the heated tools. At the highest punch speed (10 mm/s), the temperature difference between the warm die and the cold punch is maximum. In fact, the tools keep their temperature values nearly constant during the warm forming process. These results are in accordance with the ones presented by (Ma et al., 2015), reporting that high punch speed can keep heat transfer between the tools at a minimum level during the hot forming process. In fact, during the forming process, heat transfer rate between the cold punch and the heated flange zone is a function of the temperature difference between the tools, and is proportional to time. Therefore, higher punch speeds reduce the exposure time and, consequently, reduce the heat transfer between the tools.

The reduction of the temperature difference between the die and the punch with the decrease of the punch speed causes a reduction of the gap between these tools, leading to a harder ironing phase. In fact, the temperature increase leads to an increase of the punch diameter as well as the die internal diameter. For a punch speed of 0.1 mm/s, the higher punch temperature and the lowest die temperature leads to the smaller difference between these dimensions, as compared with higher punch speeds. This explains the higher forces presented during the ironing phase at the lowest punch speed, as shown in Figure 10. On the other hand, for the punch speed of 10 mm/s the gap between the die and the punch presents the highest value, resulting in the lowest ironing forces. These differences in the gap between the die and the punch are also noticed in the cup wall thickness, where the highest punch speed presents slightly higher thickness values at the end of the vertical wall, for both alloys (see Figure 11 a)). The hardening effect associated with the decrease of the punch temperature, associated to the increase of the punch speed, combined with the tools thermal dilatation influences the stress and strain distribution in the cup. These effects can explain the slight inferior thickness reduction at the cup radius zone with the increase of the punch speed, observed for the EN AW 6016-T4 alloy (see Figure 11 a)). This slight inferior thickness reduction also explains the slightly higher cup high observed with the increase of the punch speed, for this alloy (see Figure 11 b)). The EN AW 6016-T4 alloy presents higher thickness values in the ironed zone, for higher punch speeds, has a result of the tools dilation. However, there are no differences at the cup radius zone, which can be related with the softer ironing phase resulting from its lower initial thickness.

In cylindrical cup forming, the punch speed directly influences the strain rate and, consequently, the material mechanical behavior (Palumbo and Tricarico, 2007). Despite a negligible strain rate sensitivity

at RT, both alloys present a positive strain rate sensitivity in warm conditions (see Figure 4 b) and Figure 6). This positive strain rate sensitivity results in higher punch forces linked with higher punch speeds, until approximately 10 mm of punch displacement (see Figure 10). In fact, during this period the blank presents a large contact area with the heated flange, indicating that it keeps a relatively stable temperature, whatever the punch speed. Subsequently, from 10 to 19 mm of punch displacement, the blank progressively loses contact with the flange zone and its temperature is mainly imposed by the temperature difference between the die and the punch. During this period, the punch force is similar whatever the punch speed, with exception to the test performed with the EN AW 6016-T4 alloy, with a punch speed of 0.1 mm/s, as already mentioned in section 3.2.1. Globally, the higher average temperature of the blank for the punch speed of 10 mm/s may contribute to reduce the forming forces, since the material becomes softer as the temperature increases. On the other hand, the positive strain rate sensitivity leads to a harder material behavior, contributing to increase the forming forces. On the contrary, for lower punch speeds, the lower average temperature of the blank may contribute to increase the forming forces. Thus, it seems that the positive strain rate sensitivity at higher punch speeds is counterbalanced by the harder material behavior due to lower temperatures for lower punch speed. Afterwards, during the ironing phase, as explained previously, the higher punch force obtained with the lower punch speed is related with the lower gap between the die and the punch that causes a harder ironing phase.

The temperature evolution of tools and blank as a function of time (in logarithmic scale) is presented in Figure 15, enabling the analysis of the heat exchanges as a function of time, which increase as the forming time increases. The trend of the temperature evolution of TC Punch and TC B-H is mostly similar and independent of the punch speed. Concerning the TC B-H, the temperature decreases smoothly as time increases, remaining mostly above 190 ºC. The temperature of TC Punch is constant in the first second and afterward it increases as time increases. However, for the punch speeds of 0.1 and 1 mm/s the temperature of TC Punch decreases during the ironing phase. The temperature of TC Die clearly depends of the punch displacement and time; therefore its analysis is more complex. The temperature of TC Die presents an initial first period with a slight decrease, followed by a faster decrease up to attaining a plateau. This plateau corresponds to the instant that the die and the punch shoulder radii are completely formed in the part, i.e. the instant of maximal punch force, between 10 and 15 mm of punch displacement. Afterwards, the temperature of TC Die abruptly decreases during the ironing phase and increases when the die losses the contact with the blank.

Concerning the blank temperature evolution, at the highest punch speed, the blank temperature is about 0.55 seconds above 150 ºC and about 1 second between 150 ºC and 100 ºC. For the punch speeds of 1 and 0.1 mm/s, TC Blank 2 is above 150 ºC for 2.2 and 21.1 seconds, respectively. Moreover, TC Blank 2 is between 150 ºC and 100 ºC for 12.25 (14.75-2.2) and 104 (125-21.1) seconds, for the punch speeds of 1 and 0.1 mm/s, respectively. The same exposition times are valid for the temperature of TC Blank 1 in between 150 ºC and 100 ºC, for the same punch speeds.

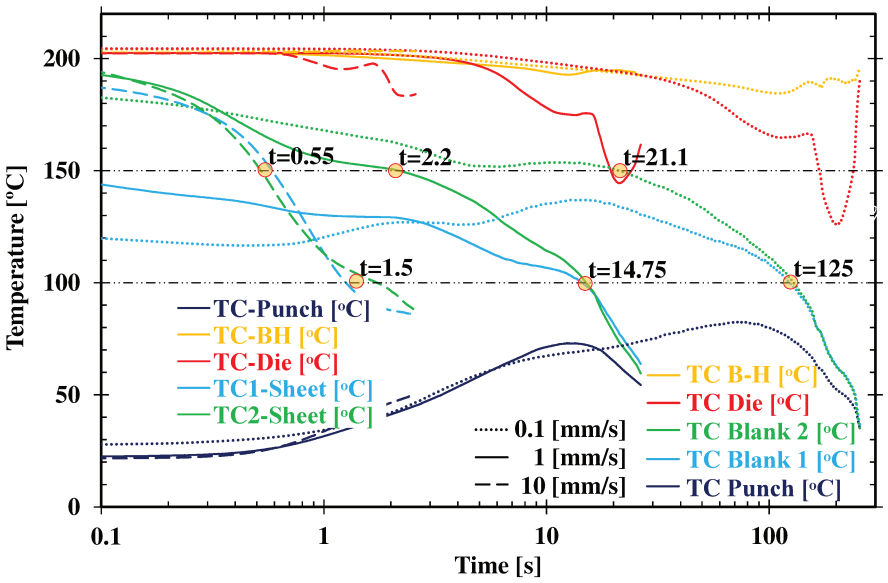

Figure 15 – Analysis of the temperature evolution in function of time presented in logarithmic scale, in warm forming of a cylindrical cup at 200 ºC for the tested punch speeds (0.1, 1 and 10 mm/s). The results presented correspond to tests for the EN AW 6016-T4 alloy natural aged of 18 months.

In section 2.2 it was shown that temperature and exposure time are major parameters affecting the mechanical behavior of the EN AW 6016-T4 alloy. To understand any microstructural modifications that may occur on the blank during warm forming, it is necessary to correlate the tensile tests results presented section 2.2 with the blank exposure time presented in Figure 15. It is clearly shown that for the punch speed of 10 mm/s the blank is exposed to higher temperatures during the forming process, however, the exposure time is very short. For the punch speed of 0.1 and 1 mm/s the blank bottom and radius (TC Blank 1 and TC Blank 2) are mostly exposed to a lower temperature range, between 150 and 100 ºC, but for a longer period. This is particularly critical for the punch speed of 0.1 mm/s leading to an exposure time of at least 125 seconds.

As previously mentioned, the test performed with the EN AW 6016-T4 alloy with a punch speed of 0.1 mm/s, presents an increase of the punch force, between 10 and 15 mm of punch displacement (see

Figure 10 a)), which is not observed for the other tests. This interval corresponds to an exposure time of about 100 seconds. This increase of the punch force can be understood with the analysis of the true stress – true strain curves, at a strain rate of $2x10^{-4}s^{-1}$ (see Figure 2 and Figure 5), where it is observed that an exposure time of about 90 seconds is enough to promote dynamic precipitation hardening, under uniaxial tensile conditions. As previously mentioned, (Ghosh et al., 2014) observed a similar behavior in the warm forming at 250 ºC, of the same alloy, where a decrease of the punch speed from 1 to 0.18 mm/s leads the material to approach the T6 condition. According to the authors, these observations can be explained in terms of dynamic precipitation, which is a common phenomenon in warm forming of heat treatable aluminum alloys. According to (Cai et al., 2004) and (Kolar et al., 2012), which studied the combined effect of deformation and precipitation on the mechanical properties of Al-Mg-Si alloys, the dislocations introduced during plastic deformation lead precipitates to growth by dislocation-assisted diffusion mechanism, reducing the time to reach the peak strength as compared to static aging. The occurrence of dynamic precipitation hardening can also explain the increase of the ring opening values with the decrease of the punch speed (see Figure 12 a)), which is more relevant for the two lower punch speed values.

5 Conclusions

For non-heat treatable aluminum alloys, as discussed in the Introduction, it has been reported that the increase of the punch speed contributes to the decrease the formability, both under isothermal conditions and non-isothermal conditions. The best formability was achieved for the tests performed at the higher temperature values with the lowest punch speed values. Additionally, it was also reported in literature an increase of springback with the punch speed increase, both under isothermal and non-isothermal condition. This corresponds to the expected behavior for materials presenting a positive strain rate sensitivity. Nonetheless, the results of this study show that, when considering non-isothermal conditions for heat-treatable aluminum alloys, the temperature gradient in the blank has a strong impact in the formability and the springback behavior. As observed for the EN AW 6061-T6 alloy, for higher punch speeds the positive strain rate sensitivity can compensate the hardening effect induced by the temperature gradient in the blank, leading to similar results whatever the punch speed. On the other hand, as observed for the EN AW 6016-T4 alloy, high punch speed values can be advantageous since they can contribute to increase the effect of the temperature gradient in the blank, with an increase of the final thickness (which may result in higher formability) and the springback reduction.

In brief, the results presented clearly show that the punch speed has a different impact in the forming behavior and springback of both heat treatable aluminum alloys. The influence of the punch speed can be divided in its impact on the material behavior and on the temperature gradient in the blank. Globally, the heat transfers that occur during the process are mostly dependent on the forming time. The higher punch speed reduces the exposure time and consequently reduces the heat exchanges. Thus, at higher punch speed, the tools keep their temperature values nearly constant during the warm forming. Additionally, for the EN AW 6016-T4 alloy high punch speed values avoid dynamic precipitation that causes additional hardening reducing the formability and increasing the springback. In this sense, a high punch speed is advantageous in warm forming under non-isothermal conditions, because it allows a better control of the process, including the temperature difference between the tools.

Acknowledgements

The authors would like to acknowledge the funding that sponsored this research work: the national funds from the French Ministry of Higher Education and the Portuguese Foundation for Science and Technology (FCT) via the project P2020-PTDC/EMS-TEC/6400/2014 (POCI-01-0145-FEDER-016876) and by UE/FEDER funds through the program COMPETE 2020, under the project CENTRO-01-0145-FEDER-000014 (MATIS). The first author V. Simões is also grateful to the FCT for the PhD grant SFRH/BD/90669/2012. The authors are also grateful to Constellium (Estelle Muller) for supplying the material. Moreover, the authors acknowledge the technical staff of IRDL, for their help in some of the experimental procedures (Anthony Jégat and Hervé Bellegou).

References

Ayres, R.A., Wenner, M.L., 1979. Strain and strain-rate hardening effects in punch stretching of 5182-0 aluminum at elevated temperatures. Metall. Trans. A 10, 41–46. doi:10.1007/BF02686404

Banhart, J., Chang, C.S.T., Liang, Z., Wanderka, N., Lay, M.D.H., Hill, A.J., 2010. Natural Aging in Al-Mg-Si Alloys - A Process of Unexpected Complexity. Adv. Eng. Mater. 12, 559–571. doi:10.1002/adem.201000041

Bolt, P.J., Lamboo, N., Rozier, P., 2001. Feasibility of warm drawing of aluminium products. J. Mater. Process. Technol. 115, 118–121.

Cai, M., Field, D.P., Lorimer, G.W., 2004. A systematic comparison of static and dynamic ageing of two Al–Mg–Si alloys. Mater. Sci. Eng. A 373, 65–71. doi:10.1016/j.msea.2003.12.035

Central Secretariat ISO, 2009. ISO 6892-1:2009 Metallic materials - Tensile testing - Part 1: Method of test at room temperature. International Organization for Standardization, Geneva, Switzerland.

Chang, Y., Tang, X., Zhao, K., Hu, P., Wu, Y., 2016. Investigation of the factors influencing the interfacial heat transfer coefficient in hot stamping. J. Mater. Process. Technol., Hot Stamping 228, 25–33. doi:10.1016/j.jmatprotec.2014.10.008

Coër, J., 2013. Mise en forme par emboutissage en température d'un alliage d'aluminium AA5754-O (PhD-thesis). Université de Bretagne Sud.

Coër, J., Bernard, C., Laurent, H., Andrade-Campos, A., Thuillier, S., 2011. The Effect of Temperature on Anisotropy Properties of an Aluminium Alloy. Exp. Mech. 51, 1185–1195. doi:10.1007/s11340-010-9415-6

Engler, O., Hirsch, J., 2002. Texture control by thermomechanical processing of AA6xxx Al–Mg–Si sheet alloys for automotive applications—a review. Mater. Sci. Eng. A 336, 249–262. doi:10.1016/S0921-5093(01)01968-2

Fan, X., He, Z., Zhou, W., Yuan, S., 2016. Formability and strengthening mechanism of solution treated Al–Mg–Si alloy sheet under hot stamping conditions. J. Mater. Process. Technol., Hot Stamping 228, 179–185. doi:10.1016/j.jmatprotec.2015.10.016

Ghosh, M., 2011. Microstructurally Controlled Mechanical Properties of Al-Mg-Si Alloys for Warm Forming Applications (PhD-thesis). Delft University of Technology, Delft, The Netherlands.

Ghosh, M., Miroux, A., Werkhoven, R.J., Bolt, P.J., Kestens, L.A.I., 2014. Warm deep-drawing and post drawing analysis of two Al–Mg–Si alloys. J. Mater. Process. Technol. 214, 756–766. doi:10.1016/j.jmatprotec.2013.10.020

Grèze, R., Manach, P.Y., Laurent, H., Thuillier, S., Menezes, L.F., 2010. Influence of the temperature on residual stresses and springback effect in an Aluminium alloy. Int. J. Mech. Sci. 52, 1094–1100. doi:10.1016/j.ijmecsci.2010.04.008

Hirsch, J., 2011. Aluminium in innovative light-weight car design. Mater. Trans. 52, 818–824.

Hu, P., Liu, Y.Q., Wang, J.C., 2001. Numerical study of the flange earring of deep-drawing sheets with stronger anisotropy. Int. J. Mech. Sci. 43, 279–296. doi:10.1016/S0020-7403(99)00119-8

H.Y. Hunsicker, 1984. Chapter 5 - Metallurgy of Heat Treatment and General Principles of Precipitation Hardening, in: John E. Hatch (Ed.), Aluminum: Properties and Physical Metallurgy. ASM International, Metals Park, Ohio, pp. 134–199.

Jelt Grease 5411 aerosol 95cSt [WWW Document], n.d. URL http://fr.rs-online.com/web/p/graisses/4612124/ (accessed 11.25.15).

Kim, H.S., Koç, M., 2008. Numerical investigations on springback characteristics of aluminum sheet metal alloys in warm forming conditions. J. Mater. Process. Technol. 204, 370–383. doi:10.1016/j.jmatprotec.2007.11.059

Kolar, M., Pedersen, K.O., Gulbrandsen-Dahl, S., Marthinsen, K., 2012. Combined effect of deformation and artificial aging on mechanical properties of Al–Mg–Si Alloy. Trans. Nonferrous Met. Soc. China 22, 1824–1830. doi:10.1016/S1003-6326(11)61393-9

Laurent, H., Coër, J., Manach, P.Y., Oliveira, M.C., Menezes, L.F., 2015. Experimental and numerical studies on the warm deep drawing of an Al–Mg alloy. Int. J. Mech. Sci. 93, 59–72. doi:10.1016/j.ijmecsci.2015.01.009

Li, D., Ghosh, A., 2003. Tensile deformation behavior of aluminum alloys at warm forming temperatures. Mater. Sci. Eng. A 352, 279–286. doi:10.1016/S0921-5093(02)00915-2

Li, D., Ghosh, A.K., 2004. Biaxial warm forming behavior of aluminum sheet alloys. J. Mater. Process. Technol. 145, 281–293. doi:10.1016/j.jmatprotec.2003.07.003

Ma, W., Wang, B., Fu, L., Zhou, J., Huang, M., 2015. Influence of process parameters on deep drawing of AA6111 aluminum alloy at elevated temperatures. J. Cent. South Univ. 22, 1167–1174. doi:10.1007/s11771-015-2630-7

Manach, P.-Y., Coër, J., Laurent, A.J.H., Yoon, J.W., 2016. Benchmark 3 - Springback of an Al-Mg alloy in warm forming conditions. J. Phys. Conf. Ser. 734, 22003. doi:10.1088/1742-6596/734/2/022003

Moon, Y.H., Kang, S.S., Cho, J.R., Kim, T.G., 2003. Effect of tool temperature on the reduction of the springback of aluminum sheets. J. Mater. Process. Technol. 132, 365–368. doi:10.1016/S0924-0136(02)00925-1

Naka, T., Yoshida, F., 1999. Deep drawability of type 5083 aluminium–magnesium alloy sheet under various conditions of temperature and forming speed. J. Mater. Process. Technol. 89–90, 19–23. doi:10.1016/S0924-0136(99)00057-6

Neto, D.M., Martins, J.M.P., Cunha, P.M., Alves, J.L., Oliveira, M.C., Laurent, H., Menezes, L.F., 2017. Thermo-mechanical finite element analysis of the AA5086 alloy under warm forming conditions. Int. J. Solids Struct. doi:10.1016/j.ijsolstr.2017.06.011

Palumbo, G., Piccininni, A., Guglielmi, P., Di Michele, G., 2015. Warm HydroForming of the heat treatable aluminium alloy AC170PX. J. Manuf. Process. 20, Part 1, 24–32. doi:10.1016/j.jmapro.2015.09.012

Palumbo, G., Tricarico, L., 2007. Numerical and experimental investigations on the Warm Deep Drawing process of circular aluminum alloy specimens. J. Mater. Process. Technol. 184, 115–123. doi:10.1016/j.jmatprotec.2006.11.024

Panicker, S.S., Singh, H.G., Panda, S.K., Dashwood, R., 2015. Characterization of Tensile Properties, Limiting Strains, and Deep Drawing Behavior of AA5754-H22 Sheet at Elevated Temperature. J. Mater. Eng. Perform. 24, 4267–4282. doi:10.1007/s11665-015-1740-6

Picu, R.C., Ozturk, F., Esener, E., Li, R., 2010. Aluminum Alloys with Identical Plastic Flow and Different Strain Rate Sensitivity. Metall. Mater. Trans. A 41, 3358–3364. doi:10.1007/s11661-010-0423-z

Shehata, F., Painter, M.J., Pearce, R., 1978. Warm forming of aluminium/magnesium alloy sheet. J. Mech. Work. Technol. 2, 279–290. doi:10.1016/0378-3804(78)90023-2

Simões, V.M., Laurent, H., Oliveira, M.C., Menezes, L.F., 2017a. The impact of warm forming in the natural aging of Al-Mg-Si alloys. Submitt. Int. J. Mater. Form.

Simões, V.M., Oliveira, M.C., Neto, D.M., Cunha, P.M., Laurent, H., Alves, J.L., Menezes, L.F., 2017b. Numerical study of springback using the split-ring test: influence of the clearance between the die and the punch. Int. J. Mater. Form. 1–13. doi:10.1007/s12289-017-1351-x

Wilson, D.V., 1988. Aluminium versus steel in the family car — the formability factor. J. Mech. Work. Technol. 16, 257–277. doi:10.1016/0378-3804(88)90055-1

Xia, Z.C., Miller, C.E., Ren, F., 2004. Springback Behavior of AA6111-T4 with Split-Ring Test, in: AIP Conference Proceedings. Presented at the MATERIALS PROCESSING AND DESIGN: Modeling, Simulation and Applications - NUMIFORM 2004 - Proceedings of the 8th International Conference on Numerical Methods in Industrial Forming Processes, AIP Publishing, pp. 934–939. doi:10.1063/1.1766647

Figure captions

Table captions

Video1

Click here to download Video Still: Video1.mp4

Video2

Click here to download Video Still: Video2.mp4

Chapter 5.

On the influence of heat-holding time on the warm forming behavior for two Al-Mg-Si alloys

This chapter contains the paper under preparation, to be submitted to be published in an international scientific journal, with the same title as the chapter. This work discusses the influence of the heat-holding time at 200°C on the thermo-mechanical behavior of the two Al-Mg-Si alloys, using uniaxial tensile tests. The results of cylindrical cup tests and split ring (springback) tests performed for different heat-holding times (from 1 to 30 minutes) are also discussed. It shows that this process parameter has to be properly controlled in case of heat treatable alloys, particularly for the naturally aged.

.

(Page intentionally left blank)

On the Influence of heat-holding time on the warm forming behavior for two Al-Mg-Si alloys

V.M. Simões[1, 2], M.C. Oliveira[2], H. Laurent[1], L.F. Menezes[2]

[1] Univ. Bretagne Sud, FRE CNRS 3744, IRDL, F-56100 Lorient, France.

[2] CEMMPRE, Department of Mechanical Engineering, University of Coimbra, Polo II, Rua Luís Reis Santos, Pinhal de Marrocos, 3030-788 Coimbra, Portugal

Corresponding author: vasco.simoes@uc.pt

Highlights

- The influence of the heat-holding time on the warm forming formability and springback was analyzed for heat treatable aluminum alloys.
- For natural aged alloys, high heat-holding times lead to static precipitation and artificial aging.
- For artificial aged alloys, high heat-holding times lead to negligible static precipitation, without over aging.
- Warm forming with low heat-holding times assures an improvement of formability and springback.

Abstract

In warm forming of heat treatable aluminum alloys, since the heat treatment and the warm forming temperatures are within the same range, changes of heat treatment conditions can occur in function of the heat-holding time compromising the success of the forming operation and in-service behavior. This study goal is to improve the understanding about the impact of different heat-holding times, in order to establish some guidelines to better control the warm forming processing condition, namely concerning formability and springback. Two heat treatable Al–Mg–Si alloys (EN AW 6016-T4 and EN AW 6061-T6) are studied between 22 ºC and 200 ºC, using tensile tests and cylindrical cup forming followed by split ring (springback) test. The tensile tests were performed using the Gleeble device and a tensile test machine coupled with a furnace. Both devices have different heating methods, which influences the thermo-mechanical behavior and leads to different strain distributions during the tensile test. For the EN AW 6016-T4, the increase of the heat-holding time up to 30 minutes leads to increase the yield stress and tensile strength, while the total elongation reduces, promoting the heat treatment change from T4 (natural aged) to T6 (artificial aged) condition. Consequently, in the warm forming tests the springback increase as the heat-holding time increases, although there are no remarkable differences in formability. Moreover, in case of prolonged natural aging, the high heat-holding time leads to the well-known negative-effect of natural aging in artificial aging. For the EN AW 6061-T6, the increase of the heat-holding time up to 50 minutes has a negligible impact on the material behavior and no over aging occurs. In brief, warm forming under non-isothermal conditions with a heat-holding time inferior to 10 minutes guarantee the increase of formability and springback reduction.

Keywords: Al-Mg-Si; Warm Forming; Heat-Holding Time; Heating methods; Springback;

1 Introduction

The benefits of warm forming in aluminum alloys are nowadays well known. Warm forming has been used as a solution to improve formability, firstly for non-heat treatable Al-Mg alloys (Ayres, 1977; Shehata et al., 1978) and later also for heat treatable alloys (Bolt et al., 2001; Wilson, 1988). Warm forming can be performed under isothermal or non-isothermal conditions, i.e. imposing a temperature gradient in the blank. (Wilson, 1988) discussed the potential arising from the use of aluminum alloys in family cars, concluding that large improvements in formability can be achieved if the flow stress of the material in the drawing zone is reduced relatively to that in the stretch-formed zone, by inducing a differential heating of the blank. Later, the studies on the warm forming under isothermal and non-isothermal conditions reported a reduction of the springback behavior for non-heat treatable alloys, either using the U-rail test (Kim and Koç, 2008; Moon et al., 2003) or the split-ring test (Grèze et al., 2010; Laurent et al., 2015). Recently, (Simões et al., 2017a) shown that warm conditions also reduce the springback for heat treatable aluminum alloys, with the advantage of being an effective solution to minimize the variability caused by the natural aging in forming operations.

In comparison with sheet metal forming processes at room temperature (RT), the warm forming requires an additional stage to increase and stabilize the temperature of the blank before the forming operation. This stage will be designated by heat-holding through this work, because it is normally difficult to separate the time required for heating and stabilizing (holding) the temperature. Several heating methods can be used in warm and hot forming processes, either in industry or in laboratory. These methods are discussed by (Karbasian and Tekkaya, 2010; Martins et al., 2015) highlighting their different heating rates. The main heating methods used are: furnaces; induction heating; and conduction heating, by direct resistance or by pre-heated forming tools. In the furnaces, the tools and the blank can be heated simultaneously or the sheet can be pre-heat in an external furnace, involving an additional transfer phase into the furnace with the heated tools. The furnaces are commonly employed in the industry due to their high production flexibility and availability, but they require a high heating time. Induction allows attaining a higher heating rate than furnaces, but the frequency and the intensity of the induced current and the distance between the inductor and the sheet has an influence on the efficiency of the heating system, as well as in the material properties. Additionally, in case of aluminum

alloys the heating stage can be long due to their low electrical resistivity. Direct resistance heating (Joule effect) also allows attaining high heating rates, but this heating system promotes inhomogeneous temperature along the component and it is difficult to heat homogeneously blanks with complex geometries, as for the industrial applications. Heating by conduction with pre-heated forming tools is also relatively fast, but has the problem of maintaining the thermal stability of the tools for long production cycles (Harrison et al., 2015).

Three heating devices are often used to characterize the thermo-mechanical material behavior under warm and hot forming conditions: classical furnace or environmental chamber; induction coil heating; direct-resistance heating (Gleeble device). In the present work, the furnace and the Gleeble devices are used to characterize the material behavior under uniaxial tension. Some of the advantages and disadvantages of using the Furnace or the Gleeble devices for the thermo-mechanical characterization were discussed by (Davis, 2004). The direct-resistance heating system of the Gleeble device allows a high heating rate but, imposes a temperature gradient along the specimen length that promotes its heterogeneous deformation. On contrary, the main advantage of the furnace device is the homogeneous temperature distribution along the specimen entire gauge length. However, the overall time needed to heat and stabilize the furnace temperature is significantly higher. Moreover, in a furnace it is difficult to have a precise control of the temperature, since the specimen and the grips are heated by convection from the surrounding atmosphere. On contrary, in the Gleeble device the temperature is precisely controlled through the digital closed-loop control system. Although, these differences are known, their impact in the thermo-mechanical characterization of the material behavior has not been yet discussed.

Warm forming of heat treatable aluminum alloys involves strain hardening, recovery, and precipitation hardening or softening (Kumar et al., 2013). Moreover, the warm forming temperatures and the aging ones are within the same temperature range. Thus, the precipitation hardening response during the warm forming process chain depends on the initial heat treatment and on the forming temperature selected (Kumar and Ross, 2016). The warm forming process chain can be considered to consist of the following steps: lubrication of the sheet and pre-heating, forming, storage and, eventually, paint baking. The paint baking is a heat treatment of precipitation hardening usually performed in heat-treatable alloys after forming

operation in order to improve their in-service strength. In the warm forming of heat treatable aluminum alloys the cycle processing time should be careful controlled in order to minimize unwanted precipitation phenomena. (Ghosh et al., 2014) studied the influence of the punch speed and the heat-holding time during warm forming of heat treatable Al-Mg-Si alloys at 250 ºC. They observed that, for a sufficiently low punch speed (i.e. 0.18(3) mm/s) or a heat-holding time higher than 10 min, the initially soft material (in T4 heat treatment) gradually becomes harder (approaching the T6 heat treatment) and reduces its ductility (i.e. a change of the initial heat treatment occurs as a result of the long exposure time at 250 ºC). In this context, (Palumbo et al., 2015) studied the influence of the pressure rate during the warm hydroforming of a heat treatable Al-Mg-Si alloy, in a temperature range from RT to 350 ºC. The best formability improvement was achieved at 200 ºC using the highest pressure rate of 25 bar/s, to minimize the exposure of the material to the warm forming temperature. For an exposure time larger than 400 seconds, at temperatures equal or higher than 250 ºC, there is an increase of the yield stress and tensile strength and reduced ductility. (Simões et al., 2017b) also studied the warm forming of an EN AW 6016-T4 alloy, showing that a low forming punch speed (i.e. 0.1 mm/s) leads to high exposure times and, consequently, the springback increases due to precipitation hardening mechanisms.

In brief, the precipitation hardening during the forming process chain depends on the initial heat treatment of the material, the forming temperature and the forming processing time. This time depends of the heating method used and, as previously mentioned, is a crucial parameter in warm forming of heat treatable aluminum alloys, in terms of their formability and springback behavior. Thus, the goal of this study to improve the understanding about the impact of different heat-holding times, in order to establish some guidelines to better control the warm forming processing condition. The present study evaluates the influence of the heat-holding time in the thermo-mechanical behavior, formability, and springback of two heat treatable Al-Mg-Si alloys. Section 2 presents the alloys selected for this study and the experimental procedures adopted for their thermo-mechanical behavior characterization. In this context, a detailed analysis of the influence of the dispositive selected is performed, considering also a non-heat treatable aluminum alloy, as reference. In Section 3, the formability and springback of the two heat

treatable Al-Mg-Si alloys were studied using cylindrical cup tests, followed by the split-ring test. Finally, the main conclusions of this study are presented in Section 4.

2 Materials and Thermo-mechanical behavior

2.1 Materials

The two alloys selected for this study are the EN AW 6016-T4 and the EN AW 6061-T6, which are commonly used for skin applications and for structural components in the automotive industry, respectively. The designation T4 indicates solution heat treated (SHT) and naturally aged to a substantially stable condition, and the designation T6 indicates SHT followed by artificial aging (H.Y. Hunsicker, 1984).

The EN AW 6016-T4 alloy was produced and provided by Constellium and the EN AW 6061-T6 alloy was acquired in the retail market. In a previous work (Simões et al., 2017a), it was shown that the mechanical properties of the EN AW 6016-T4 alloy change during storage at RT, becoming relatively stable after 7 months. At RT, the natural aging effect leads to an increase of the tensile strength and consequent increase of the drawing forces, but these effects can be highly minimized when using warm forming conditions (Simões et al., 2017a). Therefore, in order to better understand the effect of natural aging in warm forming, the tests with different heat-holding time were also performed considering the natural aging times between 1 and 18 months for the EN AW 6016-T4 alloy. The storage time at RT for the EN AW 6016-T4 is counted after the date of the SHT. The mechanical properties of the EN AW 6061-T6 remain relatively stable during the storage period (Simões et al., 2017a), therefore the natural aging analysis was not performed for this alloy.

The thermo-mechanical behavior under uniaxial tension conditions was also characterized for a non-heat treatable alloy, the EN AW 5754-H111. The mechanical properties of these alloys are presented in Table 1, for the tensile test at RT at a strain rate of $2x10^{-3}s^{-1}$, with the specimens oriented along the rolling direction (RD). The terms and definitions used throughout this work are according to the (ISO 6892-1:2009, 2009), i.e. R_m ultimate tensile strength; $R_{p0.2}$ proof strength at 0.2% of the extensometer gauge length; A_{gt} percentage of total elongation at maximum force; n_{4-6} strain hardening exponent between 4 and 6 % of plastic elongation; and

n_{10-15} strain hardening coefficient between 10 and 15 % of plastic elongation. The thickness of both alloys is approximately 1 mm, with the average value of fifty measurements also presented in Table 1.

Table 1 – Mechanical properties of EN AW 6016-T4 (Simões et al., 2017a), EN AW 6061-T6 (Simões et al., 2017a) and EN AW 5754-H111 alloys, along RD, at RT. The thickness values presented are determined by the average over fifty measurement points

	Aging time	$R_{p0.2}$	R_m	A_{gt}	n_{4-6}	n_{10-15}	Thickness
EN AW 6016-T4	1 month	101 MPa	215 MPa	23.9 %	0.32	0.26	1.047 mm
	18 months	130 MPa	247 MPa	22.8 %	0.28	0.24	
EN AW 6061-T6	–	270 MPa	325 MPa	12%	0.14	–	0.976 mm
EN AW 5754-H111	–	120 MPa	237 MPa	17.3%	0.29	0.22	0.985 mm

2.2 Tensile tests experimental procedure

The uniaxial tensile test conditions for the thermo-mechanical behavior characterization are defined by the standards (ISO 6892-2:2011, 2011) and (ASTM E21-09, 2009). According with these standards, the specimen shall be heated to the specified test temperature and shall be maintained at that temperature for a minimum holding time before loading. According with (ISO 6892-2:2011, 2011) the holding period should be at least 10 min, while the (ASTM E21-09, 2009) defines at least 20 min. Moreover, the holding time at warm temperature prior to the start of the test should be governed by the time necessary to ensure that the specimen has reached equilibrium and that the temperature can be maintained within the limits specified (ASTM E21-09, 2009). Therefore, quite often, longer times may be required to bring the entire gauge section of the specimen up to the specified temperature. Thus, it is recommended to report both times, i.e. the time to attain the test temperature and the holding time (ASTM E21-09, 2009). However, most of the studies do not report the heat and the holding times. Concerning the temperature variation, for test temperatures up to 600 ºC, it should be around ±3 ºC of the test temperature, and the temperature overshoots during heating shall not exceed this limit. Lastly, the heating apparatus and the method selected to heat the specimens should provide the temperature control necessary to satisfy the requirements previously mentioned (ASTM E21-09, 2009).

The warm forming temperature was chosen based in literature results, which often refers 200 ºC as a temperature that enables formability improvement, while keeping good post-forming mechanical properties (Fan et al., 2016; Wang et al., 2012). Additionally, in a previously study

by (Simões et al., 2017a) no significant improvements on formability or springback were found for higher temperatures, when using both heat treatable alloys under analysis. Therefore, the uniaxial tensile tests were performed using the Gleeble and furnace devices, at 200 ºC and at RT, used as a reference temperature to improve the results analysis. Different heat-holding times were considered for the tests performed at 200 ºC, taking into account the characteristics of each device, as discussed in the following section.

All tests were performed considering constant-crosshead speed conditions, with an initial strain rate of $2x10^{-3}s^{-1}$, using specimens cut aligned with the RD. The specimen used has the same shape in both devices, with a uniform section of 40 mm length and 10 mm width. According with the (ISO 6892-2:2011, 2011) and the (ASTM E21-09, 2009), when the length of the uniform section is less than 50 mm, at least two thermocouples should be attached to the specimen, one near each end of this section. In the present work, type K thermocouples were welded on the specimen surface to measure the temperature gradient. The strain fields were measured using a digital image correlation (DIC) system, from ARAMIS 4M – GOM, as described in the following section. A minimum of two tests were performed for each test condition. The reproducibility was confirmed through the average scatter of the true stress, which was less than ±1MPa for the same true strain value; therefore, only one representative test is presented for each condition. The tensile test results are presented as true stress – true strain plotted until the maximum load (i.e. the necking phase is not presented).

2.3 Tensile test devices

The assembly with the main components of the Gleeble device is schematically represented in Figure 1. Figure 1 a) highlights the relative position of the ARAMIS cameras and shows the control thermocouple (TC1), placed in the specimen middle. Three measurement thermocouples were also welded in the same straight line, with a distance of six millimeters between each other (TC2, TC3 and TC4). In the Gleeble device, the specimen is heated by direct resistance (Joule effect) via a 50 Hz AC current in a closed-loop control with the thermocouple TC1, and the grips are water cooled. This results in a temperature gradient along the specimen length with higher temperature on its center. The magnitude of this gradient depends of the material selected for the grips (cooper or steel) and from the contact area between the grips and the specimen (Davis, 2004; Norris and Wilson, 1999). However,

according with (Norris and Wilson, 1999) whatever the temperature gradient presented, the temperature variations in the specimen center are negligible within a length of 5 mm. Moreover, the device assures an uniform temperature along the width and the thickness directions. In the present work, in order to attain high heating rates, the specimen is fixed in copper wedges-grips (using pins).

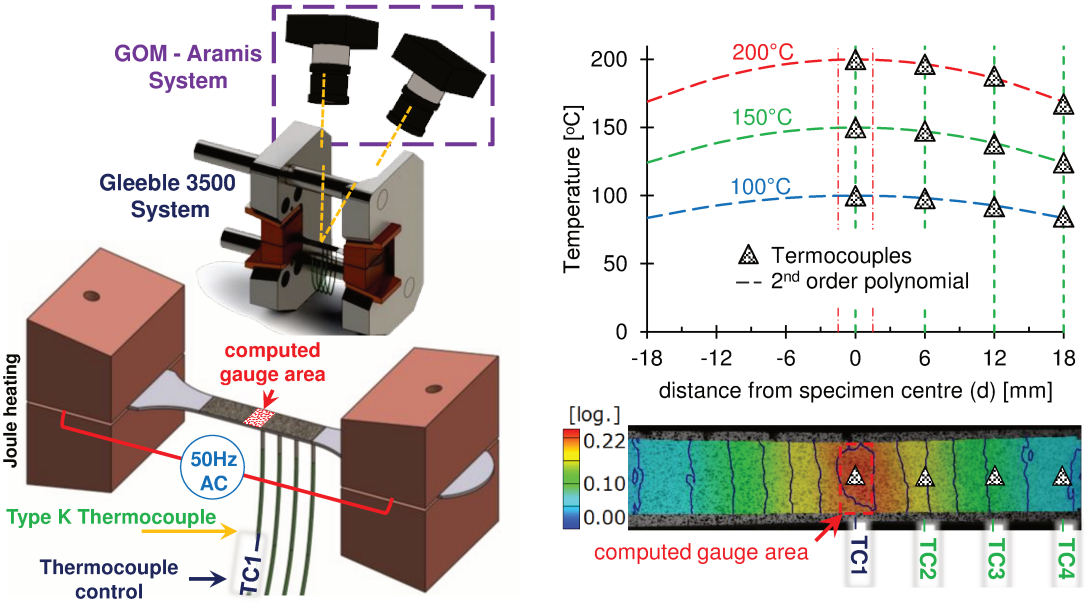

a) b)

Figure 1 – **a)** Illustration of the Gleeble 3500 device, with the ARAMIS 4M system positioned above (top). **b)** At the top: temperature distribution along the specimen length for tests performed at 100 ºC, 150 ºC and 200 ºC. At the bottom: major strain field (ε_{xx}) at the R_m instant, for a test carried out at 200 ºC, for the EN AW 6016-T4 alloy.

The heating rate measured in the Gleeble system using the copper grips was of 20 ºC/s. The temperature gradient along the specimen length is exemplified in Figure 1 b), for the test temperatures of 100, 150 and 200 ºC. Whatever the test temperature selected, the temperature gradient is well described by a 2nd order function: $T(d) = T_m - a \cdot d^2$, were T is the temperature for a point located at a distance d from the specimen center, T_m is the temperature in the specimen center and, a is a constant which value slightly increases with the increase of the value of T_m. Due to this temperature gradient, the specimen can present heterogeneous mechanical properties (temperature dependent mechanical properties) along the gauge length. In all the results analyzed in this work, this results in a strain distribution with a symmetric parabolic evolution along the specimen length, as shown Figure 1 b) – bottom, where the strain distribution corresponds to the instant corresponding to the maximal load, for a test performed

at 200 ºC. Therefore, in order to plot the true stress – true strain curves, minimizing the effect of heterogeneous thermo-mechanical properties, a rectangular gauge measurement area of 3 mm length and 6 mm width, positioned in the specimen center, is used to compute the strain (see Figure 1 b). Moreover, in the computed gauge area the temperature gradient is under 1 ºC, whatever the test temperature selected, as shown in the same figure.

Figure 2 shows the schematic representation of the classical furnace coupled with an uniaxial tensile test machine (Instron 4505). The ARAMIS system is positioned outside the furnace, acquiring the measurement area through a double-glass window. As shown in Figure 2 a), five thermocouples were used to measure the temperature in different key points (TC1 to TC5). Thermocouples TC1 acquire the environment temperature and TC5 acquire the grip temperature. Thermocouples TC2, TC3, TC4 acquire the temperature at the specimen center, end of the gauge length and in the contact zone with the grips, respectively.

The volume of air in the furnace and the mass of the grips (of 10 kg each grip) are important factors, since the heating rate decreases with the increase of the thermal inertia. The heating rate measured in the furnace air (TC1) was about 0.18 ºC/s. The heating rate measured on the grip (TC5) was about 0.085 ºC/s, which would lead to a heat time of approximately 3000 seconds to attain a stable and homogeneous temperature of 200 ºC in the specimen. Thus, in order to take advantage of the thermal inertia of the furnace and achieve a higher heating rate for the specimen, the furnace was pre-heated to a temperature slightly higher (220 ºC) than the test temperature, before placing the specimen in contact with the grips.

At the top of Figure 2 b), it is shown the temperature evolution in the furnace air (TC1), in the specimen (TC2, TC3, TC4) and in the grip (TC5), in function of the test time. As previously mentioned, the furnace and the grips were pre-heated at about 220 ºC. When the furnace door is opened to place the specimen, the furnace air temperature (TC1) immediately falls down to approximately the RT, but the grips keep their temperature at about 210 ºC (see Figure 2 b)). The specimen is placed in contact with the heated grips, and its temperature immediately rises to about 190 ºC. A minimum period of about 3 minutes is required to fix the specimen on the grips, after that the furnace door is closed. The tensile test starts when both the furnace and the specimen present a stable temperature of about 200 ºC. In the example shown in Figure 2 b)

the heat-holding time was of approximately 10 minutes. During the tensile test, a non-linear temperature variation of about 5 ºC is recorded in TC1, which results from the system incapability to maintain a constant temperature. This causes an oscillation on the specimen temperature of about 2.5 ºC. Lastly, during the tensile test, the temperature gradient between TC2 and TC4 is inferior to 3.5 ºC. Due to the reduced temperature gradient, the strain field (ε_{xx}) presents a homogeneous distribution, as shown for the instant corresponding to the (R_m) in Figure 2 b). Due to the handling difficulties associated with the placement of the specimen in the grips, it was decided to impose a minimum heat-holding time of 10 minutes. This leads to a minimum holding time inferior to the ones recommended by the standards, i.e. 10 minutes by the (ISO 6892-2:2011, 2011) and 20 minutes by (ASTM E21-09, 2009). Therefore, two different heat-holding times were selected for the tests performed in the furnace, approximately 10 and 30 minutes, while for the Gleeble device the heat-holding time was defined to be approximately 20 seconds. These ranges of heat-holding times are expected to help to understand the influence of high processing times in industrial environment and consequent microstructural modifications due to warm forming processing.

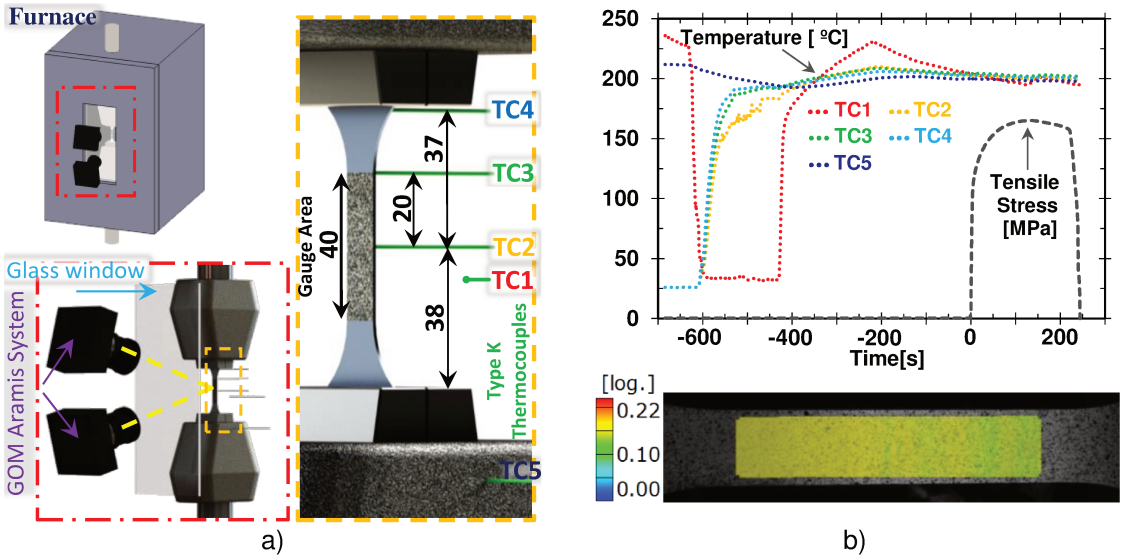

Figure 2 – **a)** Illustration of a classical furnace coupled with the Instron 4505 machine. The ARAMIS 4M system is positioned outside the furnace. **b)** At the top: temperature evolution in the five thermocouples during the heat-holding and loading tensile periods. At the bottom: major strain field (ε_{xx}) at R_m instant, for a test carried out at 200 ºC, for the EN AW 6016-T4 alloy.

2.4 Tensile test results and analysis: non-heat treatable alloy

Figure 3 a) presents the true stress – true strain curves obtained with both devices, for the EN AW 5754-H111 alloy. At RT, the true stress – true strain curves obtained with both devices are similar. However, at 200 ºC, the test performed with the Gleeble device present slightly higher stress values for the same strain value. These results are similar to the ones presented by (Coër et al., 2011), which analysis the thermo-mechanical behavior of the non-heat treatable EN AW 5754-O alloy using the same devices, at 150 ºC.

According with (Davis, 2004), when interpreting test data of warm tensile tests under constant-crosshead speed conditions, it is important to take into account strain rate variation. Thus, Figure 3 b) presents the strain rate evolution for all tests. The tensile test performed in the furnace, at 200 ºC, presents an almost stable strain rate value of ≈ $2x10^{-3}s^{-1}$, which is similar to the one measured in both devices at the RT tests. On the contrary, the tensile test performed in the Gleeble device, at 200 ºC, presents an increase of the strain rate with the increase of strain (the strain rate is determined using the gauge area in the specimen center (see Figure 1 b))). As mentioned, the crosshead speed remains constant during the test in both devices and the temperature in the specimen center is also the same. However, the temperature gradient induced by the Gleebe device (see Figure 1 b)) results in a gradient of the material mechanical properties, with the center of the specimen presenting a softer behavior due to the higher temperature. This also justifies the parabolic evolution of the major strain along the specimen length as well as the increase of the strain rate in the specimen center. The differences in the true stress – true strain curves at 200 ºC can also be related with the temperature gradient, since the slight increase of the stress values for the same strain value can be justified by the slight harder behavior of the specimen in the Gleebe device. Moreover, the EN AW 5754 alloy is known for presenting a positive strain rate sensitivity (Laurent et al., 2015). However, it should be mentioned that the strain rate increase during the tensile test at 200 ºC, performed in the Gleeble device, leads to a maximum value within the same order of magnitude. Thus, the differences observed for the true stress – true strain curves at 200 ºC (as shown in Figure 3 a)) do not significantly affect the thermo-mechanical characterization, when testing non-heat treatable aluminum alloys, as also discussed by (Coër et al., 2011).

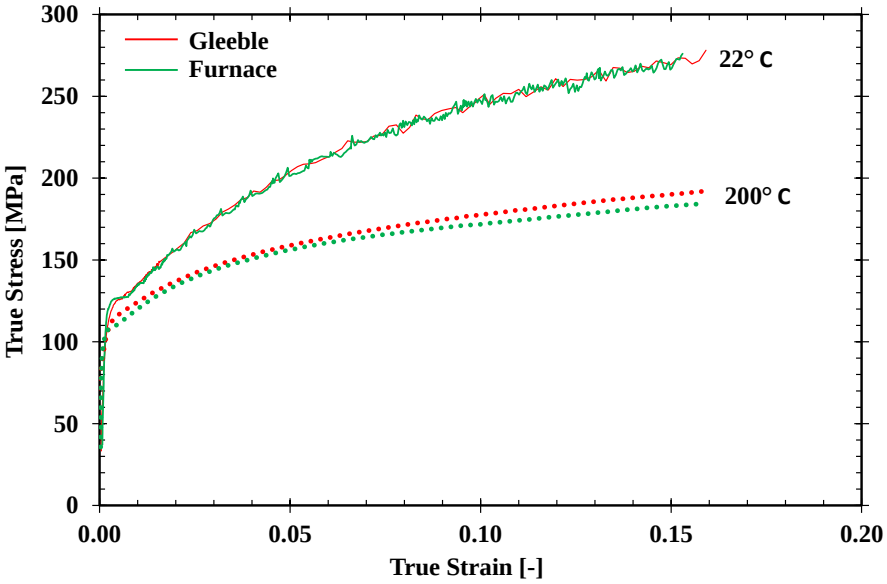

a) True stress – true strain

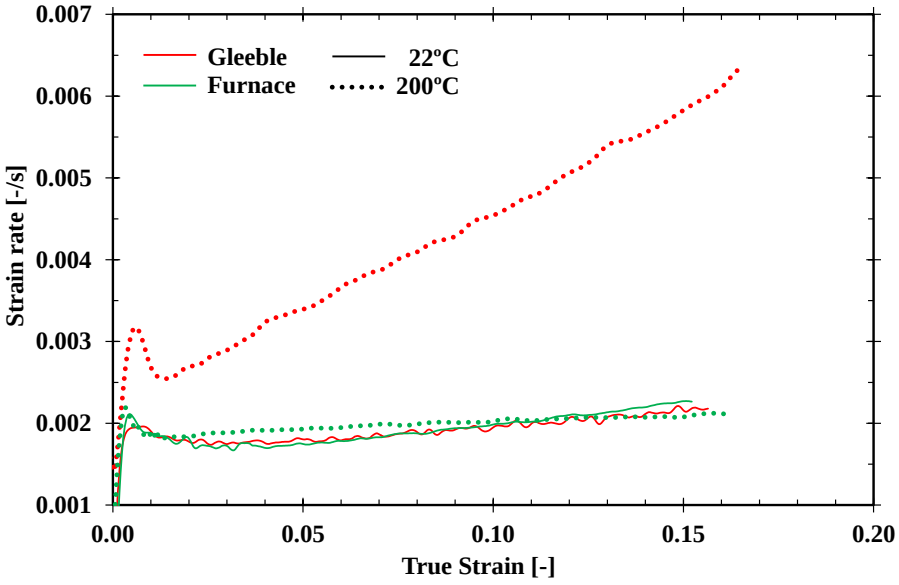

b) strain rate

Figure 3 – Analysis of the influence of testing device in material behavior thermo-mechanical characterization using the non-heat treatable EN AW 5754-H111 aluminum alloy.

2.5 Tensile test results and analysis: heat treatable alloys

Since the EN AW 6016-T4 alloy is prone to natural aging, the tensile tests were performed considering 1 and 7 months of storage time. However, at 7 months of storage time, only heat-holding times of 20 seconds and 10 minutes were analyzed. The true stress – true strain curves are presented in Figure 4 a) and b), for the EN AW 6016-T4 and the EN AW 6061-T6 alloys,

respectively. A noteworthy variation of the mechanical properties due to the heat-holding time is observed for the EN AW 6016-T4 alloy, while for the EN AW 6061-T6 alloy, the results present negligible variations. Globally, at 200 ºC, as the heat-holding time increases from 20 seconds to 30 minutes both alloys shows higher $R_{p0.2}$ and a lower strain hardening rate. This may be linked with the microstructural variations induced by static precipitation hardening promoted by warm temperatures. Regarding the influence of natural aging for the EN AW 6016-T4, for a holding time of 20 seconds, the $R_{p0.2}$ presents higher values for specimens with 7 months of storage time, while for a holding time of 10 minutes, the true stress – true strain curves of specimens with 1 and 7 months of storage time are overmatched.

For the EN AW 6061-T6 alloy, the heat-holding time has a reduced influence on the $R_{p0.2}$ variation and on the strain hardening behavior. A slightly lower stress value observed for the heat-holding time of 10 minutes, may be linked with the positive strain rate sensitivity since, as previously reported, the strain rate value is slightly higher in the Gleeble device. For a heat-holding time of 30 minutes, the $R_{p0.2}$ slightly increase, however its value at 200 ºC remains inferior than at RT. On the contrary, for the EN AW 6016-T4, the $R_{p0.2}$ is higher at 200 ºC than at RT, when considering a heat-holding time of 30 minutes. In fact, when the EN AW 6016-T4 is submitted to a heat-holding time of 30 minutes it presents strength values and a hardening behavior close to a T6 heat treatment. This is enhanced by the comparison of its mechanical behavior with the one of the EN AW 6061-T6, as shown in Figure 5. This figure compares the thermo-mechanical behavior of both alloys, considering the tests performed in the Gleeble (Figure 5 a)) and in the Furnace (Figure 5 b)) devices. At RT or at 200 ºC, for 20 seconds of heat-holding time, the alloys present a distinct behavior. However, when the EN AW 6016-T4 is submitted to a heat-holding time of 30 minutes, both alloys present a similar behavior. Therefore, the differences observed in true stress – true strain curves obtained with both devices, for the EN AW 6016-T4 alloy, are mainly related with the microstructural changes induced by the heat-holding conditions. The high heating rate attained with the Gleeble device allows minimizing the occurrence of microstructural changes, promoted by static precipitation hardening during the heat-holding period. On the other hand, the heterogeneous temperature distribution along the specimen length can promote heterogeneous dynamic precipitation and thus, heterogeneous mechanical properties along the specimen length (Simões et al., 2017b).

In this sense, the homogeneous temperature distribution along the specimen entire gauge length, attained when using the furnace device, guarantees that the microstructural modifications occur uniformly in the specimen, resulting in an easier interpretation of the influence of the heat-holding time or strain rate in the thermo-mechanical behavior.

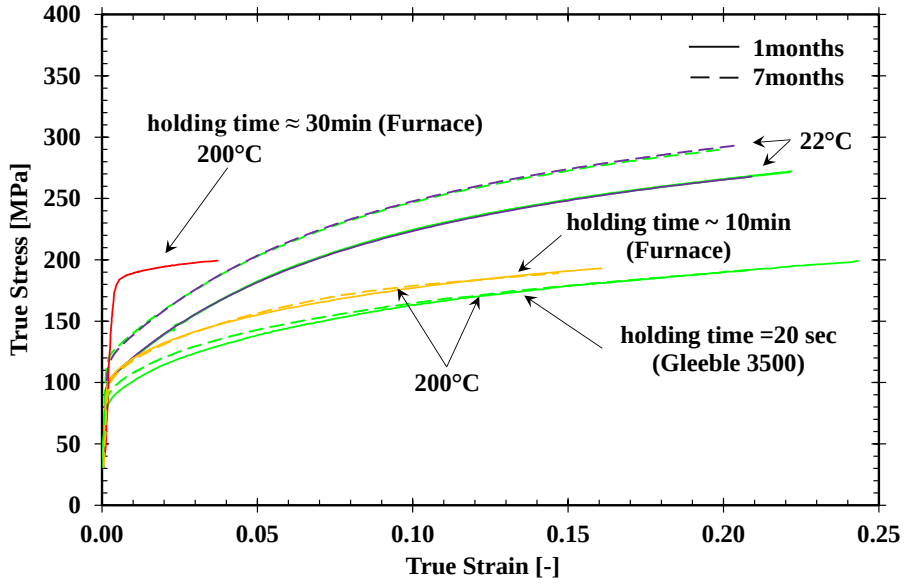

a) EN AW 6016-T4

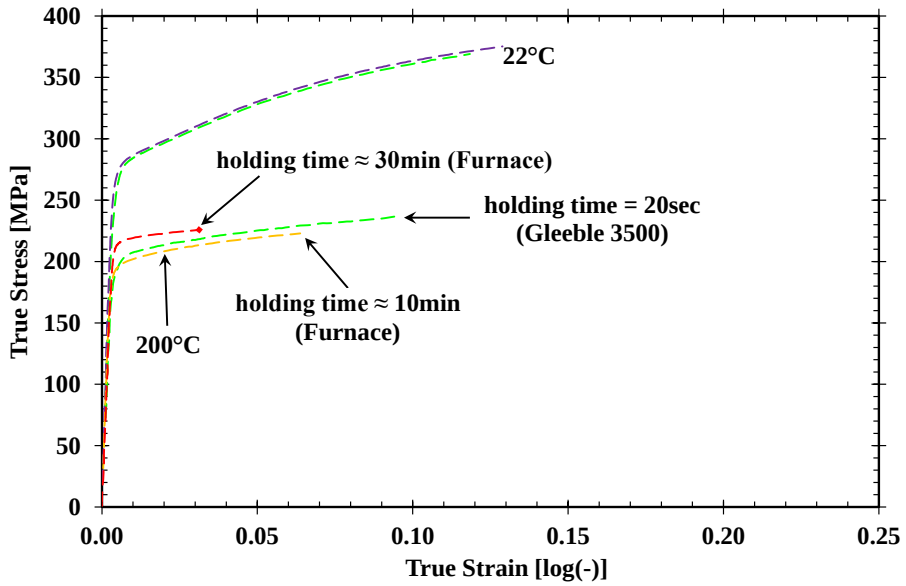

b) EN AW 6061-T6

Figure 4 – Influence of the heat-holding time on the true stress – true strain curves obtained from uniaxial tensile tests performed for specimens oriented along the RD. The green color represents the tensile test performed in the Gleeble device. The 1 month aged material is shown by solid line and the 7 months by the dash line.

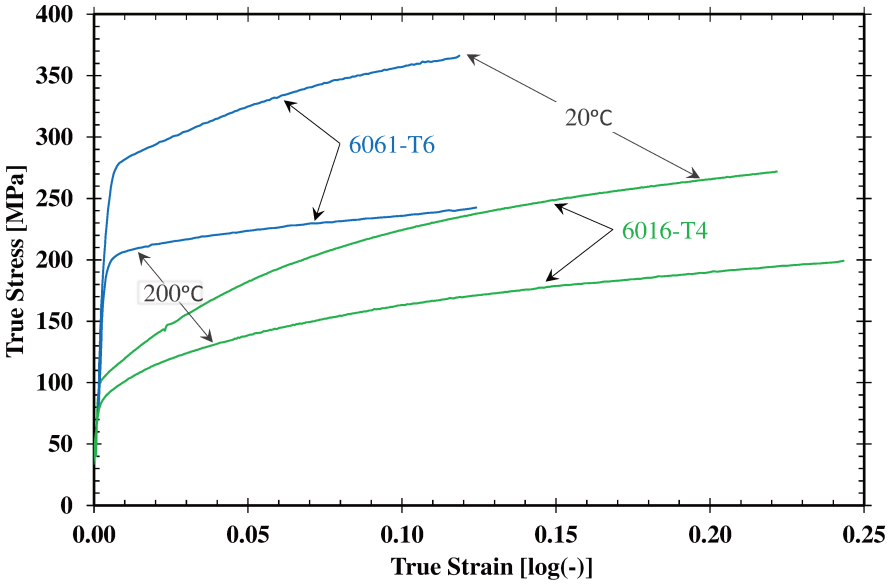

a) Gleeble 3500

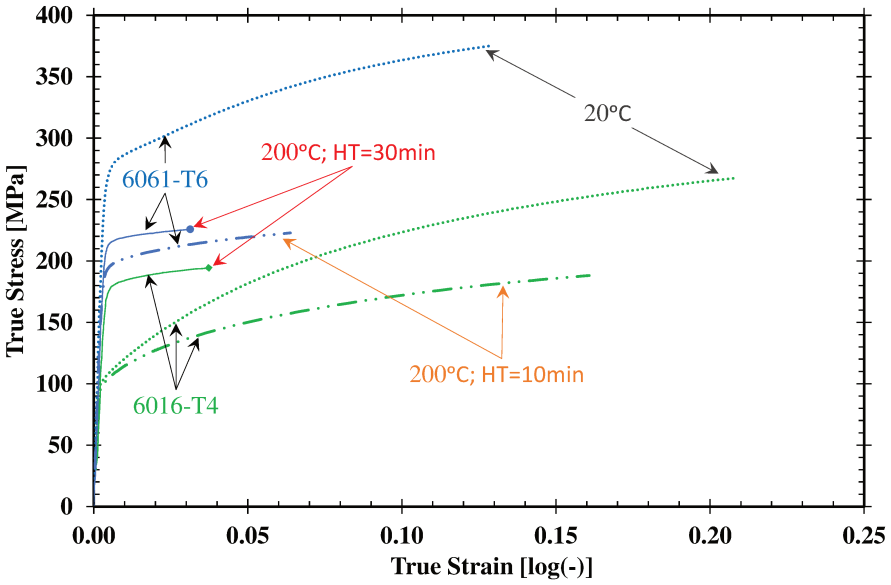

b) Instron 4505 furnace

Figure 5 – Comparison of the results obtained for the EN AW 6016-T4 alloys and the EN AW 6061-T6 alloys in function of the device used. The results presented are only for 1 month aged material.

3 Warm forming of a cylindrical cup

The cylindrical cup tests consist in forming a metal sheet with a circular shape (the blank) into a forming die by the mechanical action of a punch. A blank-holder tool is used to avoid wrinkles and to control the material flow into the die. The dispositive used was a Zwick/Roell Amsler BUP200 sheet metal testing equipment, adapted with specific tools for warm forming (Coër,

2013; Laurent et al., 2015; Manach et al., 2016). The blank has a circular shape with 60 mm of diameter. It was cut out previously to the forming process from the initial sheet by squaring shear in the Zwick BUP200 using a specific blade tool. This dispositive is composed of three main tools: die, blank-holder and punch, with the dimensions presented in Table 2. This table also summarizes the more relevant process parameters.

Table 2 – Drawing tool geometry and process parameters.

Die opening diameter	35.25	[mm]
Die radius	5.0	[mm]
Punch diameter	33.0	[mm]
Punch radius	5.0	[mm]
Gap between the punch and the die	1.15	[mm]
Blank-holder opening diameter	33.6	[mm]
Blank diameter	60.0	[mm]
Blank thickness	≈1	[mm]
Blank-holder force	6	[kN]
Punch speed	1	[mm/s]

The blanks were lubricated with a (“Jelt Grease 5411 aerosol 95cSt,” n.d.). During the heat-holding time, the water of the lubricant evaporates leaving only the lubricant on the blank. The punch force and its displacement, the blank-holder force and the temperature were acquired, as a function of time, for all tests (Coër, 2013; Laurent et al., 2015). A minimum of three reproducible tests were performed for each condition under analysis. Their reproducibility was validated by two conditions: (i) the average scatter of the punch force, which was less than ±0.1kN for the same displacement; (ii) the difference in heating time was always inferior to 30 seconds. Therefore, only one representative test is presented for each condition.

After the forming operation, the cup thickness and the cup height were measured, as schematically shown in Figure 6 a). The coordinate measurements are performed along the interior and the exterior sides of the cup, in a normal direction to the surface, such that the difference between them corresponds to the thickness value. The measurements are performed at each 45º, from 0º to 315º, to the RD. The cup height is measured at each 5º along the cup edge, and the first measurement point is at 0º to RD. In order to minimize measurement errors related with axisymmetric deviations, the thickness and height of the cup are averaged considering the cup vertical axis symmetries (i.e. the presented 1st quadrant (0º to 90º, to the

RD) is an average of 1st, 2nd, 3th and 4th quadrants). The cup was measured using a 3D measurement machine "*Brown & Sharpe Mfg. Co.*" model "*MicroXcel PFX-454*". The accuracy in the thickness measurements depends of: the 3D measurement machine accuracy (±3 μm), the control of the positioning of the cup on the measurement device (±15 μm), and of angular deviations to the RD direction (±5 μm) (Coër, 2013). The results of cup dimensions were highly reproducible within the same test conditions.

The springback analysis was performed using the split-ring test. This test consists of: i) cut a ring from the cup wall (trimming); ii) open the ring along the RD (split-ring); and iii) measure the ring opening. The variation of the ring diameter, before and after splitting, gives an indirect measure of the springback phenomenon and of the amount of the circumferential residual stresses present in the formed cup (Grèze et al., 2010). As shown in Figure 6 a), three rings were cut from the cup wall. This procedure allows a more detailed analysis of the springback behavior, since it was previously shown that the magnitude of the ring opening is influenced by its vertical position along the cup wall (Gnaeupel-Herold et al., 2005; Simões et al., 2017c; Xia et al., 2004). An electrical discharge machining (EDM) was used to cut and open the rings. The rings opening was measured using a microscope to assure high measurement accuracy, and the EDM cut thickness (0.3 mm) was taken into account in the measured value. More details concerning the experimental procedure used are given in (Simões et al., 2017a).

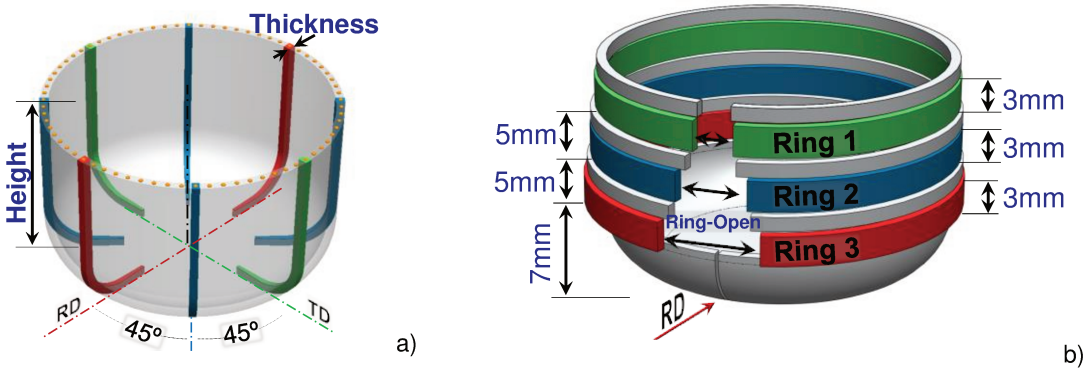

Figure 6 – Schematic representation of the drawn cup, showing the: a) reference positions for the cup dimensions measurements and b) the procedure used in the split-ring test.

3.1 Description of the warm forming procedure

A schematic illustration of the procedure used in the warm forming of the cylindrical cup is presented in Figure 7. The temperature evolution along the process is presented in Figure 8. As

shown in this Figure 8, thermocouples are placed in fixed position of the tools, enabling the acquisition of temperature values that corresponds to a local measure. A thermocouple is placed on the: (i) die radius (labeled TC Die); (ii) punch, right below the ejector (labeled TC Punch); and (iii) blank-holder, at the flange zone, on the surface contacting with the sheet (labeled TC B-H). In the blank, the thermocouples are initially placed at the center (labeled TC Blank 1) and at 15 mm (limit of the punch radius) from the blank center (labeled TC Blank 2).

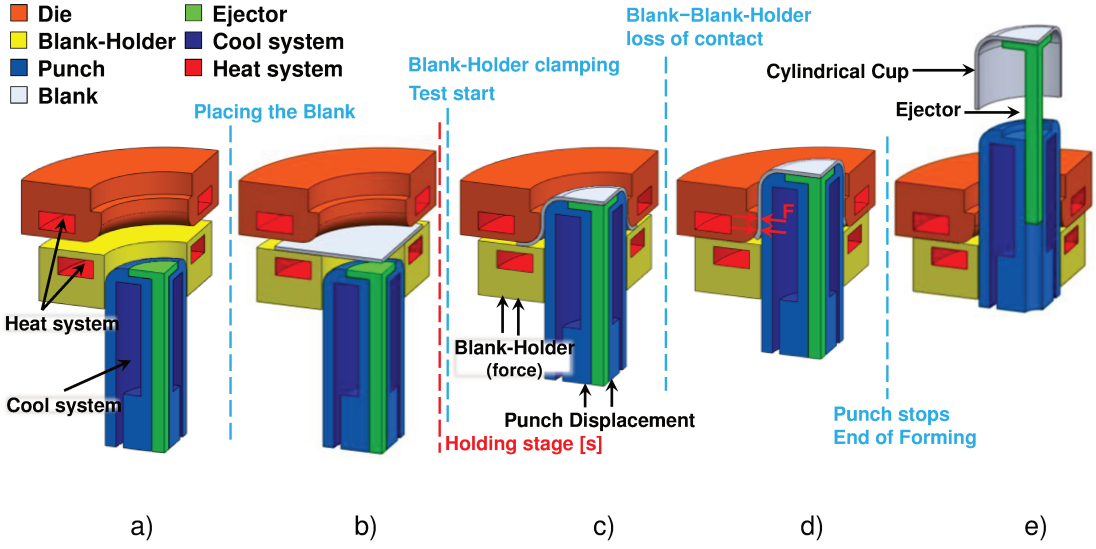

Figure 7 – Drawing of a cylindrical cup: a) Heating the die and the blank-holder, while the punch is kept at RT by the water cooling system; b) Blank heating; c) Cup drawing stage; d) Ironing stage; and e) Ejection stage.

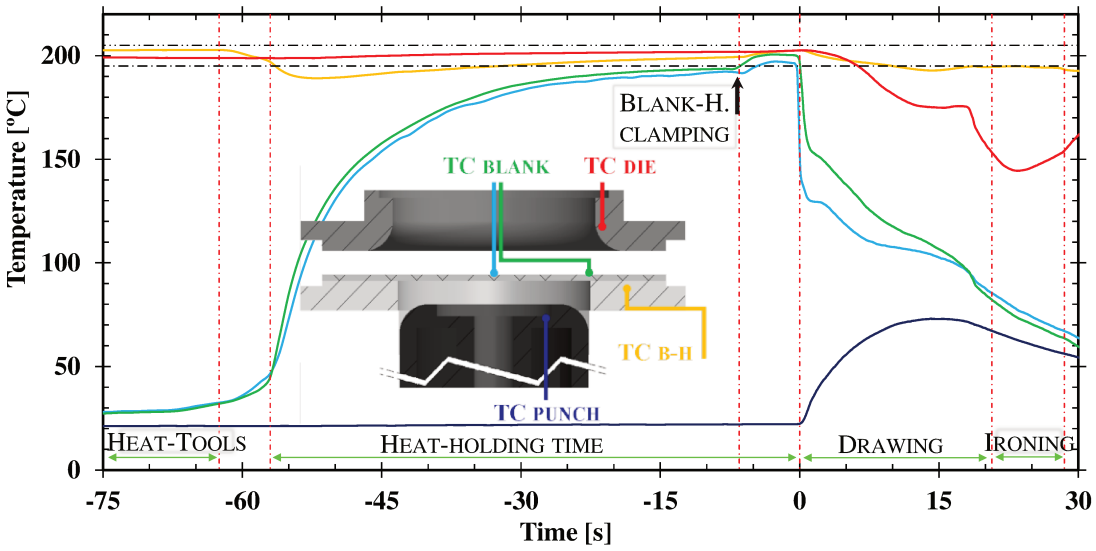

Figure 8 – Temperature evolution for the cylindrical cup test at 200 ºC, performed with pre-heated die and blank-holder and cooled punch. The negative time scale refers to the heat-holding time and the positive scale refers to the drawing and ironing stages. The results presented correspond to the test performed with the EN AW 6016-T4 alloy, with a storage period of 1 month. This test procedure is shown in **video 1**.

The heat-holding stage includes the steps previous to the forming stage, presented in Figure 7 a) and b) and in Figure 8 by the negative time interval. The warm forming procedure used to fully draw the cylindrical cup starts with the pre-heating of the die and the blank-holder, by internal electrical heating rods up to the test temperature. The punch is refrigerated to keep its temperature close to RT (Figure 7 a)). This pre-heating step aims to reduce the blank heating time. Then, the blank is positioned in the blank-holder (Figure 7 b)), taking about 60 seconds to attain the test temperature (within a margin of error less than 2.5%) (see Figure 8). In order to evaluate the influence of the heat-holding time, various exposure times of the blank at 200 ºC are tested, the called holding period (Figure 7). During the blank heat-holding and clamping stages, the punch has no contact with the blank, being at approximately 4 mm from the blank (see Figure 7 b)). However, some heat transfer occurs by convection between the blank center and the punch, consequently, the temperature of the blank center (TC Blank 1) is slightly lower than the one closer to the flange zone (TC blank 2), as shown in Figure 8.

The forming operation starts when the blank-holder clamps the sheet against the die with a force of 6 kN, then the punch moves up and makes contact with the sheet, at the time instant equal to zero. The forming phase is similar for all tests, whatever the heat-holding period considered. This means that for the 1 mm/s punch speed considered the forming operation

takes about 30 seconds. **The drawing of the cylindrical cup** begins at the instant of time equal to zero, when the punch contacts with the blank. Such contact leads to an abrupt drop of the blank temperature, in order to establish a thermal equilibrium between the tools and the blank. TC Blank 1 presents a temperature lower than TC Blank 2 since the center of the blank establishes contact with the punch first. Then, the punch moves forward into the die cavity, which corresponds to the drawing phase (see Figure 7 c)). During this phase, the blank progressively increases the contact area with the cold punch (punch bottom and radius) and with the heated die radius. This contributes to the increase of the punch temperature, while the die temperature decreases (see Figure 8). The heat flows from the flange zone, through the blank, and is dissipated by the punch cooling system, promoting a thermal equilibrium. During this time interval, the blank temperature (TC Blank 1 and TC Blank 2) follows an almost linear decrease with a reduced slope, as shown in Figure 8. This decrease is due to the heat transfer between the bottom of the cup and the cold punch.

At ≈21 seconds the **ironing stage** starts, as schematically shown in Figure 7 d). In fact, during the drawing stage, the material located in the flange area is submitted to a compression stress state in the circumferential direction (to reduce its diameter), which leads to its thickening. The ironing results from the fact that the gap between the die and the punch (1.15 mm, as shown in Table 2) is smaller than this thickness value. Thus, to promote its flow between the punch and the die, the material has to be strongly squashed and simultaneously stretched along the axial direction. This ironing stage imposes a high contact pressure that causes the deformation of the asperities at the interface (reducing the blank surface roughness) so that the actual contacting area enlarges and the thermal contact resistance decreases, resulting in an increase of the interfacial heat transfer coefficient (Chang et al., 2016). This supports the temperature decrease in the die radius during the ironing stage, as shown in Figure 8. After 24 seconds, the contact area between the blank and the die is much reduced. Consequently, the die temperature reverses its downward trajectory and increases again up to its initial temperature. The sheet and the punch temperature present a linear decrease and attain the same temperature of ≈50 ºC at the end of this stage, as shown in Figure 8 a). At the end of the process, the punch stops and the ejector is activated to remove the cup from the die cavity (Figure 7 e)).

3.2 Results and analysis

The forming behavior of the EN AW 6016-T4 alloy was analyzed for two natural aging times: 1 and 18 months, while for the EN AW 6061-T6 alloy the forming tests were only performed considering 18 months after its reception. At 200 ºC, three values of the heat-holding time were considered form the EN AW 6016-T4 alloy: ≈60 seconds (±15 seconds), 10 and 30 minutes. For the EN AW 6061-T6 alloy the heat-holding times considered were: ≈60 seconds (±15 seconds) and 50 minutes. As for the thermo-mechanical characterization, the forming tests were also performed at RT.

3.2.1 The punch force analysis

The punch force needed to fully draw the cylindrical cup is presented in Figure 9 a) and b) as function of its displacement, for the EN AW 6016-T4 alloy and the EN AW 6061-T6 alloy, respectively. Globally, the punch force decreases with the temperature increase from RT to 200 ºC, which is linked to the material softening behavior due to the temperature increase. During the forming process, two distinct stages can be considered: the drawing and the ironing (see Figure 7). As shown in Figure 9, the drawing stage occurs until ≈21 mm of punch displacement. During this stage, the punch force starts by increasing rapidly until a displacement of ≈11 mm, which corresponds to the instant that the die and the punch shoulder radii are completely formed in the part. Afterwards, the punch force decreases until it reaches a local minimum at ≈19 mm of punch displacement (see Figure 9), which is related with the fact that the tool presents no blank-holder stopper (see Figure 7). This minimum occurs just before the loss of contact between the blank and the blank-holder, since at the end of this stage the blank-holder promotes the movement of the sheet into the die cavity and, consequently, reduces the punch force. The ironing stage can be associated with the increase of the punch force until attaining a local maximum (≈23 mm of punch displacement), followed by a decrease until the end of the process. As previously mentioned, the ironing occurs because the gap between the punch and the die is not sufficiently large to allow the thicker material to flow.

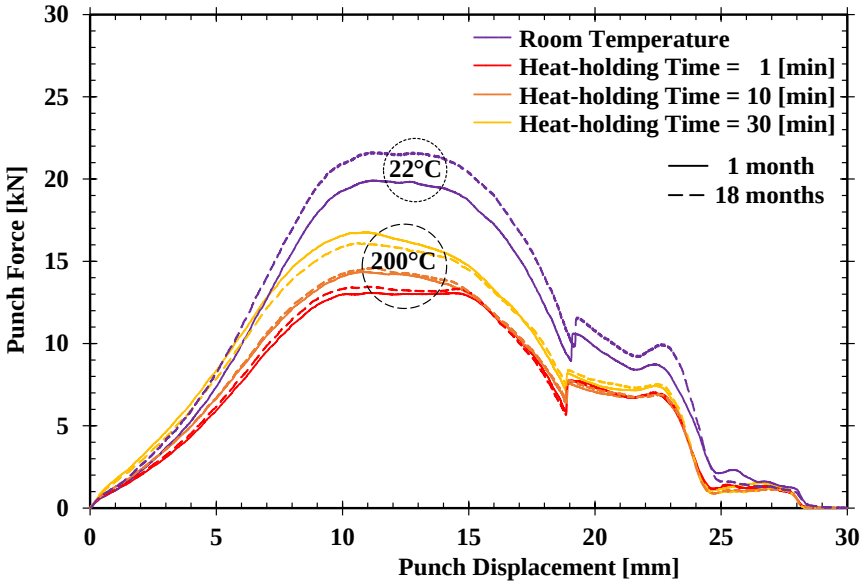

a) EN AW 6016-T4

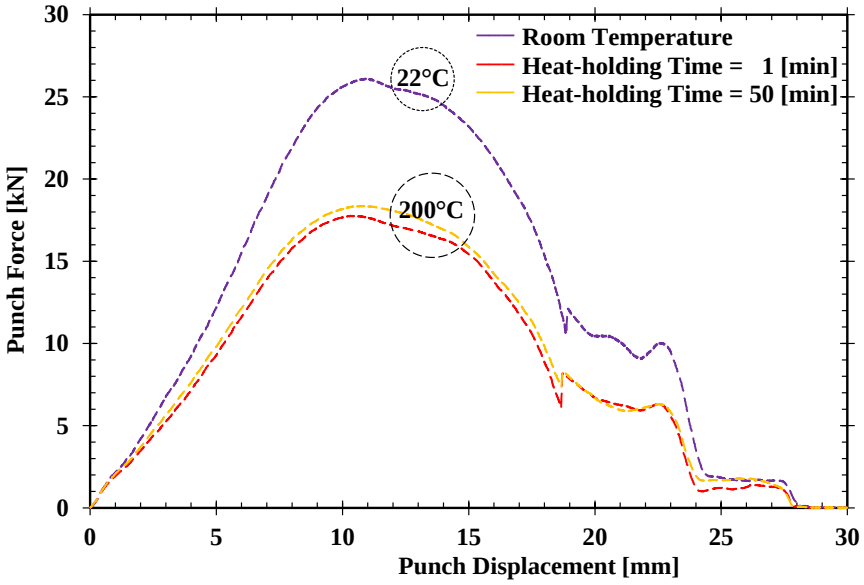

b) EN AW 6061-T6

Figure 9 – Punch force evolution as function of its displacement, for tests performed at RT and at 200 ºC, considering different heat-holding periods. The 1 month aged material is shown by the solid line and the 18 months by the dash dot line.

Table 3 shows the percentage of reduction of the punch force with the: temperature, heat-holding time, and natural aging, using the punch force at RT and 18 months of natural aging as reference. The results presented in Figure 9 and Table 3 are in agreement with the ones previously shown in section 2.5, i.e. the heat-holding time influence in the punch force is remarkable for the EN AW 6016-T4 alloy, but negligible for the EN AW 6061-T6. In fact, the natural aging state T4 is more prone to precipitation hardening than the artificial aged T6. For

the EN AW 6061-T6 alloys a heat-holding time up to 50 min, at 200 ºC, as a negligible effect on the punch force variation. On the other hand, for the EN AW 6016-T4 alloy, the increase of the heat-holding time results in a smaller reduction of the punch force, for both the drawing and the ironing stage. In fact, the punch force increases as the heat-holding time increases, which is in agreement with the thermo-mechanical behavior characterization (see Figure 4 a)). Moreover, the punch force evolution, obtained for EN AW 6016-T4 alloy with the highest heat-holding time, is similar to the ones obtained for the EN AW 6061-T6, confirming a hardening behavior close to a T6 heat treatment. In this context, it should be mentioned that the EN AW 6016 submitted to a T6 treatment presents strength values slightly smaller than the EN AW 6061-T6 (see Figure 5 b) and e.g. (Ghosh et al., 2014)).

Concerning the influence of natural aging for the EN AW 6016-T4, globally at RT and at 200 ºC for a holding time of 60 seconds, the 18 months aged material presents slightly higher strength values than the 1 month one, which is traduced by a higher punch force. Nevertheless, for a heat-holding time of 30 min this trend inverts, which may be related with the negative effect of natural aging in artificial aging, as reported by (Pogatscher et al., 2011; Werinos et al., 2016).

Table 3 – Percentage of punch force reduction as compared to RT, in function of the heat-holding time at 200 ºC and natural aging, for the EN AW 6016-T4 alloy and the EN AW 6061-T6 alloy. For both alloys the results at RT and 18 months of natural aging are chosen as reference.

		EN AW 6016-T4				EN AW 6061-T6	
		18 – m drawing	18 – m ironing	1 – m drawing	1 – m ironing	18 – m drawing	18 – m ironing
RT		0.0 %	0.0 %	7.9 %	11.0 %	0.0 %	0.0 %
200 ºC	1 min	37.4 %	30.4 %	39.3 %	31.0 %	31.3 %	35.3 %
	10 min	32.7 %	30.5 %	33.6 %	30.1 %	–	–
	30 min	25.0 %	25.3 %	22.6 %	24.8 %	–	–
	50 min	–	–	–	–	29.6 %	36.4%

3.2.2 Cylindrical Cup dimension analysis

The thickness evolution along the cup profile is shown in Figure 10 a) and b) for the EN AW 6016-T4 and the EN AW 6061-T6 alloys, respectively, considering only the measurements along RD. The thickness evolution curve presents different trends that can be associated with the zones located at the cup bottom, the punch radius and the vertical wall (see Figure 10). Two

critical points present a thickness minimum value, which are the entrance of the punch radius section and the confluence of the punch radius with the cup wall (Colgan and Monaghan, 2003; Moshksar and Zamanian, 1997). The first is the global minimum thickness value attained for both alloys, and the second a local minimum. After that, along the cup wall, the thickness increases until attaining a constant value, which is imposed by the ironing stage.

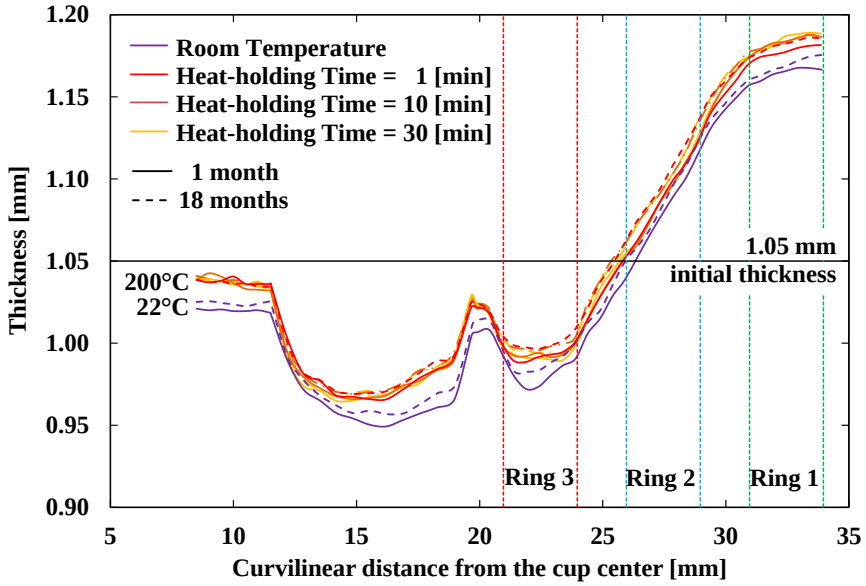

a) EN AW 6016-T4

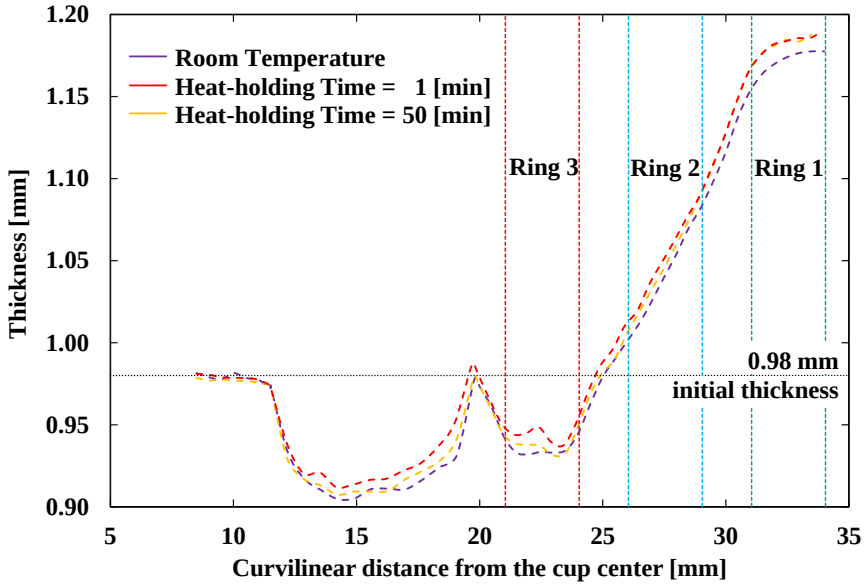

b) EN AW 6061-T6

Figure 10 – Thickness evolution along the cup profile at the RD, for tests performed at RT and at 200 ºC, considering different heat-holding periods. The 1 month aged material is shown by the solid line and the 18 months by the dash line.

Globally, the cups obtained from the tests at RT have a lower thickness than the ones at 200 ºC (Figure 10 a) and b)). This is valid for both alloys, being the thickness difference between RT and 200 ºC more remarkable for the EN AW 6016-T4 alloy. It is also noticed that the thickness imposed by the ironing stage for the tests performed at 200 ºC is higher than at RT. This difference is justified by the thermal dilatation of the tools at 200 ºC (considering the thermal expansion coefficient of 1.19×10^{-5} and the dimensions given in Table 2). Due to the volume conservation, it is possible to establish a relation between the average cup height and the average thickness, i.e. higher heights occur associated with lower average thickness values. Thus, although the cup height is not shown here, the higher average values of the cup height occur for the tests at RT. Regarding the EN AW 6016-T4 alloy, the cups obtained from 18 months natural aged material have a slightly higher average thickness than the 1 months ones, particularly for RT conditions (Simões et al., 2017a).

Comparing both alloys, it is visible that at the cup bottom and radius zone the EN AW 6061-T6 alloy present lower thickness values. This difference is linked with the lower initial thickness value of the EN AW 6061-T6 alloy (0.976mm), when compared with the one of the EN AW 6016-T4 alloy (1.047mm) (see Table 1). However, the trend of the thickness profile is independent of the initial thickness value. The influence of the heat-holding time at 200 ºC seems negligible for the EN AW 6016-T4 alloy, since there are no remarkable changes in the thickness evolution or in the cup height. On the other hand, the EN AW 6061-T6 alloy presents a slightly lower thickness evolution for the heat-holding time of 50 minutes. Nevertheless, for both alloys, the differences in the thickness evolution and height, caused by different heat-holding times, are negligible when compared with the ones caused by the temperature.

3.2.3 Springback analysis: the split-ring test

Figure 11 a) and b) shows the rings opening, measured in function of the heat-holding time, for the EN AW 6016-T4 and the EN AW 6061-T6 alloys, respectively. Concerning the influence of the axial position of the ring in the cup wall, it is observed that the opening value decreases as the distance to the cup bottom increases. In fact, Ring 3 (near to cup bottom) always presents the highest opening value, while Ring 1 (at the cup top) presents the lowest. This trend occurs for both alloys and is independent of the heat-holding time and the forming temperature. In fact, a study performed considering the same benchmark test and alloys showed that the ring

opening trend does not depend of the test temperature or of the alloy (Simões et al., 2017a). The numerical analysis of the stress condition for this benchmark test highlights the impact of the ironing phase on the residual stress distributions in the cylindrical cup. Since the ironing phase imposes high contact forces on the cup wall, ring 1 presents a lower springback, followed by ring 2 and, finally, ring 3 (Simões et al., 2017c).

The springback results at RT are presented by a horizontal line in Figure 11 a) and b), since they are used as a reference to analyze the influence of the heat-holding time at 200 ºC. Globally, for the same test conditions, the EN AW 6061-T6 alloy always presents higher springback values than the EN AW 6016-T4 alloy. This may be linked with its higher yield stress (as shown in Figure 5), since it is known that for the same Young modulus value, springback increases with the increase of the yield stress (Moon et al., 2003). For the EN AW 6016-T4 alloy, the heat-holding time has a crucial effect on the springback. The ring opening value increases linearly with the increase of the heat-holding time, while the influence of natural aging is negligible. This negligible effect of natural aging on the springback results obtained for warm formed cups at 200 ºC confirms that the influence of natural aging becomes negligible as the temperature increases, as previously reported by (Simões et al., 2017a). The increase of the ring opening values with the increase of the heat-holding time, results in springback at 200 ºC higher than at RT, for a heat-holding time of 30 min. This can be linked with the increase of the yield stress value shown in Figure 4 a), also for a heat-holding time of 30 min. The same trend is observed for the EN AW 6061-T6 alloy, with the ring opening value also presenting a linear increase with the increase of the heat-holding time. Such increase can also be linked with the increase of the yield stress value, presented in Figure 4 b) for the higher heat-holding time. However, in this case, this increase is almost negligible and, contrary to the EN AW 6016-T4 alloy, whatever the heat-holding time considered, the springback of the EN AW 6016-T4 alloy at 200 ºC is always lower than at RT.

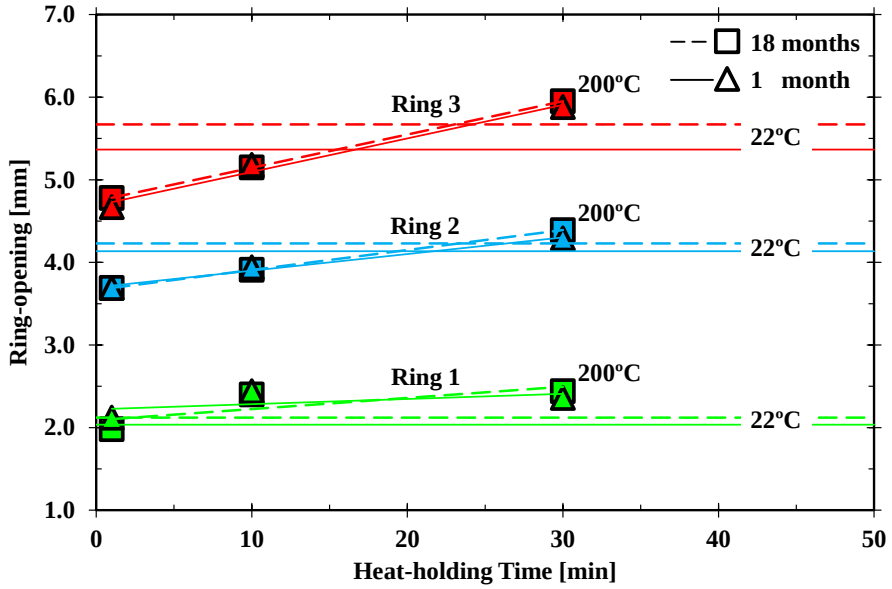

b) EN AW 6016-T4

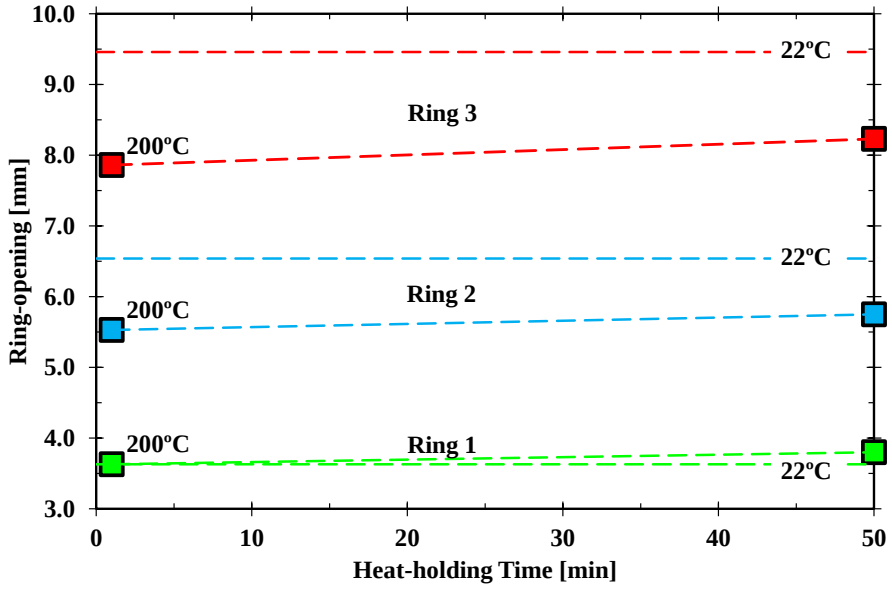

c) EN AW 6061-T6

Figure 11 – Ring-opening in function of the heat-holding time, for tests performed at RT and at 200 ºC. The 1 month aged material is shown by the solid line and the 18 months by the dash line. The horizontal lines are used to represent the reference value measured at RT for each ring, which are always represented by color: green (Ring 1); blue (Ring 2) and red (Ring 3).

4 Conclusions

In the present study the thermo-mechanical behavior, the formability, and the springback, of two Al-Mg-Si alloys (the EN AW 6016-T4 and the EN AW 6061-T6), was analyzed at RT and 200 ºC. The goal was to understand the impact of the heat-holding time in their mechanical behavior, taking into account that they present different heat treatments.

Two devices were used in the thermo-mechanical characterization of the alloys mechanical behavior: the Gleeble 3500 and the Instron tensile test machine, coupled with a furnace. Both devices present different heating methods, which lead to different strain distributions during the tensile test. In the Gleeble device, it is possible to obtain an extremely high heating rate, but there is a temperature gradient along the specimen length that causes heterogeneous deformation. On the other hand, the furnace allows attaining a homogenous temperature distribution along the specimen, which leads to a homogeneous strain field. However, the high heating time required introduces constraints to the heat-holding times that can be analyzed with this device. In case of heat-treatable alloys, the heat-holding time is a crucial parameter for the thermo-mechanical characterization, since it dictates the microstructural modifications that occur due to static precipitation. In this sense, the use of the Gleebe device renders supplementary difficulties in the results analysis, since the temperature gradient along the specimen length can also lead to a heterogeneous distribution of the mechanical properties, promoted either by static or dynamic precipitation. The direct comparison of the thermo-mechanical tests, performed with both devices for the heat-treatable alloys, shows that the differences between both devices are only negligible if: (i) the heat-holding time considered does not lead to significant microstructural changes; or (ii) the heat-treatable alloy was previously submitted to a T6 treatment, which is less prone to microstructural changes. In this context, it should be mentioned that the holding times recommend by the standards (ISO 6892-2:2011, 2011) and (ASTM E21-09, 2009) are prone to change the heat treatment condition.

The analysis of the influence of natural aging in the EN AW 6016-T4 alloy indicates that at RT natural aging results in an increase of the punch forces and springback. At 200 ºC, for a fast heat-holding time, the material natural aged for 18 months presents a slightly higher yield stress than the 1 month aged material, but the R_m is similar. This results in a slightly higher punch

force during warm forming, but a negligible effect on formability and springback. For a heat-holding time of 10 minutes, 1 and 18 months aged materials present an overmatch of both the tensile stress curves and the punch force curves during warm forming. These results shows that the control of the heat-holding time can help minimize the influence of different storages times in the mechanical behavior. For a heat-holding time of 30 minutes, the punch force evolution obtained for the 18 months aged material is lower than the 1 month one, which can be related with the well-known negative-effect of natural aging in artificial aging.

The thermo-mechanical characterization of the behavior of heat treatable alloys shows that the increase of the heat-holding time up to 30 minutes leads to an increase the yield stress and tensile strength, while it reduces the total elongation. However, such behavior was extremely marked for the EN AW 6016-T4 alloy and almost negligible for the EN AW 6061-T6 alloy. In consequence, for the warm forming tests performed with similar heat-holding times, it was observed a springback increase for the EN AW 6016-T4 alloy, which is associated to a heat treatment change from natural aged to artificial aging condition. However, it should be mentioned that the cups do not show any relevant differences in the thickness evolution along their profile, i.e. there are no remarkable differences in formability. On the other hand, in the warm forming tests performed with the EN AW 6061-T6 alloy, it was observed that an increase of the heat-holding time up to 50 minutes has a negligible impact on its formability and springback, which evidences that no over aging occurs. While for the EN AW 6061-T6 alloy the control of the heat-holding time may not be crucial, for the EN AW 6016-T4 it is recommended to use heat-holding times inferior to 10 minutes.

Acknowledgements

The authors would like to acknowledge the funding that sponsored this research work: the national funds from the French Ministry of Higher Education and the Portuguese Foundation for Science and Technology (FCT) via the project P2020-PTDC/EMS-TEC/6400/2014 (POCI-01-0145-FEDER-016876) and by UE/FEDER funds through the program COMPETE 2020, under the project CENTRO-01-0145-FEDER-000014 (MATIS). The first author V. Simões is also grateful to the FCT for the PhD grant SFRH/BD/90669/2012. The authors are also grateful to Constellium (Estelle Muller) for supplying the material. Moreover, the authors acknowledge the technical staff of IRDL, for their help in some of the experimental procedures (Anthony Jégat and Hervé Bellegou).

References

ASTM E21-09 (Ed.), 2009. Standard Test Methods for Elevated Temperature Tension Tests of Metallic Materials. ASTM Int. 03.01. doi:10.1520/E0021-09

Ayres, R.A., 1977. Enhanced ductility in an aluminum-4 Pct magnesium alloy at elevated temperature. Metall. Trans. A 8, 487–492. doi:10.1007/BF02661760

Bolt, P.J., Lamboo, N., Rozier, P., 2001. Feasibility of warm drawing of aluminium products. J. Mater. Process. Technol. 115, 118–121.

Chang, Y., Tang, X., Zhao, K., Hu, P., Wu, Y., 2016. Investigation of the factors influencing the interfacial heat transfer coefficient in hot stamping. J. Mater. Process. Technol., Hot Stamping 228, 25–33. doi:10.1016/j.jmatprotec.2014.10.008

Coër, J., 2013. Mise en forme par emboutissage en température d'un alliage d'aluminium AA5754-O (PhD-thesis). Université de Bretagne Sud.

Coër, J., Bernard, C., Laurent, H., Andrade-Campos, A., Thuillier, S., 2011. The Effect of Temperature on Anisotropy Properties of an Aluminium Alloy. Exp. Mech. 51, 1185–1195. doi:10.1007/s11340-010-9415-6

Colgan, M., Monaghan, J., 2003. Deep drawing process: analysis and experiment. J. Mater. Process. Technol. 132, 35–41.

Davis, J.R. (Ed.), 2004. Tensile Testing, 2nd ed. ASM International, Materials Park, Ohio.

Fan, X., He, Z., Zhou, W., Yuan, S., 2016. Formability and strengthening mechanism of solution treated Al–Mg–Si alloy sheet under hot stamping conditions. J. Mater. Process. Technol., Hot Stamping 228, 179–185. doi:10.1016/j.jmatprotec.2015.10.016

Ghosh, M., Miroux, A., Werkhoven, R.J., Bolt, P.J., Kestens, L.A.I., 2014. Warm deep-drawing and post drawing analysis of two Al–Mg–Si alloys. J. Mater. Process. Technol. 214, 756–766. doi:10.1016/j.jmatprotec.2013.10.020

Gnaeupel-Herold, T., Foecke, T., Prask, H.J., Fields, R.J., 2005. An investigation of springback stresses in AISI-1010 deep drawn cups. Mater. Sci. Eng. A, Measurement and Interpretation of Internal/Residual Stresses 399, 26–32. doi:10.1016/j.msea.2005.02.017

Grèze, R., Manach, P.Y., Laurent, H., Thuillier, S., Menezes, L.F., 2010. Influence of the temperature on residual stresses and springback effect in an Aluminium alloy. Int. J. Mech. Sci. 52, 1094–1100. doi:10.1016/j.ijmecsci.2010.04.008

Harrison, N.R., Friedman, P.A., Pan, J., 2015. Warm forming die design, Part III: Design and validation of a warm forming die. J. Manuf. Process. 20, 356–366. doi:10.1016/j.jmapro.2015.01.006

H.Y. Hunsicker, 1984. Chapter 5 - Metallurgy of Heat Treatment and General Principles of Precipitation Hardening, in: John E. Hatch (Ed.), Aluminum: Properties and Physical Metallurgy. ASM International, Metals Park, Ohio, pp. 134–199.

ISO 6892-1:2009, 2009. Metallic materials - Tensile testing - Part 1: Method of test at room temperature. International Organization for Standardization, Geneva, Switzerland.

ISO 6892-2:2011, 2011. Metallic materials -Tensile testing - Part 2: Method of test at elevated temperature. International Organization for Standardization, Geneva, Switzerland.

Jelt Grease 5411 aerosol 95cSt [WWW Document], n.d. URL http://fr.rs-online.com/web/p/graisses/4612124/ (accessed 11.25.15).

Karbasian, H., Tekkaya, A.E., 2010. A review on hot stamping. J. Mater. Process. Technol. 210, 2103–2118. doi:10.1016/j.jmatprotec.2010.07.019

Kim, H.S., Koç, M., 2008. Numerical investigations on springback characteristics of aluminum sheet metal alloys in warm forming conditions. J. Mater. Process. Technol. 204, 370–383. doi:10.1016/j.jmatprotec.2007.11.059

Kumar, M., Poletti, C., Degischer, H.P., 2013. Precipitation kinetics in warm forming of AW-7020 alloy. Mater. Sci. Eng. A 561, 362–370. doi:10.1016/j.msea.2012.10.031

Kumar, M., Ross, N.G., 2016. Influence of temper on the performance of a high-strength Al–Zn–Mg alloy sheet in the warm forming processing chain. J. Mater. Process. Technol. 231, 189–198. doi:10.1016/j.jmatprotec.2015.12.026

Laurent, H., Coër, J., Manach, P.Y., Oliveira, M.C., Menezes, L.F., 2015. Experimental and numerical studies on the warm deep drawing of an Al–Mg alloy. Int. J. Mech. Sci. 93, 59–72. doi:10.1016/j.ijmecsci.2015.01.009

Manach, P.-Y., Coër, J., Laurent, A.J.H., Yoon, J.W., 2016. Benchmark 3 - Springback of an Al-Mg alloy in warm forming conditions. J. Phys. Conf. Ser. 734, 22003. doi:10.1088/1742-6596/734/2/022003

Martins, J.M.P., Alves, J.L., Neto, D.M., Oliveira, M.C., Menezes, L.F., 2015. Numerical analysis of different heating systems for warm sheet metal forming. Int. J. Adv. Manuf. Technol. 83, 897–909. doi:10.1007/s00170-015-7618-9

Moon, Y.H., Kang, S.S., Cho, J.R., Kim, T.G., 2003. Effect of tool temperature on the reduction of the springback of aluminum sheets. J. Mater. Process. Technol. 132, 365–368. doi:10.1016/S0924-0136(02)00925-1

Moshksar, M.M., Zamanian, A., 1997. Optimization of the tool geometry in the deep drawing of aluminium. J. Mater. Process. Technol. 72, 363–370. doi:10.1016/S0924-0136(97)00196-9

Norris, S.D., Wilson, I., 1999. Application of 3D numerical modelling for thermal profile optimization on the Gleeble thermomechanical simulator. Model. Simul. Mater. Sci. Eng. 7, 297.

Palumbo, G., Piccininni, A., Guglielmi, P., Di Michele, G., 2015. Warm HydroForming of the heat treatable aluminium alloy AC170PX. J. Manuf. Process. 20, Part 1, 24–32. doi:10.1016/j.jmapro.2015.09.012

Pogatscher, S., Antrekowitsch, H., Leitner, H., Ebner, T., Uggowitzer, P.J., 2011. Mechanisms controlling the artificial aging of Al–Mg–Si Alloys. Acta Mater. 59, 3352–3363. doi:10.1016/j.actamat.2011.02.010

Shehata, F., Painter, M.J., Pearce, R., 1978. Warm forming of aluminium/magnesium alloy sheet. J. Mech. Work. Technol. 2, 279–290. doi:10.1016/0378-3804(78)90023-2

Simões, V.M., Laurent, H., Oliveira, M.C., Menezes, L.F., 2017a. The impact of warm forming in the natural aging of Al-Mg-Si alloys. Submitt. Int. J. Mater. Form.

Simões, V.M., Oliveira, M.C., Laurent, H., Menezes, L.F., 2017b. On the punch speed influence in warm forming and springback of two Al-Mg-Si alloys.

Simões, V.M., Oliveira, M.C., Neto, D.M., Cunha, P.M., Laurent, H., Alves, J.L., Menezes, L.F., 2017c. Numerical study of springback using the split-ring test: influence of the clearance between the die and the punch. Int. J. Mater. Form. 1–13. doi:10.1007/s12289-017-1351-x

Wang, H., Luo, Y., Friedman, P., Chen, M., Gao, L., 2012. Warm forming behavior of high strength aluminum alloy AA7075. Trans. Nonferrous Met. Soc. China 1, 1–7. doi:10.1016/S1003-6326(11)61131-X

Werinos, M., Antrekowitsch, H., Ebner, T., Prillhofer, R., Curtin, W.A., Uggowitzer, P.J., Pogatscher, S., 2016. Design strategy for controlled natural aging in Al–Mg–Si alloys. Acta Mater. 118, 296–305. doi:10.1016/j.actamat.2016.07.048

Wilson, D.V., 1988. Aluminium versus steel in the family car — the formability factor. J. Mech. Work. Technol. 16, 257–277. doi:10.1016/0378-3804(88)90055-1

Xia, Z.C., Miller, C.E., Ren, F., 2004. Springback Behavior of AA6111-T4 with Split-Ring Test, in: AIP Conference Proceedings. Presented at the MATERIALS PROCESSING AND DESIGN: Modeling, Simulation and Applications - NUMIFORM 2004 - Proceedings of the 8th International Conference on Numerical Methods in Industrial Forming Processes, AIP Publishing, pp. 934–939. doi:10.1063/1.1766647

Figure captions

Table captions

(Page intentionally left blank)

Chapter 6.

Numerical study of springback using the split-ring test: influence of the clearance between the die and the punch

This chapter contains the paper published in the International Journal of Material Forming, with the same title as the chapter. Based on a numerical analysis, this work discusses the influence of the clearance between the die and the punch on the distribution of the axial and circumferential through-thickness stress profiles along the cup height and, consequently, on springback. It shows that the ironing of the vertical wall changes the characteristic distribution of both residual stresses components, in all locations of the cup wall, even for relatively small ironing strains.

.

(Page intentionally left blank)

Int J Mater Form
DOI 10.1007/s12289-017-1351-x

SI: MODELING MATERIALS AND PROCESSES, IN MEMORY OF PROFESSOR JOSÉ J. GRÁCIO

Numerical study of springback using the split-ring test: influence of the clearance between the die and the punch

V. M. Simões[1,2] · M. C. Oliveira[2] · D. M. Neto[2] · P. M. Cunha[2] · H. Laurent[1] · J. L. Alves[3] · L. F. Menezes[2]

Received: 31 December 2016 / Accepted: 23 March 2017

Abstract The split-ring test consists in cutting a ring from the wall of a drawn cylindrical cup, which is split to measure the springback. This springback measure can also be used to estimate the circumferential residual stresses in the ring. It is known that the distribution of the residual stresses in the cup depends on the specific combination of forming parameters selected to perform the deep drawing operation, which include the depth of the cup and the clearance between the die and the punch. Moreover, the forming parameters also seem to affect the distribution of the axial and circumferential through-thickness stress profiles along the cup height, since different ring opening trends have been observed, when rings are cut from the cup wall at different heights. The focus of this numerical study is the analysis of the impact of an ironing stage on the residual stress distributions in the cylindrical cup and, consequently, in the split-ring test. The analysis is performed considering a 6016-T4 aluminium alloy, for which experimental results are available. The results show that the ironing of the vertical wall changes the characteristic distribution of the axial and circumferential residual stresses in all locations of the cup wall, even for relatively small ironing strains. This affects the trend observed for the ring opening value, when rings are cut at different heights.

Keywords Springback · Split-ring test · Finite element analysis · Ironing · Residual stresses

Introduction

The split-ring test was proposed as a springback benchmark test since it allows avoiding the problems related with the accurate measurement of springback. In fact, the use of a stamped component as the reference shape normally requires: (i) measurement fixtures that should not influence actual springback values by not restraining the formed part; and (ii) profiling equipment such as coordinate measuring machines or laser scanning, with a proper definition of the measurement

✉ M. C. Oliveira
marta.oliveira@dem.uc.pt

V. M. Simões
vasco.simoes@uc.pt

D. M. Neto
diogo.neto@dem.uc.pt

P. M. Cunha
patrick.cunha@uc.pt

H. Laurent
herve.laurent@univ-ubs.fr

J. L. Alves
jlalves@dem.uminho.pt

L. F. Menezes
luis.menezes@dem.uc.pt

[1] Univ. Bretagne Sud, FRE CNRS 3744, IRDL, F-56100 Lorient, France

[2] CEMMPRE, Department of Mechanical Engineering, University of Coimbra, Polo II, Rua Luís Reis Santos, Pinhal de Marrocos, 3030-788 Coimbra, Portugal

[3] CMEMS, Microelectromechanical Systems Research Unit, University of Minho, Campus de Azurém, 4800-058 Guimarães, Portugal

Published online: 21 April 2017

locations and directions. In many cases, most of the part will present a small springback which reduces the measurement accuracy, increasing the experimental error [1].

The split-ring test was proposed based on previous knowledge concerning the measurement of residual circumferential stresses at the surface of tubes or deep drawn cups. It consists on the cut of a ring specimen from the cup and its split longitudinally along any radial plane. The amount by which the outer diameter of the ring changes from its original value is a measure of the released residual circumferential stress. The distribution of the residual circumferential stress through the ring thickness must be determined or assumed, but it is possible to have good estimates of its magnitude based on the ring opening [1, 2].

A deep drawn cup presents significant residual stresses that result in large springback values when allowed to relax. The large springback increases indirectly the measurement accuracy and reduces the experimental error. Thus, the use of the ring opening as a standardized measure of springback enables the comparison of springback predictions using different numerical models, allowing the calibration of numerical and constitutive model parameters, to achieve a satisfactory correlation with the benchmark test results. In this context, it has been used to characterize the springback by many authors [1–8].

The accuracy of the springback prediction depends of the stress state achieved after forming, particularly its gradient through the sheet thickness. In this context, most of the studies on the analysis of residual stress, induced by forming processes and springback, resort to simpler plane strain geometries [9–12]. The springback that results from the split-ring test performed on a deep drawn cup is due to the stretch-bend process that occurs with the material flow. At the end of the forming, there are residual stresses in the cup because different locations accumulated different magnitudes of plastic strain. These stresses are a key factor for the springback, because their integral over the wall thickness yields a non-zero bending moment and thus a shape change when the ring is split [8]. The distribution of the residual stresses in the cup depends on the specific combination of forming parameters selected to perform the deep drawing operation, which include the depth and diameter of the cup, the bending radii of the tools, the gap between the die and the punch, the blank-holder force and the friction conditions. In this context, an increased depth of the cup can contribute to increase the homogeneous stretching, resulting in more uniform though-thickness circumferential and axial stresses distributions. The decrease of the bending radius of the die can cause excessive strains on both sides of the blank, reducing the springback at an increased risk of cracking on the outside, as a result of the higher tensile stresses installed [8]. However, this depends also on the combination of the other process parameters, because other authors showed that the die radius has a negligible influence on the circumferential stress distribution [2].

The stretch portion associated with the material flow depends of the restraining force applied by the blank-holder and the contact with friction conditions, meaning also that the residual stresses present in a cup are not the same for all points around and along the cup wall [1]. For the process conditions suggested in [1], it is expected that the residual stresses are largest near the top of the cup wall, due to the bending that occurred at the end of the draw, when little net tension was applied. This is confirmed by the results presented in [8] for an AISI-1010, which showed that the ring opening becomes larger for rings cut further away from the region in contact with the punch radius. However, in the analysis performed for a 6111-T4 aluminium alloy, the ring presenting the higher opening corresponds to one located closer to the middle of the vertical wall [3]. The tools dimensions used in both studies are the same, with a clearance between the die and the punch of 5 mm. However, the AISI-1010 sheet is 3.0 mm thick, while the 6111-T4 is only 0.925 mm. This indicates that the gap between the die and the punch can also affect the residual stresses distributions, as reported in [2], which show that for a clearance smaller than the blank thickness, the circumferential residual stress values are smaller. This can be related with the occurrence of an ironing stage, which has been previously reported to contribute to a reduction of the tensile residual stress values in the outer surface [13].

The residual stress distributions in the cup [13] and in the ring [7, 8] have been studied , highlighting their variation along the cup wall. In fact, in a study performed to evaluate the robustness of the split-ring test, it was found that the largest variation in the ring opening was observed when the location where the ring was cut from the sidewall was moved along the cup wall [4]. In that study, a decrease of the ring opening occurred when the ring was cut closer to the punch radius, which was associated to the corresponding decrease of the circumferential stresses toward the cup bottom. This was attributed to a rising level of accumulated plastic strain as the rings are closer to the bottom [7]. In fact, springback results from the amount of elastic energy stored in the part during the forming operation. Thus, by increasing the proportion of material submitted to plastic deformation, it is possible to reduce the change of shape induced by the elastic recovery.

The comparison of results obtained considering similar forming parameters, but different blank thicknesses (3.0 and 0.88 mm), indicates that the gap between the die and the punch results in a major discrepancy in the thickness distribution along the cup wall. For the thicker blank, the thickness value decreases toward the bottom, while for the thinner blank it increases slightly (but is still lower than the blank thickness). For the thick walled cup, a decrease in thickness is a clear indication of uniform vertical stretching (rising plastic strain), and it explains the lower springback at the cup bottom. This seems to be contradicted by the slight increase in thickness toward the bottom found for the thin walled cup. Although

there is no rise in the vertical stretching towards the cup bottom, the springback is still lower at the bottom. The explanation given by the authors is based on the different circumferential plastic flow of material during the deep drawing process, leading to higher levels of circumferential plastic strain for the thin walled cup, when compared with the thicker, where higher strains are predominantly caused by vertical stretching. Higher thickness differences along the vertical wall implies an increased circumferential material flow and higher strain levels. The latter have the effect of reducing springback as more material is deformed beyond the yield stress [4].

The results from previous studies indicate that the split-ring test is a robust springback benchmark [4], but improved knowledge is still required concerning the influence of the process parameters on the residual stresses distribution along the cup wall. In fact, experimental split-ring test results obtained in the analysis of a 6016-T4 aluminium alloy revealed a decreasing value for the ring opening with the increase of the distance from the cup bottom, which seemed to result from the fact that an ironing stage occurs during the cup forming. These results are discussed in the following section, where the forming process conditions are described, followed by the details about the numerical model adopted to perform the numerical study. The third section focus on the residual stresses distribution numerically predicted, as well as on the axial moment distribution along the cup wall, highlighting the impact of the clearance between the die and the punch and the forming depth. Finally, in the last section the main conclusions are discussed.

Description of the tests conditions

The forming process selected for the analysis and posterior springback evaluation using the split-ring test is the one used in [14], which was also proposed in the conference Numisheet 2016, as a benchmark to evaluate the springback of an AA5086 alloy under warm forming conditions [15]. The main dimensions of the tools (axisymmetric) are given in Table 1 and are schematically shown in Fig. 1. The gap between the die and the blank-holder is 1.125 mm. This means that when a 1 mm thick blank is used, if the blank thickens more than 0.125 mm, due to the compression stress state in the flange, an ironing stage will occur. The intensity of this ironing stage is strongly dependent on both the drawing ratio and the gap between the die and the punch. The circular blank presents a diameter of 60 mm, which results in a drawing ratio of 1.8.

Table 1 Main dimensions of the forming tools used in the deep drawing of a cylindrical cup [mm]

Die			Punch		Blank-holder
Opening diameter	Corner radius	Height	Diameter	Corner radius	Opening diameter
35.25	5.0	8.75	33.0	5.0	33.6

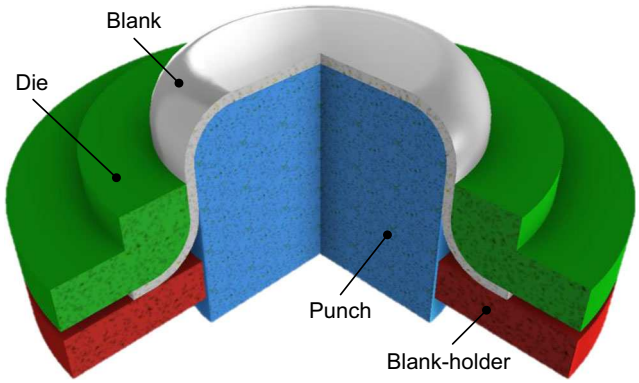

Fig. 1 Schematic representation of the forming tools considering a gap between the punch and the die of 1.125 mm

The material of the blank was taken from a rolled sheet of 6016-T4 aluminium alloy with 1.0 mm of thickness and uniaxial tensile tests were performed, enabling the identification of the material parameters required for the numerical analysis [16]. Moreover, the forming process previously described was performed using a blank-holder force of 6 kN. For further details concerning the forming tests experimental procedure, please refer to [16].

Two cups were fully drawn and three rings were trimmed at a distance of 7 mm from the cup's bottom with a height of 3 mm, with a distance between them of 2 mm, using an electro-erosion machine by wire. The positioning of the rings is schematically shown in Fig. 2 (a). The wire and the electric arc generate a cutting thickness of 0.3 mm, which is taken into account to obtain a ring of 3 mm in height. The same technique was used to split the rings along the RD. The average values obtained for the ring opening measurement from the two cups were 5.67, 4.23 and 2.12 mm, for the bottom, middle and top rings, respectively. This trend corresponds to a decreasing opening value along the cup's height. Therefore, it was decided to try to understand the impact of the ironing stage in the distribution of the residual stresses in the formed cups. This study was performed numerically, considering also two other drawing depth values of 16 and 22 mm, which are smaller than the standard value of 30 mm. For the smaller drawing depth values a single ring was cut from the cup wall, as exemplified in Fig. 2 (b), for the smaller punch displacement. Also, for the standard drawing depth, a different gap between the die and the punch was considered, using a value of 4 mm, obtained by reducing the punch diameter to 27.25 mm, which results in a drawing ratio of 2.2. This value for the clearance was selected taking as reference the one used in [3], and the tools dimensions used in the current study.

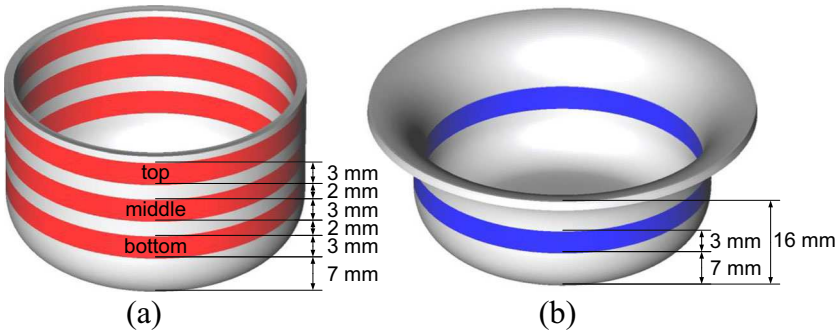

Fig. 2 Positioning of the ring(s) in the cylindrical cup: (**a**) fully drawn cup; (**b**) for a fixed punch displacement of 16 mm

Finite element model

In order to model the deep drawing process and the split-ring test, the finite element analysis is divided into four different stages: (i) deep drawing operation; (ii) unloading the cup; (iii) cutting the ring and (iv) split the ring. The numerical simulations were carried out with the in-house static implicit finite element code DD3IMP [17], specifically developed to simulate sheet metal forming processes [18–20]. The ring cut and splitting was performed with the in-house code DD3TRIM [21, 22].

Due to geometric and material symmetry conditions, only half model is simulated. This allows to simplify the analysis of the cutting and splitting stages, with the later performed by just removing the symmetry condition at one end of the ring. The blank is discretized with linear hexahedral finite elements, using a selective reduced integration technique [23] to avoid volumetric locking. The central zone of the blank (flat area of the punch) is discretized by a relatively coarse unstructured mesh, while the remaining zone is discretized with a fine in-plane structured mesh, corresponding to a total of 86 elements in the radial direction and 204 in the circumferential one. This discretization respects the recommendations of using an element size that covers 5 to 10° of the tool radius, i.e. at least 9 finite elements in contact with the radius of the die or punch, in order to accurately predict the springback [11, 12]. Springback prediction is known for being quite sensitive to the in-plane refinement but also to the number of integration points through-thickness and the integration rule adopted [12, 24]. In this study a total of 3 layers of elements through-thickness was considered, corresponding to 6 integration points in this direction, combined with the Gauss integration rule. The discretization of the blank comprises a total of 58,806 finite elements.

The forming tools are considered as rigid in the numerical simulation and its surfaces were discretized with Nagata patches [25]. The nodal normal vectors required for the smoothing method are evaluated from the IGES file, using the algorithm proposed in [26], which allows the recovery of the curvature of the surfaces with good accuracy [27] with a total of 369 Nagata patches. Further details about the blank and tools discretization can be found in [28].

Previous studies indicate that, for the conditions assumed in the experimental analysis, the deep drawing stage involves a drawing and an ironing operation. Besides, the springback prediction is quite sensitive to the numerical parameters but also to the constitutive model adopted. In this context, it was shown that the use of an orthotropic yield criterion generates a gradient for the stress distribution in the circumferential direction, which usually contributes to the underestimation of the springback [14, 29]. The 6016-T4 aluminium alloy under study presents a planar anisotropy coefficient of 0.038, which results in a small earing profile [16]. In this context, and in order to keep the results analysis as simple as possible, it was decided to assume an isotropic plastic behaviour of the material, described by the von Mises yield criterion:

$$\overline{\sigma}^{\,2} = (\sigma_{22}-\sigma_{33})^2 + (\sigma_{33}-\sigma_{11})^2 + (\sigma_{11}-\sigma_{22})^2 + 2(\sigma_{23})^2 + 2(\sigma_{13})^2 + 2(\sigma_{12})^2, \quad (1)$$

where $\overline{\sigma}$ is the equivalent stress and σ_{11}, σ_{22}, σ_{33}, σ_{23}, σ_{13} and σ_{12} are the components of the Cauchy stress tensor. The hardening behaviour is described by the Voce law [30, 31]

$$Y = Y_0 + (Y_{\text{sat}}-Y_0)\left\{1-\exp\left(-C_y\left(\overline{\varepsilon}^{\,\text{p}}\right)\right)\right\}, \quad (2)$$

since aluminium alloys are prone to exhibit saturation of the hardening behaviour. In Eq. (2), $\overline{\varepsilon}^{\text{p}}$ denotes the equivalent plastic strain, Y_0 is the initial value of the flow stress, Y_{sat} is the flow stress saturation value and C_y defines the growth rate of the yield surface. These parameters were identified based on tensile test results [16] and their values are presented in Table 2. Besides, the elastic behaviour is assumed isotropic and constant, which is described by the Hooke's law using the

Table 2 Elastic properties and Voce hardening law parameters of the 6016-T4 aluminium alloy [16]

Elastic Properties		Voce Law		
Young's modulus (GPa)	Poisson's ratio	Y_0 [MPa]	Y_{sat} [MPa]	C_y
69	0.30	131.4	312.3	12.08

parameters also listed in Table 2.

The friction between the blank and the forming tools is modelled through the classical isotropic Coulomb's law. The value of the friction coefficient used in the numerical simulations is $\mu = 0.15$ and was adjusted in order to minimize the difference between the experimental and numerical punch force evolution during the drawing stage [16].

Stress analysis procedure

Springback defines the geometrical change of a part after forming, when the forces imposed by the forming tools are removed. The accuracy of the springback prediction is strongly dictated by the stress state obtained after forming, particularly the gradient through the sheet thickness. Most of the studies on the analysis of residual stress and springback, induced by the forming process, are based on simple bending [9, 11, 24] and straight flanging [32]. For instance, the analysis of plane strain bending tests was fundamental to understand the role of a superimposed tension force in the sensitivity of springback prediction to numerical parameters, such as the number of through thickness integration points and the integration rule [12, 24].

A cylindrical cup is an axisymmetric component, as well as the ring cut from its wall. At the end of the forming process, the cup's vertical wall is submitted to residual stresses, which are usually evaluated using the cylindrical coordinate system schematically shown in Fig. 3. The cut of the ring from the cup's vertical wall contributes to the release of the radial (σ_{rr}) and axial (σ_{zz}) residual stresses. When the ring is split, the two ends of the ring open a distance that is proportional to the circumferential residual stress ($\sigma_{\theta\theta}$) [2, 3, 7, 8]. In fact, based on this knowledge, a methodology was proposed to estimate the residual stresses using the gap opening, assuming that the circumferential residual stress presents an axisymmetric distribution and it does not change along the height of ring. This methodology is based on the assumption that the elastic closing of the ring can be simplified as pure bending of a curved beam, enabling the definition of an applied bending moment, equivalent to the one generated by the ring opening [2].

This axial moment per unit length results from the through-thickness distribution of the circumferential stresses and can be evaluated as

$$M_z = \int_{-t/2}^{t/2} \sigma_{\theta\theta} \eta d\eta, \tag{3}$$

where η is the through-thickness local coordinate and t is the final sheet thickness. This enables its evaluation for each section, along the height of ring or along the circumferential direction. In this study, this moment is evaluated using the six through-thickness integration points, as schematically shown in Fig. 3, which are labelled according to their relative position. The Gauss Point (GP) located closest to the surface in contact with the punch (inner surface) is GP1 and the one closest to the surface in contact with the die (outer surface) is GP6. Also, according to the through-thickness coordinate η definition, GP1 presents always the lowest (negative) coordinate while GP6 presents always the highest (positive) coordinate. The numerical evaluation of this moment is performed using the Gauss integration rule, assuming two integration points for each finite element, such that

$$M_z = \frac{t}{6} \sum_{i=1}^{6} \sigma_{\theta\theta}(\eta_i)\eta_i. \tag{4}$$

The analysis of the through-thickness stress distributions and the axial moment will be always performed for the sections located closer to the split plane. This sections are representative of all sections situated along the circumferential direction, at the same cup height, since the isotropic von Mises yield criterion is adopted.

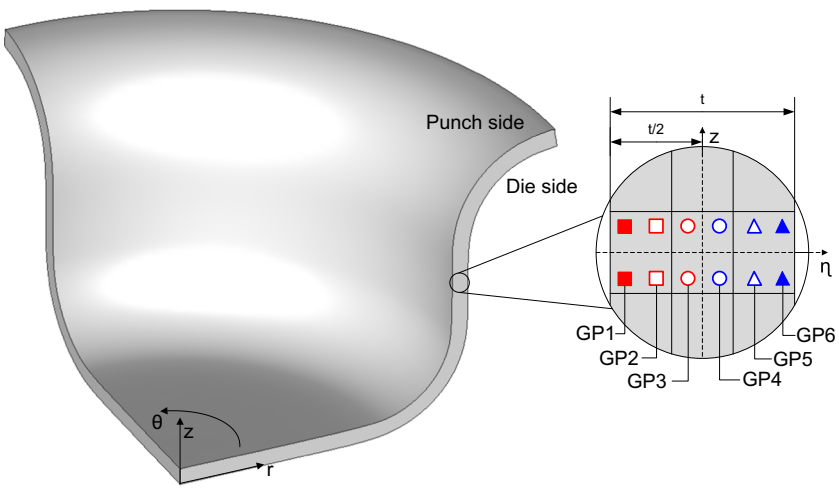

Fig. 3 Positioning of the cylindrical coordinate system in the formed cup and the local coordinate system η for the through-thickness stress analysis

Results and discussion

The numerical simulation of the deep drawing of the cylindrical cup was performed, considering the two different values of gap between the die and the punch. Figure 4 presents the punch force evolution with its displacement, highlighting the difference in the initial evolution but also on the final stage. In fact, for both cases the maximum punch force is attained for a displacement that corresponds to the instant that the die and the punch shoulder radii are completely formed in the part. However, while for the gap of 1.125 mm (labelled "Lower gap") this occurs for a punch displacement of 11–12 mm, for the gap of 4 mm (labelled "Higher gap"), this occurs only for approximately 16 mm. Moreover, for the lower gap condition the ironing stage starts to occur for a punch displacement of approximately 21 mm, while for the other condition no ironing occurs. For the lower gap condition, the maximum thickness value measured in the cup's flange, for a punch displacement of 20 mm (i.e. before the ironing stage), was approximately 1.3 mm. Therefore, the theoretical thickness reduction induced by the ironing stage is 15% [33], which can be considered a small value. The geometry of both cups is also quite different, as shown in Fig. 5, including their height. This results from the fact that different gap values induce a different thickness distribution along the cup wall, as shown in Fig. 6. In particular, a stronger thickness reduction is observed for the higher gap in the region in contact with the punch radius.

For the lower gap value, higher thinning occurs at the entrance to the punch radius section and the confluence of the punch radius with the cup wall, as previously reported in [16]. For the higher gap value, higher thinning also occurs at the entrance to the punch radius section, but a value similar to the initial one is observed afterwards, followed by a thickening with a slope similar to the one observed for the lower gap value (see Fig. 6). Moreover, for the higher gap value the cup's bottom also presents higher thinning values, which leads to a higher cup, for the same drawing depth. This effect can also be

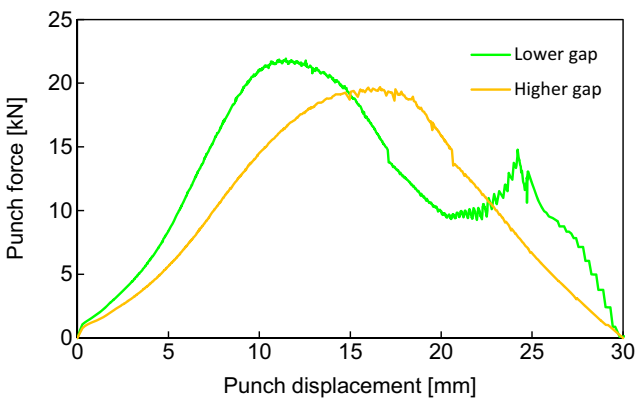

Fig. 4 Numerical punch force evolution for the two different values of gap between the die and the punch

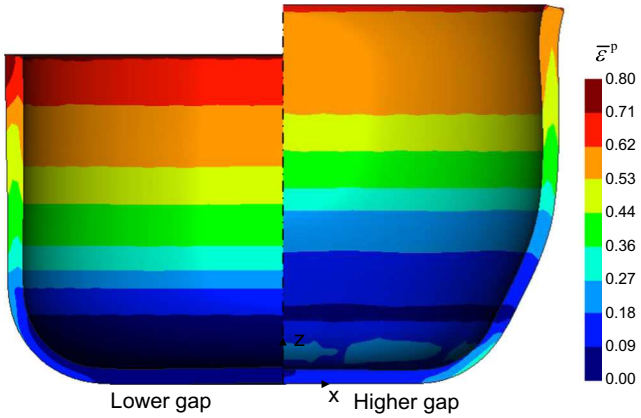

Fig. 5 Equivalent plastic strain distribution plotted on the final shape of the cylindrical cups

observed in the equivalent plastic strain distribution shown in Fig. 5. Although not shown here, the strong thinning observed for the higher gap value can be reduced by decreasing either the friction coefficient or the blank-holder force, but the trend remains unaltered. Thus, the trend for the thickness distribution is mainly dictated by the clearance between the punch and the die.

Finally, it should be mentioned that since there is no blank-holder stopper (see Fig. 1), the blank-holder only stops its vertical movement when it establishes contact with the die. Therefore, there is always some squeezing of the edge of the cup, resulting from the contact with the blank-holder [28, 29, 34].

Three rings were cut from each of the cups (see Fig. 2 (a)) and split, in order to evaluate the opening. The results are presented in Table 3, highlighting that for the lower gap value there is a clear trend for the decrease of the opening with the increase of the distance from the cup's bottom, as observed experimentally. Globally, the experimental results are accurately predicted, except for the top ring, for which the ring opening is clearly overestimated. This is certainly related with

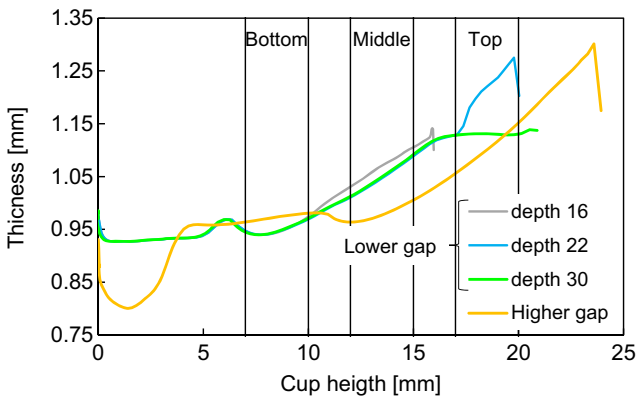

Fig. 6 Thickness distribution along the cup height at the end of the cup forming and unloading stage, for the standard punch displacement of 30 mm, for both gap values, and for the punch displacement of 16 and 22 mm for the lower gap value

Table 3 Numerical ring opening values at different positions and considering distinct process conditions. The values presented between brackets for the lower gap, full drawn cup, correspond to the experimental ones

	Punch displacement [mm]			
	30 (Full drawn cup)		16	22
Ring	Lower gap	Higher gap	Lower gap	
Bottom	6.37 (5.67)	3.59*	7.30	5.98
Middle	4.08 (4.23)	6.94	-	-
Top	3.20 (2.12)	4.05	-	-

* This ring presents an accentuated curvature in the axial direction

the underestimation of the thickening predicted by the von Mises yield criterion, for the material located under the blank-holder [29].

For the higher gap, the middle ring presents the higher opening value. This trend is similar to the one reported in [3], in the analysis of a 6111-T4 aluminium alloy, considering a similar gap with different tools dimensions. Nonetheless, it should be mentioned that for the higher gap value the bottom ring presents an accentuated curvature in the axial direction, as highlighted in the sections profiles shown in Fig. 7. A more pronounced conical shape of the ring is known to lead to a slight decrease of the ring opening [4]. Moreover, Fig. 7 also presents the relative position of the lines corresponding to the six integration points. The axial moment resulting from the residual circumferential stresses is evaluated based on the Gauss points of each element for a specific range of the longitudinal axis z, which depends on the value of the gap between the die and the punch. When the cup wall is not vertical, the Gauss points of the stacked finite elements are not aligned with the radial direction, as highlighted in Fig. 7. Therefore, the bottom ring obtained for the higher gap value will be discarded in the following analysis of the axial moment distribution along the cup wall.

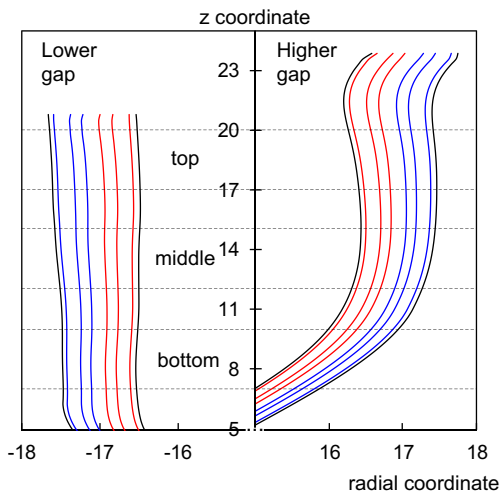

Fig. 7 Section profile of the cup wall at the end of the forming and unloading stages, highlighting the relative position of the six through-thickness integration points (red lines for the points located closer to the punch and blue lines for the ones closer to the die, as in Fig. 3)

Stress distributions

In this section the stress distributions along the cup wall are analysed, first for the cups formed to a drawing depth of 30 mm and afterwards for the two other values considered.

Analysis of the three rings

Figure 8 presents the axial stress distribution along the cups wall at the end of the forming and unloading stage, for both conditions under analysis. The through-thickness gradient is closely related with the fact that the material was bent over the die radius and straightened at the exit of the die edge, presenting a compressive value in the inner surface and a tensile one in the outer surface. The same trend is observed for the circumferential stress distribution, as shown in Fig. 9, which is in agreement with the results previously reported in [13]. Moreover, the ironing stage contributes to a change on the

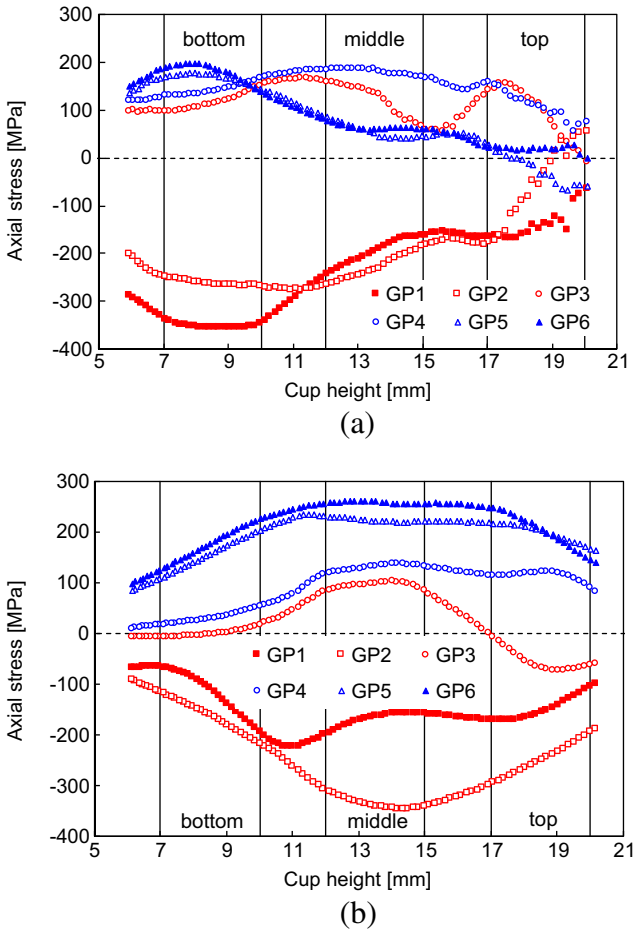

Fig. 8 Axial stress distributions along the cup wall at the end of the cup forming and unloading stage: (**a**) Lower gap; (**b**) Higher gap

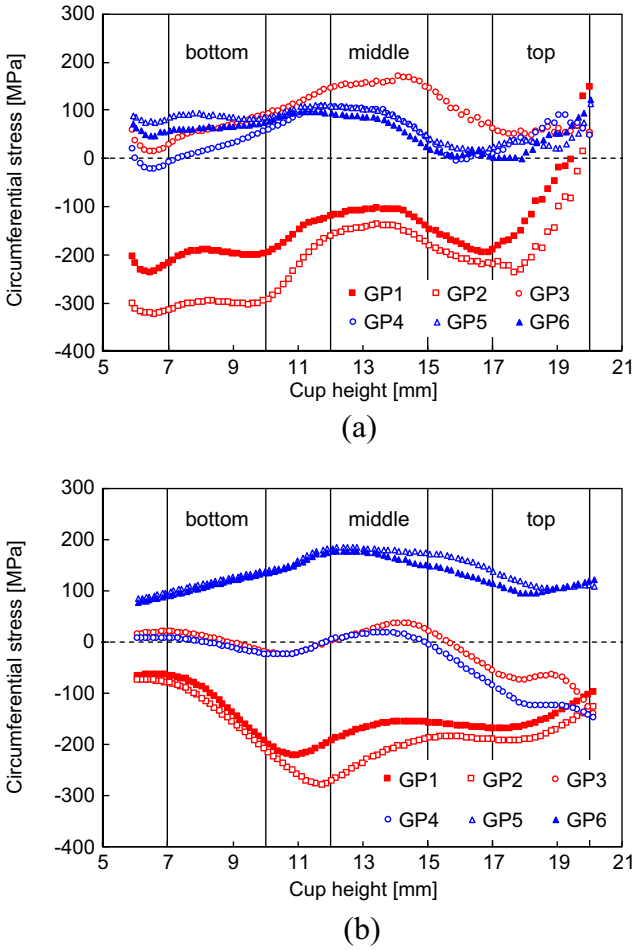

Fig. 9 Circumferential stress distributions along the cup wall at the end of the cup forming and unloading stage: (**a**) Lower gap; (**b**) Higher gap

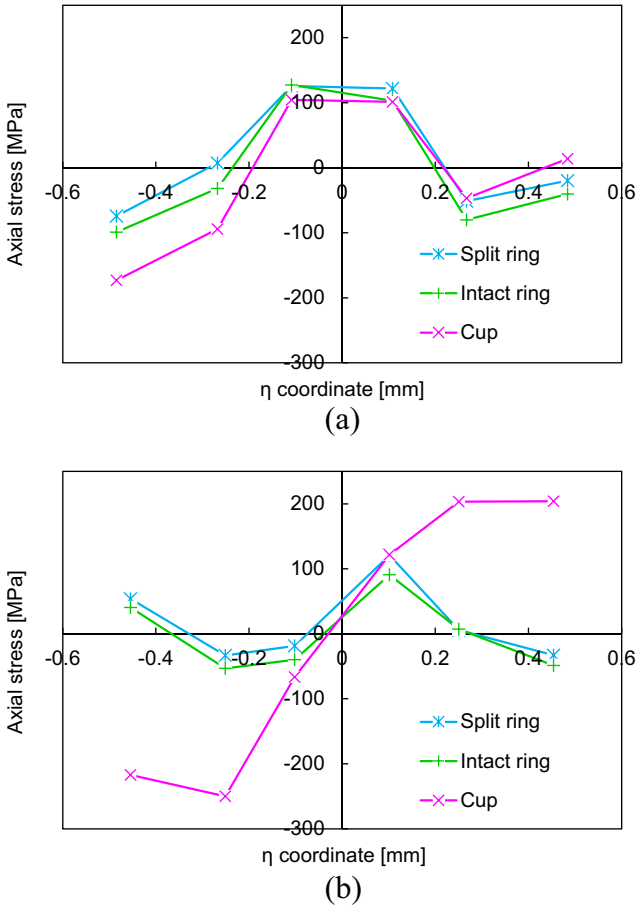

Fig. 10 Axial stress distributions along the middle section of the Top ring at the end of the forming and unloading stage, in the intact ring and in the split-ring: (**a**) Lower gap; (**b**) Higher gap

profile of both components, in particular to a reduction of the tensile residual stress values in the outer surface [13]. The radial stress distribution is not shown, since it presents a negligible magnitude when compared with the other stress components.

Figure 10 presents the through-thickness axial stress distribution in the middle section of the top ring ($z = 18.5$ mm), both for the cup, the intact ring and the split-ring. The trimming of the ring from the cup clearly contributes to the release of the axial residual stress component, while the split only has a small impact in the stress distribution, as expected. Moreover, the reduction of this stress component with the cut of the ring from the cup wall is more evident for the higher gap value. In fact, the axial stress distribution at the end of the forming process presents a distribution typical of a bending process and an "S"-curve shape after the trimming, which is typical of the unloaded state [7]. The release of the axial stress component is accompanied by the reduction of the circumferential stress component, as shown in Fig. 11. These figures highlight the interdependency between these two stress components during the ring cut stage, where the lower gap also presents a smaller variation of the circumferential stress component. The intact ring presents a through-thickness circumferential stress distribution analogous to that of a plastically bent beam in a loaded configuration, which is responsible for generating the ring opening. The stress trend observed for the intact ring obtained with the higher gap is more similar to the one previously reported in [7], although in the example under analysis the neutral line is clearly shifted to the outer surface (see Fig. 11 (b)). Besides, the neutral line location is identical to the one observed in the cup. The analysis of the circumferential stress distribution along the cup wall presented in Fig. 9, shows that there is a change of the neutral line location in function of the position along the vertical wall. For instance, for the lower gap value it is clearly shifted to the inner surface for material points located in the bottom and middle ring. In fact, the change of the circumferential stresses with the axial position has been pointed out in the literature [13, 35], with some authors reporting an increase from the mid-line towards the cup bottom [7]. Taking as reference the results shown in Fig. 9 for the cup, this trend will certainly depend on the forming parameters. Consequently, the results correlate well

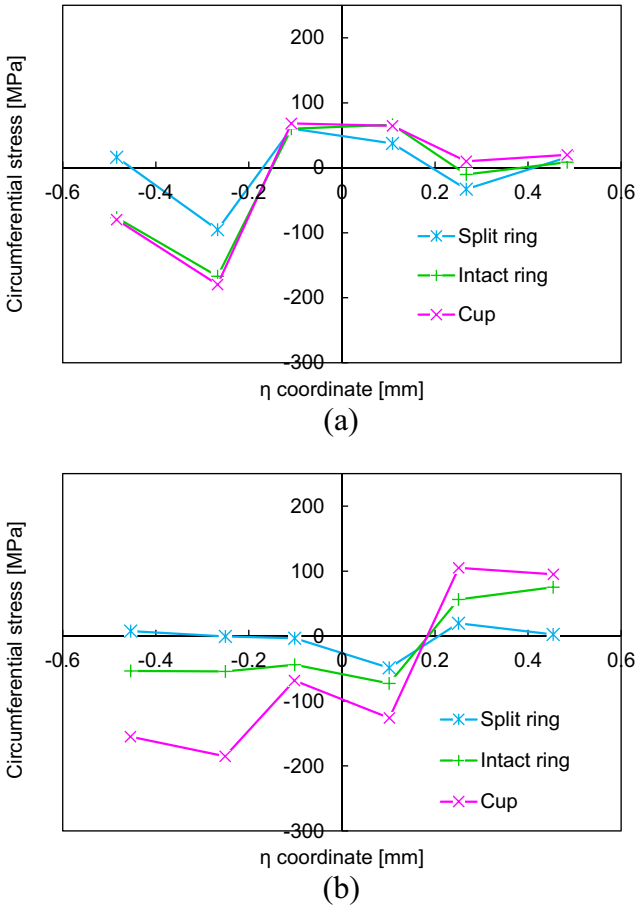

Fig. 11 Circumferential stress distributions along the middle section of the Top ring at the end of the forming and unloading stage, in the intact ring and in the split-ring: (**a**) Lower gap; (**b**) Higher gap

with the fact that the ring opening is sensitive to the vertical position along the cup wall [4] or even to the ring height [1].

The ring split stage induces a significant change in the circumferential stress distribution, which now also exhibits the "S"-curve shape, typical of the plastically bent beam in an unloaded configuration [7]. The results indicate that the axial moment for the middle section of the ring is not necessarily null, but its integration along the ring height leads to a zero value. In order to better understand the effect of the split stage, Fig. 12 presents the circumferential stress distributions obtained for the intact and split middle ring, for both gap values. This ring was selected because it presents, globally, the higher values for the ring opening and the trend observed is similar for all rings. The effect of the split is evident in the reduction of the stress values in the ring, which still presents residual stresses. The through-thickness circumferential residual stress presents an almost axisymmetric distribution, with exception of the sections located closer to the split plane, where the minimum values are attained. Moreover, there is also a gradient in the circumferential residual stresses along the ring height. It should be mentioned that, for the lower gap value, the stress distribution in the intact ring is not as axisymmetric as for the higher gap due to the fact that the ironing stage is more sensible to small shape errors induced by the tool description with Nagata patches [36].

Figure 13 presents the circumferential stress change induced by the split of the top ring, determined as the difference between the intact and the split-ring (see Fig. 11). The results obtained for the higher gap value present a more linear trend for the stress change, identical to the one previously reported in [8], while for the lower gap value the linear tendency is not so clear, although both top rings present no inelastic effects.

Analysis of the bottom ring

For the lower gap value, the analysis of the bottom ring was also performed for two other values of punch displacement, namely 16 mm and 22 mm. For a punch displacement of 16 mm the blank is still in contact with the blank-holder, presenting a small flange. The positioning of the ring is schematically shown in Fig. 2 (b). For the punch displacement of 22 mm the ironing stage has already started, but with a small value of thickness reduction (see Fig. 4 and Fig. 6). Figure 14 (a) presents the circumferential stress distribution along the middle section of the bottom ring, before the ring was cut from the cup wall, for 16 mm, 22 mm and 30 mm of punch displacement. Figure 14 (b) shows the same results obtained for the intact rings. It should be mentioned that the bottom ring is located in a region not submitted to ironing. However, as shown in Fig. 6, the ironing stage induces increased stretching, i.e. the true strains in the cup bottom become higher, acting as a stress relief and reducing the stress magnitudes [8]. In fact, as previously reported in [4], as the cup is drawn deeper, the fraction of uniform plastic strain in the cup wall increases. As a result, the material in the cup wall is deformed significantly past the yield stress, and the magnitude of the through-thickness strain inhomogeneities (difference in plastic strain from one location to another) introduced by the bending and unbending of the blank decreases. Moreover, in terms of the stress-strain curve of the material, the deformation of the entire cup wall proceeds into the strain region where large strain differences correspond to relatively small stress differences, particularly if the material hardening behaviour is well described by a saturation law.

Smaller stress differences translates into reduced residual stresses and springback. This interpretation of the influence of the drawing depth presented in [4], is corroborated by the equivalent plastic strain distribution along the cup wall, shown in Fig. 15 for the drawing depth of 16, 22 and 30 mm. In this figure it also visible the influence of the ironing stage, particularly for the outer surface, for which a higher increase is observed when compared with the inner surface, which correlates with the strong reduction of the axial component of the residual stress. Thus, as shown in Table 3, the bottom ring cut from the cup obtained with only 16 mm of punch

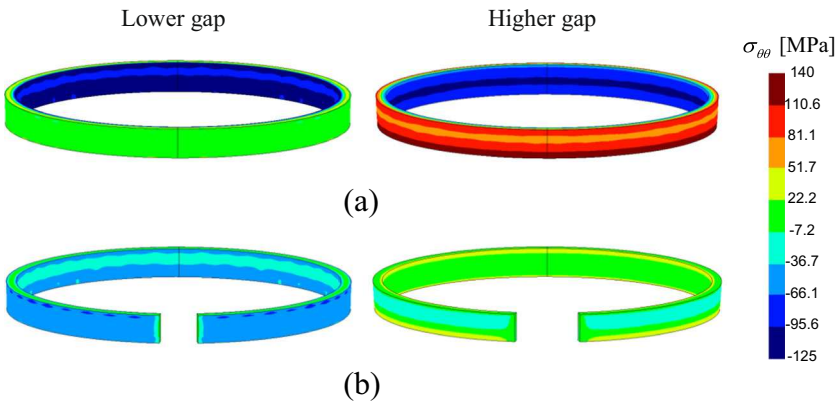

Fig. 12 Circumferential stress distributions in the Middle ring: (**a**) intact and (**b**) after the split

displacement is the one presenting the higher ring opening. However, as shown in Fig. 14 (a), the increase of the plastic strain does not necessary means the decrease of the magnitude of the through-thickness stress inhomogeneities, since similar equivalent stress values can be obtained for different stress states. Thus, the bottom ring cut from the fully drawn cup (depth 30 mm) presents a higher ring opening than the one obtained from a cup obtained with a punch displacement of 22 mm. These results show that the circumferential stress through-thickness distribution is clearly modified by the ironing stage, even for physical locations in the cup wall positioned far away from the material that is submitted to this compression state. In fact, for the full drawn cup, the trend of the circumferential stress through-thickness distribution obtained for the bottom ring is similar to the one obtained for the top ring (see Fig. 11 (a)). However, as previously stated, the ironing stage contributes to a more uniform magnitude of the circumferential stress along the thickness, which leads to a smaller ring opening.

Axial moment distributions

The axial moment per unit length, evaluated along the cup and in the ring wall, using Eq. (4), is presented in Fig. 16, for the

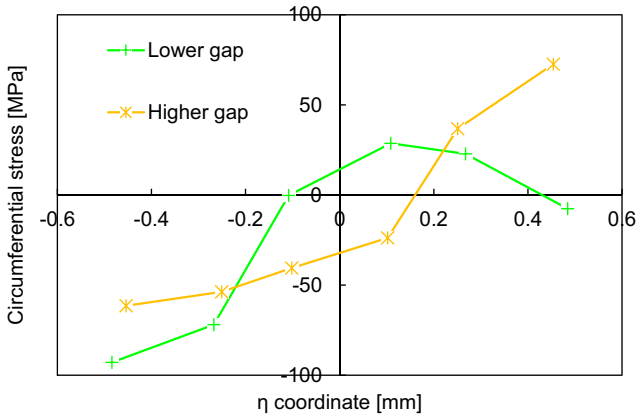

Fig. 13 Difference between the circumferential stress distributions in the intact ring and in the split-ring, at the middle section of the Top ring

through-thickness section located closer to the split position. The comparison between the values determined for the cup wall and the intact ring confirm the release of the circumferential stresses induced by the cut of the ring from the cup's wall. Moreover, the influence of the ironing stage that occurs for the lower gap, mainly for the last 5 mm of the cup's wall (see Fig. 6), is quite notorious in the smaller difference between the axial moments observed for the top ring, when

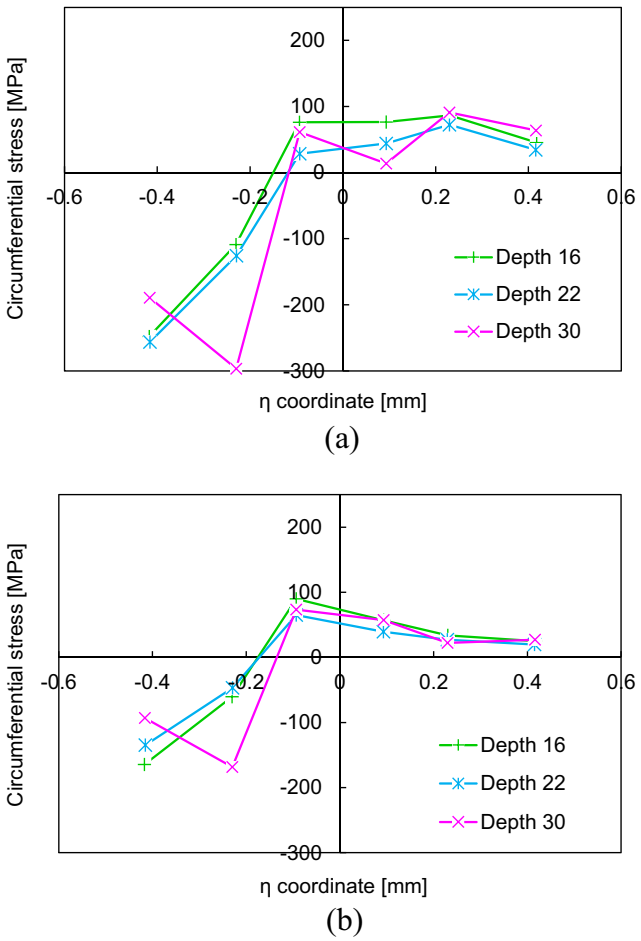

Fig. 14 Circumferential stress distributions along the middle section of the Bottom ring, obtained with the Lower gap: (**a**) at the end of the cup forming and unloading stage, (**b**) in the intact ring

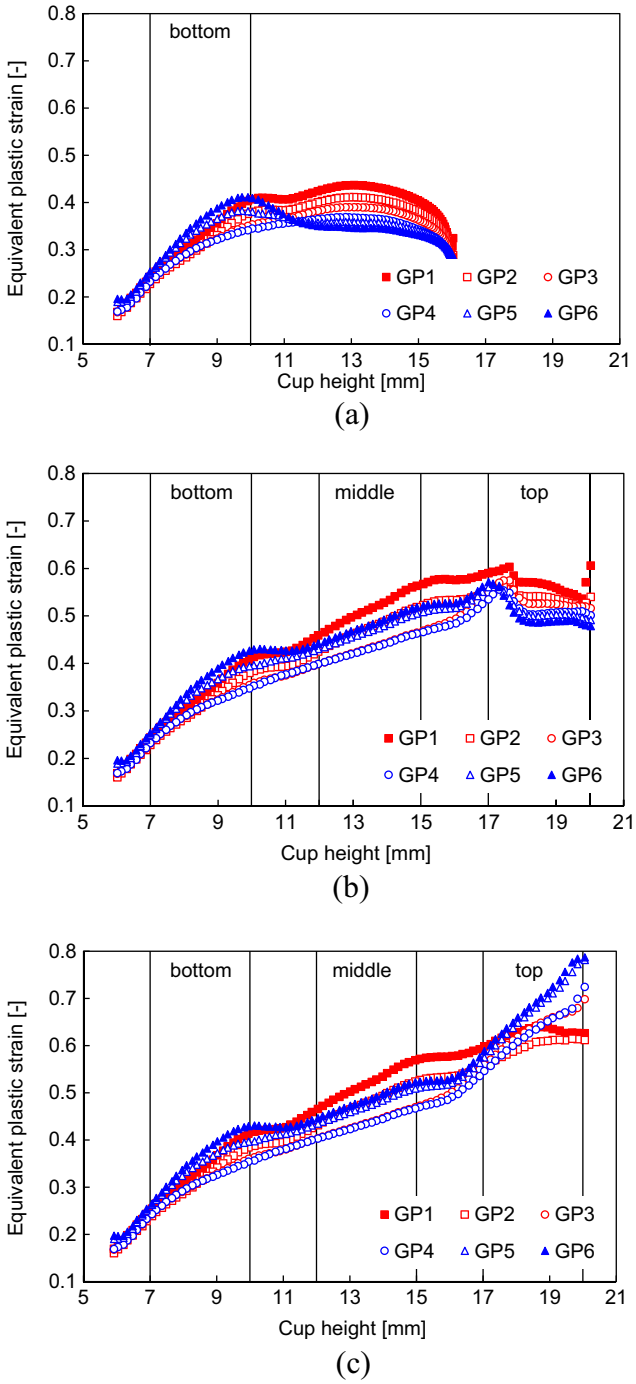

Fig. 15 Equivalent plastic strain distributions along the cup wall at the end of the cup forming and unloading stage, considering the lower gap value, for a punch displacement of: (**a**) 16 mm; (**b**) 22 mm and (**c**) 30 mm (full drawn)

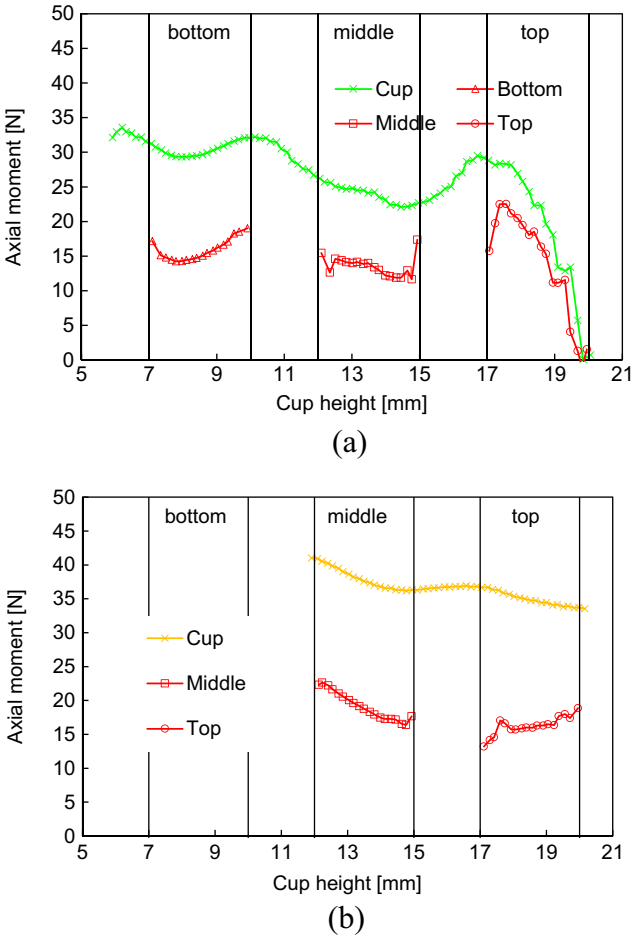

Fig. 16 Axial moment (per unit length) distributions along the cup wall at the end of the cup forming and unloading stage and in the intact ring for: (**a**) Lower gap; (**b**) Higher gap

compared with the other rings (see Fig. 16 (a)). This seems to result from the more uniform through-thickness distributions predicted in the cup for both the axial and the circumferential stresses (see Fig. 8 and Fig. 9). As discussed before for the top ring, the ironing operation changes the axial stress distribution, affecting the residual stresses predicted for the intact ring. The results confirm that the ironing changes the stress distribution, with a clear impact on the residual stresses in the cup and in the intact ring. The change in the residual stresses depends of the thickness reduction induced by the ironing operation [13], but its effect is evident even for small values as the one tested in this work.

Globally, the axial moments predicted for the higher gap condition are always higher than the ones obtained for the lower gap, which correlates with the through-thickness circumferential stress distributions along the cup wall (see Fig. 9) and with the ring opening values predicted for the middle and top rings (see Table 3). It is interesting to note that for the material located in the top ring the axial moment changes its trend upon the release of the axial stresses, which can be related with its evolution in the cup (see Fig. 8). All other axial moments present a similar trend when evaluated for the cup or the intact ring.

For both gap values, the average axial moment decreases with the increase of the distance from the cup bottom, which is in agreement with the trend observed for the opening of the rings. Moreover, in both cases it is possible to observe that the axial moment is not

constant along the cup wall, which correlates well with the sensitive of the ring opening to the positioning along the cup wall [1, 4]. In fact, even when no ironing occurs, the axial moment varies along the ring height (see Fig. 16 (b)). Nevertheless, for a higher gap value it is clear that the axial moment presents a smaller variation, which can be related with the smaller variation of the axial stress along the axial direction (see Fig. 8 (b)), associated to a smaller stretch effect (see Fig. 6) [7]. This shows that the stretch effect can also be related with the clearance between the die and the punch, besides the blank-holder force.

Figure 17 presents the axial moment distributions along the cup and the intact ring height, obtained for 16, 22 and 30 mm of punch displacement. The axial moment distributions are quite similar at the end of the cup forming and unloading, which is coherent with the fact that this part of the cup already attained a stable shape for a punch displacement of 16 mm (see also Fig. 6). Nevertheless, as shown in Fig. 14 (a), the through-thickness stress distributions are different, which confirms that similar axial moments can be determined for different stress distributions. Regarding the axial moment distribution in the intact ring, the trend is quite similar for the three depths, presenting an average value that is coherent with the ring opening values presented in Table 3, i.e. the one obtained with a drawing depth of 16 mm presents the higher value, followed by the one obtained from the full drawn cup and, finally, the one extracted from the cup obtained with a drawing depth of 22 mm. The increase in the relative difference for the axial moment evaluated in the intact ring for the three punch depths is related with the different distribution of the axial component of the residual stress, since the release of this component contributes to the change circumferential stress distribution (see Fig. 14), as discussed in the previous section.

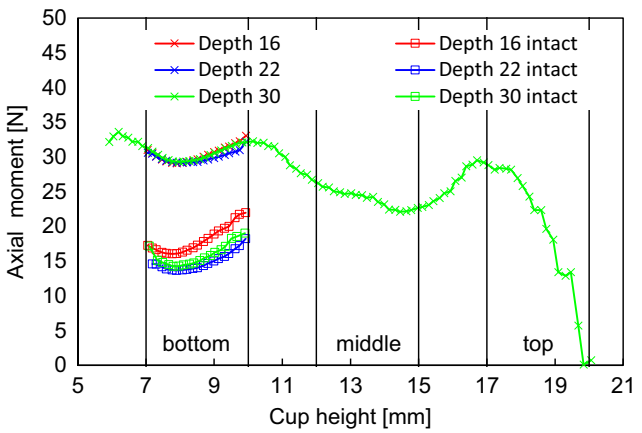

Fig. 17 Axial moment (per unit length) distributions along the cup wall at the end of the cup forming and unloading stage and in the intact ring for the Lower gap, using different punch displacements

Conclusions

The results show that deep drawn cups present axial and circumferential residual stresses of high magnitude, which are tensile at the outer surface and compressive at the inner surface, with profiles similar to what is expected from a bending-unbending operation [8, 13]. The ironing of the vertical wall changes the stress distribution along the cup wall outer surface, with a decrease of the axial stresses from a maximum near to the cup bottom to a minimum along the wall, while the circumferential residual stresses are distributed more uniformly along the cup wall [13]. This change in the characteristic residual stresses distribution is observed in all cup wall, i.e. it is not limited to the material that was submitted to the through-thickness compression state. Moreover, as stated in [13], the reduction in the residual stresses after deep drawing and ironing is observed even for relatively small ironing strains.

The axial and circumferential stress profiles exhibit a strong dependence on the axial position, which reflects the effect of bending under stretching. This effect is dictated by the blank-holder force selected, but also by the clearance between the die and the punch. The cut of the ring from the cup releases the residual axial stress component, as well as a part of the circumferential stress component, presenting an interdependency between these two components. In fact, since the ironing stage induces a more uniform through-thickness distribution of the axial stress component in the cup, the variation of the circumferential stresses between the cup and the intact ring is also smaller. Globally, the introduction of an ironing stage contributes to the reduction of the circumferential stress component through-thickness gradient, leading to a smaller ring opening, as observed also in [2]. However, this effect depends on the vertical position of the ring and the drawing depth, since the ironing stage changes the characteristic distribution of the residual stress component. The trend observed for several rings cut along the cup wall reflect the strong dependence on the axial position of both the axial and circumferential through-thickness residual stress profiles, which are strongly affected by a relatively small ironing strain.

Acknowledgements The authors gratefully acknowledge the financial support of the Brittany Region (France), the Portuguese Foundation for Science and Technology (FCT), under projects PTDC/EMS-TEC/0702/2014 (POCI-01-0145-FEDER-016779) and PTDC/EMS-TEC/6400/2014 (POCI-01-0145-FEDER-016876), and by UE/FEDER through the program COMPETE 2020. The first and the third author are also grateful to the FCT for the Doctoral grant SFRH/BD/90669/2012 and the Postdoctoral grant SFRH/BPD/101334/2014, respectively.

Compliance with ethical standards

Conflict of interest None.

References

1. Demeri MY, Lou M, Saran MJ (2000) A benchmark test for springback simulation in sheet metal forming. doi:10.4271/2000-01-2657
2. Xiao L-H, Yuan D-H, Xiang J-Z et al (2016) Residual stress in the cylindrical drawing cup of SUS304 stainless steel evaluated by split-ring test. Acta Mech Sinica 32:125–134. doi:10.1007/s10409-015-0516-4
3. Xia ZC, Miller CE, Ren F (2004) Springback behavior of AA6111-T4 with split-ring test. In: AIP Conf. Proc., pp 934–939. doi:10.1063/1.1766647
4. Foecke T, Gnaeupel-Herold T (2006) Robustness of the sheet metal springback cup test. Metall Mater Trans A 37:3503–3510. doi:10.1007/s11661-006-1045-3
5. Laurent H, Grèze R, Manach PY, Thuillier S (2009) Influence of constitutive model in springback prediction using the split-ring test. Int J Mech Sci 51:233–245. doi:10.1016/j.ijmecsci.2008.12.010
6. Laurent H, Greze R, Oliveira MC et al (2010) Numerical study of springback using the split-ring test for an AA5754 aluminum alloy. Finite Elem Anal Des 46:751–759. doi:10.1016/j.finel.2010.04.004
7. Gnaeupel-Herold T, Prask HJ, Fields RJ et al (2004) A synchrotron study of residual stresses in a Al6022 deep drawn cup. Mater Sci Eng A 366:104–113. doi:10.1016/j.msea.2003.08.059
8. Gnaeupel-Herold T, Foecke T, Prask HJ, Fields RJ (2005) An investigation of springback stresses in AISI-1010 deep drawn cups. Mater Sci Eng A 399:26–32. doi:10.1016/j.msea.2005.02.017
9. Oliveira MC, Alves JL, Chaparro BM, Menezes LF (2007) Study on the influence of work-hardening modeling in springback prediction. Int J Plast 23:516-543. doi: 10.1016/j.ijplas.2006.07.003
10. Lee MG, Kim SJ, Wagoner RH et al (2009) Constitutive modeling for anisotropic/asymmetric hardening behavior of magnesium alloy sheets: application to sheet springback. Int J Plast 25:70–104. doi:10.1016/j.ijplas.2007.12.003
11. Li KP, Carden WP, Wagoner RH (2002) Simulation of springback. Int J Mech Sci 44:103–122. doi:10.1016/S0020-7403(01)00083-2
12. Meinders T, Burchitz IA, Bonte MHA, Lingbeek RA (2008) Numerical product design: Springback prediction, compensation and optimization. Int J Mach Tools Manuf 48:499–514. doi:10.1016/j.ijmachtools.2007.08.006
13. Ragab MS, Orban HZ (2000) Effect of ironing on the residual stresses in deep drawn cups. J Mater Process Technol 99:54–61. doi:10.1016/S0924-0136(99)00360-X
14. Laurent H, Coër J, Manach PY et al (2015) Experimental and numerical studies on the warm deep drawing of an al-mg alloy. Int J Mech Sci 93:59–72. doi:10.1016/j.ijmecsci.2015.01.009
15. Manach P-Y, Coër J, Laurent AJH et al (2016) Benchmark 3 - Springback of an al-mg alloy in warm forming conditions. J Phys Conf Ser 734:22003. doi:10.1088/1742-6596/734/2/022003
16. Simões VM, Laurent H, Oliveira MC, Menezes LF (2016) Natural aging effect on the forming behavior of a cylindrical cup with an al-mg-Si alloy. In: AIP Conf. Proc, p 200021:1–6. doi:10.1063/1.4963639
17. Menezes LF, Teodosiu C (2000) Three-dimensional numerical simulation of the deep-drawing process using solid finite elements. J Mater Process Technol 97:100–106. doi:10.1016/S0924-0136(99)00345-3
18. Oliveira MC, Alves JL, Menezes LF (2008) Algorithms and strategies for treatment of large deformation frictional contact in the numerical simulation of deep drawing process. Arch Comput Methods Eng 15:113-162. doi:10.1007/s11831-008-9018-x
19. Menezes LF, Neto DM, Oliveira MC, Alves JL (2011) Improving computational performance through HPC techniques: case study using DD3IMP in-house code. AIP Conf Proc. 1353: 1220-1225. doi:10.1063/1.3589683
20. Neto DM, Oliveira MC, Menezes LF (2015) Surface smoothing procedures in computational contact mechanics. Arch Comput Methods Eng 24:37–87. doi:10.1007/s11831-015-9159-7
21. Barros PD, Baptista AJ, Alves JL et al (2015) Trimming of 3D solid finite element meshes: sheet metal forming tests and applications. Eng Comput 31:237–257. doi:10.1007/s00366-013-0344-8
22. Baptista AJ, Alves JL, Rodrigues DM, Menezes LF (2006) Trimming of 3D solid finite element meshes using parametric surfaces: application to sheet metal forming. Finite Elem Anal Des 42: 1053–1060. doi:10.1016/j.finel.2006.03.005
23. Hughes TJR (1980) Generalization of selective integration procedures to anisotropic and nonlinear media. Int J Numer Methods Eng 15:1413–1418. doi:10.1002/nme.1620150914
24. Wagoner RH, Li M (2007) Simulation of springback: through-thickness integration. Int J Plast 23:345–360. doi:10.1016/j.ijplas.2006.04.005
25. Neto DM, Oliveira MC, Menezes LF, Alves JL (2014) Applying Nagata patches to smooth discretized surfaces used in 3D frictional contact problems. Comput Methods Appl Mech Eng 271:296-320. doi: 10.1016/j.cma.2013.12.008
26. Neto DM, Oliveira MC, Menezes LF, Alves JL (2013) Nagata patch interpolation using surface normal vectors evaluated from the IGES file. Finite Elem Anal Des 72: 35-46. doi:10.1016/j.finel.2013.03.004
27. Nagata T (2005) Simple local interpolation of surfaces using normal vectors. Comput Aided Geom Des 22:327–347. doi:10.1016/j.cagd.2005.01.004
28. Neto DM, Martins JM, Cunha PM et al Thermo-mechanical finite element analysis of the AA5086 alloy under warm forming conditions. Submitted to Int J Solids Struct. http://hdl.handle.net/10316/40114. Accessed 30 March 2017
29. Coër J, Laurent H, Oliveira MC et al Detailed experimental and numerical analysis of a cylindrical cup deep drawing. Submitted to Int J Mater Form. http://hdl.handle.net/10316/40113. Accessed 30 March 2017
30. Voce E (1948) The relationship between stress and strain for homogeneous deformations. J Inst Met 74:537–562
31. Voce E (1955) A practical strain-hardening function. Meta 51:219–226
32. Livatyali H, Altan T (2001) Prediction and elimination of springback in straight flanging using computer aided design methods: part 1. Experimental investigations J Mater Process Technol 117:262–268. doi:10.1016/S0924-0136(01)01164-5
33. Danckert J (2001) Ironing of thin walled cans. CIRP Ann - Manuf Technol 50:165–168. doi:10.1016/S0007-8506(07)62096-4
34. Rabahallah M, Bouvier S, Balan T, Bacroix B (2009) Numerical simulation of sheet metal forming using anisotropic strain-rate potentials. Mater Sci Eng A 517:261–275. doi:10.1016/j.msea.2009.03.078
35. Yuying Y, Chunfeng L, Hongzhi X (1992) A study of longitudinal cracking and the forming technology for deep-drawn austenitic stainless-steel cups. J Mater Process Technol 30:167–172. doi:10.1016/0924-0136(92)90344-R
36. Neto DM, Oliveira MC, Alves JL, Menezes LF (2014) Comparing faceted and smoothed tool surface descriptions in sheet metal forming simulation. Int J Mater Form 8:549–565. doi:10.1007/s12289-014-1177-8

(Page intentionally left blank)

Chapter 7.

Conclusions and Perspectives

This chapter presents the main conclusions from this work as well as some of the opened perspectives to increase the robustness of warm sheet metal forming operations and the exploitation of the database of experimental results.

.

(Page intentionally left blank)

7.1. Conclusions

The main goal of this dissertation is the analysis of warm forming conditions of heat treatable aluminum alloys, taking into account the natural aging, in order to propose solutions that can contribute to the increase of robustness of sheet metal forming operations. The work was supported on a campaign of experimental tests, performed for two Al-Mg-Si alloys (EN AW 6016-T4, EN AW 6061-T6) and taking into account their storage time. The thermo-mechanical behavior of both alloys was characterized using uniaxial tensile tests and stress relaxation tests. The cylindrical cup deep drawing test was also performed in a range of temperature between RT and 250°C, enabling the indirect evaluation of the residual stresses using the split ring (springback) tests. The conclusions drawn from the results can be summarized as follows.

Regarding the influence of **Temperature**:

- For both alloys, the temperature increase leads to a decrease of the yield stress and the work hardening rate. Compared to RT, warm forming reduces the drawing forces, indicating the presence of lower internal stress, which leads to lower springback values.
- For both alloys, the orthotropic behavior trend does not change due to temperature increase, thought the planar anisotropy coefficient slightly decreases with the temperature increase. It results in a slight decrease of the cylindrical cup earing with the temperature increase.
- The temperature increase leads to an increase of the post-uniform elongation, which is higher for the EN AW 6061-T6 alloy than for the EN AW 6016-T4 alloy, although it has a small influence in uniform elongation. This increase in ductility is advantageous to improve formability in sheet metal forming parts.

Regarding the influence of **Strain Rate and Punch speed**:

- Both alloys present a negligible strain rate sensitivity at RT, which was confirmed from both the uniaxial tensile tests and the forming tests results.
- At 200 °C, both alloys present a positive strain rate sensitivity. This was evaluated by the uniaxial tensile tests, being the stress-relaxation stages extremely useful to understand the dynamic precipitation phenomena occurring at warm temperatures, for the EN AW 6016-T4 alloy.
- In warm forming tests, the low punch speed leads to high exposure time that counteracts the effects of the non-isothermal conditions, promoting the tools thermal equilibrium. On the other hand, at higher punch speed, the tools keep their temperature values nearly constant during the warm forming.

- In warm forming tests, due to high exposure time at the low punch speed, dynamic precipitation hardening occurs on the EN AW 6016-T4 alloy. Therefore, the increase of the punch speed leads to a punch force and springback reduction and improves formability.
- The punch speed has a negligible influence in formability and springback of the EN AW 6061-T6 alloy, despite its positive strain rate sensitivity. In fact, for higher punch speeds the positive strain rate sensitivity can compensate the hardening effect induced by the lower average blank temperature at lower punch speeds, leading to similar results whatever the punch speed.
- The results here reported about the influence of punch speed in Al-Mg-Si alloys are opposed to the ones found in the literature for non-heat treatable aluminum alloys, which report a decrease of formability and an increase of springback with the punch speed increase, for both under isothermal and non-isothermal conditions. This corresponds to the expected behavior for materials presenting a positive strain rate sensitivity. Nonetheless, the results of this study show that, when considering non-isothermal conditions for heat-treatable aluminum alloys, the temperature gradient in the blank has a strong impact in the formability and the springback behavior, which can be explored to counteract the positive strain rate sensitivity.

Regarding the influence of **Holding time**:

- For the EN AW 6016-T4 alloy, the increase of heat-holding up to 30 minutes leads to a change its mechanical behavior to the one typical of an artificial aging (T6) heat treatment. In consequence, it was observed a punch force and a springback increase.
- For the EN AW 6061-T6 alloy, the tensile test results show a slight increase of yield stress and tensile strength (with similar strain hardening) as the heat-holding time increases up to 30 minutes, which results in a slight increase of the punch force. However, this has a negligible effect in formability and springback. Moreover, the heat-holding of 30 minutes does not induce the over-aging of this artificially aged alloy, on the contrary it causes an increase of strength. The occurrence of over-aging depends on the initial T6 treatment, which for this alloy seems to present some potential for strength increase, with the corresponding loss in total elongation.

Only the mechanical behavior of the EN AW 6016-T4 alloy is strongly influenced by natural aging. Thus, the natural aging study focuses only on this alloy. Regarding the influence of **Natural Aging**:

- At RT (from 1 to 18 months), the yield stress and tensile strength increase as the storage time increases, which leads to an increase of the maximum drawing forces (about 10%) and springback (about 10%).

- The orthotropic behavior trend does not change due to natural aging, though the planar anisotropy coefficient slightly increases due to natural aging.
- The influence of natural aging in the variations of yield stress and tensile strength is reduced by the temperature increase. Thus, whatever the storage time, in warm forming between 200 and 250 °C with a punch speed of 1 mm/s, the drawing force required to produce the cylindrical cups is nearly the same, as well as the thickness evolution along the cup, and the springback.
- At 200 °C, whatever the punch speed adopted the variability caused by natural aging was negligible at warm forming, which validates the effectiveness of warm forming as a solution to minimize the variability caused by the natural aging in forming operations.
- At 200 °C, for a fast heat-holding time, the material natural aged for 18 months presents a slightly higher yield stress than the 1 month aged material, but the tensile strength is similar. This results in slightly higher punch force during warm forming, and a negligible effect on formability and springback. For a heat-holding time of 10 minutes, 1 and 18 months aged material present an overmatch of both the tensile stress curves and the punch force curves during warm forming. For a heat-holding time of 30 minutes, the punch force evolution obtained for the 18 months aged material is lower than the 1 month one. This can be related with the known negative-effect of natural aging in artificial aging.

Moreover, a **numerical study focusing on the split-ring test** was performed, to enable an improved understanding about the influence of the processing condition in the ring opening trend and its link with the internal stress distribution in the cup wall. The conclusions drawn from this study can be summarized as follows.

- At the end of forming process, the cup presents axial and circumferential residual stresses of high magnitude, which are tensile at the outer surface and compressive at the inner surface, with profiles similar to what is expected from a bending-unbending operation.
- The ironing of the vertical wall changes the stress distribution along the cup wall outer surface, with a decrease of the axial stresses from a maximum near to the cup bottom to a minimum along the wall, while the circumferential residual stresses are distributed more uniformly along the cup wall. Moreover, the reduction in the residual stresses after deep drawing and ironing is observed even for relatively small ironing strains.
- The cut of the ring from the cup releases the residual axial stress component, as well as a part of the circumferential stress component, presenting an interdependency between these two components.
- The trend observed for several rings cut along the cup wall reflects the strong dependence on the axial position of both the axial and circumferential

through-thickness residual stress profiles. This explains the lower sensitivity of the ring located in the top of the cup (ironed zone) to the changes in material and process conditions.

In summary, the results highlight the potential of warm forming, when performed under non-isothermal conditions with high punch speeds and heating rates, as an effective solution to improve formability and springback. Additionally, warm forming contributes to minimize the influence of natural aging in sheet metal forming parts variability. From an industrial point of view, higher punch speed is advantageous since it allows higher production rates. Moreover, warm forming can also be used to reduce the variability originated by the use of different batches or different manufacturers.

7.2. Perspectives and suggestions for future studies

This work contributes to the rise and better understanding of some issues that deserve to be better analyzed in future work:

- The results of this study show that, when considering non-isothermal conditions for heat-treatable aluminum alloys, the temperature gradient in the blank has a strong impact in the formability and the springback behavior. In this context, in order to contribute to a more extensive used of warm forming in the industrial field, it is important to be able to perform its virtual try-out. This requires thermo-mechanical models, able to describe the heat transfer phenomena as well as the mechanical behavior of the materials. According to the study results, these models need also to be able to take into account the tools dilatation, particularly if the forming process involves ironing stages.
- The results of this study highlight the fact that when modeling the mechanical behavior of heat-treatable alloys different approaches can be adopted. In fact, the hardening models adopted for artificially aged alloys can be similar to the ones used for non-heat treatable alloys, i.e. take into account temperature and strain rate sensitivity. However, for naturally aged alloys the hardening model should also be able to describe the static and dynamic precipitation hardening, particularly if long heat-holding times need to be considered. The experimental results obtained within this work constitute an excellent database to study the potentialities of different hardening models already available in the literature, or even develop new models.
- The analysis or development of a hardening model always involves a strategy for its parameters identification. The direct comparison of the thermo-mechanical tests, performed with the Gleeble device and the Intron tensile test machine coupled with the furnace, indicate that the temperature gradient that occurs in the first device can promote heterogeneous artificial aging

conditions along the specimen's length. Thus, the development of parameter identification strategy based on results obtained with the Gleeble device should take into account this effect.

- The results of this study show that the temperature increase leads to a decrease of the yield stress and the work hardening rate. Therefore, it is expected to have slighter differences in the mechanical behavior of different batches or different manufacturers, when using warm conditions. This should be confirmed with an experimental study.

(Page intentionally left blank)

Appendix 1

Natural Aging Effect on the Forming Behavior of a Cylindrical Cup with an Al-Mg-Si Alloy

This appendix contains the paper presented at the ESAFORM 2016, the 19th International ESAFORM Conference on Material Forming and published in: AIP Conference Proceedings, with the same title as the appendix. This work presents a finite element analysis of the cylindrical cup test, using DD3IMP-in-house code, performed for RT conditions and considering the EN AW 6016-T4, showing the impact of thickness deviations and natural aging in the prediction of the experimental results.

.

(Page intentionally left blank)

Natural Aging Effect on the Forming Behavior of a Cylindrical Cup with an Al-Mg-Si Alloy

V.M. Simões[1, 2, a)], H. Laurent[1,b)], M.C. Oliveira[2, c)], L.F. Menezes[2, c)]

[1]*Université de Bretagne-Sud, EA 4250, LIMATB, F-56100 Lorient, France*
[2] *CEMUC, Dep. de Eng. Mec., Univ. de Coimbra Polo II, Pinhal de Marrocos, 3030-788 Coimbra*

[a)]Corresponding author: vasco.simoes@univ-ubs.fr
[b)]herve.laurent@univ-ubs.fr
[c)]{marta.oliveira, luis.menezes}@dem.uc.pt

Abstract. Natural Aging of EN AW 6016-T4 is experimentally evaluated under uniaxial tensile test and forming of a cylindrical cup. The uniaxial tensile tests were performed 4 days, 1, 4, 7 and, 18 months after the alloy quenching. The results shows an increase of the proof and tensile strengths, while the in-plane anisotropy remains globally invariable with the increase of the storage time. The forming of cylindrical cups was performed too, with specimens at 1 and 18 months of natural aging. The increase of the proof and tensile strengths leads to an increase of the punch force during the deep drawing process. However, the effect on the thickness evolution along the cup's wall and on the cup's height is negligible. In fact, the numerical simulation results indicate that these parameters are more sensitive to the initial sheet thickness (considering the mean value of 1.047mm or the approximated one of 1.000mm) than to the changes induced by aging in the hardening behavior.

INTRODUCTION

Al-Mg-Si are frequently used Al-based alloys due to the good formability in non-aged state and, due to the possibility to be bake-hardened ("artificial aging" achieved by an age hardening at ≈180ºC during ≈30 min) to medium strength. Therefore, these alloys have many applications in transports industry, namely in automotive industry. Al-Mg-Si alloys are delivered in supersaturated states due to quenching, and may often present an increase of the proof and tensile strength, due to storage at room temperature. This effect, known as natural aging, occurs after quenching when the alloys are stored at room temperature (RT) during a time period (storage time). In general, natural aging is considered to be not relevant from the technological point of view for Al-Mg-Si alloys, since they are always submitted to artificial aging [1]. Nevertheless, natural aging is often analyzed in order to understand its "negative effect" in the subsequent bake hardening step, since it causes longer precipitates with a lower volume fraction. This leads to lower peak hardness and increased ductility after bake hardening [1]. During natural aging stage the proof strength ($R_{p0.2}$ [2]) and the tensile strength (R_m [2]) increases and ductility is reduced [3,4]. In fact, it has been proposed to represent the evolution of the $R_{p0.2}$ with the natural aging time (t_{NA}) using a logarithmic function, such that $R_{p0.2} = k \cdot \log(t_{NA}) + R_i$, where k is a natural aging kinetics parameter and R_i represents the initial yield strength of the alloy (after quenching and storage at room temperature for ≈1 h) [5-7].

Since it was first observed by Wilm in 1904 [8], the study of the age hardening behavior process has contributed greatly to the optimization of aluminum alloys performance. This complex process was first explained by Guinner and Preston in 1938 [9,10] for the Aluminum alloys and, later for Al-Mg-Si Alloys [11]. Nevertheless, the scientific knowledge about the mechanisms is still rather fragmentary due to the difficulties on its analysis [1,12]. In fact, the study of natural aging in 6000 series alloys is complicated because: firstly, the content of Mg and Si is always very low, i.e. 1.5 or 1.2wt% for each of the elements Si and Mg, respectively; secondly, Mg, Al, and Si are neighboring elements in the periodic table [1].

ESAFORM 2016
AIP Conf. Proc. 1769, 200021-1–200021-6; doi: 10.1063/1.4963639
Published by AIP Publishing. 978-0-7354-1427-3/$30.00

This work is focused on an EN AW 6016 alloy that is used in automotive industry and is expected to show superior formability and higher corrosion resistance with a low paint baked strength. The main goal is to understand the influence of natural aging on the forming behavior of this Al-Mg-Si alloys. Therefore, the natural aging was evaluated by performing tensile test at 1, 4, 7 and 18 months after quenching.

SELECTED MATERIAL AND EXPERIMENTAL PROCEDURE

The EN AW 6016-T4 alloy is known as a Si excess alloy since the Mg/Si ratio in mass fraction percentage [wt.%] is less than one. The sheets were made and supplied by Constellium with a Mg/Si ratio equal to 0.19 [wt.%] and were cold rolled up to 1.04mm thickness, annealed, quenched and natural aged (T4). The mechanical properties were evaluated by the supplier using uniaxial tensile tests, performed after 4 days of maturations at RT and are presented in Table 1.

TABLE 1. Mechanical properties of EN AW 6016-T4 (supplier results). R_m tensile strength. $R_{p0.2}$ proof strength at 0.2% of the extensometer gauge length. Ag percentage of non-proportional elongation at maximum force. n_{4-6} strain hardening coefficient between 4 and 6 % of plastic elongation. n_{10-15} strain hardening coefficient between 10 and 15 % of plastic elongation (terms and definitions according with the European Standard EN 10002-1 [2]).

R_m	$R_{p0.2}$	Ag	n_{4-6}	n_{10-15}
198 MPa	88 MPa	24.6 %	0.32	0.27

The static strain aging due to material storage at room temperature was evaluated using uniaxial tensile tests performed 1, 4, 7 and 18 months after the heat treatment. The strain rate of $2x10^{-3}s^{-1}$ was adopted as reference and used in all tests. At least two tensile tests were performed for each test condition and the results were always reproducible with an average scatter of true stress less than ±1MPa, for the same value of true strain. Thus, in the following section only the result of one of the tests is presented. The strain fields were measured by Digital Image Correlation (DIC) technique using ARAMIS 4M 3D optical system. The anisotropic behavior was analyzed for specimens with 1 and 7 months of storage time, by performing test with three different in-plane directions: 0°, 45° and 90° to rolling direction (RD).

The formability was evaluated using the cylindrical cup benchmark test, with the tools dimensions shown in Fig. 1 a). The circular blank with an initial diameter of 60 mm is radially drawn into the die by the punch movement (Fig. 1 b)) to obtain a cylindrical cup (Fig. 1 c)). The blank-holder force of 6 kN was selected in order to avoid wrinkles and the punch force is recorded during the test. The blank is lubricated with an Aerosol Oil Spray [13] in an amount which avoids the occurrence of galling.

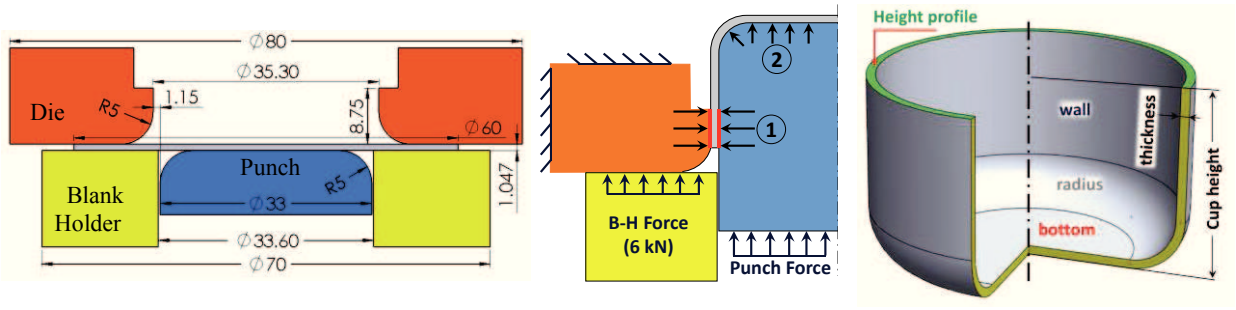

(a) (b) (c)

FIGURE 1. Deep drawing of a cylindrical cup: (a) Tools in initial position with dimensions; (b) Ironing phase; (c) Final cup geometry and its sections.

The cylindrical cup tests were performed in a Zwick BUP200 machine [14]. The cup thickness and height measurements (Fig. 1 c)) were performed using a 3D machine "Brown & Sharpe Mfg. Co.", model "MicroXcel PFX-454". The thickness is evaluated based on the coordinates measurements performed along the interior and the exterior sides of the cup, in a normal direction to the surface; the difference between the interior and exterior coordinates is the thickness value. The measurements were performed along several directions to the RD, such that the value presented corresponds to the average of the results obtained, as follows: 0º to RD (average of 0º and 180º); 45º to RD

(average of 45º, 135º, 225º and 315º); 90º to RD (average of 90º and 270º) [15]. The cup height is measured from 0º to 355º to RD with a step of 5º [15]. The cup height measurements are presented from 0º to 90º taking into account average the assumed cup symmetries. The results presented for the punch force, cup thickness and cup height are the average of the results obtained for the three cylindrical cup tests performed.

TENSILE TESTS RESULTS

The tensile test results obtained with specimens with different storage time are presented in Fig. 2. Figure 2 a) shows the influence of natural aging on the mechanical properties along the RD. Globally, natural aging leads to an increase of the yield and ultimate tensile stresses(or R_{02} and R_m) with the increase of the storage time [3,4], with a negligible influence in the hardening coefficient. In an initial period there is a fast increase of both R_{02} and R_m, which tends to stabilize for longer storage time periods. As previously mentioned, this behaviour can be described with a logarithmic function [5], as shown in Fig. 2 b) for the material under analysis.

Concerning the in-plane anisotropic behaviour, the results show a negligible influence of natural aging for both the flow stresses (see Fig. 2 c)) and the r-values (see Fig. 2 d)). Despite the small differences reported for the r-values, the trend is globally the same. Other works have also reported that this alloy keeps the same anisotropic trends despite the negligible influence of natural aging [3].

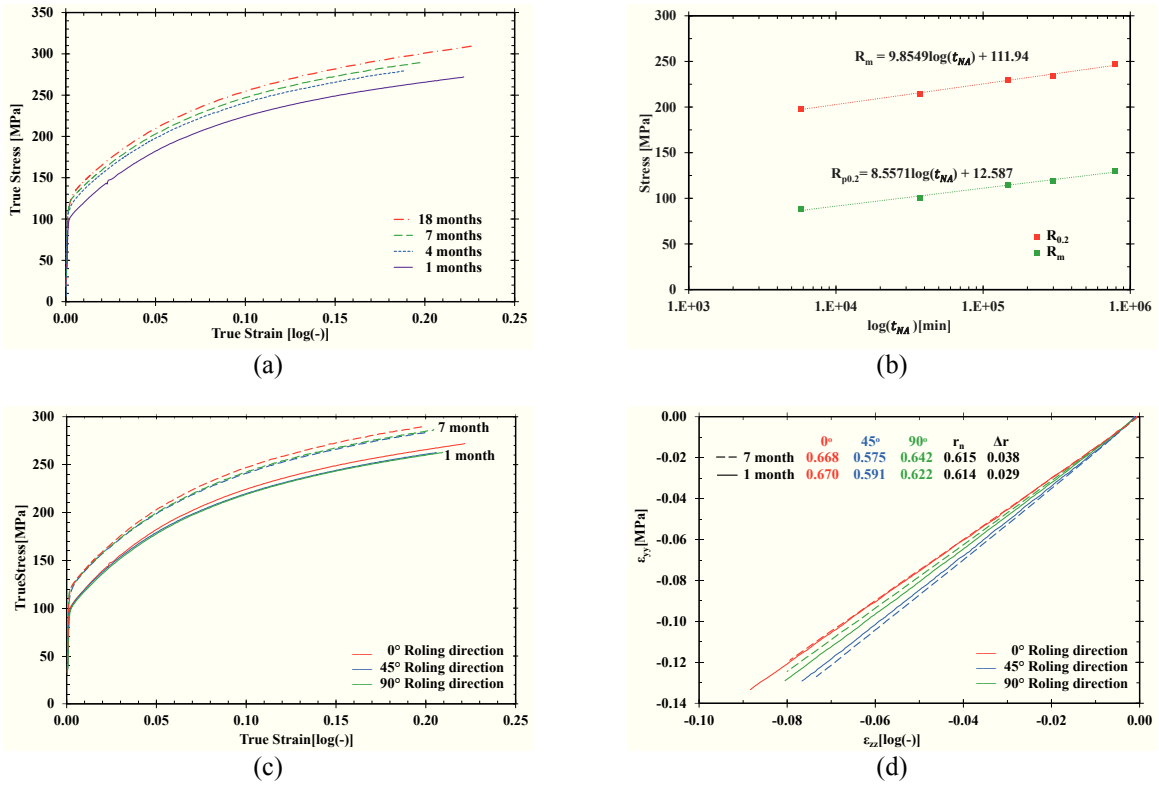

FIGURE 2. Natural aging effect on material behavior: a) Stress-strain curves along RD, obtained from uniaxial tensile tests performed at different storage time; b) Logarithmic evolution of the yield and ultimate tensile stresses with natural aging time (average of 6 test minimum including different anisotropic directions); Influence of natural aging on anisotropic behavior: c) stress-strain curves and d) r-values.

Based on this set of experimental results, the constitutive parameters for the isotropic hardening Voce law ($Y = Y_0 + (Y_{sat} - Y_0)[1 - \exp(-C_Y \bar{\varepsilon}^p)]$) [16] and the Barlat et al. (1991) yield criterion (YLD'91) [17] were identified using the in-house code DD3MAT [18], for 1 and 18 months of storage. It should be mentioned that in order to ameliorate the definition of the in-plane stress directionalities for the yield criterion parameters identification, the experimental values considered correspond to an equivalent plastic strain $\bar{\varepsilon}^p$ value of 5%. Also, it is assumed that the r-values remain unchanged after 7 months of storage time. The identified parameters are presented in Table 2.

TABLE 2. Parameters identified for the constitutive model adopted using the in-house code DD3MAT [18]

	Voce Law			**Yld91** (m=8)				
	Y_0	C_Y	Y_{sat}	C_1	C_2	C_3	C_4= C_5	C_6
1 months	109.9	11.58	280.9	1.1078	1.0866	0.9684	1	0.9917
18 months	131.4	12.08	312.3	1.0899	1.0699	0.9533	1	0.9758

FORMING TESTS RESULTS

Figure 3 presents the results obtained for the cylindrical cup tests performed with the sheet after a storage time of 1 and 18 months. Figure 3 a) presents the punch force evolution with punch displacement, highlighting the two distinct phases that occur during the process: drawing and ironing. The drawing phase involves the deformation up to ≈19mm of punch displacement, where a noticeable local minimum of the punch force occurs when the blank loses contact with the blank-holder. After that point the ironing phase starts, with an increase of the punch force until attaining a local maximum (≈23mm of punch displacement), followed by a decreases until the end of the process. Ironing occurs since the thickness of the blank is higher than the gap between the die and the punch (1.150mm). Therefore, the sheet is strongly compressed between the punch and die (see Fig. 1 b)), which typically imposes high contact forces, normal to the surface of the punch and the die. Globally, the results show an increase of the punch force with increasing aging time, which can be related with the increase of the flow stress presented in Fig. 2 a).

In order to better understand these experimental results, the numerical analysis of the cylindrical cup forming process was performed using the in-house code DD3IMP [19]. The blank is discretized with 3-D solid elements with 8 nodes. The tools are assumed to behave rigidly with the die modeled using Nagata surfaces [20] and the blank-holder and the punch with Bézier surfaces. The elastic regime assumes an isotropic behavior, described by the Young's modulus (E=69 [GPa]) and the Poisson ratio (ν=0.33). The constitutive model adopted for both specimens uses the parameters previously shown in Table 2. Regarding the sheet thickness, as previously mentioned, the supplier indicates a value of 1.04 mm. In fact, the average value obtained for more than 130 measurements was 1.047mm. Therefore, two models were considered: one with 1.000 mm and another with 1.047mm, of initial blank thickness. The friction is modelled with the Coulomb's law using a constant value of 0.15, since it allows a good reproduction of the punch force during the drawing phase, as shown in Fig. 3 a) for the 1.047mm thick blank.

Globally, the numerical simulation results for the drawing stage corroborate the influence of natural aging on the punch force evolution, i.e. the increase of the punch force associated to the increase of the flow stress. Figure 3 b) compares the punch force evolution for both specimens, as predicted by the models with different initial blank thicknesses. The results show that an increase of ≈0.05mm (≈5%) in the sheet thickness, globally, it has the same impact in the punch force during drawing as the increase of the flow stress due to natural aging.

The punch force evolution results clearly show that the ironing stage is not well predicted. Nevertheless, it should be mentioned that it is known that this stage is quite sensitive to the gap value between the punch and the die [21] (see Fig.1) as well as to the friction conditions [15,22]. In this context, Fig. 3 c) presents the thickness evolution along a curvilinear coordinate, corresponding to the distance to the cup's center. The profile of the thickness evolution clearly shows the two critical points where the minimum thickness value is typically obtained, corresponding to the begin and end of the punch radius [23]. Along the cup's wall, the thickness increases until attaining a constant value, which was imposed by the ironing stage. Thus, it is possible to confirm that the gap between the die and the punch is slightly higher in the experimental device than in the numerical model.

The experimental results indicate that natural aging has a negligible effect in the thickness evolution (Fig. 3 c)), which is corroborated by the numerical analysis. A slight decrease in thickness is observed for the material with 1 month of storage time, due to the lower flow stress value, in both experimental and numerical results. On other hand, the initial thickness of the blank used in the numerical simulation is a major factor to accurately predict thickness evolution. The results considering an initial thickness of 1.047mm show a very good agreement with the experimental ones. The small differences in the cup's bottom can be associated to the fact that the parameters for the YLD91 yield criterion were identified without any information regarding the equi-biaxial stress state behavior. In addition, the differences in the cup's wall can be related with the stronger ironing stage imposed by the numerical model, since this slope is influenced by the value for the maximum thickness allowed.

Figure 3 d) presents the cup's height profile which shows always the same trend: maxima at RD and TD and minimum at 45^0 to RD and equivalent positions. Thus, it can be stated that the ear profile is not influenced by natural aging, which is in agreement with the trend observed for the in-plane anisotropic behaviour in the uniaxial tensile tests. In the experimental results, the amplitude of the ears (difference between maximum and minimum height) is higher for the 18 months naturally aged material, which also seems to be in agreement with the slightly higher value for Δr (see Fig. 2 d)). The global cup's height is underestimated in the numerical simulations as a sequence of a smaller flow of the blank during the drawing step (loss of contact with the blank-holder occurs later). Although the numerical results obtained with an initial blank thickness of 1.047mm show a slightly higher profile, this seems to be caused by the strong stretching during the ironing stage.

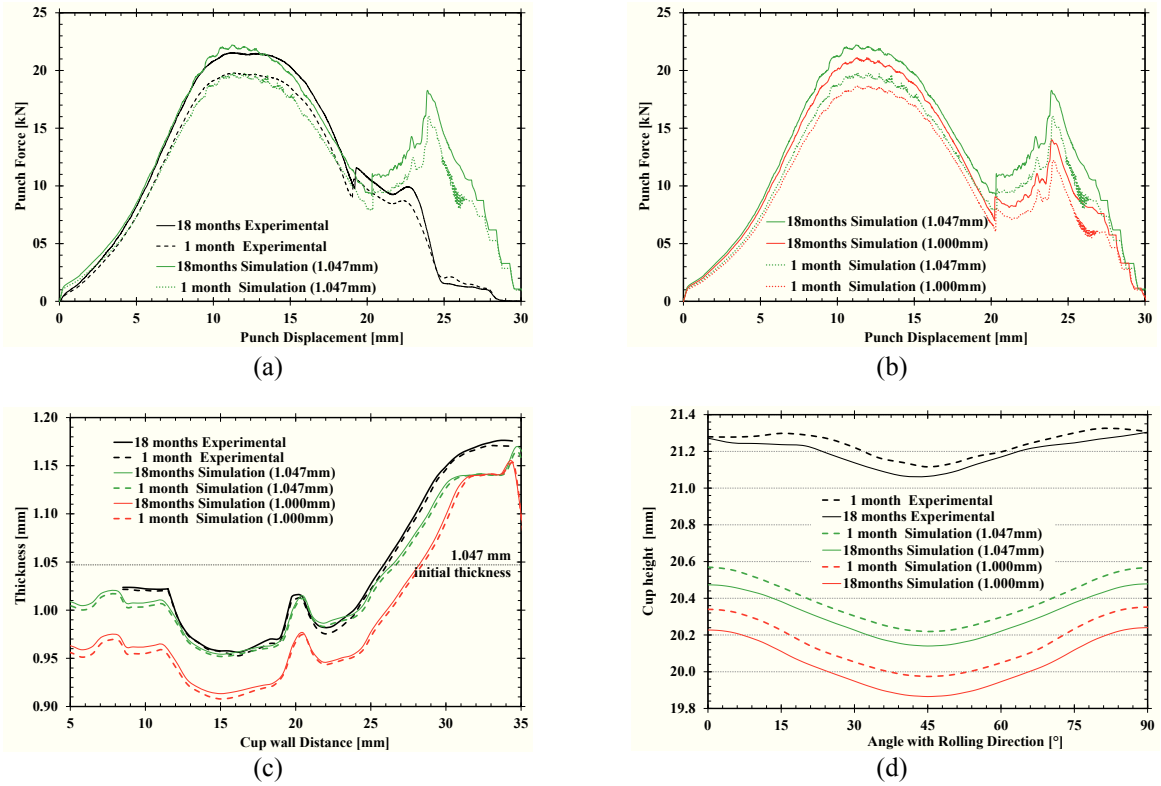

FIGURE 3. Results of the cylindrical cup forming:
Punch force evolution with punch displacement (a) Experimental results *vs* numerical results with a blank with an initial thickness of 1.047mm, for 1 and 18 months of storage time, (b) Numerical results with blanks with initial thickness of 1.000mm and 1.047mm, for 1 and 18 months of storage time;
Experimental results vs Numerical results with blanks with initial thickness of 1.000mm and 1.047mm, for 1 and 18 months of storage time: (c) Thickness evolution along the cup's and (d) Cup's height.

Summary:

A study on the natural aging effect on EN AW 6016-T4 formability was performed. The alloy shows a logarithmic increase of the proof and tensile strength with storage time increase. The anisotropic behavior is negligible influenced by the natural aging, which leads to minor variations of the thickness evolution along the cup's profile and also of the cup's height. Thus, although there is a slight increase of the force needed to deform the blank this is not a relevant factor from an industrial point of view. The numerical simulation results highlight the importance of the accuracy in the initial blank thickness, in order to be able to predict accurate distributions for this parameter, which is often used to evaluate the constitutive models performance.

ACKNOWLEDGMENTS

This research work is sponsored by national funds from the French Ministry of Higher Education and the Portuguese Foundation for Science and Technology (FCT) via the project PTDC/EMS-TEC/1805/2012 and by FEDER funds through the program COMPETE – Programa Operacional Factores de Competitividade, under the project CENTRO -07-0224 -FEDER -002001 (MT4MOBI). The authors are also grateful to Constellium for supplying the material to perform the experimental tests. The first author is also grateful to the FCT for the PhD grant SFRH/BD/90669/2012.

REFERENCES

1. J. Banhart, C.S.T. Chang, Z. Liang, N. Wanderka, M.D.H. Lay, and A.J. Hill, Adv. Eng. Mater. **12**, 559 (2010).
2. Central Secretariat ISO, *ISO 6892-1:2009 Metallic Materials - Tensile Testing - Part 1: Method of Test at Room Temperature* (International Organization for Standardization, 2009), p. 65.
3. A. Mishra, Experimental Investigation and Numerical Prediction of Rupture in Bending of Metallic Sheets, Université de Bretagne-Sud, 2013.
4. A. Cuniberti, A. Tolley, M.V.C. Riglos, and R. Giovachini, Mater. Sci. Eng. A **527**, 5307 (2010).
5. S. Esmaeili and D.J. Lloyd, Scr. Mater. **50**, 155 (2004).
6. S. Esmaeili, D.J. Lloyd, and W.J. Poole, Acta Mater. **51**, 3467 (2003).
7. S. Esmaeili and D.J. Lloyd, Acta Mater. **53**, 5257 (2005).
8. A. Wilm, Metall. Z. Für Gesamte Hüttenkd. **8**, 225 (1911).
9. André Guinier, Nature **142**, 569 (1938).
10. G. D. Preston, Nature **142**, 570 (1938).
11. P. Brenner and H. Kostron, Z Met. **4**, 89 (1939).
12. L. Ding, Z. Jia, Z. Zhang, R.E. Sanders, Q. Liu, and G. Yang, Mater. Sci. Eng. A **627**, 119 (2015).
13. Jelt Grease 5411 aerosol 95cSt.
14. H. Laurent, J. Coër, P.Y. Manach, M.C. Oliveira, and L.F. Menezes, Int. J. Mech. Sci. **93**, 59 (2015).
15. J. Coër, Mise En Forme Par Emboutissage En Température D'un Alliage D'aluminium AA5754-O, Université de Bretagne Sud, 2013.
16. E. Voce, J. Inst. Met. **537** (1948).
17. F. Barlat, D.J. Lege, and J.C. Brem, Int. J. Plast. **7**, 693 (1991).
18. J. L. Alves, M.C. Oliveira, and L.F. Menezes, in *AIP Conf. Proc.*, **712**, 1645 (2004).
19. L.F. Menezes and C. Teodosiu, J. Mater. Process. Technol. **97**, 100 (2000).
20. D.M. Neto, M.C. Oliveira, L.F. Menezes, and J.L. Alves, Comput.-Aided Des. **45**, 639 (2013).
21. V.M. Simões, Analysis of the Influence of Process Parameters in the Deep Drawing of a Cylindrical Cup, Universidade de Coimbra, 2012.
22. V.M. Simões, J. Coër, H. Laurent, M.C. Oliveira, J.L. Alves, P.Y. Manach, and L.F. Menezes, Key Eng. Mater. **554-557**, 2256 (2013).
23. M. Colgan and J. Monaghan, J. Mater. Process. Technol. **132**, 35 (2003).